UNIVERSITY OF STRATHCLYDE

Department of Biomedical Engineering



# Development of Microfluidic Systems for Studying Functional Connectivity Between *In Vitro* Neuronal Co-Cultures

Graham Robertson

A thesis presented in partial fulfilment of the requirements for the degree of Doctor of Engineering

2015

# Declaration of Authorship

This thesis is the result of the author's original research. It has been composed by the author and has not been previously submitted for examination which has led to the award of a degree.

The copyright of this thesis belongs to the author under the terms of the United Kingdom Copyright Acts as qualified by University of Strathclyde Regulation 3.50. Due acknowledgement must always be made of the use of any material contained in, or derived from, this thesis.

Signed:

Date:

# Abstract

The brain is a fascinating machine that is fundamental to our existence as conscious individuals. This is highlighted during neurological disorders that can have a devastating impact on the sufferer's aptitude and quality of life. There is much which is not yet understood about what happens during neurological disorders including the changes which occur at a cellular level that affect synaptic communication between neurons.

One method of studying these synaptic connections and how they change during disorders is through *in vitro* neuronal cell cultures which are a valuable tool for investigating cellular mechanisms. Recently, microfluidic techniques have enabled new methods of patterning cells *in vitro* and can provide precise control of the extracellular environment. Compartmentalised devices have been created that allow for certain characteristics of neurological disorders to be modelled *in vitro*. However, current methods of applying drugs to neuronal network in such devices are often performed manually which can limit their value as it is impractical to switch between multiple solutions.

In this thesis, a method is initially developed for quantifying the synaptic communication that occurs between functionally connected neural networks that are held in isolated environments. This was investigated using primary hippocampal neurons grown in a compartmentalised device. One sub-network of neurons was chemically stimulated while both presynaptic and postsynaptic responses were observed simultaneously using $Ca^{2+}$ imaging. Additionally, to address the currently limited methods of altering the extracellular environments in neuronal microfluidic devices, a microfluidic perfusion system was developed that can switch between multiple solutions. This was applied to compartmentalised neural networks while their cellular activity was monitored using $Ca^{2+}$ imaging. Overall, the methods developed here can be used to study neurological mechanisms in a controlled manner and have the potential to be used in the screening of novel drugs and therapeutics targeted at neurodegenerative disorders.

# Acknowledgments

# Contents

# Figures

# Tables

# Abbreviations

| | |
|---|---|
| **AMPA** | α-amino-3-hydroxy-5-methyl-4-isoxazolepropionic acid |
| **ATP** | Adenosine triphosphate |
| **BSA** | Bovine serum albumin |
| **CCD** | Charge-coupled device |
| **CNS** | Central nervous system |
| **DIV** | Days *in vitro* |
| **DL-AP5** | DL-(-)-2-amino-5-phosphonopentanoic acid |
| **EM** | Electron multiplier |
| **FOV** | Field of view |
| **GABA** | γ-aminobutyric acid |
| **GFAP** | Glial fibrillary acidic protein |
| **GFP** | Green fluorescent protein |
| **HDMS** | Hexamethyldisilazane |
| **iGluR** | Ionotropic glutamate receptor |
| **MAP2** | Microtubule-associated protein 2 |
| **mAβ** | Monomer β-Amyloid |
| **MCPG** | (R,S)-α-Methyl-4-carboxyphenylglycine |
| **MEA** | Microelectrode array |
| **mGluR** | Metabotropic glutamate receptor |
| **NBQX** | 2,3-dioxo-6-nitro-1,2,3,4-tetrahydrobenzo[f]-quinoxaline-7-sulfonamide |
| **NCX** | $Na^+/Ca^{2+}$ pump |
| **NFU** | Normalised fluorescence units |
| **NMDA** | N-methyl-D-asparate |
| **OA** | Okadaic acid |
| **PBS** | Phosphate buffered saline |
| **PDMS** | Polydimethylsiloxane |
| **PFA** | Paraformaldehyde |
| **PNS** | Peripheral nervous system |
| **RFP** | Red Fluorescent protein |

| | |
|---|---|
| **ROI** | Region of interest |
| **TTX** | Tetrodotoxin |
| **UV** | Ultraviolet |

# Chapter 1. Background

## 1.1. Introduction

The brain is an interconnected network of cells which work together and form an exceedingly intricate biological mechanism. The purpose of this thesis is to investigate and develop a microfluidic tool that can help in the understanding of the underlying mechanisms of the brain in health and disease. *In vitro* microfluidic systems will be initially investigated to show that communication can occur between isolated environments. Further development of this system to improve its capabilities by incorporating perfusion will then be described.

The nervous system is essential for the control and management of the human body and has been called the most complicated machine in the known universe [1]. It is comprised of the central nervous system (CNS), made up of the brain and spinal cord, and the peripheral nervous system (PNS), which includes all of the nervous system outside of the CNS [2]. The components of the CNS are responsible for information processing, decision making, integrating sensory signals and sending motor commands [3]. The PNS is principally concerned with sending sensory information to the CNS and delivery commands from the CNS to effectors [3].

The nervous system is composed of neural tissue, which includes a range of cell types. The main functional unit, responsible for communication, is the neuron of which there are around 100 billion in the human brain [4]. Supporting and augmenting the neurons are the glial cell types, which in the CNS includes oligodendrocytes, astrocytes, and microglia that each have a range of functions required to maintain the neuronal population [2].

### 1.1.1. Neurons – Specialised for Communication

Neurons are cells that are capable of communication and signal processing [5], [6]. There are several different sub-types of neuron found in the nervous system which all function using the same principal mechanisms. Within a network of neurons, a single neuron has the ability to excite or inhibit the excitation of another cell and in turn it

can be excited or inhibited by other neurons [7]. The cell can be divided into sections, where each region plays a role in the cell's functionality.

The cell body is called the soma and it contains the nucleus and the locus where the inputs and outputs of the cell extend from [8]. Surrounding the nucleus is the perikaryon that contains organelles essential for the cell's viability, such as the mitochondria needed for the large amount of adenosine triphosphate (ATP) production that an active neuron requires [2]. Neurons need energy from ATP for maintaining the resting membrane potential, recovering from depolarisation, and for the synthesis, release and recycling of neurotransmitters [9]. Nissl bodies in the perikaryon are formed by fixed and free ribosomes that group together with the rough endoplasmic reticulum and give the cell a grey appearance, hence the term grey matter [10]. The structure of the cell is supported by neurofilaments and neurotubules where bundles of these neurofibrils, extend out of the cell soma into processes that project from the cell body. In the most common type of neuronal cell, a multipolar neuron, multiple of these processes form dendrites that act as inputs to the cell while a single projection will become the output of the cell, the axon. Both the dendrites and axons can branch to form many connections with other cells (Figure 1.1).
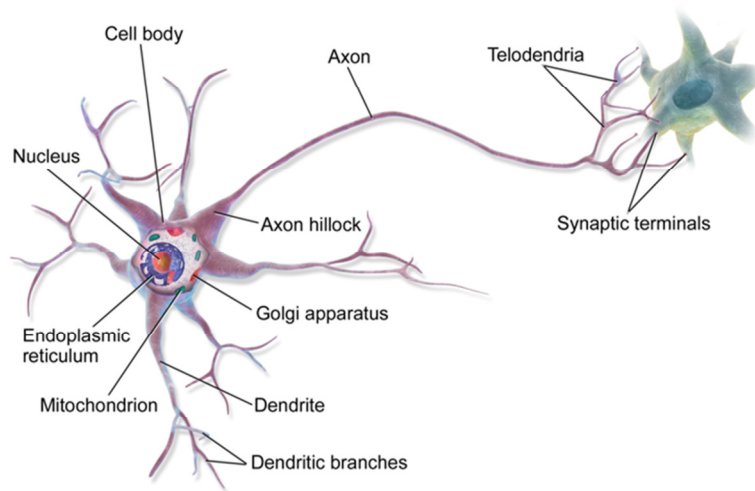


**Figure 1.1 The anatomy of a neuron. Many dendrites converge on the cell soma where an axon is projected from via the axon hillock.** *Image by BruceBlaus*

## 1.1.1.1. Dendrites and Axons

The dendrites are processes that extend from the cell soma and are responsible for conducting signals from other neurons towards the cell body. They may branch and be connected to, and excited by, many other cells in the network. These processes are covered in fine studs (dendritic spines) that are used to form connections with axons, called synapses [2].

A neuron also projects a single axon (that may branch) from the soma that is responsible for carrying information away from the neuron to other connected neurons and effectors [2] (Figure 1.1). The axon is joined to the soma at a thickened region called the axon hillock [11]. The distal end of the axon terminates with fine branches (telodendria) which end with a synaptic terminal. Internally, the axon contains neurofibrils and neurotubules for structural support, mitochondria to produce ATP, various enzymes required for functioning, and synaptic vesicles that contain neurotransmitters. Externally, the axon membrane may be exposed to the interstitial fluid or it may be sheathed in myelin which enables faster conduction of action potentials along the length of the axon to the synapse [12].

## 1.1.1.2. Synapse

The communication from the axon of one neuron to the dendrite of another occurs at a synapse [5]. This is formed between a presynaptic terminal, on the axon of one neuron, and the postsynaptic membrane, on the dendrite of the receiving neuron, with a region called the synaptic cleft between the two. The presynaptic cell, upon receiving an action potential at the synapse, releases vesicles containing neurotransmitters into the synaptic cleft. The depolarisation of the presynaptic terminal opens voltage-gated calcium ($Ca^{2+}$) channels which allow $Ca^{2+}$ to flow into the cell. The increased concentration of $Ca^{2+}$ in the presynaptic terminal causes the synaptic vesicles, containing neurotransmitters, within the presynaptic terminal to be exocytosed into the synaptic cleft [13]. The neurotransmitters then bind to receptors in the postsynaptic membrane which can trigger either a depolarisation or hyperpolarisation of the postsynaptic cell membrane, depending on the

neurotransmitter released, and consequently instigating or preventing a new action potential in the post synaptic cell.

## 1.1.1.3. Action Potentials

Actions potentials arise from a local depolarisation of a cell's membrane from the resting membrane potential [4]. In neurons, the resting membrane potential is approximately –70 mV between the inside of the membrane and the outside of the membrane (Figure 1.2). This is maintained due to a combination of electrochemical gradients and active pumping of ions in and out of the cell.

In a cell, the ionic composition of the intracellular fluid and extracellular fluid differs significantly [2]. For neurons, there is a high concentration of potassium ($K^+$) ions inside the cell and a high concentration of sodium ($Na^+$) and chloride ($Cl^-$) ions in the extracellular fluid (Figure 1.2A). A concentration difference of a particular charged species across a cell membrane gives rise to an electrical potential across the membrane. The voltage, $V_{eq}$, is dependent on both the charge carrier concentration outside, $[X]_{out}$, and inside the cell membrane, $[X]_{in}$, as described by the Nernst equation [14], Equation 1.

$$V_{eq} = \frac{RT}{zF} \ln \frac{[X]_{out}}{[X]_{in}}$$

**Equation 1**

Where $z$ is the valency of the ion in question, $F$ is the Faraday constant, $R$ is the ideal gas constant, and $T$ is the temperature of the solution in Kelvin. Each species of charge carrier will create a potential according to their concentration distribution across the cell membrane. The overall transmembrane potential is a summation of each individual Nernst potential.

The membrane of the cell is not freely permeable to ions and is instead selectively permeable through ion channels situated in the membrane. Some ion channels may be continuously open or may be triggered by the binding of an agonist, or electrically, by changes in the local electric field potential between different parts of the channel. Other channels are active and use energy released from ATP hydrolysis to actively pump specific ions through the cell membrane. One of the main pumps in a neuron that helps maintain the transmembrane potential is the sodium-potassium

pump that actively transports $Na^+$ out of the cell and $K^+$ into the cell. These ion channels, pumps and electrochemical gradients all contribute to the resting membrane potential.
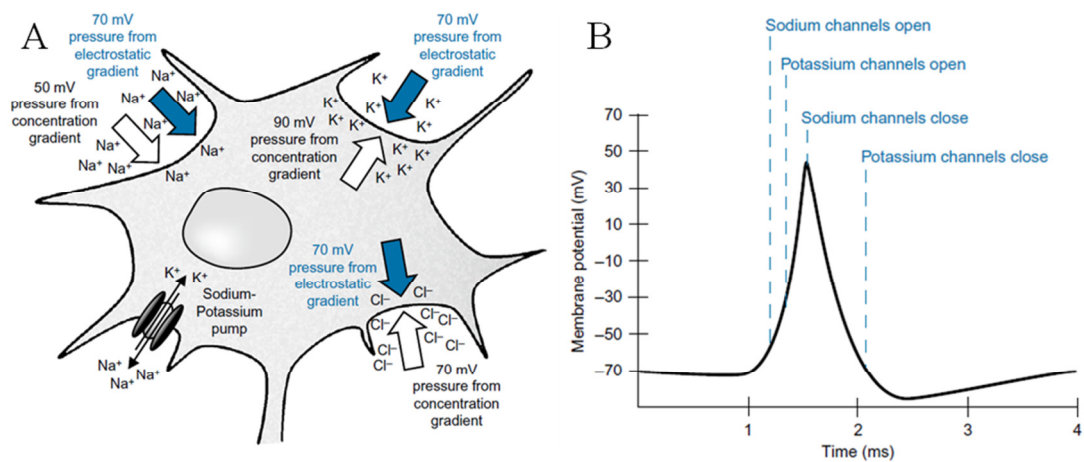


**Figure 1.2 The transmembrane potential of a neuron. (A) A combination of chemical concentration gradients and electrostatic gradients are involved in creating the transmembrane potential. Sodium, potassium and chloride ions are chiefly responsible for creating the potential difference of –70 mV between the inside and outside of the cell. Active pumping by ion channels, such as the sodium-potassium pump, is crucial in sustaining the membrane potential. (B) During an action potential voltage gated sodium channels are responsible for depolarising the cell while voltage gated potassium channels are responsible for repolarising the cell. Once activated the voltage gated channels cannot be reactivated for a short period of time called the refractory period. *Figure adapted from* [4].**

During an action potential a local region of the cell's transmembrane potential is reduced due to a change in the local concentrations of different ions. This can be caused by either neurotransmitter activity or proximity to part of the membrane that is already depolarised [2]. If the transmembrane potential changes, to reach a sufficient threshold, then voltage-gated $Na^+$ channels will open, causing an influx of $Na^+$ that depolarises the cell to +30 mV (Figure 1.2 B). This depolarisation in turn triggers the voltage-gated $Na^+$ channels to close and other voltage-gated channels to open, such as the voltage-gated $K^+$ channel which opens causing an efflux of $K^+$ that is sufficient to repolarise the cell. This cascade process normally takes around 1 ms, after which there is a relative refractory period where voltage-gated channels are reset and there is a brief period of hyperpolarisation to -90 mV. During the initial cascade there is an absolute refractory period where no other action potentials can

occur, while during the relative refractory period a higher than normal stimulus is required to instigate an immediate action potential. The depolarisation/repolarisation of the transmembrane potential occurring at one location causes the surrounding membrane to reach the threshold and trigger its own depolarisation/repolarisation cascade, thus propagating a wave of depolarisation/repolarisation along the cell membrane. The refractory periods of the voltage-gated ion channels help to maintain the directionality of the action potential as it travels along an axon membrane.

Oligodendrocytes in the CNS and Schwann cells in the PNS can form insulating layers of myelin around sections of axons. Between each insulated section is a region of the axon membrane that is exposed to the extracellular fluid, called a node of Ranvier [12], which contains a high density of ion channels. The insulated regions are formed by many layers of lamellae (10–160 layers) wrapped around the axon, which act in series to greatly increase the resistance between the intracellular fluid of the axon and the extracellular fluid. This effectively blocks ion flow through the membrane at these regions and concentrates it at the nodes of Ranvier [14]. When a node of Ranvier is depolarised during an action potential, the electrochemical gradient produced is sufficient for the subsequent node to reach the threshold voltage and trigger a depolarisation/repolarisation cascade. By skipping the insulated regions of the myelinated axon, the action potential is able to propagate along the axon at an increased speed of up to $150\,\mathrm{m\cdot s^{-1}}$, compared to $0.5–10\,\mathrm{m\cdot s^{-1}}$ for unmyelinated axons [15].

## 1.1.1.4. Neurotransmitters

The neurotransmitter is a chemical messenger that activates receptors in the postsynaptic membrane [5]. These receptors may act to either depolarise the cell membrane, an excitatory action, or to hyperpolarise it, an inhibitory action. Alternatively, neurotransmitters may bind to G protein-coupled receptors (GPCRs) that can influence the cell behaviour through intracellular mechanisms [16]. The most abundant excitatory neurotransmitter in the CNS is glutamate, which acts on receptors to trigger excitation in the postsynaptic cell [17]. The most common inhibitory neurotransmitter in the CNS is GABA ($\gamma$-aminobutyric acid)[18].

## 1.1.1.4.1. Glutamate Receptors

Glutamatergic neurons release glutamate which can activate two main receptor groups [19]. When glutamate binds to ionotropic glutamate receptors (iGluRs) a directly produced excitatory post synaptic current is produced. Alternatively, when binding to metabotropic glutamate receptors (mGluRs) a biochemical cascade within the cell is triggered, which may either increase or decrease excitability (Figure 1.3).

Glutamate can act on several ionotropic receptors, such as AMPA (α-amino-3-hydroxy-5-methyl-4-isoxazolepropionic acid), NMDA (N-methyl-D-asparate) and Kainate, to produce excitatory responses [17], [19]. These receptors are located on the postsynaptic membrane and when bound allow cations to pass into the cell, reducing the transmembrane potential, potentially causing an action potential to occur if a threshold of depolarisation is achieved. There is some evidence that NMDA and Kainate receptors can also be located in the presynaptic membrane [20]. Each receptor has two agonist-binding sites that must be occupied for the ion channel to open. AMPA receptors are responsible for the fast excitatory transmission in the brain and have a low affinity for glutamate. When open, AMPA receptors become permeable to $Na^+$, $K^+$, and sometimes $Ca^{2+}$. NMDA receptors have a higher affinity for glutamate than AMPA receptors; however, they require the co-agonist glycine to bind to the receptor for the ion channel to open. Once open, the ion channel allows the flow of non-specific cations including $Ca^{2+}$. Kainate receptors can have low or high affinities for glutamate and become permeable to $Na^+$, $K^+$, and slightly to $Ca^{2+}$ upon activation.

Alternatively, glutamate can act on several metabotropic receptors that have been identified [17], [19]. These receptors are coupled to secondary systems within the cell that activate a variety of G-proteins. These can modify a range of cellular functions including the performance of voltage-gated ion channels which can alter the cell's excitability. These are found in both the presynaptic terminal, where they can decrease the release of both excitatory and inhibitory neurotransmitters, and the postsynaptic membrane, where they can inhibit or potentiate ion channel activity [21]. Due to the signalling cascade involved, the result of metabotropic receptor activation is slower than that of ionotropic receptors; however, their effect

can be more pronounced as single metabotropic receptor activation can result in many cascade reactions within the cell. This can lead to sustained alterations inside the cells such as altered plasticity and excitability of the cell.
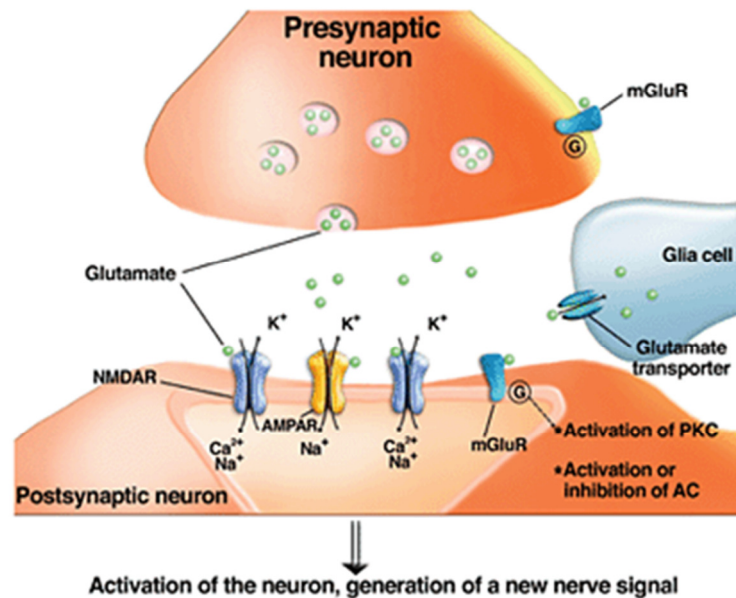


**Figure 1.3 The neurotransmitter glutamate acts on many receptors in the postsynaptic neuron. When a glutamatergic synapse is activated, glutamate is released and can act on both iGluRs and mGluRs to produce an excitatory response in the postsynaptic neuron. Glial cells can also absorb excess glutamate to modulate the synaptic activity. There is also evidence of mGluRs being present on astrocytes** [21]**. *Image from* [22]**

## 1.1.1.4.2. GABA Receptors

Conversely, GABAergic neurons release GABA which acts as an inhibitory neurotransmitter [23], [24]. When GABA binds to the ionotropic $GABA_A$ receptors they open, allowing $Cl^-$ to pass into the neuron. The influx of $Cl^-$ ions increases the transmembrane potential, hyperpolarising the membrane and inhibiting its depolarisation. The effect of stimulating GABAergic neurons is to lower the excitability of the neuronal network. The $GABA_A$ receptors can be blocked using drugs such as bicuculline methiodide [25], [26], which reduces the inhibitory influence of this neurotransmitter and therefore increases the overall excitability of the neuronal network.

GABA can also bind to the metabotropic $GABA_B$ receptors [24]. These activate G proteins which in turn act on ion channels in both the presynaptic and postsynaptic

membrane. In the presynaptic membrane they inhibit $Ca^{2+}$ channels which reduce $Ca^{2+}$ influx and thus the release of neurotransmitters. In the postsynaptic membrane $GABA_B$ receptors act to open $K^+$ channels resulting in the hyper-polarisation of the postsynaptic cell. Both of these metabotropic mechanisms act to prevent the signalling of action potentials from one neuron to another. GABA receptors have also been found on astrocytes where they are thought to play a role in further modulating the synaptic communication between neurons [27].

## 1.1.2. Glia – Supporting Neuronal Function

While neurons are specialised for communication they cannot maintain the extracellular environment and are dependent on glia [2] (Figure 1.4). These cells generally support the neuron functionality by maintaining the extracellular environment and augmenting functional properties of the neuron [28]. The main glial cells found in the CNS are astrocytes, oligodendrocytes and microglia. The smallest of the glial cells are called microglia which act as the brain's innate immune system and maintain the interstitial environment by performing phagocytosis to absorb pathogens, waste products, and cellular debris. Oligodendrocytes have large processes that wrap around axons to form a myelin sheath. Several myelinated sheathes, generally 1–2 mm in length, can cover the entire length of the axon enhancing the signal propagation along it. Between adjacent sheathes is a node of Ranvier [12], which contains a high density of $Na^+$ channels necessary for the axon to conduct action potentials between nodes.

The most prevalent glial cell in the CNS is the astrocyte which is the largest of the glial cells [2]. It has a diverse range of functions that are essential for healthy brain function. As the CNS is isolated from blood supplies, due to the blood-brain barrier, astrocytes bind to capillaries, completely covering the endothelial layer to maintain the interstitial environment [29]. They regulate the concentration of ions, nutrients, and dissolved gasses in the interstitial fluid as well as providing structural support in the brain. Additionally, astrocytes have increasingly been found to play a role in synaptic communication [30], [31]. By absorbing and recycling neurotransmitters these cells can suppress or enhance synaptic communication between cells.
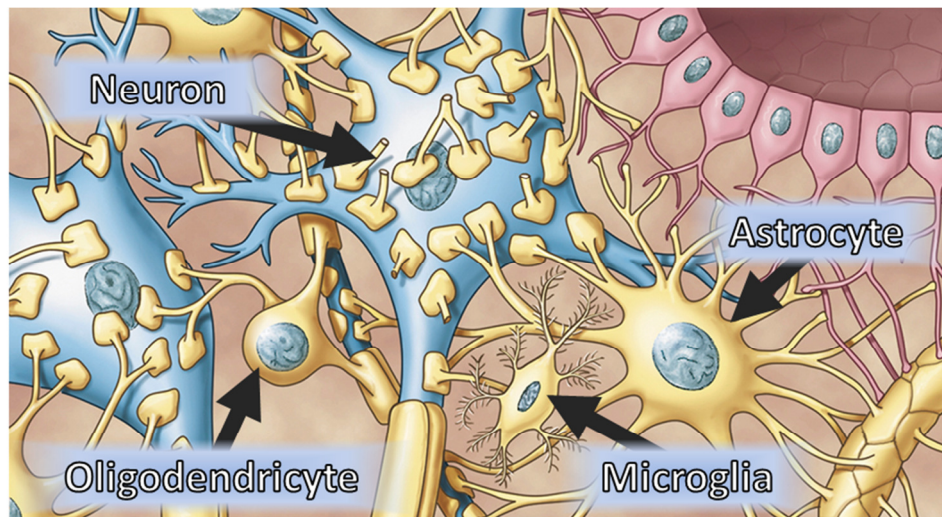
**Figure 1.4 Glial cells in the CNS. Neurons are surrounded by glial cells in the CNS.** *Astrocytes* **bind to capillaries and neurons,** *Oligodendrocytes* **form myelin sheaths around axons to aid in action potential propagation and** *Microglia* **absorb pathogens and waste products found in the interstitial environment.** *Modified image from* [2]

## 1.2. Disease States

The diversity of the vast network of interconnected cells that comprise the CNS make it difficult to study when it functions properly and hinders research into what happens during CNS disorders. Brain disorders can have a devastating impact on those affected and are a significant burden on the global economy. In Europe the estimated annual cost of mental and neurological disorders is €798 billion [32], [33], while in the UK alone a 2010 survey revealed that the economic cost was €134 billion due to approximately 45 million cases of brain disorder [34]. These costs are expected to rise in the future as the conditions are generally long term and the average age of the population increases [33], [34]. The poor understanding of mental and neurodegenerative disorders poses a problem that has been highlighted as one of the "grand challenges" of our time [35].

In general CNS disorders are difficult to treat due to the poor understanding of physiological changes that occur at a cellular level, the difficulty in getting treatments to the affected area, and the poor translation of treatments from animal models to the human disease [36]. The primary route of delivery for a pharmacological treatment to the CNS is the blood, however the brain is protected

from many molecules in the blood by the blood-brain barrier [37]. This is because the CNS requires a specialised environment that is different to the rest of the body. It is a challenge to develop drugs that can readily cross the barrier as well as treat a disease condition. Additionally, while animal models are often used in research of treatments, the diseases that they reproduce are often induced artificially and do not represent all aspects of the disease [37]. This can lead to treatments that fail during clinical trials even though results in animal models appeared promising.

One of the most well known disorders is dementia, which affects over 35 million people around the world, with the most common form being Alzheimer's disease [38], [39]. This condition is diagnosed symptomatically, however it is characterised by tau aggregation and β-amyloid plaques that are found throughout the brain [40]. The amyloid hypothesis suggests that the formation of β-amyloid plaques, formed by the aggregation of excessive β-amyloid peptides, drives the progression of the disease including the characteristic tau hyperphosphorylation leading to neurofibrillary tangles and neurodegeneration [41]. More recently is has been hypothesised that it is in fact tau mutations and aggregations that have a central role in the underlying mechanisms that lead to the propagation of the disease. These mechanisms are thought to include microglia which can release cytotoxic factors when activated leading to neuronal damage and the release of tau oligomers. These tau oligomers are thought to have a role in triggering further neurotoxic actions [42].

Overall, it is thought that the disease originates in part of the brain and spreads to other regions, however the exact mechanism of propagation between neurons is still unknown. The malformations adversely affect the communication between neurons by deteriorating synaptic connections, and ultimately result in a severely degraded overall brain structure [40] (Figure 1.5).
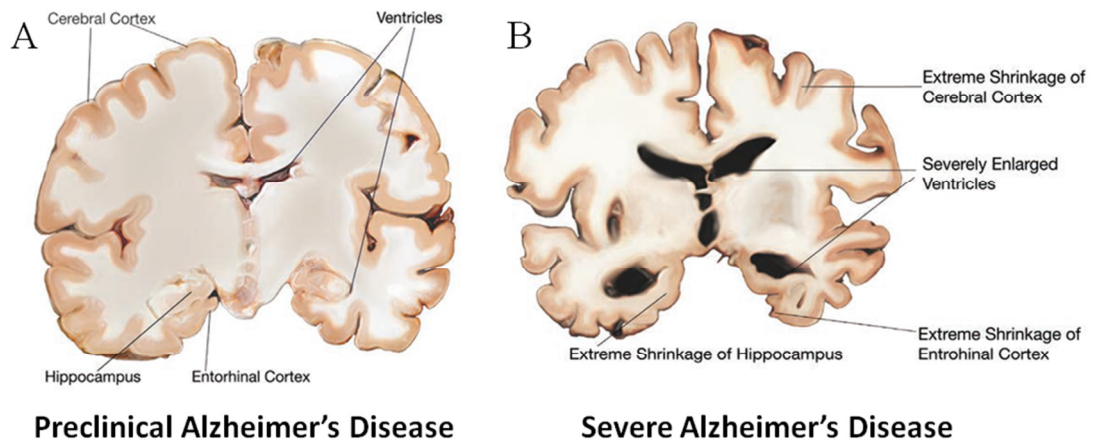
**Figure 1.5 Alzheimer's disease degrades the structure of the brain. During the development of the disease structural changes alter the normal structure of the brain (A). Regions of the cerebral cortex and hippocampus shrink while the ventricles become enlarged.** *Image modified from* [40]

Other forms of neurological disorder, such as epilepsy and multiple sclerosis, also have unique mechanisms of action which are only partially understood [43]. In each of these conditions it is difficult to determine the exact mechanisms of action at a cellular level. To properly understand these neurological disorders requires fundamental neuroscience research which is important and generally underfunded given the potential impact on society [32]. There are also limitations in current research into therapeutics that rely on using animals to model human disorders that the animals do not naturally present [37]. In these cases there can be very specific known causes and symptoms, however, the animal models used may only partially replicate the disorder leading to poor translation from animal models to the human disease. While there is a range of techniques that are traditionally used in neuroscience research, there is also a need for new multidisciplinary approaches which can provide more detailed information on fundamental neurobiology mechanisms [44].

Of all of the structures in the brain, the hippocampus is one of the most widely studied [45] due to its important roles in learning and memory as well as its association with neurodegenerative disorders. In particular the hippocampus has been linked to Alzheimer's disease amongst other disorders such as temporal lobe epilepsy and schizophrenia [43]. This makes the hippocampus a prime target for exploring how the brain works and for devising therapeutic strategies against neurodegenerative disorders.

## 1.3. Studying Neuron Physiology

### 1.3.1. *In Vivo* versus *In Vitro*

There are many methods of studying neural physiology, interactions and degeneration. Both *in vivo* and *in vitro* techniques have advantages and disadvantages. *In vivo* provides the most physiologically relevant environment to study neural tissue that *in vitro* studies can only hope to achieve. However, *in vitro* environments allow for the isolated study of the neural tissue without the confounding influences of a dynamic living environment. This allows for specific sub-cellular properties to be analysed in isolation. Indeed it was only through an *in vitro* study, over a century ago, that the first direct observation of a neurite growing was achieved [46]. While *in vitro* cultures allow for simplified control over individual cellular mechanisms, it is an unnatural environment for CNS cells to grow and can lead to changes in cellular behaviour. Many factors can affect the rate of maturity of neurons *in vitro*, where higher cell densities and 3D cell culture can lead to earlier synaptic activity and help neurons to mature at a closer rate to those *in vivo* [47], [48].

### 1.3.2. Methods of Studying Synaptic Communication

There are several methods available that make it possible to study the communication between connected neurons. These vary in terms of signal quality, interpretation and efficiency. The functional activity of a neuron can be described in terms of the number of action potentials it produces over time or in terms of intercellular chemical fluctuations. There are several methods of recording this activity, both electrically and optically.

### 1.3.3. Electrophysiology

Electrophysiology is the study of the electrical properties of a cell or tissue [4]. For neuronal cultures the electrical activity of individual cells can be recorded using whole cell patch-clamping or multiple cells can be recorded using a planar microelectrode arrays.

## 1.3.3.1. Patch-Clamping

Patch-clamping is the current gold standard for recording ion channel activity of cell membranes. This technique uses a glass micropipette, with a wire electrode inside, to form a tight connection with the cell membrane called a gigaohm seal [4], [49]. Typically a silver/silver chloride (Ag/AgCl) electrode is inserted into the micropipette that contains a physiological salt solution. This type of electrode is non-polarisable and reversible, where $Cl^-$ ions in the solution are exchanged for electrons at the interface between the electrode and solution [50]. This allows currents to flow through the electrode which can be used to measure voltages relative to the reference electrode.

There are a number of configurations possible for the micropipette depending on the experiment [51]. Whole cell patch-clamp recording involves breaking into the cell so that both electrical potentials and currents from the entire cell can be measured. Alternative methods include removing part of the cell membrane to be analysed in isolation (Figure 1.6). A second electrode, elsewhere in the extracellular solution, acts as a grounding wire so that the patched electrode can be used for controlling the membrane voltage or current and for collecting data. There are two main modes of operation that the microelectrode can be used to interrogate the cell. In current clamp mode, the current through the membrane is fixed and the transmembrane potential is free to fluctuate. In voltage clamp mode, the voltage across the membrane is fixed and the current through the membrane is recorded. Current clamp mode can be used to record the firing of action potentials of a neuron, and voltage clamp mode can characterise voltage gated ion channels within the membrane. While the patch-clamp technique can record signals from neurons in high resolution, it does have a few significant drawbacks. The process requires specialist equipment such as sensitive amplifiers and micro manipulators that require an experienced operator. Due to the time required to carefully form and manipulate delicate seals, the technique is low throughput. There is commercial equipment available for higher throughput automated patch-clamp systems that can perform multiple patches simultaneously on suspended cells [52], however these systems are typically very expensive. Other

automated patch-clamping systems require complex customised systems to manipulate electrodes and form seals on neurons of interest [53].
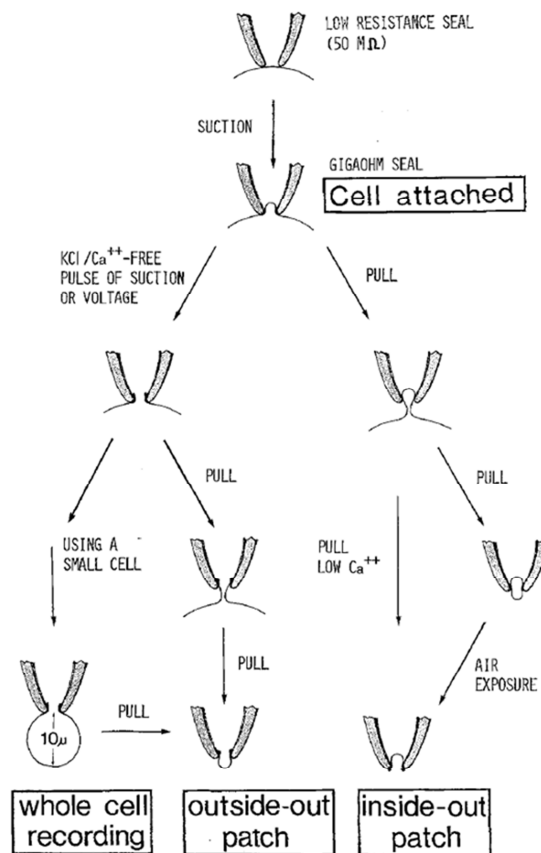


**Figure 1.6 Patch-clamping techniques for studying membrane properties. Initially the micropipette electrode is lowered onto the cell and slight negative pressure applied to form a gigaohm seal. From this cell attached mode it is possible to manipulate the cell membrane to perform whole cell recording and outside-out or inside-out membrane analysis.** *Image taken from* [51]

## 1.3.3.2. Microelectrode Arrays (MEAs)

An alternative method of measuring bulk electrical activity is to use planar micro electrodes in close proximity to a cell or a group of cells [54] (Figure 1.7). These can be used with *in vitro* cell cultures, *ex vivo* brain slices, or *in vivo* with probes inserted into the brain. Changes in local potentials can be detected and amplified to give a measure of time dependent activity around the location of the electrode. Typically polarisable metal electrodes are used, where at the interface of the metal conductor and electrolyte solution a leaky capacitive interface is created [55], [56]. This is due

to the tendency of an electrode with a charge to attract oppositely charged ions whilst repelling similarly charged ions. This polarises the ions and electrons at the surface of the metal with respect to the potential of the solution, forming an electrical double layer [56]. Just like a capacitor, the build-up of ions on the electrode's surface gives the interface high impedance to low-frequency signals but low impedance to high-frequency signals which is suitable to detect fast extracellular events such as action potentials [55].

Arrays of these electrodes can be fabricated to cover a surface allowing an entire sub-network to be monitored simultaneously. By monitoring a structured array of electrodes it is possible to determine the connectivity between parts of the network using computational analysis. However, as each electrode in the array is fixed spatially with respect to the rest of the array, monitoring a pseudo-randomly distributed neuronal network poses some problems. Since the accuracy of a single electrode's measurement depends on its proximity to a neuronal cell a fixed array can result in some electrodes becoming redundant. *In vitro*, it is possible to reduce redundant electrodes by encouraging growth near them. In general electrodes will record the electrical activity of groups of neuronal cells over a large area; this makes it difficult to attribute single action potentials to individual cells.
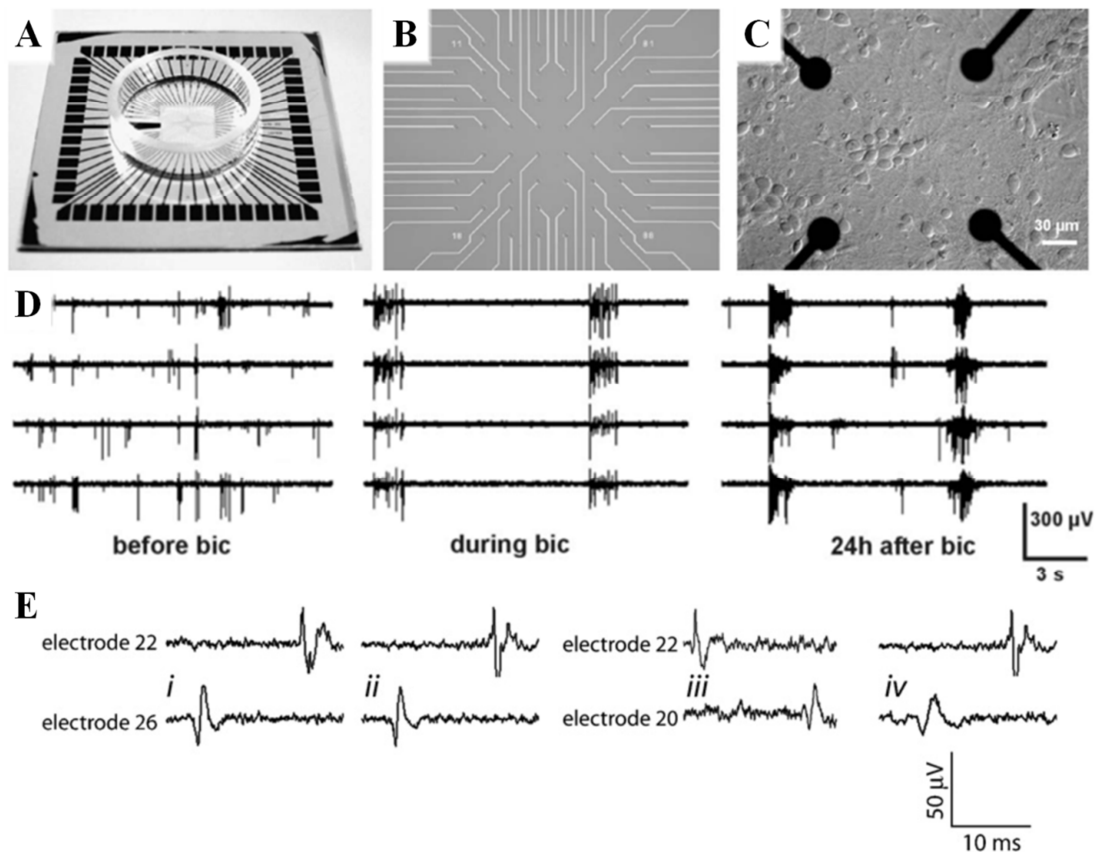
**Figure 1.7 Microelectrode array and experimental recordings. Planar MEAs can be used to record from a large region of cells *in vitro*. (A) A large chip is used to make contacts with an amplifier and recording device. At the centre of the chip is the MEA (B) which can either be used to grow cells *in vitro* (C), or be used with brain slices. (D) Each electrode records the activity from multiple cell sources making action potentials that are detected difficult to associate with specific individual cells. (E) Signals from individual electrodes recorded with an MEA (from a different experiment [57]) show that individual spikes can be seen and used to correlate the activity between areas of the neuronal network. *(A–D) Images adapted from* [54]*, (E) Image adapted from* [57]**

## 1.3.3.3. Alternative Electrophysiology Techniques

An alternative to the patch-clamp technique is the use of "sharp" electrode intracellular recording [49]. Similar electrodes are used, however the glass micropipette used for the electrode has a smaller diameter (<1 μm), and is directly inserted through the neuronal membrane [58]. Due to the reduced tip diameter any change to the intracellular fluid composition is minimised. However, while the quality of cell activity recording is similar to that of patch-clamp recording, it has been found that the sharp electrode technique can damage the cell membrane and cause significant leakage between the intracellular and extracellular fluid [59].

Extracellular field potentials are electrical potentials that are generated by cells and surround them. These fluctuate in neurons during the depolarisation caused by action potentials. The change in voltage of the cell field potential is greatly attenuated when detected by the extracellular recording electrode (1/100–1/1000) and so only a small voltage (0.1–1 mV) can be detected during an action potential [60]. Simultaneous action potentials from multiple neurons will be integrated at the electrode and can generate stronger signals. However, due to the large attenuation, the technique is "blind" to sub-threshold activity of the neuron, i.e. changes in potential that are insufficient to cause an action potential. Field potentials can be recorded by either planar MEAs or extracellular micropipette electrodes [60], [61].

## 1.3.4. $Ca^{2+}$ Imaging

An optical measurement of neuronal cell activity can be achieved using a $Ca^{2+}$ sensitive fluorescent probe. $Ca^{2+}$ is an ion that has a range of functions in cell physiology and monitoring the intracellular concentration of $Ca^{2+}$ can reveal the activity of the cell. In neurons an influx of $Ca^{2+}$ at the synaptic terminal is responsible for the exocytosis of neurotransmitters. The increase in $Ca^{2+}$ concentration is due to the influx of $Ca^{2+}$ through voltage gated $Ca^{2+}$ channels, located predominantly at the synaptic terminal, as well as the release of $Ca^{2+}$ from the intracellular stores of the endoplasmic reticulum located throughout the cell [62] (Figure 1.8).

A commonly used, non-ratiometric probe is Fluo4 AM [62]. It is a molecule conjugated with an ester group which allows it to be transported across the cell membrane and be internalised. Once inside the cell, the ester group is removed by the cell enzymatic activity, making the fluorescent probe charged which reduces its ability to pass back through the cell membrane. The intensity of the fluorescent probe's fluorescence can increase 100 fold upon binding to $Ca^{2+}$[63], allowing fluctuations in $Ca^{2+}$ concentrations within the cell to be monitored optically without interfering with the cell. As $Ca^{2+}$ fluctuations within neuronal cells correlate to functional communication between neuronal cells, $Ca^{2+}$ activity can be monitored to determine the neuronal activity.
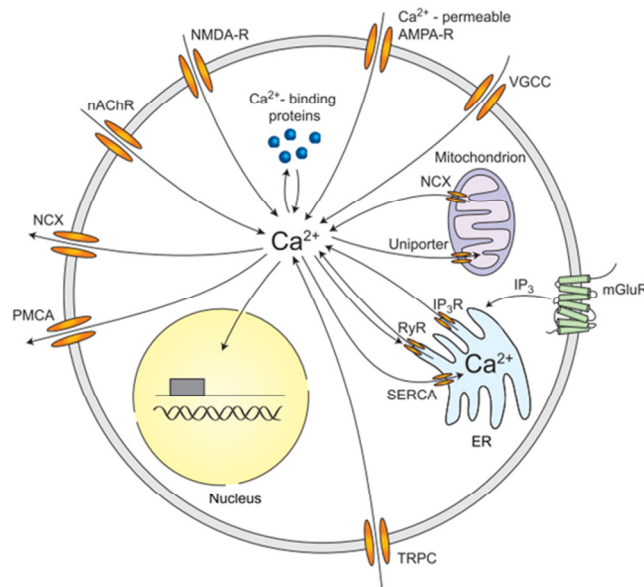
**Figure 1.8 Ca$^{2+}$ signalling in the neuron. There are several sources of Ca$^{2+}$ influx in a neuron. Ca$^{2+}$ is allowed into the neuron via NMDA-Receptors, AMPA-Receptors, and voltage gated Ca$^{2+}$ channels and can also be released from the endoplasmic reticulum. It is actively removed from the cell by the Na$^+$/Ca$^{2+}$ pump (NCX) and the plasma membrane ATPase (PMCA) or stored in the endoplasmic reticulum.** *Image taken from* [62]

Ca$^{2+}$ imaging has been used to monitor both individual cells as well as large networks of neurons simultaneously [64]. In general only bursts of synaptic activity are observable due to the fast Ca$^{2+}$ dynamics (typically less than 1 ms [65]) and the typical equipment used for the fluorescent imaging, however, there are examples where single action potentials have been detected using a high frame rate during recording [66].

This technique can also be used to monitor Ca$^{2+}$ fluxes in other cells types including astrocytes whose activity can influence the synaptic communication between neurons. Being able to simultaneously monitor activity from multiple cell types can be advantageous when determining how different cell types interact.

## 1.3.5. Cell Stimulations

For most *in vitro* studies of neuronal functionality it is necessary to probe the cell using some form of stimulation. This can be in the form of chemical, electrical, or optical stimulation where the response can be assessed to reveal a mechanism of action.

## 1.3.5.1. Chemical Stimulation

Chemical stimulation of *in vitro* neurological cultures can take many forms, both in terms of the chemical administration and the method of delivery. One method of chemical stimulation can induce activity by forcing the neuron to depolarise, such as applying a high concentration of potassium chloride (KCl) to the extracellular solution [67]. Other methods of chemical stimulation used can target receptors or ion channels to either excite or inhibit neuronal activity through a variety of pharmacological mechanisms. Examples of these include the external application of neurotransmitters such as glutamate to excite neuronal cells or the perfusion of glutamate blockers to inhibit synaptic communication.

There are several methods of administering chemicals to neuronal cultures *in vitro*. In normal perfusion systems chemicals can be added to the perfusate, or perfusates can readily be switched to wash on new drugs of interest. This exposes the whole culture to the chemical of interest, and the effects of that can be observed using electrophysiology or $Ca^{2+}$ imaging.

Global perfusion of substances has been used to great effect in studying neuronal physiology and while it is the simplest of the perfusion techniques it does require a degree of expertise to implement. It also requires exposing the whole culture to the substances of interest which can make it difficult to determine the exact method of action and whether there are confounding influences from the whole culture. In the brain, single neurons can also traverse multiple regions with various differing micro-environments. To better study how changes within one region of a culture can affect the other cells within the network it is desirable to produce local environments *in vitro*.

In contrast to global exposure, it can be of interest to specifically stimulate a single neuron (or a group of neurons) to monitor the effect produced on surrounding synaptically connected neurons (Figure 1.9). This can be achieved using a micro-pipette system, called a picospritzer, to introduce a small concentrated volume of a drug to the targeted neuron [68]. The small volume of the drug diffuses to an

insignificant concentration within the solution to reduce its action on other neurons nearby.
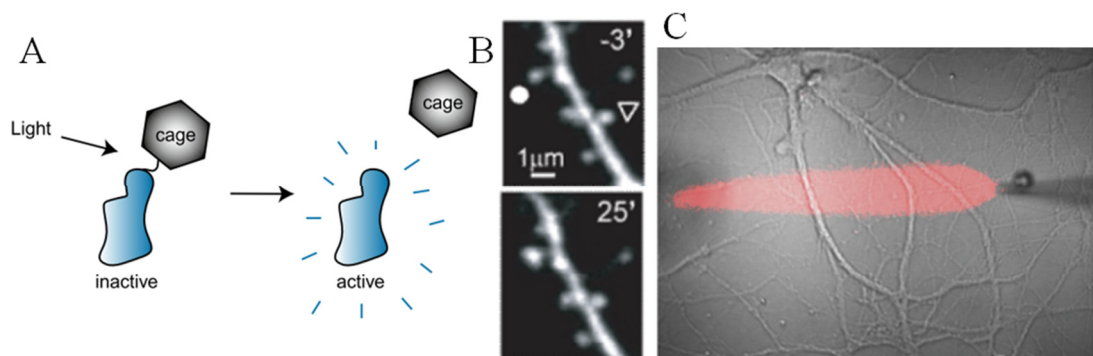


**Figure 1.9 Glutamate uncaging and micropipette perfusion for regional stimulations. (A) Light is used to activate caged glutamate by removing the obstructive caging molecule. (B) A dendrite's response before and after light is used to uncage glutamate in its vicinity (white dot). (C) Micropipette perfusion (red) can be used during normal perfusion experiments to stimulate a selected region of dendrites.** *(A) image taken from* [4]*, (B) image taken from* [69]*, (C) image modified from* [70]

An alternative method of local stimulation is the process of glutamate uncaging. The glutamate molecule is bound to a cage that renders it inactive and is introduced to the perfusate. Specific regions of the network are then stimulated by illuminating them with an appropriate wavelength and intensity of light that uncages the glutamate molecule freeing it to act on the neuron [69].

While both forms of local stimulation can provide greater insight to the physiology of neuronal function there are a few disadvantages. Micro-pipettes require skilled operation to ensure that the chemical of interest envelops the region of interest and does not diffuse into surrounding regions. The remainder of the culture downstream will also be exposed to various concentrations of the chemical stimulus. Glutamate uncaging requires the molecule to be introduced to the entire solution potentially acting in an unexpected manner.

## 1.3.5.2. Electrical Stimulation

Neurons can also be excited electrically using electrodes either to stimulate a region of a culture with an MEA, or a specific region of a single cell using the patch-clamping method. A microelectrode, such as those used in patch-clamping or MEAs,

can be used to cause a local change in the electrochemical gradient around the membrane of the neuron. This can depolarise a region of neurons near the electrode which can instigate action potentials to the rest of the network. Alternatively, using the whole cell patch-clamping method described earlier, it is possible to actively stimulate a single neuron or even an individual neurite. This is often done when the functionality of a synapse between two neurons is being investigated. The presynaptic neuron is patched to provide a controlled stimulation while the postsynaptic neuron is patched to record the resulting communication. It was using this method that it was found that extracellular $Ca^{2+}$ is required for synaptic communication to occur [71].

## 1.3.6. Problems Faced in Neuroscience Research

Studying the brain and neurological disorders is one of the great challenges of our time. The complexity of the vast numbers of neurons and glial cells arranged in an ordered integrated manner makes it difficult to isolate a particular problem of interest *in vivo*, and so *in vitro* techniques have been used for the last century to investigate these systems and interactions on a cellular level [72].

Patch-clamping, MEAs, $Ca^{2+}$ imaging, chemical perfusion are all valuable techniques for studying neural cultures *in vitro* and many are still the gold standard of *in vitro* neuroscience research. However, there are limitations that are difficult to overcome with some traditional techniques. For example, the ability to locally stimulate cells requires complex molecules, such as caged glutamate, or setups, such as micro-pipettes or light sources, to be used. Furthermore, there is a key challenge when spatially controlled microenvironments are required within a network of cells, making it difficult to develop complex *in vitro* experiments that better represent the *in vivo* environment.

Over the last 15 years [72] a set of fluid handling techniques called *microfluidics* has been applied to neuroscience research to enable more advanced experiments. Notable advantages are the greater spatial and temporal control over the cell network microenvironments that can be achieved. These techniques are therefore well suited to studying neural cultures *in vitro* and will be described in the following sections.

## 1.4. Microfluidics

Microfluidics is the term used to describe an area of technology relating to the use and manipulation of volumes of fluid that are of the microlitre scale (and lower) contained within microchannels [73]. The precise control of fluids in such confined environment is very appropriate for biological systems where cells can be exposed to multiple environments for discrete times. Additionally, microfluidic systems allows the *in vitro* environment to more closely resemble what is found *in vivo* [74], [75]. This is applicable to neural studies where it is desirable to control the extracellular environment both spatially and temporally, as well as retaining control over the cell distribution and growth within microchannel networks.

While the field of microfluidics has grown almost exponentially in recent years it is still a relatively new area that has had limited impact in the process of drug discovery and biomedical research [76]. The number of publications surrounding microfluidics has been generally engineering focussed rather than biomedical related [76]. The engineering based publications usually feature proof of concept studies where the aim is to develop assays in a microfluidic format that have already been well established using macroscopic techniques. Indeed, macroscopic techniques are still the gold standard for high throughput drug screening and analysis [77].

One area of scientific research that microfluidics is beginning to make an impact relate to chemistry based problems such as chemical synthesis and protein crystallisation [77]. In biology however, the biggest impact has been on diagnostic techniques, where established principles are miniaturised and optimised to provide low cost dedicated devices. These are particularly beneficial in resource limited situations, such as developing countries, where the infrastructure to access centralised laboratories does not exist [76]. On the whole, microfluidics holds great promise for future drug development, screening and biomedical research, however it may be argued that it has yet to find a definitive application that may replace currently established techniques.

The fabrication of microfluidic devices for research and development is relatively simple and low cost. The most common method used in research labs for production

involves a process called soft lithography (Figure 1.10), during which a template of the microfluidic system is created. Polydimethylsiloxane (PDMS) is ideal for rapid fabrication, as replica moulding of the microfluidic template can create many nearly identical devices in a quick and cost effective manner [72]. PDMS is a biocompatible and gas permeable polymer, widely used in microfluidic cell culture [78], and is also optically transparent, a feature that allows it to be used with conventional microscopes for imaging.
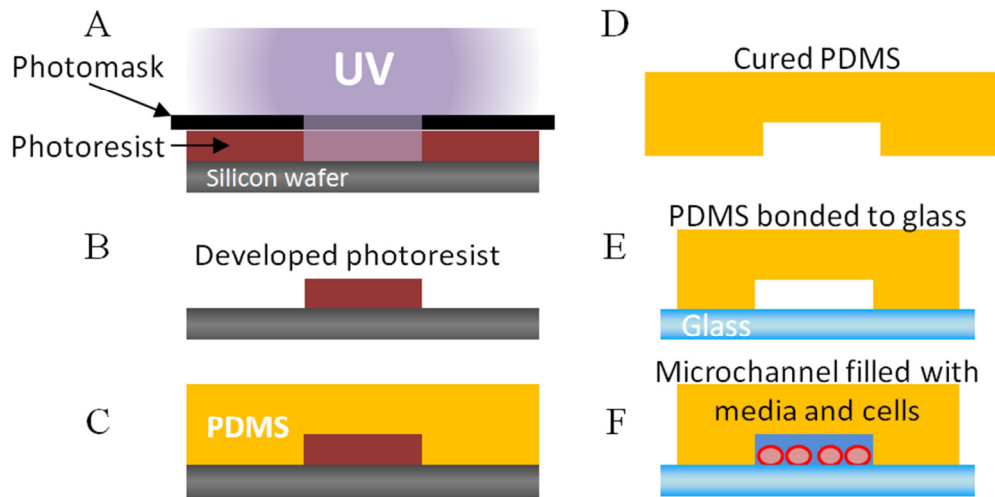


**Figure 1.10 Fabrication of microfluidic devices for biological applications. Microfluidic masters are created using photolithography, where the system is initially designed and transferred onto a photo-mask. (A–B) Creating the microfluidic template. (C–F) Replica moulding of the template to produce a microfluidic device. (A) Photoresist is spun on a silicon wafer to produce a layer of uniform thickness and ultraviolet (UV) light is projected through the mask onto the photoresist. (B) Once processed to remove the excess resist, a raised surface is left that depicts the fluidic design. This is hard baked and the surface is treated to prevent adhesion which completes the master mould. (C) PDMS is a liquid polymer that can be mixed with a curing agent and poured over the master mould where it will cure in place. (D) Once solidified, the cast can be removed from the master mould revealing an impression of the fluidic design. (E) This patterned piece of PDMS can then be trimmed, with inlets and outlets punched, before being bonded to glass. (F) The final device is a hollow structure that can be surface treated and used to contain cells and culture medium.**

## 1.4.1. *In vitro* Applications of Neural Microfluidics

In the last 15 years [72] there has been a surge in publication of neuroscience research that makes use of disposable microfluidic systems based on PDMS due to its ease of use and relatively low cost. Provided here is a brief overview of the most

relevant microfluidic devices in the field of neuroscience along with their possible applications.

## 1.4.2. Compartmentalised Systems

As described earlier (see Section 1.3.5), it is desirable to have cultures of neurons with fluidically addressable microenvironments. One of the key advances that microfluidics has offered is the ability to produce structures on the same scale as neuronal processes. This has enabled the fabrication of microstructures which contain multiple connected compartments, where neurons grown in a compartment may develop neurites that spread to other compartments. Since the compartments are semi-isolated from each other, they can contain different fluids to create local microenvironments. This concept was actually realised in the 1960's with the use of Campenot chambers to isolate peripheral neurons from their neurites under normal cell culture conditions [79]. However, its application was limited to neurons of the PNS due to the size of compartments involved [72].

More recently, compartmentalised structures constructed using PDMS have been used for a wide range of applications with various neuronal subtypes. One of the first forms of compartmentalisation described in the literature involved the creation of two symmetrical culture chambers separated by an array of microchannels [80] (Figure 1.11). These channels are small enough to prevent cell somas from entering but are large enough for the fine processes of neurons to grow through to the other side. This method of creating structured microenvironments has become the most widely adopted technique for forming customised networks. The simple design and fabrication process has made it more favourable than alternative methods of creating customised structures of neurons that depend on valves [81] or the integration of microelectrodes [82].
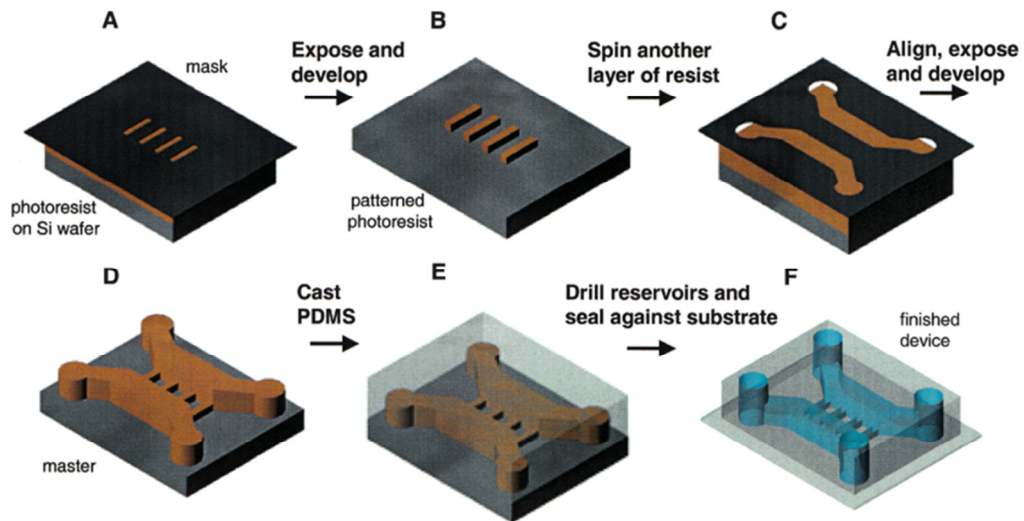
**Figure 1.11 Compartmentalised structure for axon isolation. (A–D) The fabrication process for creating the multilayered microfluidic master mould is shown. (E-F) Replica moulding is used to create the finished microfluidic device. The structure consists of 4 large open well reservoirs for storing media and accessing the two culture chambers. Each culture chamber holds around 2 μL of fluid and is connected directly to a reservoir at either end. Between the two culture chambers is an array of microfluidic channels, measuring 10 μm wide and 3 μm deep. This structure creates a physical barrier between the two chambers with imbedded grooves for neurites to grow through.** *Image reproduced from* [80]

Compartmentalised structures have been used for a wide range of applications in neuroscience, including: the fluidic isolation of axons for injury, transduction [83], and distal stimulation [83]–[86]; the compartmentalisation of co-cultures (of neurons or glial cells) to observe their interactions and better mimic the *in vivo* structured order of the nervous system [87], [88]; and fluidic isolation of sub-populations of neuron-neuron co-cultures [85], [89], [90]. Of particular interest is the compartmentalisation of neuronal sub-networks that allow for different treatments to be applied to specific regions of the cell network [74], [75]. These structured approaches to *in vitro* cell culture resemble the compartmentalised nature of the nervous system where physiological processes may traverse multiple cell types and environments. There have been many variations of compartmentalised structures produced, the most relevant of which will be described here.

## 1.4.2.1. Compartments for Axon Isolation

The microfluidic structure introduced by Taylor *et al.* (Figure 1.11) was originally used to isolate axons from their soma and dendrites [80], [84]. This was achieved by seeding neurons in a single compartment, called the "somal compartment", and leaving the other compartment empty, called the "axonal compartment". It was found that if the central barrier was greater than 450 μm in length then only axons were able to grow into the axonal compartment [84] (Figure 1.12). The reduced growth of dendrites compared to axons prevents them from completely crossing the whole microchannel [86] (Figure 1.12C).
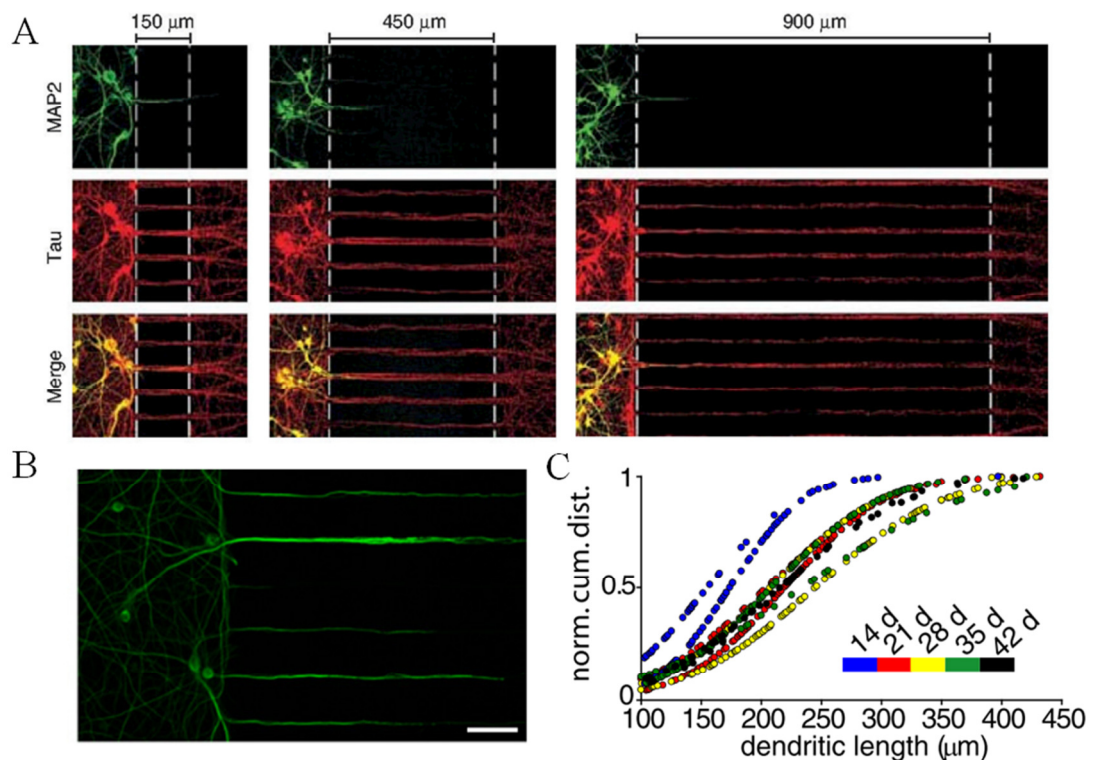


**Figure 1.12 The length of the microfluidic barrier can prevent dendrites from crossing into the opposing culture. (A) Neurons were seeded in one compartment of the device, where both axons (Tau) and dendrites (MAP2) can grow into the central microchannels as shown with immunofluorescent imaging. (B) MAP2 staining was used to determine the distance that dendrites extended into the microchannels depending on the number of days they were grown, as shown in (C).** *(B) Scale bar: 50 μm. (A) Image taken from* [84]*, (B & C) images modified from* [86]

This device structure has enabled new studies of axons in isolation. It is possible to extract axonal mRNA for analysis as well as to perform gene therapy on axons [83].

In similar structures it is possible to induce damage of the axons and subsequently to monitor their recovery. Axonal injury has been achieved with a variety of methods including physical mechanical contact [91], optical laser ablation [92], and chemical application [85], [93].

## 1.4.2.2. Compartments for Cell Co-culture

The compartmentalised format of the microfluidic structure under analysis allows the study of multiple populations of different cell types that are functionally connected. Similar structures have been used to grow neuro-glial co-cultures where neurons and glial cells are seeded in separate compartments using a variety of configurations [87], [88]. This allows the interactions between axons and glial cells to be studied in a controlled manner (Figure 1.13).
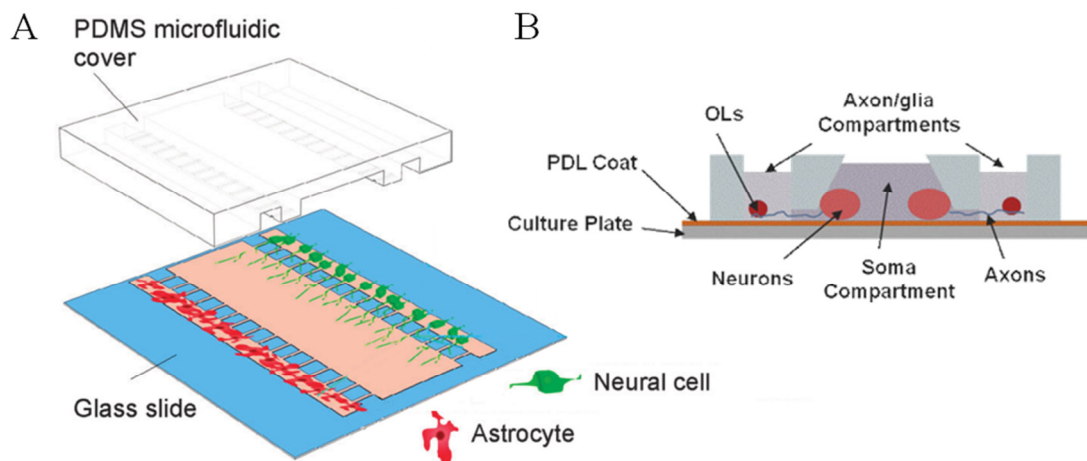


**Figure 1.13 Neuron glia co-culture in compartmentalised structures. (A) Neurons and astrocytes are seeded in outside chambers and are separated by an unoccupied central chamber. Neurites can grow from the neuronal side to the glial side and the central chamber can be used to target them with concentration gradients across the width of the chamber. (B) Neurons are seeded into a central compartment where their axons can extend into multiple connected compartments that contain glial cells such as oligodendrocytes (OLs).** *(A) Image modified from* [88]*, (B) Image taken from* [87]

## 1.4.2.3. Compartments for Structured Networks

Other studies have chosen to examine populations of different types of neuron, such as corticostriatal co-cultures [85], [89], [90], though some have modified the structure of the microchannels to preferentially allow axons to grow in one

direction [89]. These *axon diodes* act to make one chamber presynaptic and the other postsynaptic due to the directional influence on axonal growth (Figure 1.14). The structure uses tapered microchannels where large openings are presented to the presynaptic chamber while smaller openings allow access to the postsynaptic chamber. This has been used to demonstrate *in vitro* that cortical neurons can induce synchronous $Ca^{2+}$ activity in their striatal co-culture [89].
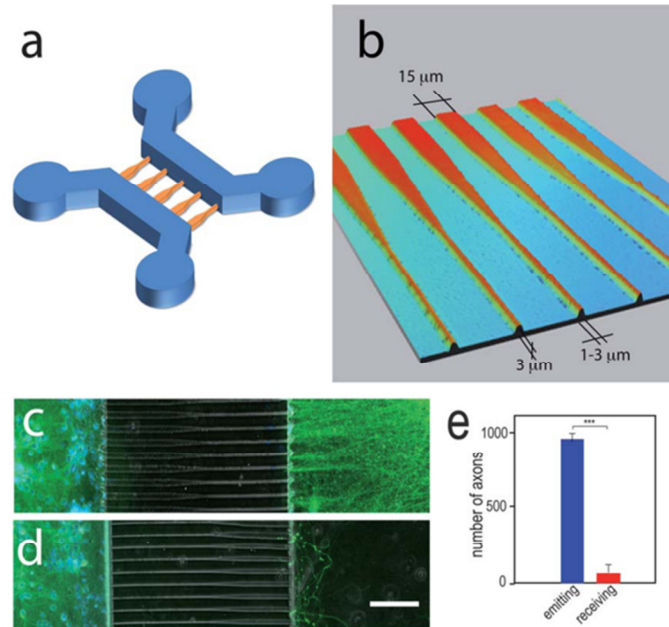


**Figure 1.14 The structure for "axon diodes" promotes simplex connectivity between networks. (A) Schematic of the multi-layered microfluidic master. (B) An optical profile of the devices structure showing the dimensions used to create the "axon diodes". (C–E) Cells grown in the device, on either side of the diodes, show preferential growth in one direction. Immunofluorescent staining for α-tubulin (green) and Hoechst (blue).** *(C & D) Scale bar: 50 μm. Figure modified from* [89]

## 1.4.2.4. Compartments to Model CNS Disease

With the use of compartmentalisation as a tool to separate different regions of neurons it is possible to build a reconstructed neuronal network that can represent structures of the brain [85], [89], [94], [95] as well as disease conditions [74], [75], [85], [88]. An example of the conditions demonstrated so far is Alzheimer's disease where differing approaches create models that are not possible using traditional *in vitro* methods.

One approach uses compartments of neuronal co-cultures with an additional empty central compartment (Figure 1.15). Neurites from each side compartment are able to spread into this central chamber to form synapses between the two cultures. The central chamber acts to create a concentration gradient between the chambers when one chamber is chemically insulted to produce a "diseased network" that is in contact with a "healthy network". The diseased network is created by treating one compartment of cells with okadaic acid (600 nM) for 75 minutes to inhibit the dephosphorylation of Tau microtubules [74], creating a network with hyperphosphorylated Tau that is one of the symptoms found in Alzheimer's disease. This system demonstrated the gradient control of Tau phosphorylation states and resulted in co-pathological states of neurons within a single device that could potentially be used as a new platform for drug screening.
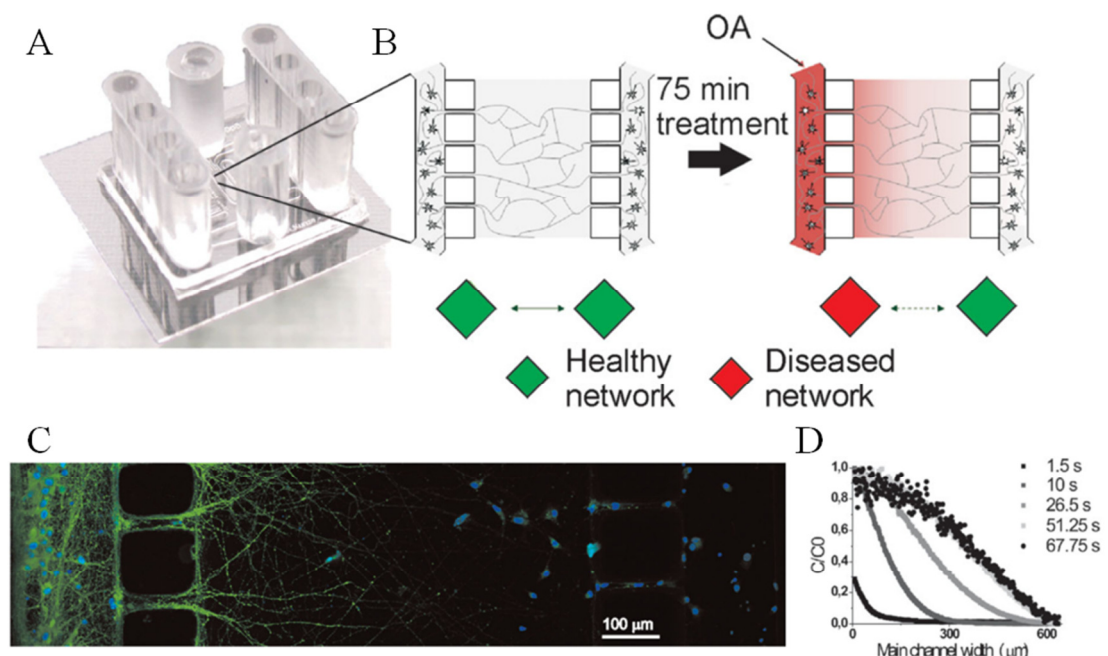


**Figure 1.15 *In vitro* model for Alzheimer's disease. (A & B) The device shown is used to produce a Neuron-neuron co-culture separated by a central chamber. One compartment of the device is treated with okadaic acid (OA) to promote the formation of hyperphosphorylated tau. (C) Immunocytochemical staining for hyperphosphorylated tau, (Phospho-Tau Ser262: green, DAPI: blue). (D) Shows the time dependant establishment of a concentration gradient across the width of the central microchannel. *Images modified from* [74]**

A different approach to modelling AD *in vitro* is to focus on one aspect of the disease such as the spread of β-Amyloid through different regions of the brain

(Figure 1.16). Using multiple compartments a large network of neurons was created that are grouped into isolated regions. A fluorescently labelled β-Amyloid construct was subsequently introduced to one chamber and monitoring of the protein's location was performed using confocal microscopy 6 hours later [75]. It was ultimately found that the β-Amyloid construct could be transmitted to the neighbouring compartmentalised co-cultures and that the method may be mediated by direct neuron-neuron contact.
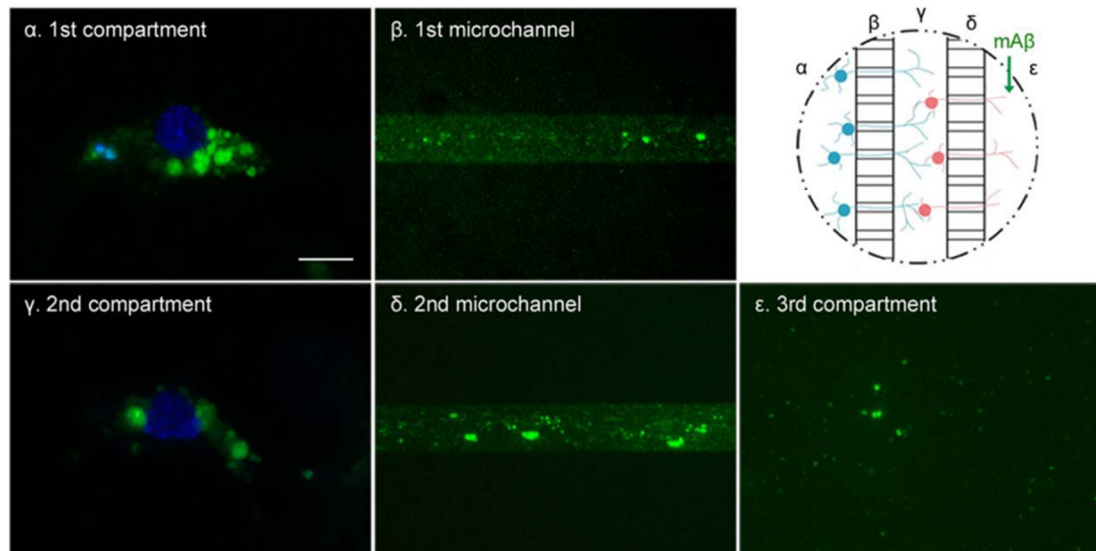


**Figure 1.16** ***In vitro*** **model of β-Amyloid spread in a multicompartment system. Three chambers are connected in series by arrays of microchannels to create a structured network. After 2 weeks of culture, fluorescently tagged β-Amyloid (fluorescein isothiocyanate monomer β-Amyloid, *mAβ*) was then introduced to the third compartment, *ε*. Fluorescent images were taken of the microchannels and compartments after 6 hours to show the localisation of mAβ (green), DAPI (blue), which showed that the mAβ molecule was found to have spread to both the directly connected compartment, γ, and the indirectly compartment, α.** ***Scale bar: 10 μm. Image modified from*** [75]

## 1.4.3. Stimulating Cells in Microfluidic Devices

Interrogating cells within these microfluidic environments has been carried out in several ways. Stimulation is normally performed chemically [74], [85], [86], [88], [89], [94] due to the restricted access to the cells, however it is also possible to physically alter the cell with valve enabled microfluidics [91] or a laser source [96]. While chemical applications to sub-networks of cells can be a useful tool in determining the effects of local application it is important to ensure that these stimuli

are confined to the desired sub-compartment of the device. When the compartmentalised structure was introduced, a method for fluidically isolating a compartment was also described [80], [84] (Figure 1.17). This involves creating a pressure gradient between the cell culture compartments. The pressure gradient can induce a fluid flow that is sufficient to counter diffusion from one chamber to the other, although diffusion in the opposite direction is sustained. The pressure gradient is simple to achieve as each chamber is generally connected to an open well, which acts as a reservoir for cell culture medium, and a small volume difference between reservoirs is all that is required to create the pressure difference [80]. In most designs this is sufficient for short term isolation of a chamber, however it may not allow for long term isolation, of several days, as the volume difference will eventually equilibrate due to the flow of fluid from one chamber to the other.
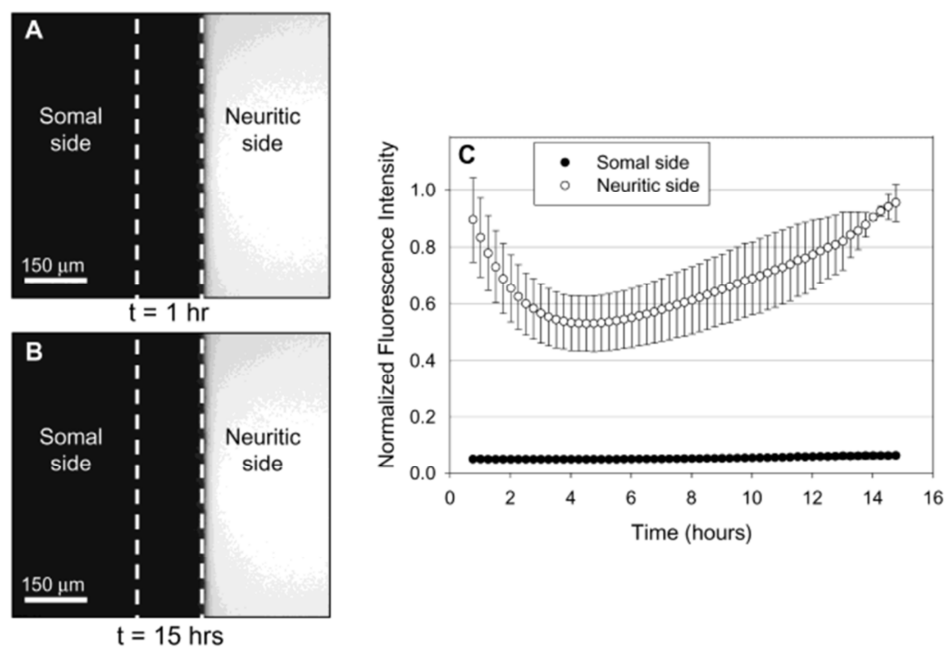


**Figure 1.17 Fluidic isolation between microfluidic compartments. To demonstrate that one compartment can be fluidically isolated from the other fluorescein was used to optically measure the diffusion that occurred. (A) The two chambers (labelled Somal side and Neuritic side) were loaded by adding 125 µL of PBS to the Somal side and 100 µL of Fluorescein to the Neuritic side. (B) The volume difference between the sides created a sufficient pressure gradient to prevent diffusion of fluorescein between the chambers. (C) The fluorescein concentration on the Neuritic side initially decreased due to the net flow of fluid from the Somal side.** *(A & B) Dotted lines represent the edges of the microchannel barrier. Image taken from* [80]

## 1.4.4. Measuring Outcomes from Microfluidic Devices

While various methods have been used to stimulate cells within microfluidic systems, there are several methods that have been used to gauge the effects on neuronal cultures. Electrophysiology, $Ca^{2+}$ imaging, immunocytochemistry and transcript microarrays have all been used to measure cell activity and sub-cellular characteristics within sub-compartments of microfluidic devices.

## 1.4.4.1. Electrophysiology in Microfluidic Devices

An MEA can be used as a substrate to grow a neuronal network in a microfluidic device by aligning the PDMS fluidic layer with the electrodes (Figure 1.18). This can provide electrophysiological measurements from both sub-networks simultaneously to provide functional readouts from a wide area and in depth network connectivity analysis. Such systems have been used to evaluate corticothalamic co-cultures [90], [95] in addition to providing a method of culturing a target system alongside an environmentally coupled twin control system [97].
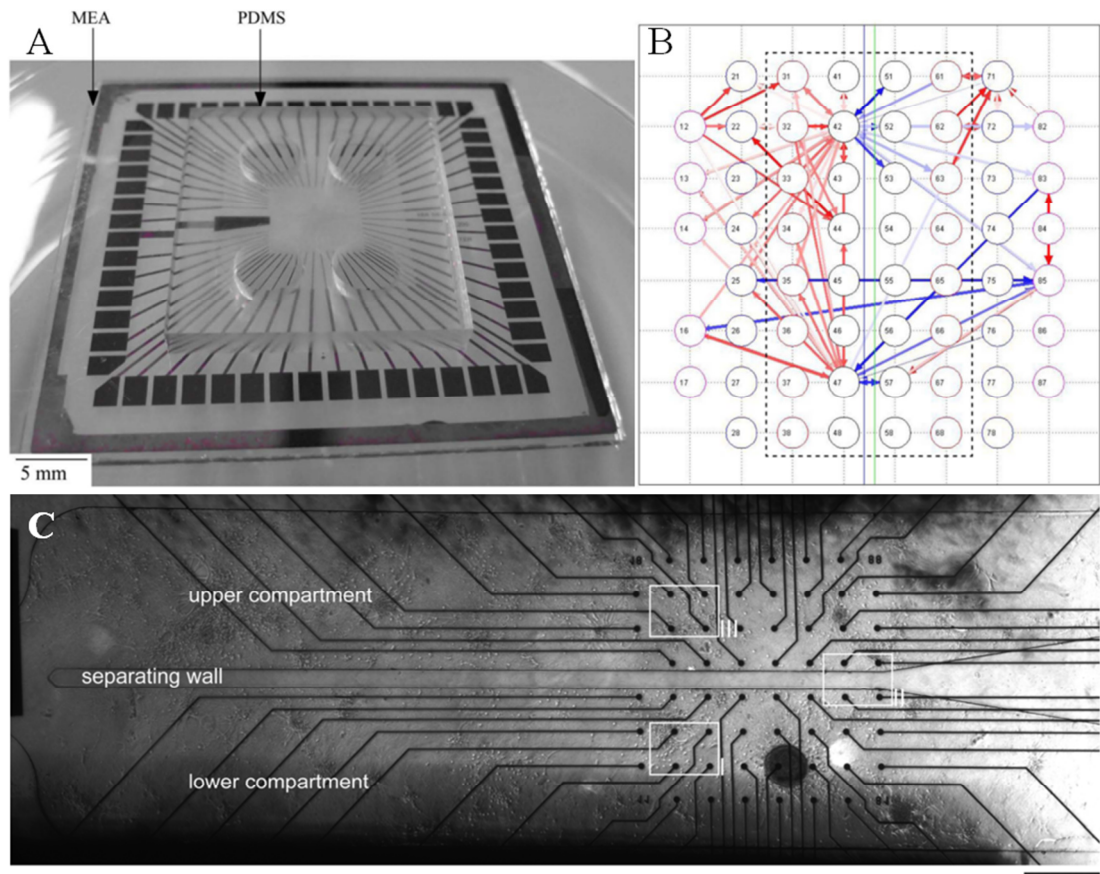
**Figure 1.18 Examples of microelectrode arrays used in microfluidic devices. (A) A PDMS structure, similar to the design by Taylor, is reversibly bonded to a micro electrode array chip. The MEA is at the centre of the device while the electrode contacts are around the edges. (B) A network connectivity map shows the apparent strength of cell signalling between each electrode. Only the top 100 connections are shown, and the blue and green vertical lines represent where the microfluidic barrier between compartments is located. (C) A different structure that uses an MEA to monitor two neuronal compartments within a device. Here the compartments are not interconnected with microgrooves and instead one network is used as a control while the other is chemically targeted. In both devices (A & C) a 60 electrode MEA is used.** *(C) Scale bar: 500 μm. (A & B) Image modified from* [98]*, (C) Image modified from* [97]

A modified, multi-layered PDMS device was also used to provide direct electrophysiological measurements through patch-clamping [99] (Figure 1.19). The multi-layered structure is required to provide a suitable reservoir volume of medium for normal culture conditions while also allowing unhindered access to the cells required for patch-clamping.
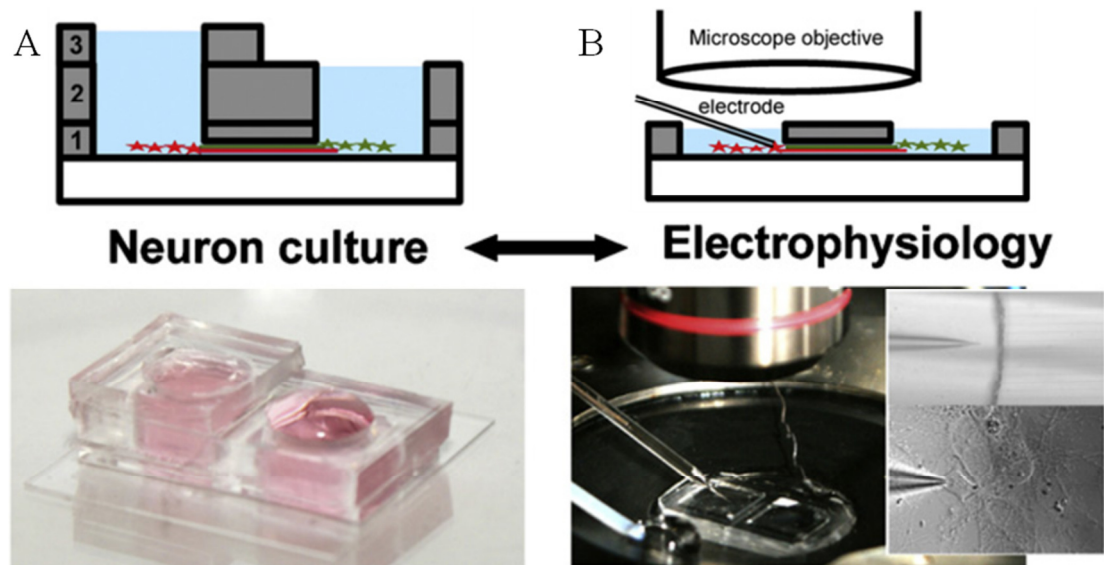


**Figure 1.19 A multi layered compartmentalised device for patch-clamping. (A) A multilayered device, consisting of 3 individual PDMS layers, is used to grow populations of neurons in separate compartments. (B) By removing the upper PDMS layers it is possible to gain access to the cells for use in patch-clamping studies.** *Image modified from* [99]

## 1.4.4.2. Fluorescent Imaging in Microfluidic Devices

An alternative method of examining cell functionality within microfluidic devices is $Ca^{2+}$ imaging. Since many microfluidic devices are made using glass as a substrate for growing the cells it is possible to perform $Ca^{2+}$ imaging studies using an inverted microscope. With standard *in vitro* experiments $Ca^{2+}$ imaging has been performed to study neuronal responses in both individual and large networks of cells and has even been used to detect single action potentials. In neuronal microfluidic systems it has been used to study single cell responses to synaptic insults [86] and to monitor groups of neurons for synchronous behaviour [89] (Figure 1.20). Using fluidically isolated neurites in a microfluidic channel it was possible to selectively stimulate dendrites and monitor the intracellular change in $Ca^{2+}$ over time [86]. Both the

stimulated dendrite and cell soma were monitored separately to show that the dendritic concentration of $Ca^{2+}$ increased more rapidly than in the soma. On a larger scale, $Ca^{2+}$ imaging has been used to synchronously monitor a small network of neurons to determine their activity and synchronicity in response to different, directly applied insults [89].
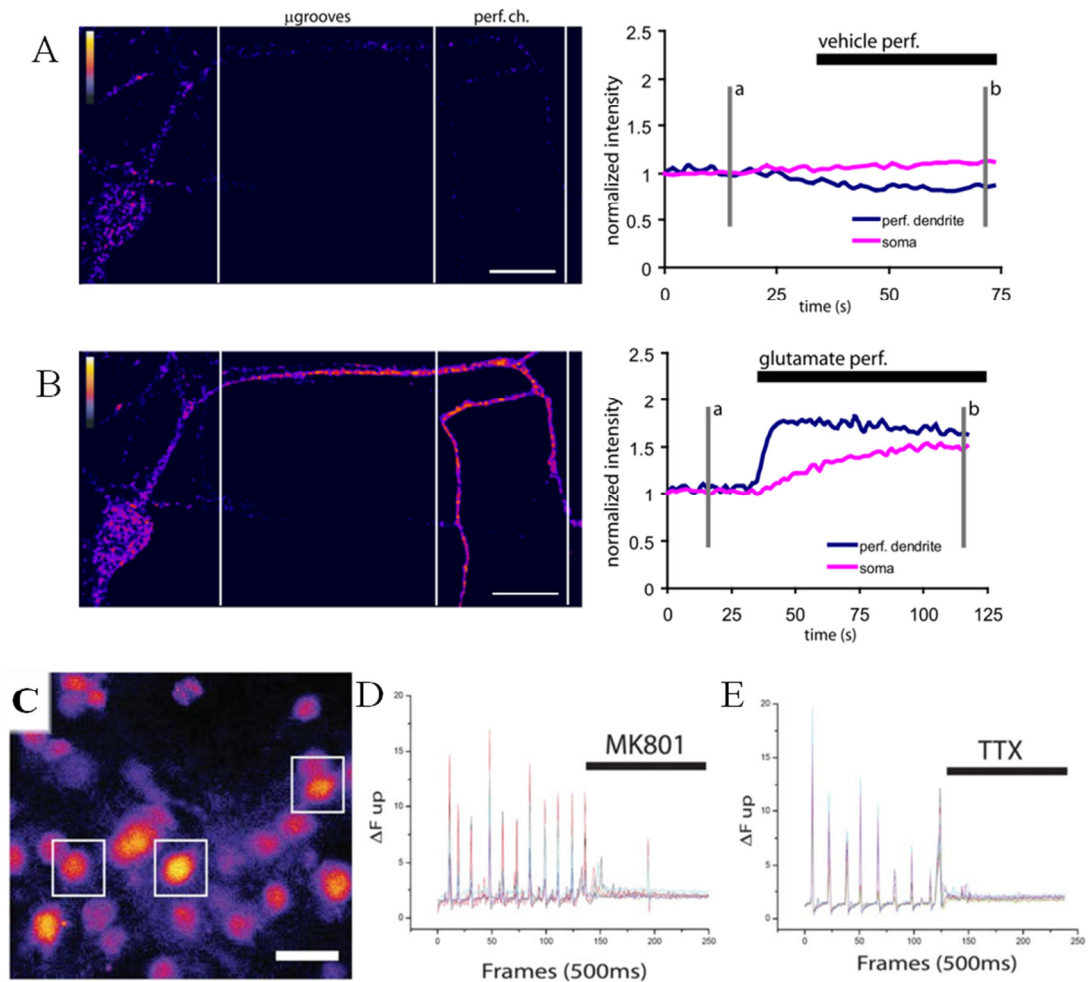


**Figure 1.20 Examples of $Ca^{2+}$ imaging in microfluidic devices. (A & B) A compartmentalised structure was used to isolate a dendrite from its soma. The dendrite was manually perfused with vehicle (A) and glutamate (B) while changes in the dendritic and somal $Ca^{2+}$ were recorded using $Ca^{2+}$ imaging. (C) $Ca^{2+}$ imaging was performed on groups of thalamic neurons that were connected to cortical neurons. (D and E) Activity from multiple cells was recorded simultaneously to show their response to directly applied compounds. (A & B) Scale bars: 25 µm, (C) scale bar: 20 µm. (A & B) Images taken from** [86]**, (C–E) images modified from** [89]**.**

## 1.4.4.3. Immunocytochemistry in Microfluidic Devices

Immunofluorescent staining of fixed cultures and fluorescent imaging of live cultures are widely used methods for measuring cell growth and protein expression in microfluidic devices. While standard fluorescent microscopy does not show functional communication between cells it is generally of interest to identify neurons within mixed cultures and also to ensure that neurites are growing between compartments as required. Popular targets for staining fixed cultures include; MAP-2 [84]–[86], [94], [99] which is a somatodendritic marker, β-III-Tubulin and Tau [74], [100], [101] which are present in neuronal cytoskeletons. Identification of synapses can be performed by staining for synaptic markers such as Synapsin1 and v-GLUT1 [85], [99] (Figure 1.21).
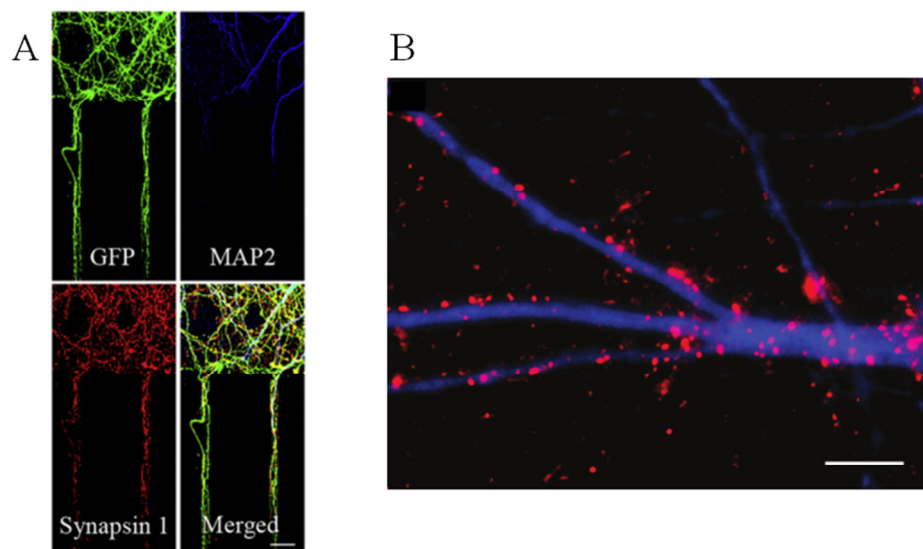


**Figure 1.21 Immunocytochemistry in microfluidic devices. Examples of fluorescent imaging in microfluidic devices show that it is possible to detect markers of interest both within the microfluidic barrier (A), and within the cell chamber.** *(A) Scale bar: 25 μm, (B) Scale bar: 20 μm. (A) Image taken from* [99]*, (B) Image taken from* [85]*.*

Imitated disease states have also been characterised by locating hyperphosphorylated Tau [74] and fluorescently labelled β-Amyloid [75] within cultures (Figure 1.15 & Figure 1.16). It is also possible to visualise protein regulation and sub-cellular localisation which has been performed using fluorescently labelled proteins of interest such as ERK [89] and pCREB [94]. Alternative methods for determining protein expression involves the harvesting of cellular tissue from selected

compartments to use in semiquantitative RT-PCR [84] or in conjunction with RNA transcript microarrays [101] (Figure 1.22).
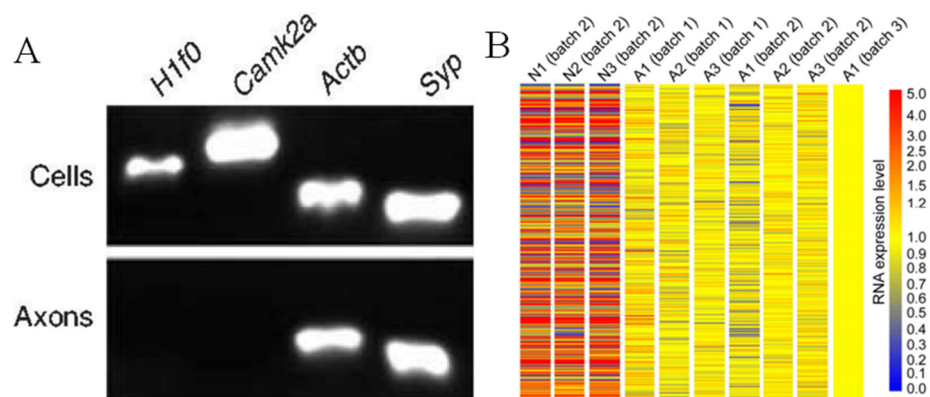


**Figure 1.22 Examples of mRNA gathered from different compartments of a compartmentalised device. Both (A & B) were from similar experiments where neurons were seeded in the Somal side of the Taylor device, and cell material was collected following the growth of axons into the axonal compartment. (A) RT-PCR was used to analyse samples from both the Cell side and the axonal side, showing that the expression of specific proteins of interest differed between compartments. (B) A RNA microarray was used to analyse samples from the neuronal side (N1–3) and the axonal side (A1–3). The image shows a heat map of calculated expression level of 2484 transcripts.** *(A) Image taken from* [84]*, image taken from* [101]*.*

In some cases it is of interest to visualise growing neurites or to fluorescently detect live neurons. GFP, mCherry, RFP, and fluorescently labelled tau have been introduced virally to cultures to express fluorescent proteins of different colours making it possible to monitor growth as well as to distinguish between neurites from different compartments [81], [86], [91]. Fluorescently monitoring live cells provides unique information in some studies, such as being able to visualise the growth, injury and recovery of a single axon [91] (Figure 1.23).
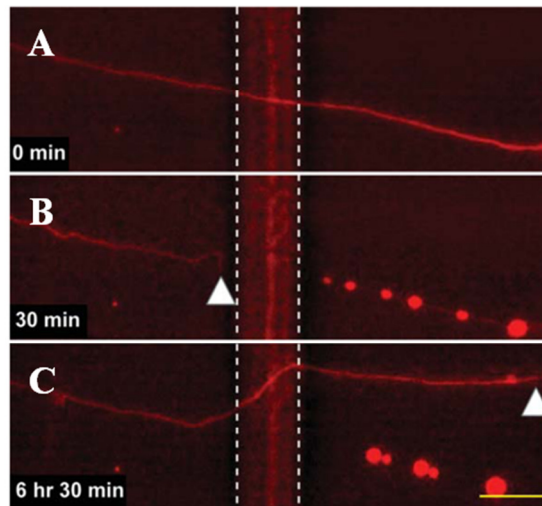
**Figure 1.23 Fluorescence imaging of tau in an injured axon. Cells in a valve-based microfluidic device were tau-labelled (microtubule marker: red). (A) Initially an axon was allowed to grow in the microfluidic device. (B) The valve (white dotted lines) compressed the axon, and the distal segment degraded. (C) Following 6 hours the axon has partially recovered.** *Scale bar 25 μm. Image modified from* [91]

## 1.4.5. Current Limitations in Neural Microfluidics

While microfluidic techniques have provided insight into some areas of fundamental neurobiology there are still areas that can be improved upon. There are many examples where neuron to neuron co-cultures in separate compartments require the interaction of neurites between the compartments. However, in the majority of cases, this communication between compartments is often left assumed or unexploited. For example, in the demonstration of axon diodes [89] only the effects of applying drugs directly to the recorded cells were reported and not the indirect effects of drug application to the connected co-culture. Showing that there is functional communication between two co-cultures has so far only been demonstrated with the use of MEAs [90].

In all of the devices described, each system has been fundamentally limited by the nature of fluidic perfusion within the device. While using open wells provides a simple means of adding compounds of interest to a selected culture, the lack of an active perfusion system prevents that compound from being removed. Crucially this limits any experiment to single applications of a drug which prevents physiologically relevant experiments that require multiple stages. The addition of a volume of

solution to an open well will alter the system's state of equilibrium causing a movement of fluid over the cell culture. This change in fluid flow may physically stimulate the cells of interest, potentially confounding the observed results and so must to be taken into consideration.

Overall, the lack of perfusion in neuronal microfluidic devices restricts their application to basic two stage experiments. Multistage experiments are achievable, however, they depend on the use of MEAs that permit the device to be moved and washed between stages without altering the position of the electrodes relative to the cells [95]. While this can be of use in some circumstances it does not solve the problem of inconsistent fluid flow due to the addition of new solutions to the system.

## 1.5. Objectives

The ability to assess the functional connectivity between neuronal co-cultures in a compartmentalised device as well as integrating a perfusion system in such a device would be beneficial to the field of neuroscience. Overcoming these challenges could enable new *in vitro* disease models to be created with drugs applied to targeted regions.

In this thesis, the challenges surrounding the concept of compartmentalised co-cultures of neurons shall be investigated. Designs similar to the Taylor device [80] shall be used as the basis of these investigations as it has proven to be a definitive design for achieving compartmentalisation. Initially, a new method for assessing the synaptic communication between primary hippocampal co-cultures in a compartmentalised shall be considered using $Ca^{2+}$ imaging and chemical stimulation. Secondly, various methods of perfusion shall be considered and their ability to perfuse multiple solutions to selected compartments shall be evaluated.

## 1.5.1. Thesis Outline

This background chapter, Chapter 1, has given a brief overview of neuroscience and the standard techniques used to study the phenomena. It has discussed a few of the limitations faced in the field and described a handful of the new frontiers being explored with novel *in vitro* microfluidic devices as well as the mathematical

techniques required to understand them. Finally, several areas of neuronal microfluidics have been highlighted that require further development.

Chapter 2 will describe various materials and methods that were required to carry out the design, fabrication and experimental setup of microfluidic devices for use in Chapter 3 and Chapter 4.

Chapter 3 will describe the use of $Ca^{2+}$ imaging to demonstrate functional connectivity between compartments in a microfluidic device. This chapter uses a compartmentalised structure, similar to that described by Taylor *et al.*, to show that chemically stimulating neurons in an isolated compartment can alter the activity of synaptically connected co-cultured neurons in an adjacent compartment.

Chapter 4 describes progress towards a microfluidic perfusion system that is compatible with the compartmentalised microfluidic structure. It will demonstrate the automated repeated stimulation of neurons that have been cultured in a microfluidic chamber. In addition, and building on the work from chapter 3, a multistage perfusion experiment will be described that demonstrates the blocking of induced synaptic activity between chambers.

Chapter 5 shall discuss the implication of the outcomes from Chapter 3 and Chapter 4 with reference to the material cover in Chapter 1. It shall also contain some highlights concerning collaborative work that has resulted from this project, before finally concluding this work.

# Chapter 2. Materials and Methods

This thesis details the development of a suitable system that uses microfluidic structures for studying neurological mechanisms *in vitro*. During this project a range of compartmentalised devices have been created, characterised and tested with primary neuronal cultures. These microfluidic devices were ultimately based on earlier concepts and structures designed by Taylor *et al.* [80], and this work has endeavoured to increase their functionality with regards to studying functional neuronal communication.

In this chapter several components of standard cell culture and device fabrication processes that were carried out are described. In addition, a variety of experimental methods and approaches to data analysis were used based on conventional techniques. All work, including cell culture, device design, fabrication and preparation, experiments, data analysis and coding were carried out by the author unless stated otherwise.

## 2.1. Materials

The following equipment and chemicals were used during various stages of the project.

### 2.1.1. Equipment

| Equipment | Brand / Supplier |
|---|---|
| Microscope: Axio Observer A1 | Zeiss |
|     Objectives: *5×, 10×, 20×* | Zeiss |
| Microscope: BX51WI | Olympus |
|     Objectives: *40× (water immersion),* | Olympus |
|               *60× (water immersion)* | Olympus |
| Cooled EM CCD camera LucaR | Andor Technologies |
| Cooled CCD camera 01-RET-EXI-F-M-12-C | QImaging |
| Millex syringe-driven filter unit (0.22 μm) | Millipore, UK |
| Plastic Syringe | Fisher Scientific, UK |
| Glass Syringe | SGE Analytical Science, UK |

| | |
|---|---|
| Photo-mask: Chrome on glass | JD Photo-Tools, UK |
| Photo-mask: Acetate | JD Photo-Tools, UK |
| Oxygen plasma asher | Pico A, Diener Electronic, Germany |
| Biopsy punches 8mm and 4mm | Stiefel, SmithKline Beecham ltd, UK |
| Needle for syringe | Fisher Scientific, UK |
| Microscope slides | Fisher Scientific, UK |
| Coverslip slides | VWR, UK |
| Round coverslips | VWR, UK |
| Syringe pump AL-1000 | WPI, UK |

## 2.1.2. Chemicals

| Chemical | Supplier |
|---|---|
| Neurobasal A | Life Technologies Ltd, UK |
| B27 supplement 50M | Life Technologies Ltd, UK |
| L-Glutamine 200 mM | Life Technologies Ltd, UK |
| Potassium chloride (KCl) | VWR, UK |
| Sodium hydrogen carbonate (NaHCO$_3$) | VWR, UK |
| Sodium dihydrogen phosphate (NaH$_2$PO$_4$) | VWR, UK |
| Magnesium sulphate (MgSO$_4$) | VWR, UK |
| Sucrose | VWR, UK |
| CaCl$_2$ | VWR, UK |
| KH$_2$PO$_4$ | BDH Laboratory Supplies, UK |
| Sodium chloride (NaCl) | Sigma-Aldrich Company, UK |
| Ethylene-di-amine tetra-chloro-acetate (EDTA) | Sigma-Aldrich Company, UK |
| D-Glucose | Sigma-Aldrich Company, UK |
| Papain | Sigma-Aldrich Company, UK |
| HEPES | Sigma-Aldrich Company, UK |
| MgCl$_2$ | Sigma-Aldrich Company, UK |
| Phosphate buffered solution (PBS) Tablets | Sigma-Aldrich Company, UK |
| Bovine serum albumin (BSA) | Sigma-Aldrich Company, UK |
| Fetal bovine serum (FBS) | Sigma-Aldrich Company, UK |
| Fluorescein | Sigma-Aldrich Company, UK |

| | |
|---|---|
| Poly-L-lysine | Sigma-Aldrich Company, UK |
| Paraformaldehyde (PFA) | Sigma-Aldrich Company, UK |
| Triton X-100 | Sigma-Aldrich Company, UK |
| Trypan blue | Sigma-Aldrich Company, UK |
| Acetone | Fisher Scientific, UK |
| Methanol | Fisher Scientific, UK |
| Isopropanol | Fisher Scientific, UK |
| L-Glutamic acid | Tocris Bioscience, UK |
| Bicuculline Methiodide | Abcam, UK |
| 2,3-dioxo-6-nitro-1,2,3,4-tetrahydrobenzo[f]-quinoxaline-7-sulfonamide (NBQX) | Abcam, UK |
| DL-(-)-2-amino-5-phosphonopentanoic acid (DL-AP5) | Abcam, UK |
| (R,S)-α-Methyl-4-carboxyphenylglycine ((R,S)-MCPG) | Abcam, UK |
| Chicken anti-MAP2 | Millipore, UK |
| Mouse anti-Synaptophysin | Millipore, UK |
| Rabbit anti-β-III-tubulin | Sigma-Aldrich Company, UK |
| Mouse anti-GFAP | Sigma-Aldrich Company, UK |
| Rabbit anti-β-tubulin | Sigma-Aldrich Company, UK |
| Alexa Fluor 488 Goat anti-chicken | Life Technologies Ltd, UK |
| Alexa Fluor 555 Goat anti-rabbit | Life Technologies Ltd, UK |
| Alexa Fluor 488 Donkey anti-mouse | Life Technologies Ltd, UK |
| Hexamethyldisilazane (HDMS) | Sigma-Aldrich Company, UK |
| AZ 4562 | MicroChemicals, Germany |
| AZ400K Developer | MicroChemicals, Germany |
| SU-8 3010 | Chestech Ltd, UK |
| SU-8 3035 | Chestech Ltd, UK |
| MicroPosit EC solvent | Rohm and Haas, US |
| Trichloro(1H,1H,2H,2H-perfluorooctyl)silane | Sigma-Aldrich Company, UK |
| Sylgard 184 Silicone Elastomer (PDMS & Curing agent) | DowCorning, Michigan |

## 2.2. Microfluidic Systems

Several iterations of devices have been fabricated during the course of this project. This section comprises a list of standard procedures used to fabricate the microfluidic devices.

### 2.2.1. Design

Devices were designed using a computer aided drawing package (CorelDRAW X5). The systems' topologies in the x & y-axis were designed, whilst the z-axis was determined by the thickness of material used in the fabrication process. Masks for both positive and negative photo-resists were created in this manner.

Devices were created using a two-layer fabrication procedure (Figure 2.1) where the general layout of the structure consisted of two culture chambers (typically 100 µm deep) with inlets and outlets that were separated by a central microchannel barrier (typically 5 µm deep). This barrier was necessary for the formation of a suitable fluidic barrier that generates a higher fluidic resistance than the adjoining chambers in order to implement the desired fluidic driven assay. Careful consideration was given to the design of the layers which allowed for them to be misaligned by a few millimetres in any direction and still be functionally appropriate (Figure 2.1). Guidelines to aid in the alignment of multiple layers were also included in the designs, such as boundary markings and channel labels.
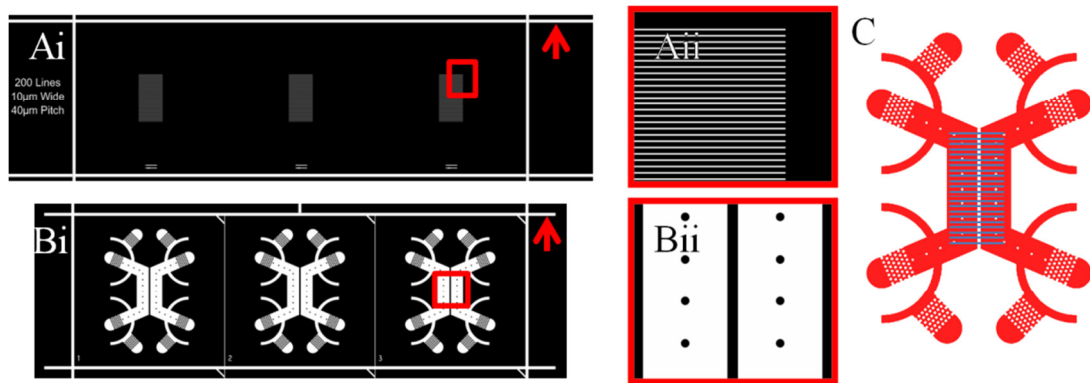
**Figure 2.1 Example photo-masks used in the construction of two-layered devices. (A) In this mask example, the thin layer consisted of sets of parallel lines that would form the microchannels. (B) In this mask example the thick layer consists of parallel chambers for each device with markings to punch out open wells for seeding the device and storing medium. In both layers there are several marking lines (Red Arrow) outside of the features that aided in manual alignment during fabrication. (C) An overlay of the device shows how the features in each layer are aligned after fabrication.**

Photo-masks were created externally (JD photo-tools, UK). The thin layer, containing the microfluidic channels that cross the central barrier, required a chrome on glass mask to be made as the minimum dimension of the features were typically 5–10 µm. The thick layer, containing the chambers, wells, channels and other superficial markings, had larger minimum features with dimensions of 50+ µm which were printed on lower quality acetate.

## 2.2.2. Fabrication

The initial fabrication of a master mould was only required when a new system was designed. The mould could be subsequently reused several times for the creation of devices. Devices were made of PDMS casts of the mould and bonded to glass before being prepared for cell culture.

### 2.2.2.1. Two Layer Fabrication Using Photolithography

Master moulds were created using standard photolithography techniques [84] involving a two-stage photolithography procedure resulting in photo-resist patterned onto a silicon wafer Figure 2.2A). Initially a silicon wafer was cleaned via 3 minute sonications in acetone, methanol and isopropanol before being dried on a hotplate (180℃ for 20–60 minutes). The first thin layer of SU8 (SU8 3010) was spun onto this (5000 rpm for 30 s) to create a layer thickness of ~5–10 µm, and pre-baked at

95℃ for 5 minutes. Once cooled, the layer was exposed to collimated UV light ($>10$ J·cm$^{-1}$ for 20 s) patterned by the thin layer mask before being post-baked at 65℃ for 60 s, then 95℃ for 5 minutes. After baking the layer was allowed to cool to room temperature to reduce internal stresses within the resist. The exposed surface was then developed for 300 s in MicroPosit EC solvent to reveal the thin layer pattern. The developed pattern was hard-baked on a hotplate (200℃ for 20 minutes) which also served to evaporate any remaining solvents before the next layer was added.

Early on in the project an alternative method of producing the thinner layer was used which required the positive photoresist AZ4562. Initially the cleaned silicon wafer was spun with HDMS (an adhesion promoter) for 5 s at 4000 rpm. Immediately after this, AZ4562 was spun onto the wafer. For layers greater than 20 μm, spin rates of less than 1000 rpm were used. For thin layers of 6 μm, a spin rate of 4000 rpm was used. The coated wafer was then pre-baked at 110℃ for 5 minutes and allowed to cool down to room temperature. A photo-mask was then positioned over the wafer before exposing it to collimated UV light ($>10$ J·cm$^{-1}$) for 20 s. The exposed wafer was then developed in AZ400K (diluted 1:3, developer:DI water) for 10 minutes or until the features were clearly apparent. It was then rinsed with DI water and dried with nitrogen ($N_2$) gas. The wafer was finally hard-baked on a hotplate at 125℃ for 25 minutes.

The second, thicker layer was formed by spinning of SU8 3035 (800 rpm for 30 s) onto the wafer containing the first layer and then pre-baked at 95℃ for 5 minutes. This achieved a thickness of 95–100 μm. The mask for the second layer was aligned by eye to markings in the first layer and exposed to the collimated UV light source ($>10$ J·cm$^{-1}$ for 80 s). Once exposed, the layer was post baked for 5 minutes at 65℃ and then 20 minutes at 95℃. This layer was allowed to slowly cool down to room temperature before being developed for 300 s in MicroPosit EC solvent to reveal the two-layer pattern. The features on the wafer were checked using a filtered-corrected upright microscope and further development carried out with fresh solvent until the central microchannels could be clearly seen between the chambers. The patterned wafer was hard-baked to create the final master mould by ramping up the

temperature in an oven to above 180℃ for 30 minutes and then allowing it to slowly cool down to room temperature. Completed master moulds were visually inspected using an upright microscope.
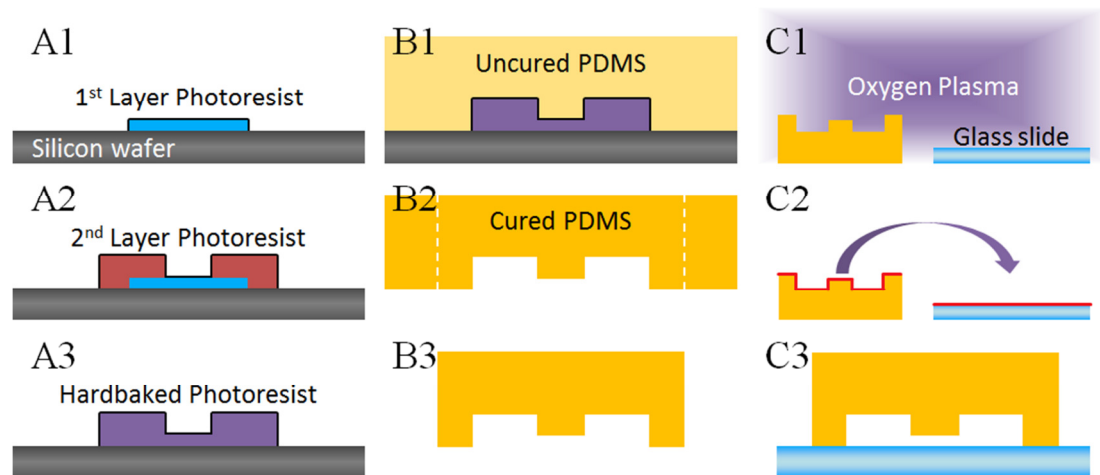


**Figure 2.2 Summary of the fabrication procedure. (A1) The first layer of SU8 or AZ photo resist was patterned onto a silicon wafer. (A2) The second thicker layer of SU8 was aligned and patterned on top of the first layer. There was sufficient overlap between layers to compensate for partial misalignment. (A3) The entire structure was hard-baked and silanised to form the completed master mould. (B1) Liquid PDMS was poured over the master mould, degassed and baked to promote polymerisation. (B2 & B3) The cured PDMS could be removed from the mould and trimmed as required. (C1) The cleaned PDMS and glass slide were exposed to oxygen plasma. (C2 & C3) The exposed surfaces were brought into contact to form the completed device.**

## 2.2.2.2. Silanisation of the Master Mould

To prevent PDMS adhesion to the silicon surface, the master mould was exposed to oxygen plasma (0.26 mBar, 200 W for 2 minutes) prior to silanisation. The mould was placed in a vacuum chamber with a separate dish containing 50 µL of trichloro(1$H$,1$H$,2$H$,2$H$-perfluorooctyl)silane, and left under low pressure for 45 minutes to complete the vapour deposition. Once silanised the mould could then be set and used with PDMS.

## 2.2.2.3. PDMS Casting

PDMS was cast on the mould to acquire an impression of the features (Figure 2.2B). Liquid PDMS was mixed with a curing agent (10:1 w/w, base:curing agent) and poured over the master mould, typically to a depth of ~5 mm. This was degassed in a vacuum chamber for 30 minutes to remove bubbles that form from the mixing and

polymerisation process. The degassed PDMS was placed in an oven at 80℃ to cure for 3 hours. Once completely set the PDMS was removed from the oven and allowed to cool before preparation. The master mould was visually inspected after each casting to ensure that features of the design did not degrade through successive casting procedures. If there was any degradation of the master mould during this process it would result in features noticeably lifting off which would render the mould unusable. In general, there was no degradation of the master moulds used and there was excellent reproducibility between successive castings.

## 2.2.2.4. PDMS Preparation

The PDMS was removed from the wafer by cutting around the features with a scalpel. The block of PDMS containing several devices was then sliced into individual devices according to the optimal guidelines present on the surface. Holes to form the wells that connected to both ends of the cell culture chambers were then cut using either a 4 mm or 8 mm diameter biopsy punch. In some cases fluidic inlets and outlets, to be connected to syringe pumps, were also necessary. These were cut using a sharpened flat tipped needle (0.723 mm diameter).

## 2.2.2.5. Cleaning of PDMS and Glass

Once the PDMS was prepared, the structure had to be bonded to glass to form a completed device. For general use, microscope slides were found to be adequate, however for higher magnification microscopy (40× or greater) coverslip slides were used due to the limitations of the objectives present. Both devices and the glass had to be cleaned to help ensure the bonding process was successful. The glass was cleaned by sequential sonications in acetone, methanol and isopropanol for 3 minutes each. PDMS was cleaned by sonication in methanol for 3 minutes only. Once cleaned, the PDMS devices and glass slides were both dried with $N_2$ gas and then placed in an oven (>80℃) for 30 minutes.

It was also possible to quickly clean both the devices and the glass using scotch tape [102], [103]. Tape would be pressed firmly onto the surface of all features and onto the area of the glass slide to be bonded before being gently peeled off. This was repeated with fresh tape to ensure that the surface was sufficiently cleaned. In general this method was preferred as it reduced the time taken to perform bonding

and also the amount of solvents used during the cleaning process. However, as it is not possible to clean coverslips using this method, sonication in solvents was always used to clean coverslip slides.

## 2.2.2.6. Bonding of PDMS to Glass

Bonding of PDMS to glass was carried out using an oxygen plasma asher (Figure 2.2C). By briefly exposing the surfaces of PDMS and silicon glass to low pressure oxygen plasma, silanol groups (–Si–OH) are formed on the treated surfaces. When both surfaces are brought into contact they quickly form covalent bonds (–Si–O–Si–) making the PDMS inseparable from the glass [104], [105].

Cleaned PDMS devices were placed feature side up into an oxygen plasma chamber (Pico A, Diener Electronic, Germany) along with the glass slides. Once exposed to oxygen plasma (0.26 mBar, 90 W, 6 s), the devices were picked up and placed, feature side down, onto the surface of the glass. Manual compression between the PDMS and the glass was used to ensure conformal contact.

Alternatively, devices could be reversibly bonded to the glass via conformal contact alone [102]. By pressing the PDMS, feature side down, firmly onto the glass a weak seal could be achieved. While this seal was general strong enough to hold fluid, care was required to ensure that the PDMS was not disturbed. This occasionally led to devices that leaked their contents or even complete detachment of the PDMS from the glass. In general, permanent bonding was preferred due to its reliability.

## 2.2.3. Preparation of Devices for Cell Culture

There were several conditions that had to be met in order for the device to be ready for cell culture. It must be able to contain medium, be coated in poly-l-lysine (PLL) and finally had to be sterile.

Once fabricated the PDMS quickly becomes hydrophobic when left in air. This poses a problem with regards to filling microchannels with water based solutions. Force filling the chambers while the PDMS is hydrophobic results in air bubbles being present in the channels that prevent the system from functioning properly. However, upon oxygen plasma exposure, the surfaces of PDMS are temporarily rendered hydrophilic. When preparing the device the entire system was exposed to oxygen

plasma (200 W) for 1 minute before the wells were filled with deionised water. Keeping the surfaces wet prevented the PDMS from becoming hydrophobic and allows the water to be washed off with medium at a later stage. Devices at this stage could be kept in the fridge and used at a later date providing they did not dry out.

Once flooded with water the devices were sterilised. Groups of devices were placed inside a large glass Petri dish and left with the lid open inside a UV sterilisation cabinet for 20 minutes. The lid was then closed and the dish left under UV light for a further 20 minutes. The closed dish, now containing sterilised devices, was removed and transported to a sterile cell culture hood.

To promote cell adhesion the sterilised devices were required to be coated with PLL solution diluted to 0.01 mg/mL and filter sterilised from a stock solution of 0.1 mg/mL. Water was emptied from the wells in each device, using a P200 pipette, with the chambers and microchannels being left wet. The top wells of each device were then half filled with the PLL solution. This was left for 60 minutes at room temperature, before being washed off 3× with the cell culture medium.

Once coated and washed with medium the devices were ready to be plated with cells. They could also be stored in the hood or incubator for later use, within 1–2 days, however best results were achieved when the device was prepared with PLL on the same day as the cell culture.

## 2.3. Cell Culture in Microfluidic Devices

Over the progression of this project the cell culture technique and use of cells was refined, resulting in the optimised use of one animal for up to 15 devices. The dissection of the hippocampus was carried out using standard culture techniques [106], [107] where the sole difference from these techniques was the final concentration of the cell suspension.

### 2.3.1. Preparation of Cell Culture Medium and Enzyme Solutions

Cell culture medium was prepared by using Neurobasal A medium supplemented with L-glutamine (2 mM) and B27 (2% v/v). This was passed through a sterile filter (Millex 0.22 μm, Millipore, UK) and incubated at 37℃ prior to use with the cells.

Enzyme solution consisted of (in mM): NaCl 3.39, KCl 0.201, NaHCO$_3$ 1.092, NaH$_2$PO$_4$ 0.078, MgSO$_4$ 0.123, EDTA 0.073, Glucose 2.252, CaCl$_2$ 0.11. This was filter sterilised prior to use.

Two variations of the enzyme solution were also required. Papain solution was made by adding 7.5 mg papain to 5 mL of enzyme solution. BSA solution was made by adding 60 mg BSA to 6 mL of enzyme solution. Both of these solutions were incubated at 37℃ and filter sterilised prior to use.

## 2.3.2. Hippocampal Dissection and Cell Suspension

Sprague Dawley rat pups (1–2 days old) of either sex were used in all cell cultures. A total of 27 pups were used to produce the work detailed in this thesis. These were killed via cervical dislocation (in accordance with Schedule 1 UK Home Office guidelines) and decapitated. The skin and skull were cut with small scissors and peeled back, partially exposing the brain, then part of the skull was removed with forceps to allow access to the whole brain. The optical nerves were severed and the brain was removed and placed onto sterile filter paper. The hemispheres were separated with a scalpel and rolled apart (ventral side up). Removal of the cerebellum and midbrain exposed the hippocampus which was dissected out and placed into enzyme solution. This was done for both hemispheres.

The hippocampal tissue was diced and incubated in papain solution for 20 minutes at 37℃. To inactivate the papain and turn the tissue into a cell suspension, serial trituration of the tissue was carried out in BSA solution with flame polished glass pipettes of decreasing diameter. Fragments within the cell suspension were removed and disposed of before the remaining cell suspension was spun down (2,000 rpm for 2 minutes) and resuspended in 1 mL of cell culture medium. Cells were stained with trypan blue (0.4%) and live cells were counted using a haemocytometer. The cells were then resuspended at concentrations of $3\times10^5$ cells/mL for coverslips or $3\text{-}5\times10^6$ cells/mL for devices.

## 2.3.3. Loading Cells into Devices

Initial devices required a low cell seeding concentration as they incorporated open wells, where the cells were grown, but not a microfluidic culture chamber. In these

devices open wells were emptied of medium by pipette and loaded with 100 µL of cell suspension ($3 \times 10^5$ cells/mL). This was then incubated for 1 hour (37℃, 5% $CO_2$). The medium was then withdrawn and fresh medium added until each well was filled (~200 µL) and returned to the incubator (37℃, 5% $CO_2$).

In general, devices consisted of pairs of open wells that were linked by a microfluidic chamber for cell culture. Due to the high surface area to volume ratio, a greater cell concentration was required to load the device ($3$–$5 \times 10^6$ cells/mL). The medium already in the open wells, from the preparation stage, was extracted. Cells were loaded into the device by pipetting 5 µL into the well while holding the pipette tip beside the inlet to the microchannel. Only one well attached to each chamber was loaded to ensure that the cells were able to flow through chamber. The device was then incubated for 10 minutes (37℃, 5% $CO_2$), before each well was topped up with fresh medium and returned to the incubator. The addition of extra medium to the wells was staggered to reduce the flow rate across the recently plated cells.

All devices were placed in Petri dishes along with a smaller dish containing a few millilitres of cell culture medium. This external (to the device) medium served to increase the humidity within the closed Petri dish and prevented significant evaporation from the device wells. Without the external medium the cell culture medium in the device would evaporate quickly, even in a humidified incubator, due to the high surface area to volume ratio. Sterile water could not be used as a replace for the external medium as it resulted in diluting the culture medium within the wells; however, a sufficiently salty solution is a suitable alternative. The Petri dish containing the device was kept in an incubator to maintain constant conditions (37℃, 5% $CO_2$). Every 2–3 days the devices would have half of the medium removed from each well before being topped up with fresh medium.

## 2.4. Immunocytochemistry

Staining of devices was performed to identify neurite growth, differentiate between astrocyte and neurons and to view synaptic vesicles. While the staining method remained consistent, there were two types of imaging systems used to view the stained devices at low and high magnification.

## 2.4.1. Immunocytochemical Staining

Initially the cells were washed 3 times in phosphate buffered saline (PBS). Washing was performed by gradually removing the contents of all wells, half filling each well with PBS and then repeating this. It was important to keep each of the wells connected to chamber at similar volumes during this procedure to minimise the flow rate over the cells. The emptied wells were then half filled with ice cold paraformaldehyde (PFA) 4% for 10 minutes, washed 3 times with PBS, half filled with ice cold 100% methanol for 10 minutes, washed 3 times with PBS, half filled with 0.01% Triton-X100 for 10 minutes and washed 3 times with PBS.

Non-specific binding was blocked by incubation with a blocking solution (PBS with BSA 1% w/v and FBS 5% v/v), half filled into each well, for 1 hour at room temperature. Primary antibodies were then diluted in blocking solution to their standard concentrations and 20–100 µL were loaded into the top-wells only. This was kept at 4℃ for 16–18 hours.

The devices were washed 3 times, in the manner described previously, with blocking solution. Secondary antibodies were diluted in blocking solution (1:200, secondary antibody:blocking solution) and 20–100 µL were loaded into the top well of each channels. The device was incubated in darkness for 1 hour prior to a final wash with PBS. Wells were left filled with PBS to keep the cell chambers wet.

Due to the PDMS permeability to water vapour it is impractical to seal the devices after staining. As such the system should be kept wet using PBS. Filter sterilised PBS can improve the duration that the device can be viewed for. The labelled devices could be stored by keeping the wells filled with PBS, placing the device in a Petri-dish, sealing the dish with parafilm and covering it in tinfoil. This can be stored in a fridge for up to two months to be imaged later, though the quality will deteriorate over time.

## 2.4.2. Immunocytochemical Imaging

Imaging was performed using either an inverted microscope (Axio Observer A1, Zeiss), or an upright microscope (BX51WI, Olympus) for higher magnification of devices on coverslips using a 40× or 60× water immersion lens. With an inverted

microscope, the device remained upright while all wells were filled with PBS and the features imaged. With an upright microscope, the majority of the fluid was emptied from each well, leaving the bottom of each well a little wet, to prevent spillage onto the microscope and the device was inverted. A few drops of PBS were applied to the glass coverslip of the inverted device before imaging with water immersion objectives. During imaging with the upright microscope it was necessary to periodically check that the channels remained wet.

For the inverted microscope, images were captured using a cooled EM-CCD camera (LucaR, Andor Technologies) and processed using Andor SOLIS for Imaging (version 4.19.30001.0). For the upright microscope, images were captured using a cooled CCD camera (01-RET-EXI-F-M-12-C, QImaging) and processed using a combination of WinFluor imaging software (J. Dempster, University of Strathclyde) and ImageJ (version 1.47). Both setups produced greyscale images which were coloured and merged, where appropriate, using GIMP (version 2.8).

## 2.5. $Ca^{2+}$ Imaging

To monitor activity within and between live cells, a $Ca^{2+}$ sensitive indicator was used to visualise activity of both neurons and astrocytes.

### 2.5.1. $Ca^{2+}$ Imaging – Preparation

To image $Ca^{2+}$ activity, a physiologically relevant solution was required to maintain the live cell culture. External solution consisted of (in mM): NaCl 122, KCl 5, HEPES 10, $KH_2PO_4$ 0.5, $NaH_2PO_4$ 0.5, $MgCl_2$ 1, D-Glucose 11, $CaCl_2$ 1.8. The solution was adjusted with NaOH to a pH of 7.4 and the osmolarity was adjusted with sucrose to 310 mOsm.

Devices to be $Ca^{2+}$ imaged were taken from the incubator and cleaned in freshly prepared external solution. The cells were loaded with a $Ca^{2+}$ sensitive dye, Fluo4 AM (5 µM in external solution), for 1 hour in darkness at room temperature. The cells were then washed with external solution and the device was attached to the microscope stage. To help prevent the device from moving during an experiment tape was used to secure the glass slide to the stage.

## 2.5.2. Ca$^{2+}$ Imaging – Microscopy Setup

Specific settings for the camera and microscope setup varied between experiments. In general the light intensity from the mercury arc lamp (HBO 100W) had to be reduced with a neutral density filter to 20% (FL attenuator, position 5) since there was no electronic shutter on the light source to pulse the illumination. To monitor cell activity the excitation light had to be left on continuously and so the reduced intensity helped to prevent the light from bleaching the fluorescent dye, degrading the cell viability or potentially inducing cell responses. A 5× objective was used to image the cells which in combination with the camera (LucaR, Andor Technologies) provided a field of view (FOV) of around 2.7 mm$^2$. The camera was set to have an exposure time of 0.4s, a frame rate of 2 Hz, no pixel binning and an electron multiplier (EM) gain of 50–200. The EM gain was set at the start of each experiment depending on the baseline fluorescence of the loaded cells.

## 2.5.3. Ca$^{2+}$ Imaging – Signal Processing

Once an experiment was completed, the file could be analysed using Andor SOLIS (version 4.19.30001.0) for Imaging and MATLAB (R2011b). A standard routine of processing the Ca$^{2+}$ image sequences was followed to provide consistent signal processing and analysis (Figure 2.3). Regions of interest (ROIs) were drawn around each cell that fell within the FOV using Andor SOLIS for Imaging with the average intensity of each ROI per frame exported. This provided an array of the raw intensity values from each ROI which was loaded into MATLAB for further analysis. To aid with signal processing of multiple experiments, the first ROI drawn in all cases was of a region devoid of any visible cell or cell process which served as the background recording.
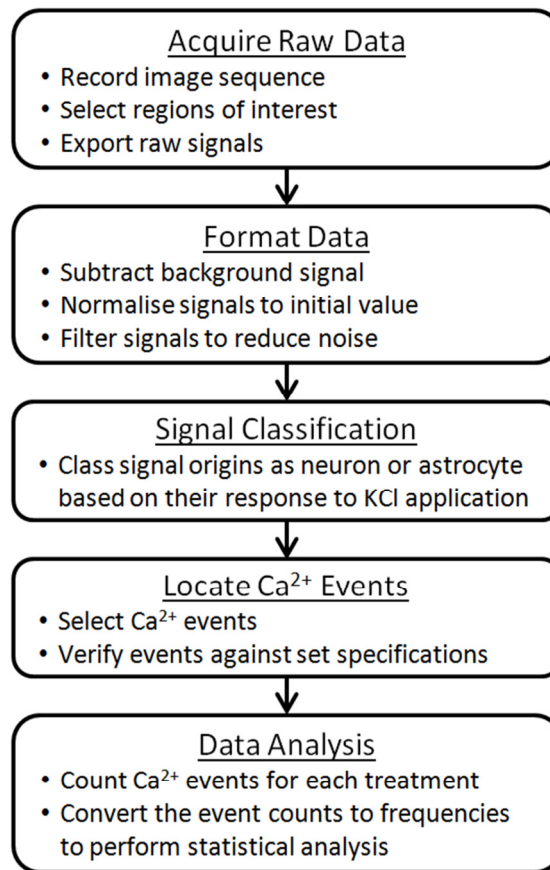
**Figure 2.3 Flowchart of the signal processing stages required. Ca$^{2+}$ image sequences of cell networks were recorded and converted into a set of Ca$^{2+}$ intensities. These signals were formatted prior to inspection, where they were classed as neuronal or astrocytic and their Ca$^{2+}$ events were selected. Each Ca$^{2+}$ event was checked against a set specification to determine if it qualified before being counted towards the total events that occurred for a specific treatment. The number of events per treatment could be statistically analysed to determine if significant changes in Ca$^{2+}$ activity had occurred.**

Processing of the signals was performed using several scripts that were written in MATLAB (see MATLAB Files – Processing Ca$^{2+}$ Imaging, page 162) to aid in the predominantly manual analysis of image sequences. Signals were initially converted into a standard format by deducting the background and dividing the entire signal by its initial value. These normalised signals were then filtered to reduce noise by using a moving average filter (window size 11). After this process, if any signals were found to have any negative values they were removed as errors.

The manual characterisation of these pre-processed signals started with identifying the cell type of the signal. As Ca$^{2+}$ imaging reveals both neuronal and astrocytic activity it is important to differentiate between the two types of signal. Every

experiment carried out contained a stage of direct neuronal depolarisation using KCl (25 mM). By observing a signal, at the stage of KCl application, it was possible to distinguish between neurons and astrocytes [67], [106] (Figure 2.4). This classification was carried for each signal that was shown sequentially by the MATLAB script used. Afterwards all of the signals could be displayed according to each category, and individually displayed if required.
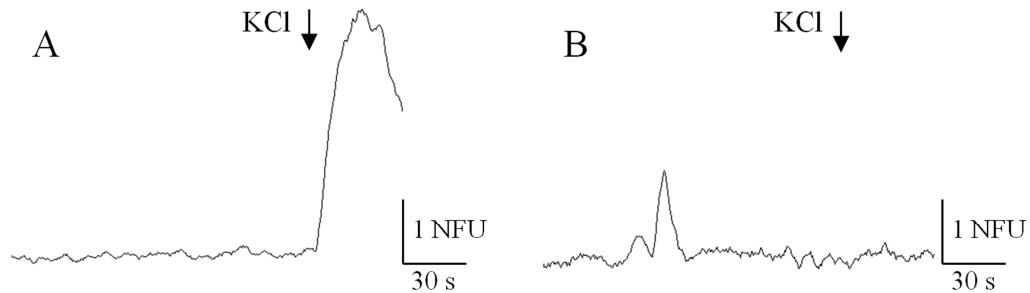


**Figure 2.4 KCl application identifies cells as either neuronal or astrocytic. (A) A typical neuronal signal has a distinct sharp rise in Ca$^{2+}$ upon KCl (25 mM) stimulation. (B) A typical astrocyte signal does not show a response to KCl stimulation.**

Once categorised, the signal activity was quantified. A MATLAB script was used to display all of the signals in sequence while the start and peak of each Ca$^{2+}$ event was manually identified (Figure 2.5). This information was stored so that it could be used later to identify the location and magnitude of each Ca$^{2+}$ event.
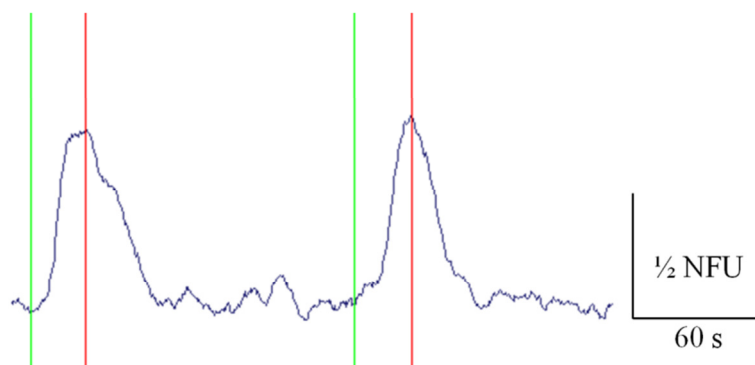


**Figure 2.5 Manual identification of events using a computer interface. A user interface was created in MATLAB to select specific regions of each signal. For each Ca$^{2+}$ signal the start of each event is selected (marked with a green line) and the initial peak of the event is also selected (marked with a red line). This allows the event information to be stored in terms of location and magnitude of the event.**

Attempts at producing a program to automatically identify regions of interest to quantify $Ca^{2+}$ activity were not successful. While this could greatly enhance the speed of the quantification and analysis, the attempts were ultimately unreliable and could not be used. In general, the concept of automatic characterisation of cell type and $Ca^{2+}$ signalling is beyond the scope of this project.

## 2.5.4. $Ca^{2+}$ Imaging – Statistical Analysis

Once the data surrounding each event was gathered from the signal processing stage the statistical significance of changes in cell activity could be derived using MATLAB. During experimental recordings, the onset of each treatment was recorded accordingly in terms of frame number. This allowed the periods of treatments to be synchronised with the processed signals. For each treatment used, its duration became a separate analytical zone for processing changes in activity. The number of events in each analytical region was automatically counted. As each analytical region could vary by some time, it was decided to use the event frequency per region rather than the number of events per region as this would be an unfair comparison of experiments if regions were not uniformly distributed.

For an experimental routine, consisting of several stages which are repeated using multiple devices, all of the resulting cell signals were analysed as a single data set in terms of event frequency per region. The average frequencies of events per region were compared to determine if cell activity was significantly different between regions. Since each sample from the data set, containing the frequency over multiple regions, originates from a single cell it is appropriate to use a paired student's t-test to determine the significance in changes between regions.

## 2.6. $Ca^{2+}$ Imaging Experiments – Procedural Setups

Initial experiments carried out consisted of sequentially applying chemicals to targeted channels within the microfluidic devices during a continuous recording. While this allowed for the local application of the chemical it did not allow for the washing off of the chemical applied. A perfusion system was subsequently developed to permit discrete application of chemicals that could be applied to localised chambers and washed off automatically. All $Ca^{2+}$ imaging experiments

were carried out on the inverted microscope (Axio Observer A1, Zeiss) with a cooled EM CCD camera (LucaR, Andor Technologies).

## 2.6.1. Non-perfusion Based Experiments

Experiments that were performed without perfusion relied on manual pipetting of solutions to and from the open wells of the device. By altering the volume in each well it was possible to control the flow of fluid and selectively apply drugs to areas of the device. This was done with care to prevent the devices from being nudged during the experiment as the cells will be continually recorded. Apart from the preparation of solutions utilised during this type of experiment, there was no additional setup of equipment required.

## 2.6.2. Perfusion Based Experiments

The perfusion system, developed to apply chemicals and wash them off, required the additional setup of syringe pumps and connections to the device. Solutions for each stage were prepared and loaded into syringes. Glass syringes (5 mL, 10.301 mm internal diameter, SGE, UK) with plastic tipped metal plungers were used to minimise the lag associated with syringe driven fluidic systems. Syringes loaded with solution had bubbles removed and were positioned into programmable syringe pumps (AL-1000, WPI, UK). A syringe pump was capable of actuating a syringe plunger at a rate of $1.4 \times 10^{-3}$ mm/min up to 184 mm/min, to provide a range of flow rates between 0.11667 µL/min and 15334 µL/min (assuming a 5 mL syringe). Syringes to be used for withdrawal were loaded with DI water, de-bubbled, and positioned into the appropriate pumps.

Connections between the syringes were made using a series of needles and tubing. A blunted needle tip (0.405 mm diameter, ~15 mm length) is attached to the syringe which is connected to PTFE tubing (0.255 mm diameter, ~700 mm length) via a short piece of Tygon tubing (~10 mm length). At the device end the PTFE tubing is connected to a needle segment (0.723 mm diameter, ~15 mm length, both ends flattened and blunted) via another piece of Tygon tubing. Fluid was allowed to flow through the tubing at this stage which demonstrated the integrity of the tubing as well as priming the tubes with fluid. The exposed section of needle at the end of the tubing was then connected to the device by inserting it into pre-punched inlets and

outlets. This connection was sealed with a small amount of silicone grease to ensure that the interface did not leak.

For procedures using the pumps, it was necessary to switch between solutions with minimal transition time so that pressure conditions within the system were kept constant. It was also desirable for experimental routines to be pre-set and automatically controlled throughout the entire experiment. To achieve this, the pumps were networked together which allowed them to be controlled by a single computer using a communication protocol based on RS232 (as detailed in the user manual). To send commands, an interface was built using MATLAB that was able to control multiple pumps simultaneously (Figure 2.6A). Alternatively, pre-set instructions were added to a MATLAB script that would carry out the entire routine automatically (Figure 2.6B). Up to six pumps were controlled during experiments using these interfaces. The code for both programmes is attached in appendix (see MATLAB Files – Syringe Pump Control, page 182).
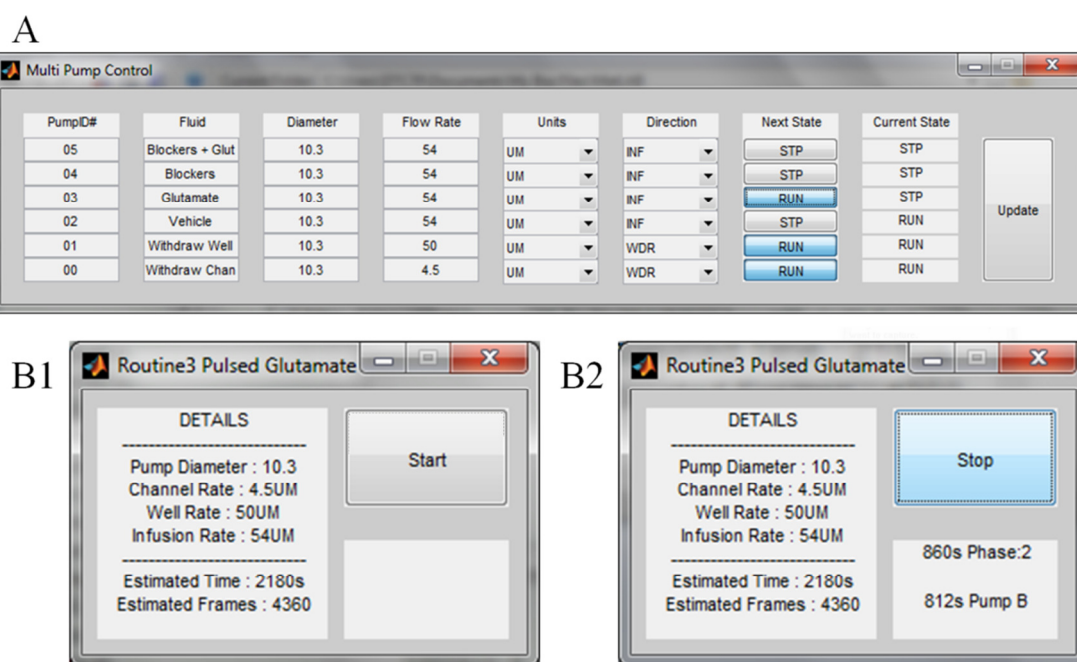


**Figure 2.6 Multiple syringe pumps were controlled via computer interface. (A) It was possible to control all of the pump parameters using the program including Syringe Diameter, Flow Rate, and Direction. Multiple pumps could be updated simultaneously to reduce switching times between solutions. (B) Programmed routines could also be implemented, where the interface would provide relevant information about the current stage of the program (B2) for the operator to use during the experiment.**

# Chapter 3. Synaptic Communication between Isolated Hippocampal Co-cultures

There are several advantages of using microfluidic devices for *in vitro* cell culture including the ability to pattern cells and selectively manipulate their environment. Using a compartmentalised device it is possible to grow primary hippocampal co-cultures that can form synaptic connections with each other. This is demonstrated in this chapter by immunofluorescent staining of cell processes to show the physical connections and $Ca^{2+}$ imaging to show functional synaptic activity.

Elsewhere, multiple networks of neurons have already been grown in compartmentalised devices [75], [86], [89]. However, functional communication between compartmentalised networks has generally been assumed or demonstrated using MEA setups [95]. Here, functional communication between isolated neuronal networks is demonstrated using a novel combination of $Ca^{2+}$ imaging and selective chemical stimulation in a microfluidic device.

## 3.1. Introduction and Hypothesis

Synaptic communication is a fundamental process in the CNS. It is also a key function to become affected during several neurological disorders including Alzheimer's disease. It is useful to study fundamental cell physiology *in vitro* where the number of confounding influences on the cell can be reduced as the extracellular environment can be carefully controlled. Compartmentalised microfluidic systems have recently become a powerful tool for studying the interaction of different cell phenotypes, including cortical-striatal co-cultures [89] and neuron-glia co-cultures [87]. One of the main assumptions from these types of study is that synaptic communication is not influenced by the microfluidic barrier between the cultures. The use of compartmentalised systems is advantageous for studying synaptic communication as differing pre and postsynaptic culture environments can be achieved. This allows chemical stimuli on one culture to affect the activity of the other via synaptic communication.

In this chapter, the assumption of synaptic communication is addressed through functional testing of the neuronal networks involved. Primary hippocampal co-cultures are grown in compartmentalised microfluidic systems to form a congruent network with two sub-networks that are held in environmentally isolated conditions. The suitability of the device created was evaluated to ensure that fluidic isolation of a sub-network could be achieved. A functional test was developed to determine if synaptic communication occurred between the fluidically isolated sub-networks.

While the overall aim is to develop a device for use in synaptic communication studies, there are several points that warrant evaluation to ensure that the system works as designed. The main issues to be investigated are the system's capability of producing reliable sub-network formation and that these networks are synaptically connected, as well as confirming that no cross-contamination is present during the evaluation of functional connectivity.

To find out if the system developed allows for the formation of synaptically connected co-cultures, neuronal cell cultures have to be observed growing within the device with cultures sending neurites towards each other to form a larger network. The neurites between the networks will be examined for synapse formation by imaging for synaptic markers.

The evaluation of synapses between the neuronal networks formed involves a live cell assay to assess their functionality. By chemically stimulating a change in activity in one network the other network should respond if it is functionally connected. The cell responses will be assessed using $Ca^{2+}$ imaging.

The fluidic isolation of one network from the other will be evaluated to ensure that a chemical stimulus from one culture does not diffuse across the barrier and directly stimulate the opposing culture. Essentially, this involves modelling the system to ensure that one chamber can remain fluidically isolated for the duration of the experiment.

## 3.2. Design and Development

The development of a device for studying synaptic communication required some refinements of both the design layout and fabrication techniques used for creating the master mould. While the overall aim is to show synaptic functionality the first goal was to produce consistent cultures that could physically form a connected neuronal network.

## 3.2.1. Design Development

Initially the connection of two or more cultures was attempted using a series of square well connected via a series of long microchannels. This master mould was created using a single 20 μm layer of AZ photoresist as described in Section 2.2.2. Ultimately the device proved unsuccessful due to the lack of growth towards the microchannels (Figure 3.1). This was potentially due to the distance between the adjacent open wells being greater than 3 mm. In addition, a significant number of microchannels became blocked from the open wells during the bonding process since there was a significant overhang between the channels and the hole punched out to form the well. Cells were seeded in 3 of these devices from the same culture, at concentrations of $1.5 \times 10^5$–$6 \times 10^5$ cells/mL, with similar results in each.
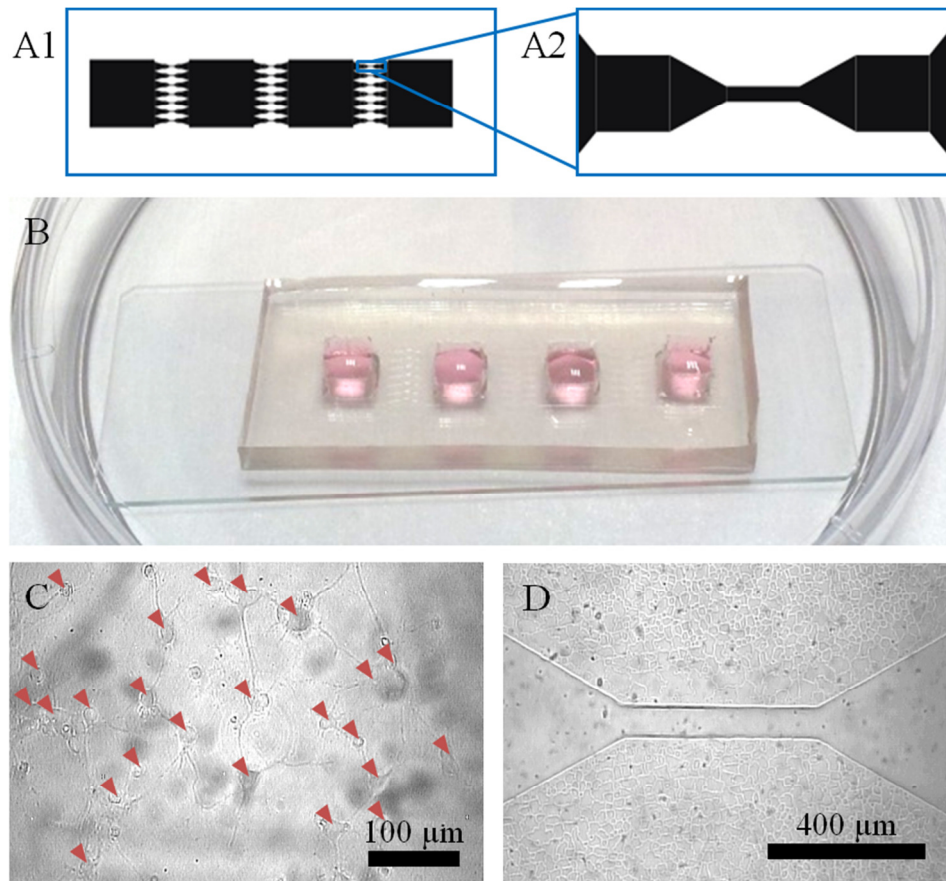
**Figure 3.1 Primary hippocampal cells grown in initial PDMS structures. (A) Schematic of the 4 square open wells connected via arrays of microfluidic channels (A2). (B) A fabricated device consisting of 4 square open wells cut out of PDMS with a set of microchannels connecting each well. The device is filled with cell culture media and kept in an individual Petri dish for cell culture. (C) Numerous cells, identified with a marker, were found growing and appeared to have processes that connected to each other, apparently forming networks in each open well of the device. (D) No cell processes were found growing in the microchannels between the open wells. The microchannels were 500 μm long, and located 1.5 mm away from the open well.**

A new device geometry, based on a design previously used for axonal isolation [80], was then fabricated. The design consists of two parallel chambers for cell culture with a barrier separating them. Along this barrier there is a series of microchannels suitable for cell processes to grow through and connect to the culture on the other side. This required a master that was fabricated from two layers of photoresist; a thin layer for the central barrier and a thick layer for the culture chambers (Figure 3.2).
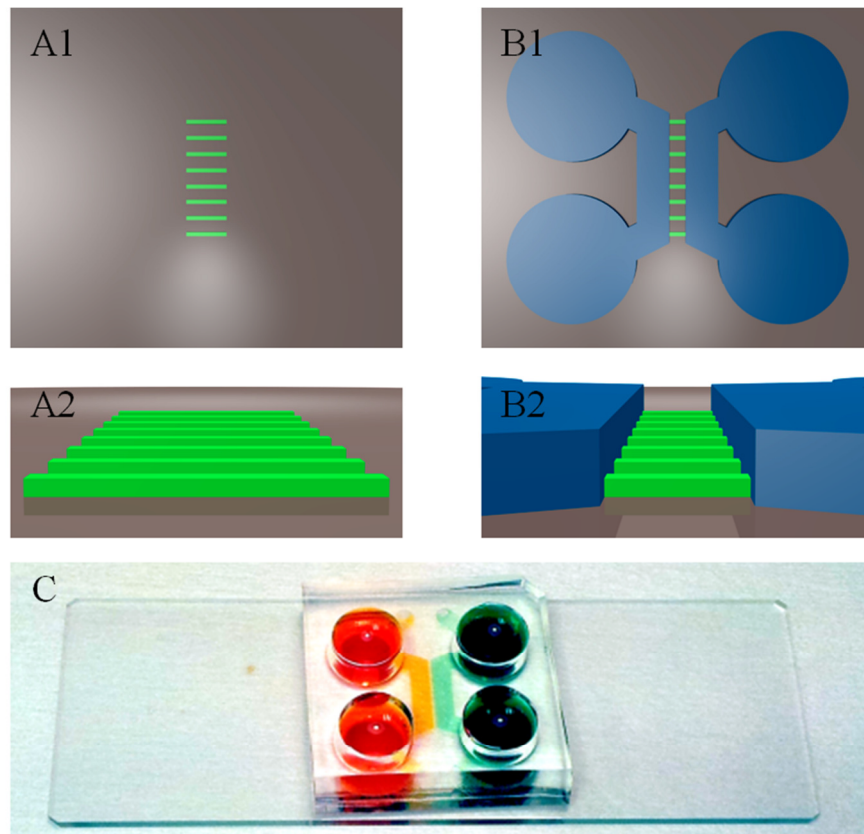
**Figure 3.2 Fabrication of the two layer device master and a completed PDMS device. (A) The first layer of photoresist is patterned onto a silicon wafer; A1 – top view, A2 – side view. The thin layer consists of solely of the microchannels located between the culture chambers. These are 10 µm wide and 5–10 µm deep with a pitch of 40 µm. (B) The second thicker layer of photoresist is patterned onto the silicon wafer with the first thin layer; B1 – top view, B2 – side view. This consisted of two parallel chambers that were 2 mm wide, 90–100 µm deep, and had an average path length of 10.2 mm. The distance between the chambers was 250 µm which set the length of the microchannels in the central barrier. The larger chambers were for the cell cultures to grow while the smaller microchannels provided paths for neurites to grow and form connections with the network on the other side. Markings were also included in the thick layer to show where PDMS should be cut out to form the large open wells at either end of the chamber structure. (C) Image of a fully fabricated device loaded with food colouring to highlight the different chambers. The device is bonded to a standard microscope slide (75 mm × 25 mm).**

## 3.2.2. Device Fabrication

To create devices for cell culture, PDMS is cast onto a master mould consisting of a silicon wafer and a pattern of photoresist. The patterned PDMS is bonded to a glass slide, forming a hollow chamber for cell culture.

During the fabrication process of the master mould, two methods were used. The initial method involved AZ photoresist for the thin layer of microchannels and SU8-3035 for the thicker layer of chambers. While the initial devices proved successful for cell culture, some issues were encountered in relation to the formation of microchannels in the barrier between the culture chambers. Poor bonding between the AZ layer and the SU8 layer allowed PDMS to creep between the layers during casting and degassing procedures. This led to several microchannels in the barrier being blocked and preventing some cell process growth between the chambers (Figure 3.3).
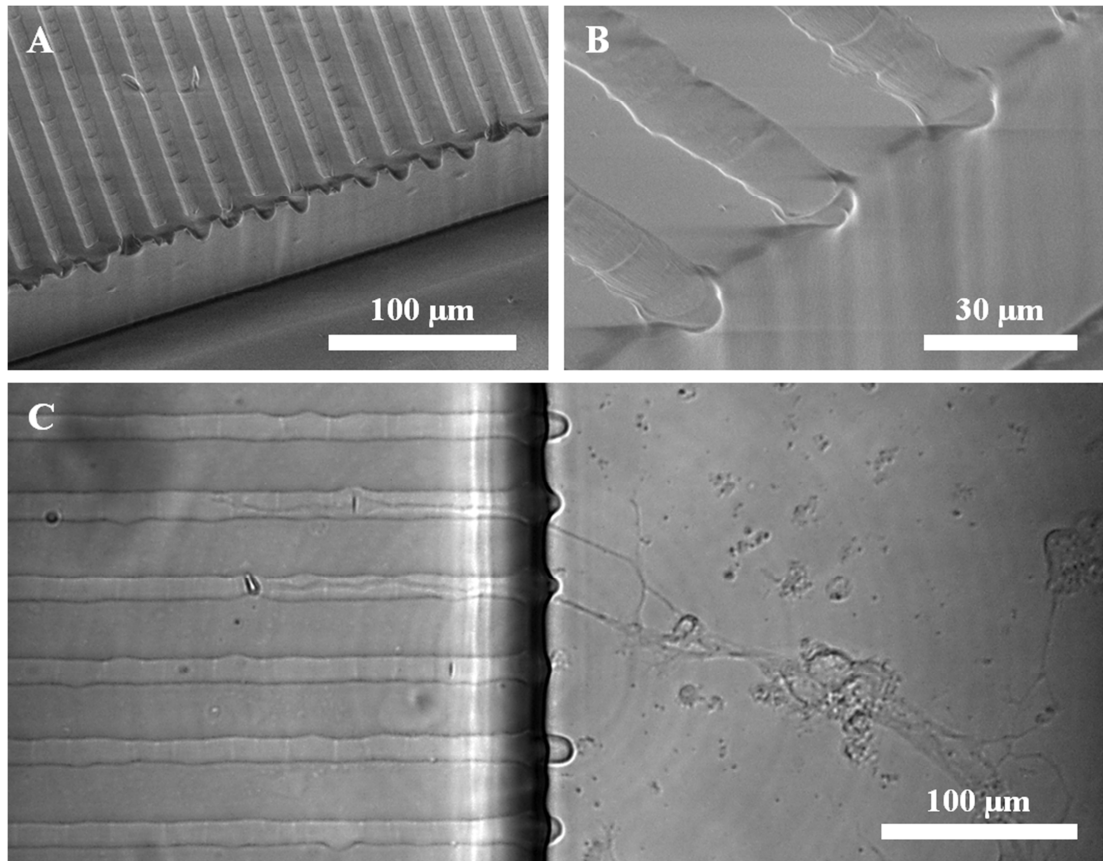
**Figure 3.3 Images of PDMS structures from casts of SU8 on AZ templates. (A) An SEM image of the resulting PDMS structure between the culture chambers. It can be seen that the majority of channels are well defined but closed at the end of each channel. (B) An SEM image of three microchannels shows the curved profile of the reflowed AZ resist. These channels appear to be blocked by PDMS that has seeped between the AZ and SU8 of the master. (C) A bright field image of the PDMS barrier (left) and the cell culture chamber (right). Irregular PDMS lips can be seen suggesting potentially blocked channels; however, a neuron can still be seen to extend processes towards and through two of the microchannels, navigating around the blockage.**

An alternative method of fabricating the master was to use SU8-3010 for the thin layer. SU8-3035 was found to bond consistently with the thin layer of SU8-3010 leading to higher quality results (Figure 3.4). The final PDMS casts were found to have well defined channels using the SU8 on SU8 method.
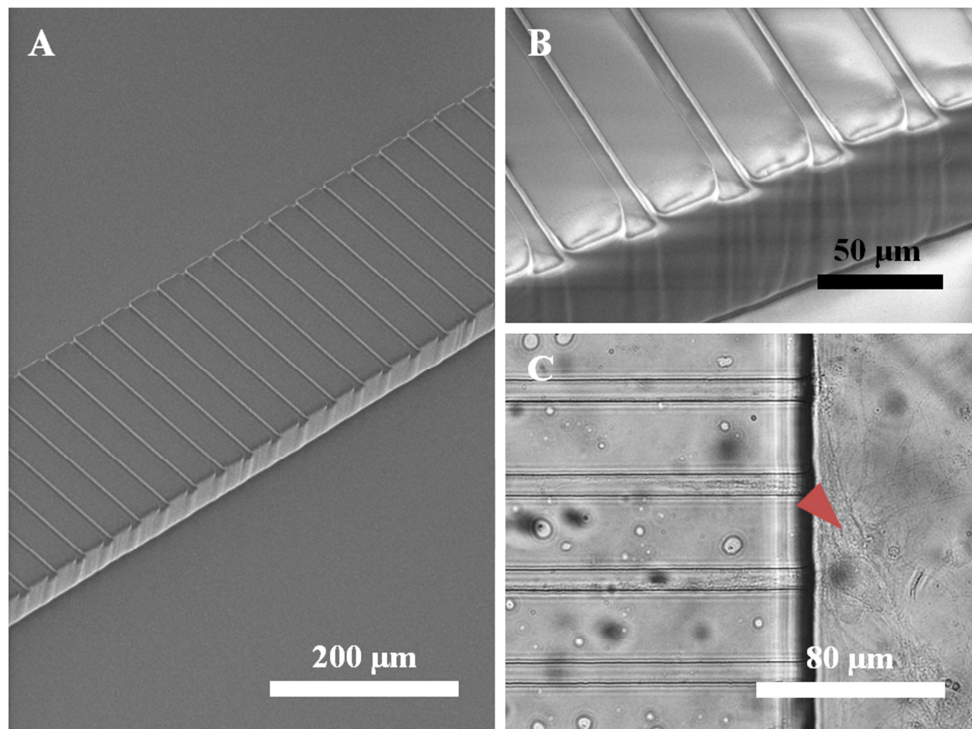
**Figure 3.4 Images of PDMS structures from casts of SU8 on SU8 templates. (A) An SEM image of the resulting PDMS microfluidic barrier between two larger cell culture chambers. (B) A close inspection of the barrier reveals regular, well defined microchannels with no blockages. (C) A bright field image of a neuron in the culture chamber, growing processes into multiple microchannels of the barrier.**

## 3.2.3. Cell Culture

Cells were cultured in the devices in a very similar manner to standard techniques used routinely for culturing hippocampal cells on coverslips [106], [107], (see Section 2.3.2. The preparation of the cell culture to be loaded into the device is based on the standard preparation of primary hippocampal cultures with the only difference being the final concentration of cells used, $3$–$5\times10^6$ cells/mL compared to $3\times10^5$ cells/mL. The change in concentration was required so that a similar density of cells would be achieved. Under normal conditions for culturing cells on coverslips, typically 100 µL of cell suspension is plated onto a glass coverslip, resulting in a droplet that has a height of around 1 mm. In comparison, the microchannels used here have a height of ~100 µm, so a much larger concentration of cells is required to achieve a similar spacial density when initially plating cells in microfluidic channels. Once loaded into devices the media was half refreshed every 2–3 days. The resulting

cultures varied in terms of cell distribution throughout the network (Figure 3.5), as some cultures formed networks with uniformly distributed neurons while others formed clusters with larger bundles of neurites between them. In both cases individual cells were observable during $Ca^{2+}$ imaging (see Section 2.4) and so both were used for experiments. In all cases there was a clustering of cells near the open wells, as the residual seeding volume results in an unusually high cell concentration in these areas.
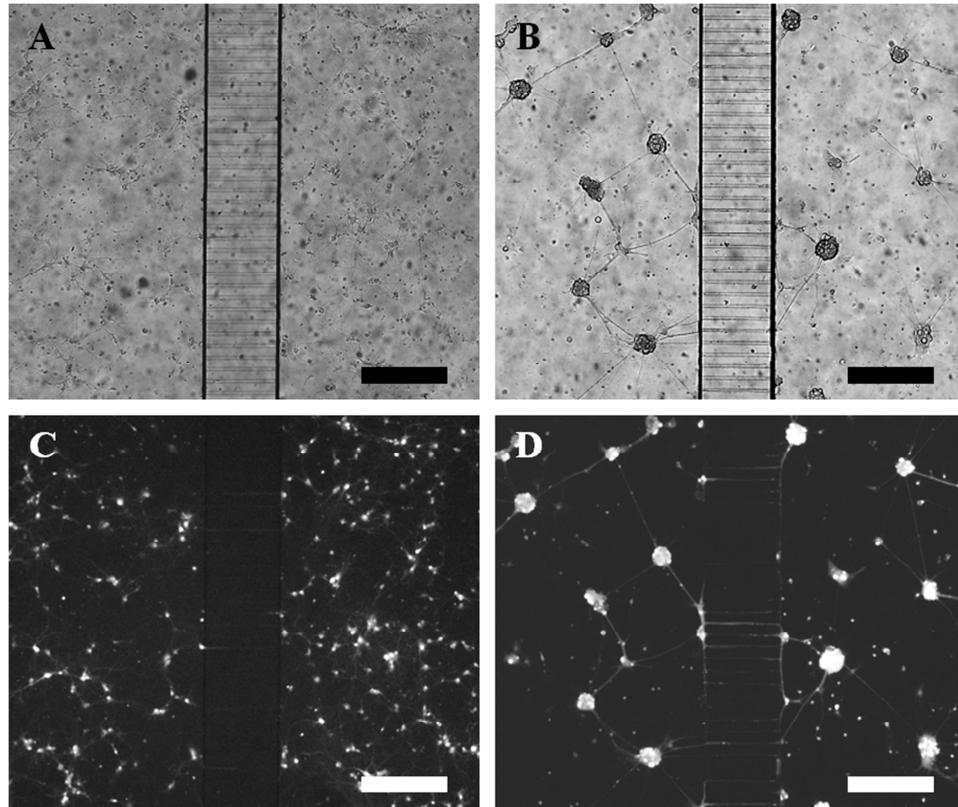


**Figure 3.5 Bright field and $Ca^{2+}$ images of cultures grown in devices. (A, B) Bright field images of typical cultures that were distributed (A) and clustered (B). (C, D) The respective fluorescent images of the bright field examples taken during $Ca^{2+}$ imaging experiments help to visualise the cell distribution, where individual cells are still apparent in the clusters (D). *(A–D) Scale bars: 300 μm.***

## 3.3. Immunocytochemistry

Immunofluorescent staining was used to determine whether cells cultures grown within the devices were forming synaptic connections with the co-culture through the microfluidic barrier. Primary hippocampal cultures were grown within devices for 3-17 DIV prior to staining as described previously (see Section 2.4). The stained

cultures were used to determine whether cell processes grow through the microchannels and that synaptic mechanisms are indeed present.

### 3.3.1. MAP2 and β-III-Tubulin

To image neuronal growth within the device, neuronal processes were stained with two different primary antibodies, MAP2 (1:5000 dilution) is a somatodendritic marker and β-III-tubulin (1:500 dilution) as a neuron specific cytoskeleton marker revealing the entire structure of the neuron including the axon. Appropriate secondary antibodies (1:200 dilution) were used to reveal the corresponding primary antibody (Figure 3.6).
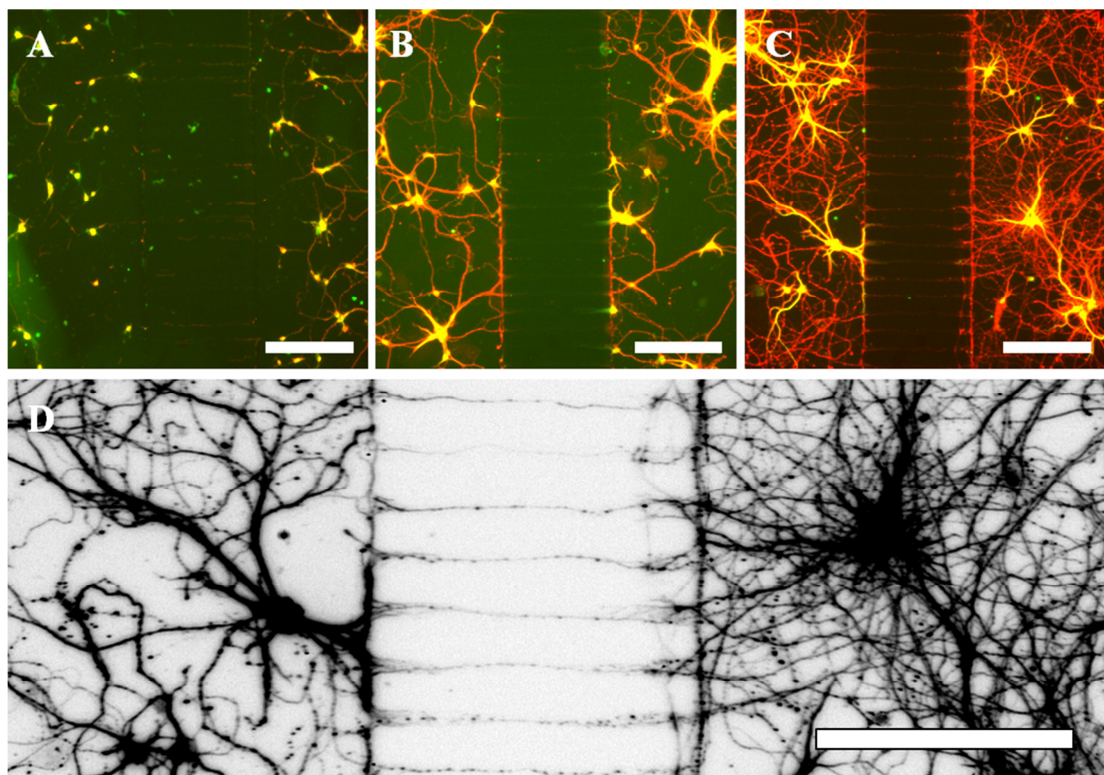


**Figure 3.6 Immunofluorescent staining of MAP2 and β-III-tubulin. Cultures were grown and fixed on 3 DIV (A), 6 DIV (B), and 10 DIV (C). These were stained for MAP2 (neuronal somatodendritic marker – green) and β-III-tubulin (neuronal cytoskeleton marker – red). Some projections can be seen entering the microchannels after 3 DIV, with most of the microchannels containing projections by 10 DIV. (D) An enhanced image of the 10 DIV culture clearly shows cell processes that have grown through the microchannels and connected with the opposing culture. *(A–D) Scale bars: 200 μm.***

The staining reveals that neuronal processes begin to grow within the microchannels from an early stage (at least 3 DIV). Later, 6–10 DIV, it is possible to see that the majority of channels are filled with cell processes. Axons are distinct from dendrites in the images as they stain positive for β-III-tubulin (shown in red) and negative for MAP2 (green), consequently axons appear red while dendrites will stain positive for both β-III-tubulin and MAP2 and therefore appear yellow. Both axons and dendrites are shown to enter the microchannels, however in the centre of the microchannel predominantly axons (red processes) are observed. It was not possible to determine the origin of processes within the microchannels from these images. The locations of synapses were also impossible to determine from the staining. While these figures show that neuronal processes cross the microchannels and appear to link to the opposing culture, it is not clear whether the mechanisms for synaptic communication develop within the microchannels in a similar manner to synapses formed outside of the microfluidic channels.

## 3.3.2. β-III-Tubulin and Synaptophysin

Staining for the synaptic marker, synaptophysin (1:500 dilution), reveals the location of the synaptic vesicles which are required for synaptic communication [108]. This immunocytochemistry was performed along with staining for β-III-Tubulin (1:500 dilution), as it is a marker for the whole neuron including the axon where the synaptic vesicles should be most abundant. To reveal these structures the primary antibodies used were for synaptophysin and β-III-Tubulin with corresponding fluorescently labelled secondary antibodies (1:200 dilution) used to identify the primary antibodies (Figure 3.7).
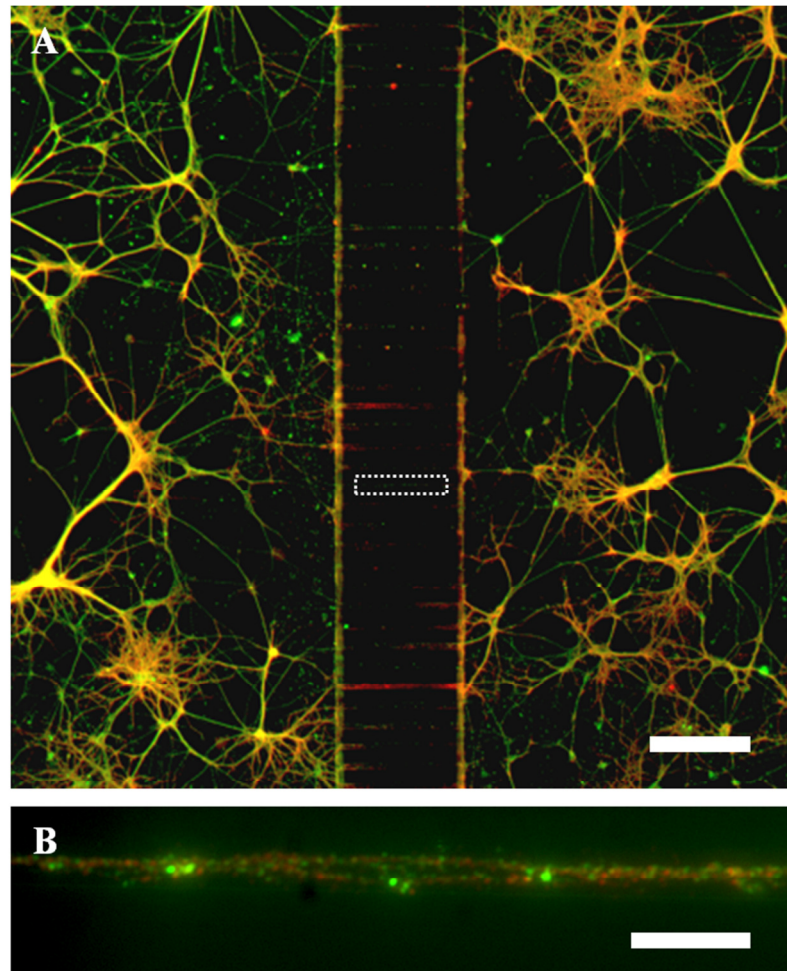
**Figure 3.7 Immunofluorescent staining of β-III-tubulin and synaptophysin. (A) A low magnification (5×) image shows that synaptophysin (synaptic vesicle marker: red) is co-located (yellow) with neuronal bodies and processes (β-III-tubulin: green) in both cultures. (B) A high magnification (50×) image of the microchannels shows that synaptophysin is also present within the connections between cell cultures.** *(A) Scale bar: 200 μm. (B) Scale bar: 20 μm.*

From the imaging of the microchannels it is possible to see that synaptic vesicles are present and co-located with neuronal processes. This suggests that the mechanisms for synaptic communication are in place and that synapse formation may be occurring within the microchannels themselves. The presence of synaptophysin is similar to that found outside of the microchannel which suggests that synapse formation is not being impeded by the constraints of the microchannels.

While it is important to confirm the presence of synapse formation, it is also essential to show that these synapses are functional. To confirm the synapses are indeed

functional, a live cell experiment is required to show dynamic communication between the two cultures.

### 3.3.3. β-III-Tubulin and GFAP

The primary hippocampal cultures used are expected to grow both neurons and astrocytes. In the CNS, astrocytes help to form and regulate the blood-brain barrier and, while providing trophic support for the neurons, are increasingly thought to play a role in synaptic communication [27], [109]. To visualise how astrocytes were growing alongside the neurons within the chambers, cultures in the devices were stained with the astrocytic marker GFAP (1:500 dilution) and β-III-tubulin (1:500 dilution), and the corresponding secondary antibodies (1:200 dilution) (Figure 3.8).
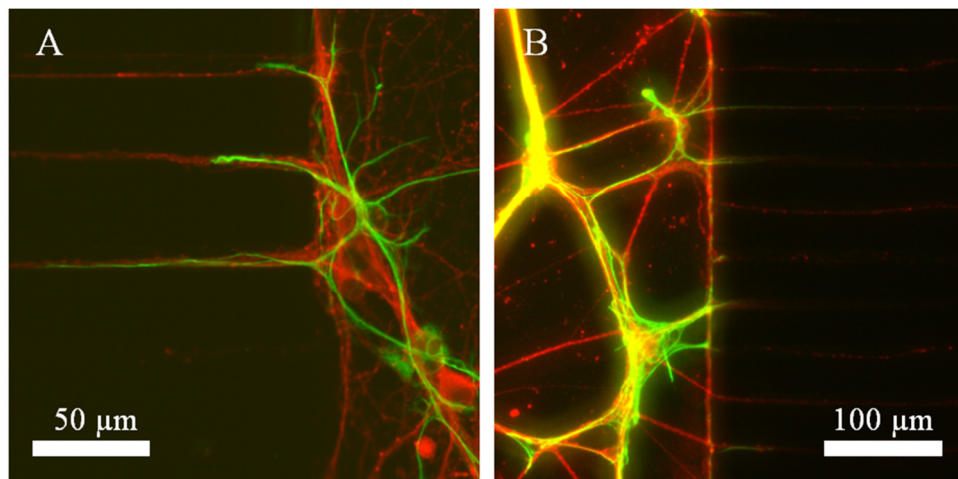


**Figure 3.8 Immunofluorescent staining for neurons and astrocytes. (A & B) Devices from 2 different cultures were stained to detect the presence of both neurons (β-III-tubulin – red) and astrocytes (GFAP – astrocyte marker – green). Astrocytes were found to have grown alongside the neurons as shown and even extended processes into the microchannels. However, no astrocytes were found to extend far enough to reach the other culture and no astrocyte cell bodies were found within the microchannels themselves.**

From these images it can be seen that astrocytes grow alongside neurons and send projections into the microchannels. Out of the microchannels imaged, none of the astrocytic processes were seen to completely traverse the gap to the other side.

## 3.4. System Characterisation for Functional Testing

While the immunocytochemical staining strongly suggests that the two cultures are synaptically connected, it cannot reveal if these connections are functional. To show functionality, a live cell assay using $Ca^{2+}$ imaging was developed to show that one cell culture can alter the activity of the other using synaptic activity. This assay needs to be validated to show that there is no cross contamination in the system that may confound experimental outcomes.

## 3.4.1. Experimental Procedure

To determine that the synapses between the cultures were functional, one culture would be chemically stimulated while the activity of the other was monitored via $Ca^{2+}$ imaging. For a chemical to be selectively applied to a single culture it is required that one culture is fluidically isolated from the other. If there is a pressure difference between chamber A and chamber B, then the resulting fluid flow between the chambers should be sufficient to fluidically isolate one chamber from the other. This hypothesis is tested and found to be valid in Section 3.4.3.

The experimental procedure consisted of: fluidic isolation of chamber A from chamber B, indirect application of vehicle (direct to chamber B), indirect application the chemical stimulus (KCl or glutamate, direct to chamber B), and final direct depolarisation using KCl (direct to chamber A, Figure 3.9). The fluidic isolation of side A from side B causes chemicals that are applied to side B to only stimulate the side B culture. This *indirectly* stimulates the side A culture via synaptic transmission. Chemicals applied to side A *directly* stimulate the side A culture, however the chemicals will act both *directly* and *indirectly* on side B due to the nature of the fluidic isolation.
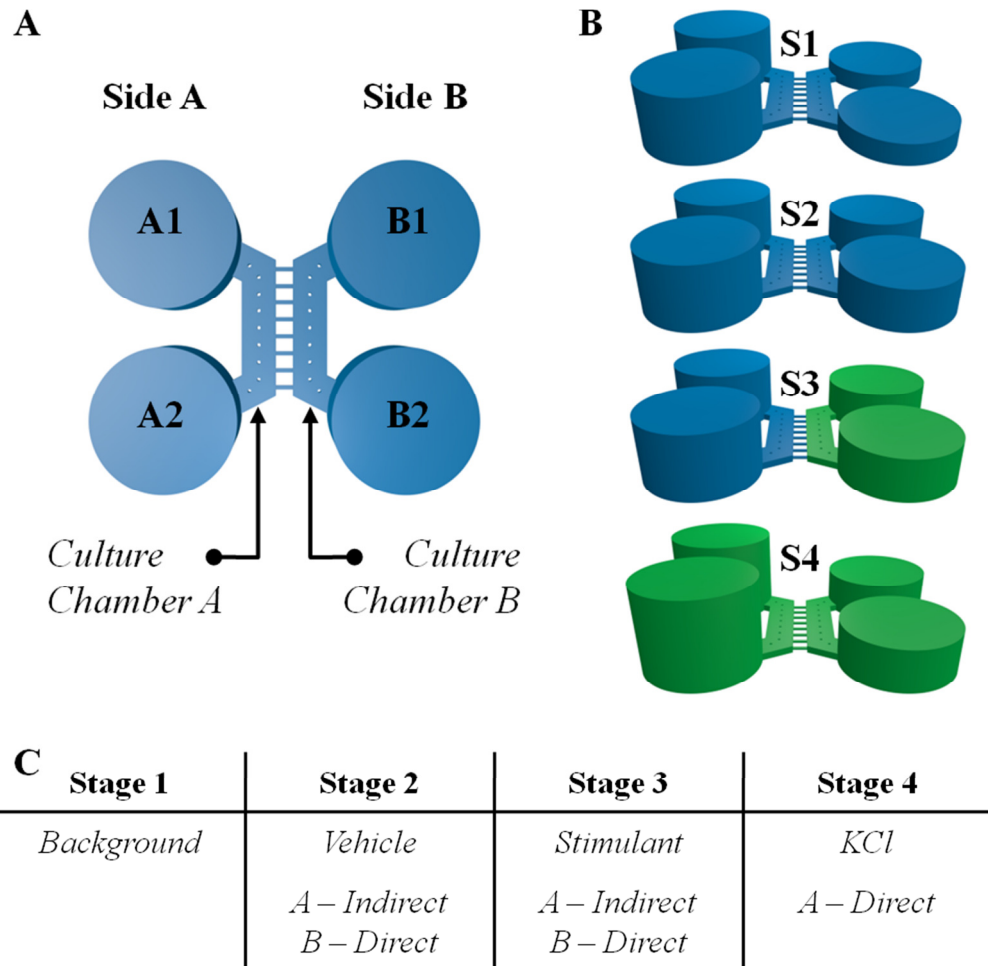
**Figure 3.9 Ca$^{2+}$ imaging experimental setup. (A) The layout of the device and labelling of the open wells and chambers is provided as it is practical to have a reference for each side and individual open wells. (B) Each stage of the experiment is shown with external solution (blue) and a stimulant (KCl – green), along with a brief table describing what takes place (C). Stage 1 (S1); the open wells are loaded with different volumes to fluidically protect side A from chemicals applied to side B. Stage 2 (S2); a volume of external solution (vehicle) is applied to B1 followed by B2. Stage 3 (S3); half of the solution is removed from B1 and B2, followed by an application of the stimulant (KCl or glutamate). Stage 4 (S4); finally A1 and A2 are loaded with a volume of KCl to directly depolarise the neuron on side A. A continuous recording was taken throughout the experiment with each stage lasting approximately 5 minutes.**

## 3.4.2. Electrical Equivalent Model

To determine how fluid flows through the microchannels it is possible to create an electrical equivalent circuit of the fluidic network [110]. This provides a simplification of the complex fluidic dynamics that occur and so close approximations of fluid flows can be determined. The fluid dynamics of microfluidic

systems are well documented as being analogous to electrical circuits [110]. This can aid in the analysis of such fluidic networks due to the established mathematical techniques used in circuit analysis, Table 1.

**Table 1 Extracts from a comparison of microfluidic networks and electric circuits** [110]

| Microfluidics | | Electronics | |
|---|---|---|---|
| Volumetric flow rate | $Q$ / m$^3$·s$^{-1}$ | Electric current | $I$ / Amp |
| Pressure drop | $\Delta P$ / Pa | Voltage drop | $\Delta V$ / Volt |
| Hydraulic resistance | $R_h$ / Pa·s$^3$·m$^{-1}$ | Electric resistance | $R_e$ / $\Omega$ |
| Hydraulic capacitance | $C_h$ / m$^3$·Pa$^{-1}$ | Capacitance | $C$ / F |
| Hagen-Poiseuille's law | $\Delta P = Q \cdot R_h$ | Ohm's law | $V = I \cdot R_e$ |
| Law of mass conservation (at a node) | $\sum Q_n = 0$ | Kirchhoff's current law (at a node) | $\sum I_n = 0$ |
| Law of energy conservation (in a closed path) | $\sum \Delta P_n = 0$ | Kirchhoff's voltage law (in a closed path) | $\sum V_n = 0$ |
| Fluid flow source | | Current source | |
| Pressure source | | Voltage source | |

The overall structure of the device can be broken down into separate fluidic components that can be analysed individually (Figure 3.10). These consist of open reservoirs and fluidic conduits for storing and directing fluid flow.

The open wells act as reservoirs for storing fluid, where the geometry confines the fluid, and a volume of fluid results in a pressure at the bottom of the well. The volume in a cylinder is $V = \pi r^2 h$, where having height creates a pressure due to gravity, $P = \rho g h$. These are solved to give Equation 2.

$$P = \frac{\rho g}{\pi r^2} V \qquad \qquad \textbf{Equation 2}$$

$$C_h = \frac{dV}{dP} \qquad \qquad \textbf{Equation 3}$$

Where $P$ is the pressure at the bottom of the well, $\rho$ is the density of the fluid, g is the acceleration due to gravity, $V$ is the volume of fluid contained in the well, and $r$ is the radius of the well (for a cylindrical well). The open wells act as capacitors with a

constant for hydraulic capacitance, $C_h$, where $dV$ is the change in volume experienced for a given change in pressure $dP$, Equation 3.

The culture chambers and microchannels are conduits for fluid flow which will passively resist fluid flow due to an inherent hydraulic resistance. The resistance depends on the fluid viscosity and the dimensions of the chamber itself. Each culture chamber acts as a single resistance between two open wells, while the central microchannels of the barrier act in parallel between the two culture chambers. There are two formulae for cuboidal channels, depending on the shape of their cross-section. The culture chambers and microchannels both have a rectangular cross-section, where their height, $h$, is less than their width, $w$, and so Equation 4 can be used [111]. For channels with a square cross-section, where $h = w$, Equation 5 should be used [111]. Both of these equations make several assumptions about the fluid flow and channels they are characterising. It is assumed that the channel is straight with a constant cross-section and that fluid in contact with the surface does not move (no-slip boundary condition). It is also assumed that through the channel there is pressure driven, laminar flow of an incompressible Newtonian fluid, generally referred to as Poiseuille flow [111].

$$R_h = \frac{12\mu L}{wh^3 \left(1 - 0.630\frac{h}{w}\right)}$$ **Equation 4**

$$R_h = \frac{28.4\mu L}{h^4}$$ **Equation 5**

$$R_{Par}^{-1} = \sum_{i=1}^{N} R_i^{-1}$$ **Equation 6**

Where $R_h$ is the hydraulic resistance, $L$ is the length of the channel, and $\mu$ is the dynamic viscosity of the fluid flowing through the channel. For multiple individual resistances acting in parallel, $R_i$, their combined resistance $R_{Par,}$ is given by Equation 6.

These equations allow the fluidic components to be represented mathematically which is useful in the understanding of how fluid will flow in the system and allows for experimental setups to be optimised. From the dimensions of the well, the capacitance of each chamber is calculated as $5.12 \times 10^{-9}$ m$^3$·Pa$^{-1}$ (assuming a perfect

cylinder or radius 4 mm). Chambers were assumed to have a constant rectangular cross-section and the fluid is assumed to be water as it is the main solvent for all of the solutions used during experiments. Using Equation 4, the chamber resistances are approximated as $7.36 \times 10^{10}$ Pa·s·m$^{-3}$. The resistance of a single microchannel is approximated to be $1.56 \times 10^{15}$ Pa·s·m$^{-3}$, with the combined parallel resistance of the 200 microchannels being $7.80 \times 10^{12}$ Pa·s·m$^{-3}$.
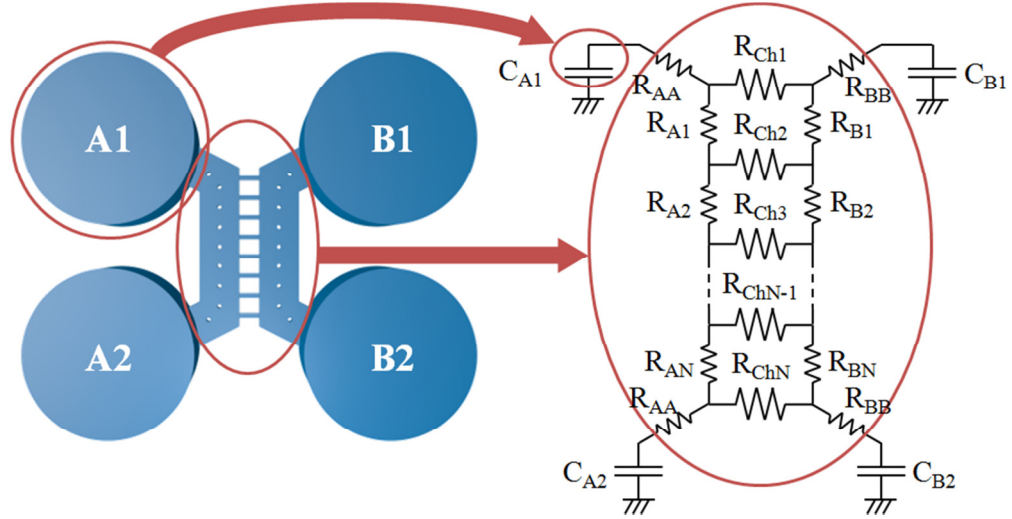


**Figure 3.10 The fluidic system converted into an electrical equivalent circuit diagram. In the conversion each well becomes a capacitor and each channel becomes a resistor. For each well (radius ≈ 4 mm) the calculated capacitance is $5.12 \times 10^{-9}$ m$^3$Pa$^{-1}$. For resistor network $R_A$ and $R_B$ the resistance is calculated to be $7.36 \times 10^{10}$ Pa·s·m$^{-3}$. For each central microchannel $R_{Ch}$, the resistance is $1.56 \times 10^{15}$ Pa·s·m$^{-3}$, with the combined resistance of 200 channels in parallel being $7.80 \times 10^{12}$ Pa·s·m$^{-3}$.**

There will be some discrepancies between the calculated ideal values of the system and the physical parameters of the system. The actual resistance of the chambers will be slightly larger than the calculated value due to the periodic pillars used to support the structure. The capacitance will also be non-linear due to the slight variability of the well diameter throughout the height of the well.

The capacitors (open wells) can be charged by increasing the volume of fluid it contains, creating a potential energy source. The flow of fluid between two open well pressure sources, $P_1$ & $P_2$, through a channel of resistance $R_h$ is given in Equation 7.

$$Q = \frac{\Delta P}{R_h}$$

**Equation 7**

Chapter 3

Where $Q$ is the volumetric flow rate between the two source and $\Delta P$ is the pressure difference between $P_1$ and $P_2$, $\Delta P = P_2 - P_1$. This allows the flow rate through the culture chamber to be determined by knowing the dimensions and the volumes of fluid in both connected open wells.

Noting that the fluidic resistance of the central microchannels is two orders of magnitude greater than the hydraulic resistance of the side chambers, the system can be assumed to operate in 2 independent modes. The first mode of operation is that of quickly equalising any pressure difference between two wells that are directly connected by the culture chamber. The second mode is that of two directly connected wells from one side slowly equalising with the directly connected wells of the other side via the central microchannels. For each mode of operation it is possible to estimate the amount of time it takes to equalise a volume difference between two sources connected to a microchannel.

Over time the system continually changes as the flow of fluid will alter the volumes stored in each open well and thus affect the flow of fluid. Without active intervention the system tends to a condition of equilibrium where there is no sustained fluid flow. The volume exchanged between open wells over time, $V(t)$, when connected via a chamber of resistance $R_h$, will follow and exponential decay to an equilibrated volume with the connected well, Equation 8.

$$V(t) = \frac{\Delta V}{2}\left(1 - e^{-\frac{2t}{R_h C_h}}\right)$$
**Equation 8**

Where $\Delta V$ is the initial volume difference between the two open wells at $t = 0$. A measure of how long it takes the system to reach equilibrium is given by the time constant based on Equation 8, $\tau = \frac{RC}{2}$. This is the time taken for the system to reach $(1 - 1/e) \approx 63\%$ of the equilibrium condition given a step change in volume. Comparing the time constants of the two operational modes, it can be seen that the second mode takes a greater duration of time to equalise a volume difference than the first mode (Figure 3.11).
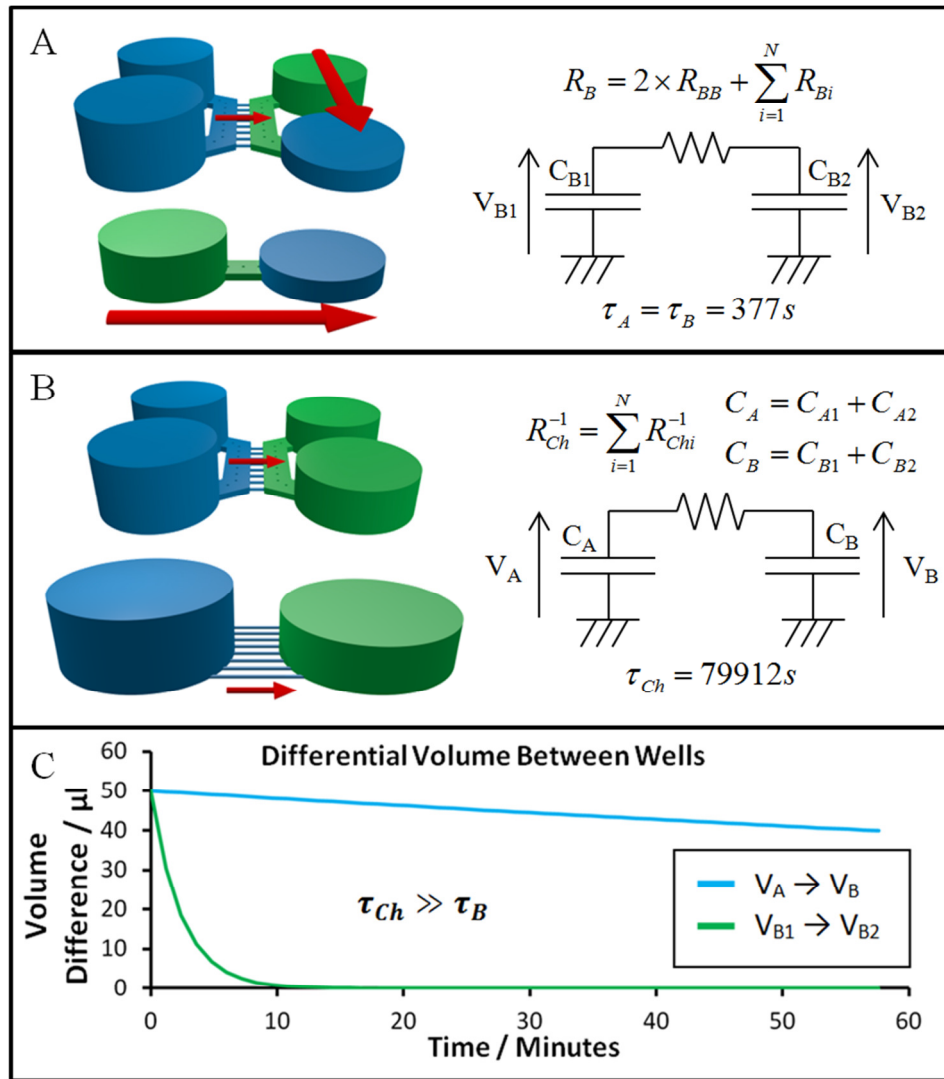
**Figure 3.11 There are two modes of operation that are apparent within the system. (A) When the volumes in the wells of one side are dissimilar, the majority of the flow will work to equilibrate this inequality before working to equilibrate the inequality between sides. As the resistance of the central microchannels is significantly greater than the resistance of chamber B, $R_{Ch} \gg R_B$, the effect of the central microchannels on fluid flow can be ignored over short durations. This results in an equilibration time constant of $\tau_A = \tau_B = 377$ seconds. (B) Once each side has equilibrated, the potential difference between the two sides remains and is now the only source of flow. With a time constant of $\tau_{Ch} = 79912$ seconds, its effects can be ignored over short durations. (C) A graph of the calculated volume difference between wells over time highlights the difference in time constants. In general, because $\tau_{Ch} \gg \tau_B$, the effects of fluid flow between sides can be ignored for $t < \tau_B$ and do not become significant until t approaches $\tau_{Ch}$.**

## 3.4.3. Characterisation of Mass Transfer Within a Device

It is essential to rule out the possibility of cross contamination between the culture chambers to determine if any results observed are due to synaptic stimulation. This can be done by replicating the experiment using a fluorescent probe instead of a non-observable stimulant in addition to building a computational model of the system. The completed device contains four open wells as part of the structure for use in loading and feeding the cells with culture medium. The volumes in these wells are related to the pressure at each end of the culture chamber and are used to manipulate the fluidic flow both within each chamber and between the two chambers. While these have now been modelled, it is necessary to understand how the time dependent factors act on fluid flow and diffusion within the system to confine an added chemical to a single chamber.

## 3.4.3.1. Single Isolated Applications of Fluorescein

The experimental conditions to be used were evaluated using the fluorescent probe fluorescein. This molecule has a diffusion coefficient of $4.9–6.4 \times 10^{-6}$ $cm^2s^{-1}$ [112], [113], which is smaller than both glutamate, $7.6 \times 10^{-6}$ $cm^2s^{-1}$ [114], and potassium ($K^+$), $19 \times 10^{-6}$ $cm^2s^{-1}$ [115]. For the purpose of evaluation, $K^+$ is the worst case scenario as it has the highest coefficient, making it the most able to rapidly diffuse and contaminate the opposing culture. However, as it is not practical to experimentally determine the diffusion of $K^+$ within this system, fluorescein was used initially to evaluate a computational model. Once validated, the computational model can then be used to determine if smaller more diffusive molecules like $K^+$ contaminate the opposing culture during the timescale of the experiment.

The principle of fluidic isolation has been characterised in the past [80], however as each device fabricated will vary in terms of dimensions achieved it is appropriate to demonstrate this for any new system used. By applying the experimental conditions (Figure 3.9), which include a fluidic isolation condition, to a device using fluorescein instead of the chemical stimulant, it is possible to tell if the applied substance is isolated to one chamber (Figure 3.12).
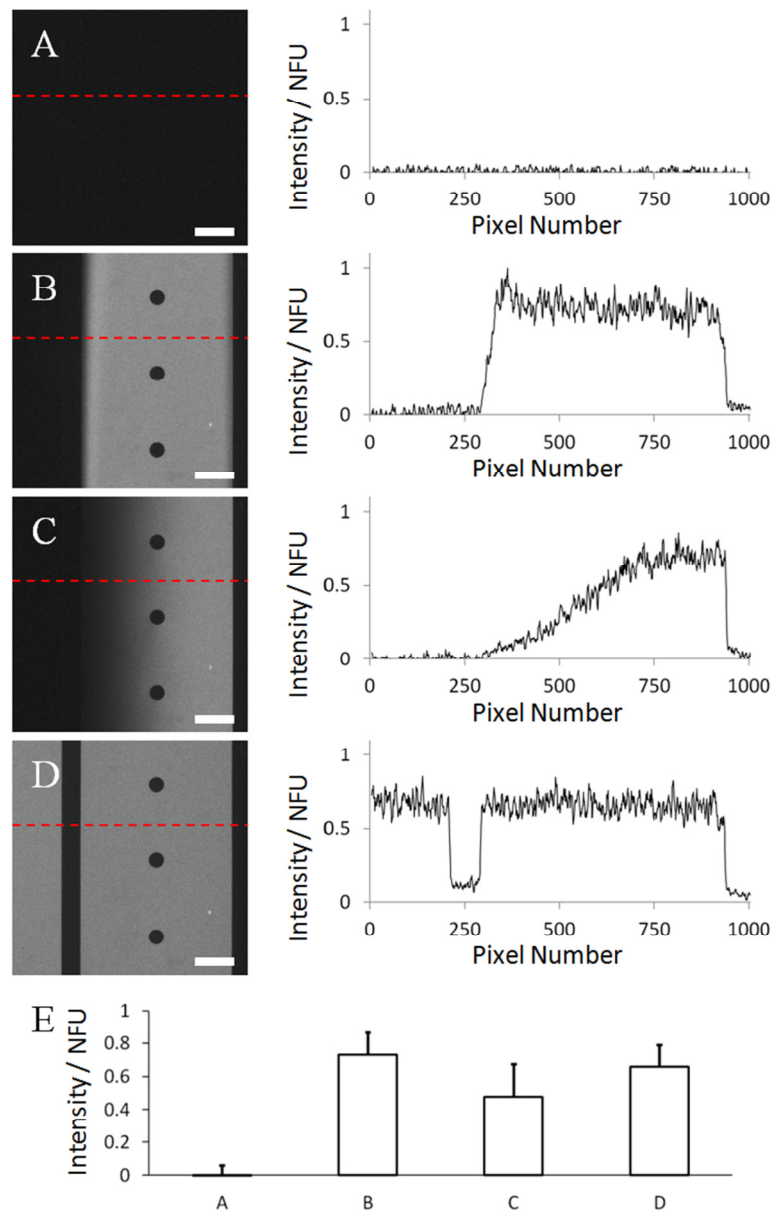
**Figure 3.12 Experimental evaluation using fluorescein. A device loaded with water was used to characterise the dispersion of fluorescein over time. (A) Initially sides A and B were filled respectively with 150 μL and 50 μL of water. (B) At t = 0, 50 μL of fluorescein (30 μM) was added to well B1, followed by well B2. (C) t = 5 minutes, the device was recorded for the typical duration of a chemical application to side B. No fluorescence was observable in side A during this time. (D) Finally, both chambers were flooded with fresh fluorescein (at a final concentration of 15 μM). The images taken during the experiment have higher noise than usual. This is because of the magnification (2.5×) required to show an entire channel and the low intensity of illumination used to reduce photobleaching of the fluorescein. (E) The average fluorescent intensity found within chamber B at each stage of the experiment. The intensity was taken as an average of the fluorescent intensity over the central 80% of the channel width and can be used to compare the total concentration of fluorescein in the chamber at different stages of the experiment. *(A–D) Scale bars: 500 μm.*

While this experiment shows that fluorescein is indeed contained within the microchannels it does not directly resolve the question of how other chemicals, which are not fluorescently detectable and have different molecular weights, will diffuse between the chambers. To address this issue, the system must be modelled and the model must be compared to the equivalent experiment with fluorescein to determine its validity. After this, it is reasonable to assume that, if the diffusion coefficients for other compounds are known, the advection-diffusion conditions for other chemicals, including $K^+$ and glutamate, can be estimated with an acceptable degree of accuracy.

## 3.4.3.2. Computational Model

Once the pressures that occur within the system were calculated, they were used to provide the constraints and parameters for a 3D computational model. Solving Fick's law in 3 dimensions, to calculate diffusive transport, whilst taking into account the Navier-Stokes equation, for fluid flow due to pressure differences, is too complex to solve manually and so a computer simulation is required. A model of the system was provided courtesy of Dr Michele Zagnoni. The model was initially used to simulate the diffusion of fluorescein under standard experimental conditions which could be compared to the actual experimental results (Figure 3.13). When it was confirmed that the model could reliably predict fluorescein's concentration, it was used to model the diffusion of the smaller particles of $K^+$ ions which has a greater diffusion coefficient.

Each simulation, of fluorescein and $K^+$, was conducted under the parameters that would be used in an actual experimental test. These focussed on the conditions that would occur during KCl or glutamate applications. Immediately prior to chemical application, side A wells would hold 150 µL each, while side B would hold 50 µL each. The stimulus would be applied in 50 µL applications to well B1 and B2. This results in a 50 µL/well volume difference between the two sides which is designed to maintain the fluidic isolation of side A from side B. It is this condition that must be evaluated with fluorescein and simulated for $K^+$ ions.
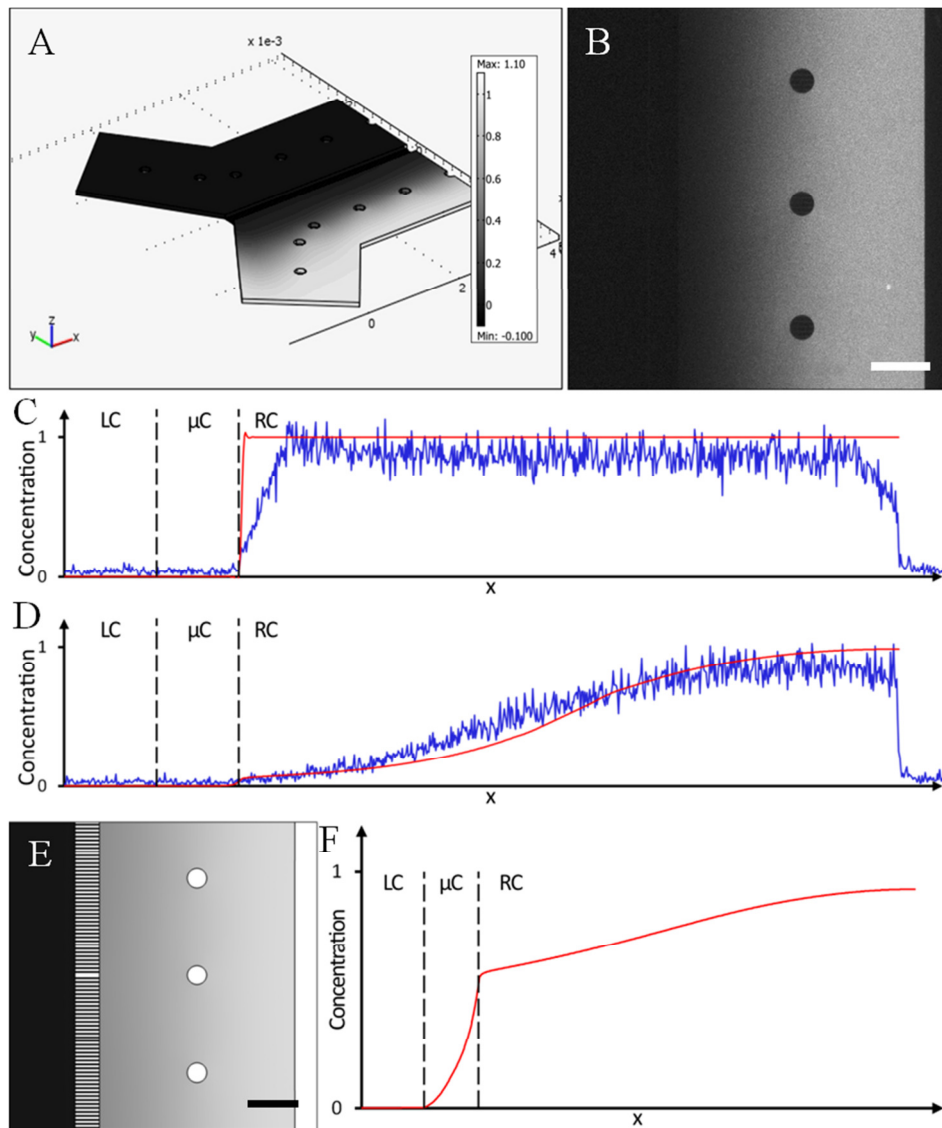
**Figure 3.13 The computer simulation confirms that K$^+$ ions do not contaminate the fluidically protected culture.** Initially a simulation of fluorescein was performed as it can be compared to experimental results to validate the computer model. **(A)** An image of the 3D computer model that can be used to solve the combined effects of fluid flow and diffusion. **(B)** A fluorescent image taken from 5 minutes into a mock experiment using fluorescein. **(C)** The concentration profile predicted by the simulation (red line) compared to the measured profile from the experiment (blue line) at t = 0 s. **(D)** The concentration profile predicted by the simulation (red line) compared to the measured profile from the experiment (blue line) at t = 300 s. The simulation provided a good fit to the experimental data, with correlation coefficients between each simulation and the corresponding experimental data of 0.93 **(C)** and 0.97 **(D)**. **(E)** This allowed for a simulation to be run for K$^+$ ions, t = 300s. **(F)** The corresponding concentration profile in the simulation of K$^+$ ions shows that there is no leakage of K$^+$ ions through to the opposing chamber after 300 seconds. *(B, E) Scale bars: 500 μm.*

From the simulations it is possible to see that there is a slight discrepancy between the simulation and the experimental results at the edge of the microchannel (Figure 3.13C). This is due to the non-uniform signal from the fluorescent experiment and could be caused by non-vertical channels walls, or residual fluid flow within the channel which would have a similar parabolic flow profile. Overall, the simulated concentration of fluorescein still closely matches the concentration obtained in practice with a satisfactory degree of accuracy. This validates the model and so it is suitable for predicting the diffusion of other compounds in similar experimental conditions. The simulation of $K^+$ showed that there is no diffusion from one chamber to the other within the time period of the experimental procedures used. Therefore, cross-contamination of both glutamate and $K^+$ is not possible during the experiment and any subsequent rise in activity in the indirectly stimulated side must be due to synaptic activity.

## 3.5. $Ca^{2+}$ Imaging

Initially cells were loaded with Fluo4 AM (5 µM) for 45 minutes as described previously (see Section 2.5.1), and the experiment was carried out using an inverted microscope with a 5× objective. The fluidic barrier was introduced by loading each well with 150 µL of external solution, then withdrawing 50 µL from both wells B1 & B2. Once these conditions were established, a background recording of the cell activity was recorded for 5 minutes. To apply a new solution to side B, 50 µL was withdrawn from B1 & B2 then 50 µL of the new solution was added. This was performed once with vehicle and then once with either high KCl solution or glutamate with a final concentration of 25 mM or 100 µM respectively. For each solution applied to side B, the concentration used was double the target concentration due to the residual volume that results in a 2× dilution. For high KCl, the target concentration was 25 mM and so 45 mM was applied (as the external solution already contains 5 mM). Similar concentrations of KCl are widely used to stimulate and depolarise neurons [57], [86], [116]. For Glutamate, the target concentration was 100 µM and so 200 µM was applied. After each new solution a maximum of 5 minutes was allowed for the resulting cellular activity to be recorded. Finally,

50 µL of KCl (100 mM) was added to A1 & A2, with the recording terminating shortly after.

The initial application of vehicle to B1 & B2 is required to provide a kinetic stimulation. Any sudden change in volume stored in a well will create a temporary pressure gradient that induces a fluid flow. This fluid flow potentially can cause a sheer stress on the cells which may induce synaptic activity that would falsely be represented as chemically induced activity. As such, a solution change of vehicle provides a control to which other solution changes can be compared against. This means that the chemical action of a solution change can be separated from the physical action of changing the solution itself.

This experimental procedure was carried out on an epifluorescene inverted microscope. A 5× objective was chosen to provide a field of view (FOV) of approximately 2.68 mm$^2$ (Figure 3.14). This area encompassed a region of both A & B culture chambers which contained 100–200 cell bodies.
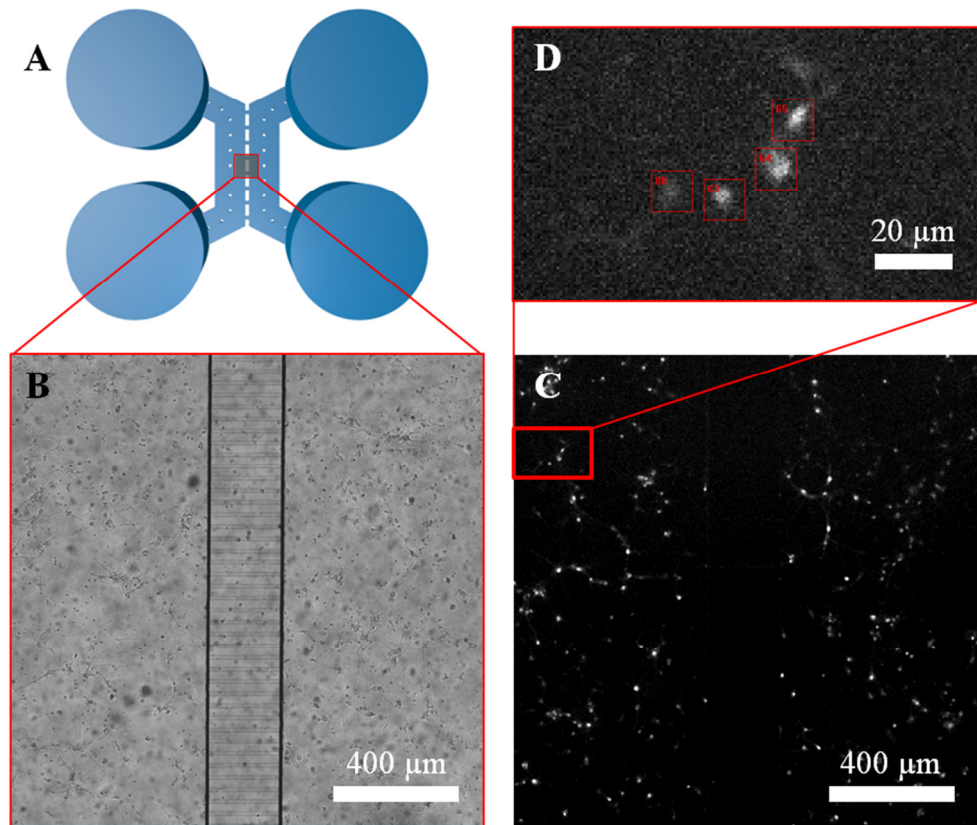
**Figure 3.14 Image processing for the Ca$^{2+}$ imaging experiments. (A, B) The field of view (FOV) during the Ca$^{2+}$ imaging experiments was centred on the central barrier of the device so that cells on both sides would be recorded. A low magnification was used to record the experiments so that a large population of neurons on both sides could be observed. (C) A typical fluorescent image (corresponding to *B*) would show approximately 200 cells on each side of the barrier. (D) A magnified area of the FOV shows regions of interest that were manually selected to contain individual cell soma.**

## 3.5.1. Experimental Analysis

From the time-lapse images recorded for each experiment, a range of cells could be identified on either side of the barrier. To analyse each cell's individual signal over time, several regions of interest (ROIs) were selected using the image capture software Andor Solis. The resolution of each image was such that only the larger structures of the cell bodies were clearly identifiable, while cell projections were not generally visible. Each ROI contained a bright-spot in the image corresponding to a single cell. The minimum size for a ROI was 50 pixels (approximately 10×10 μm) where an average of all the pixels provided the fluorescent intensity value for that individual ROI. An ROI was also selected containing no visible cells or processes to provide a background signal.

Once the image sequences were reconstructed as an array of intensity values, they could be processed as time dependant signals and displayed as graphs for analysis (Figure 3.15). The signals were conditioned by subtracting the background signal to remove fluctuations in the background illumination. The first 20 frames of each signal were averaged to provide the baseline for that signal and the entire signal was divided by this baseline to normalise the starting values to 1. The normalisation of the signal means that any increase in fluorescence is proportionate to the starting value and is measured in normalised fluorescence units (NFU). Once normalised, the signals were then filtered (moving average filter, window size 11) to reduce the apparent noise in the signal.
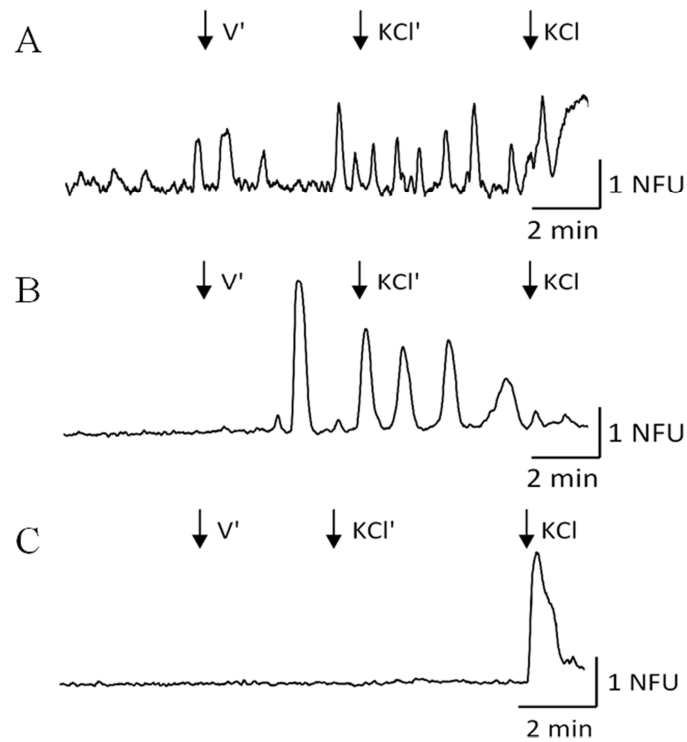
**Figure 3.15 Example signals retrieved from during Ca$^{2+}$ imaging. Intensity signals were processed to remove background fluctuations, filtered and normalised to achieve clear time varying intensity signals. The representative traces shown are taken from side A, featuring the background signal, the response to indirect vehicle (V'), the response to indirect potassium (KCl'), and the response to direct potassium (KCl). (A) A typical neuronal signal, identified by its response to direct potassium, whose activity increases when potassium solution is applied to the opposing culture. (B) Other signals that were clearly active but did not respond to direct potassium were classed as astrocytes. (C) Some cells did not respond to indirect stimulation but were responsive to direct potassium solution suggesting that they were neurons that did not connect to the other culture. These disconnected neurons act as internal controls and show that the culture on side A were not directly stimulated by solutions applied to side B.**

The formatted signals could then be categorised and the number of Ca$^{2+}$ events during each part of the procedure counted. Signals were categorised as neuronal or astrocytic by analysing their response to the final direct application of KCl. Neuronal cells, which depolarise in high KCl solutions, respond with a large influx of Ca$^{2+}$ resulting in a sharp increase in the corresponding fluorescent signal from which the cell does not typically recover if the stimulus is not removed. Cells that did not respond to the direct application of KCl were classed as astrocytes as previously

described [67], [106]. Signals that did not have any significant $Ca^{2+}$ events were discarded along with signals where the cell type could not be determined.
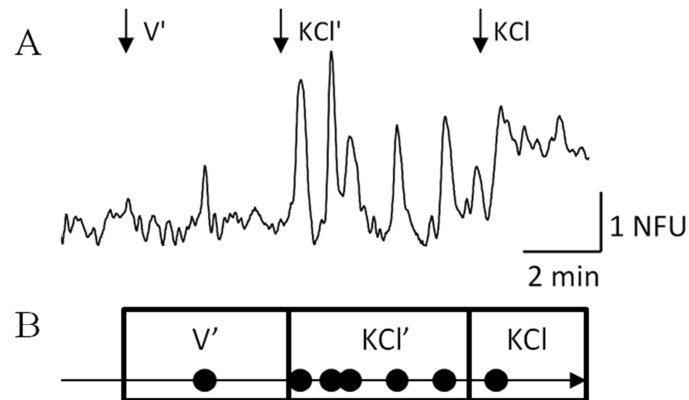


**Figure 3.16 Example of $Ca^{2+}$ event selection. (A) An example trace from a neuron where the $Ca^{2+}$ events are shown in the dot trace below (B). Each $Ca^{2+}$ event must have a rise in fluorescent intensity of at least 0.5 normalised fluorescence units (NFU) above the baseline, and once identified is validated before being counted in the region that it was found. This allows the number of events in each region to be compared with each other.**

Events from each signal were then counted using a routine written in MatLAB (see Section 2.5.3). A $Ca^{2+}$ event was defined as an increase in fluorescence from the baseline level of greater than 0.5 NFU that occurred during a measurement period of the experiment. This threshold was set so that only large $Ca^{2+}$ fluctuations were counted and also to eliminate noise. Some cells appeared to generate spontaneous $Ca^{2+}$ events prior to any applied treatment, however these tended to be smaller than the events during treatments and in most cases were below the defined threshold for $Ca^{2+}$ activity. As there was difficulty in analysing the initial spontaneous activity, prior to the control conditions being applied (indirect vehicle application), it has not been included in the following analysis. Multiple events were possible within a single measurement period if the signal had sufficiently recovered before the subsequent event occurred (Figure 3.16). Once the event details were collected they were grouped into each region of the experiment and counted to determine if there was a significant change between different regions of the experiment. Due to slight variations in the duration of each experimental period the event frequency per region was used, rather than the number of events per region, to statistically analyse the

change in events between regions. To find the event frequency the number of events was divided by the duration of the period.

To determine if there was a significant change in event frequency between periods a statistical comparison test was used on all of the events collected for each experiment type. As the event frequency was stored on a cell by cell basis it was possible to performed a paired student's t-test comparing the vehicle to the stimulus.

To aid in the signal formatting, processing and analysis several scripts were written in MATLAB (see MATLAB Files – Processing Ca2+ Imaging, page 161). Some scripts assisted the user to perform manual categorisation of the signals and event selection. The event selection script allowed the user to select any region in the graph that could possibly be an event and then later the event was automatically removed if it did not comply with the defined attributes of an event. The grouping of events, validation and analysis of event frequency were carried out automatically via the customised scripts.

## 3.5.2. Experimental Results

A range of different chemical stimuli were used to obtain multiple sets of results. The stimulations used were high KCl solution (25 mM) and glutamate (100 μM). Tests using KCl and glutamate as the stimulation on side B provided response increases on side A. All experiments in devices were performed using at least 2 different culture dates.

Experiments were carried out as described using 4 devices which provided an average of 97 functional cells per device that could be identified from side A. As the main purpose of the device was to assess changes in the general activity of a culture, all of the cells visible in a given field of view were analysed to give the best impression of the $Ca^{2+}$ activity of the culture. Of these cells, 235 were classed as neurons and 152 as astrocytes depending on their response to direct KCl. Both the astrocytes and the neurons were found to have an increased rate of $Ca^{2+}$ events after KCl stimulation of the cells in side B (Figure 3.17). The average $Ca^{2+}$ event frequency for neurons after indirect vehicle stimulation was $3.54 \times 10^{-3} \pm 0.33 \times 10^{-3}$ events/second which rose to $5.01 \times 10^{-3} \pm 0.45 \times 10^{-3}$ events/second after indirect KCl

stimulation, an increase of 41% (n = 235, p < 0.001). While the experiment was initially designed to monitor neuronal activity it was noted that astrocytes also exhibited $Ca^{2+}$ events which increased in frequency between indirect vehicle stimulation, $2.47\times10^{-3} \pm 0.37\times10^{-3}$ events/second, and indirect KCl stimulation, $5.36\times10^{-3} \pm 0.51\times10^{-3}$ events/second, a rise of 117% (n = 152, p < 0.001). The astrocyte population only included active astrocytes as all non-active cell signals were discarded.
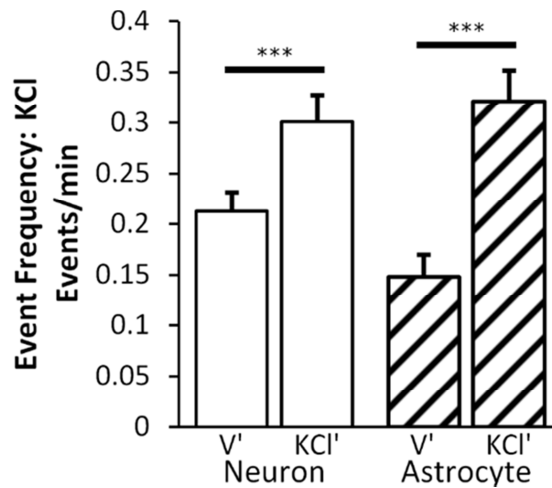


**Figure 3.17 Effects of indirect potassium stimulation (25 mM) on neurons and astrocytes. The bar chart shows the average frequency of $Ca^{2+}$ events observed in each cell from side A during the chemical stimulation of side B using vehicle (V') and then potassium (KCl'). Both neurons (n = 235) and astrocytes (n = 152) showed a significant increase in the number (and therefore frequency) of $Ca^{2+}$ events following KCl stimulation of side B.**

To test the system with a physiologically relevant stimulus, glutamate was used to antagonise cells in side B. Glutamate is one of the main excitatory neurotransmitters and, being water soluble, can replace the $K^{+}$ that was previously used without modification to the rest of the experiment. A total of 3 cultures in devices were tested using this method with 286 neurons and 57 astrocytes being identified from the subsequent signal analysis (Figure 3.18). From side A the neuronal response to vehicle was $1.68\times10^{-4} \pm 0.38\times10^{-4}$ events/second which rose to $8.64\times10^{-4} \pm 0.8\times10^{-4}$ events/second upon indirect glutamate stimulation. This rise was found to be significant, 415% (n = 286, p < 0.001), and was greater than the increase from KCl stimulation. The initial activity of the astrocytes was $4.70\times10^{-4} \pm 1.4\times10^{-4}$ events/second, and rose 83% to $8.6\times10^{-4} \pm 2.1\times10^{-4}$ events/second (n = 57, p < 0.05).
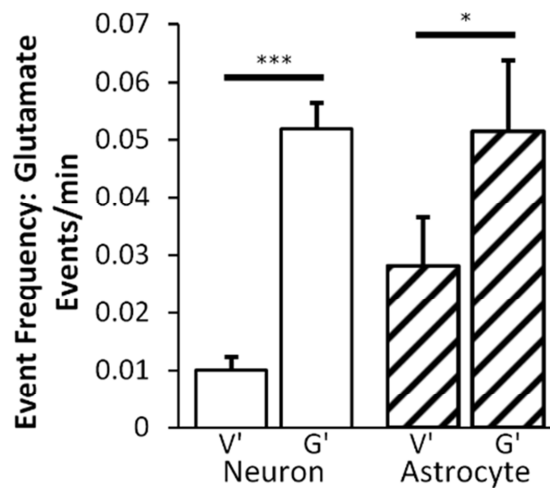
**Figure 3.18 Indirect glutamate (100 μM) stimulation produced a significant increase in activity of both neurons and astrocytes. The bar chart shows the average frequency of Ca$^{2+}$ events observed in each cell from side A during the chemical stimulation of side B using vehicle (V') and then glutamate (G'). Both neurons (n = 286) and astrocytes (n = 57) showed a significant increase in the number (and therefore frequency) of Ca$^{2+}$ events following KCl stimulation of side B.**

## 3.6. Discussion

This chapter has described the development of a microfluidic device for testing synaptic communication between neuronal co-cultures. There was considerable work required to refine the fabrication of devices and cell culture process to reliably produce appropriate cell cultures. Once these production processes were improved, it was necessary to determine that the devices were suitable for monitoring synaptic communication. Initial immunocytochemical staining revealed the connections that formed between co-cultures grown in separated chambers. However, this does not confirm functional connectivity and so a live cell experiment was developed to show synaptic communication between the co-cultures.

### 3.6.1. Cell Culture

Cells were found to grow well within the device and formed processes in the microchannels between cultures from as early as 3 DIV. It could be seen from the immunofluorescent imaging that the cultures were connected by neuronal cell processes in the majority of the microchannels. These neuronal processes were shown to contain synaptic vesicles that are found in presynaptic terminals and are

commonly used to show the formation of stabilised synapses [74], [108], [117]. This suggested that synaptic communication was possible within the microchannels themselves. The general growth of the neurites is similar to other microfluidic devices used for neuroscience research that use the same structure [84], which found neurites would traverse the channel even with the absence of neurons on the other side.

It was also shown that astrocytes can grow into the microchannels. Some sources have shown neurons and astrocytes to be motile and may pass between chambers in their systems which contain a similar microfluidic barrier [74]. However, here no cells were observed in the process of migrating between channels during any of the staining performed. The astrocytes observed here were only found in the vicinity of neurons and while they did extend processes into the microfluidic channels, they did not appear to traverse the barrier.

## 3.6.2. Functional Communication

While immunofluorescent staining for synaptophysin is strongly suggestive of stable synapse formation it cannot confirm the functionality of these synapses. As such it was necessary to show functionality via another mechanism and so a new test was devised. $Ca^{2+}$ imaging is a common *in vitro* technique for monitoring the functional activity of neuronal cells [67], [89], [106]. As an optical microscopy technique it is well suited for use in optically transparent microfluidic devices used here and elsewhere [86], [89] in situations where standard electrophysiology techniques are difficult to apply. A key advantage of $Ca^{2+}$ imaging is that it allows for the simultaneous capture of many signals, as demonstrated here, which increases the throughput of the device [64], [66]. It is difficult to directly compare the $Ca^{2+}$ imaging results from this chapter to conventional cultures that are plated on coverslips. Typically $Ca^{2+}$ imaging is performed on coverslips under perfusion [67] which may affect the spontaneous activity of cells since the extracellular fluid is constantly being refreshed. Additionally, it is difficult to stimulate sub-populations of cells on coverslips especially if there is not perfusion applied to the system.

The functional test used here essentially involves monitoring a culture's functional activity while chemically stimulating a synaptically connected, fluidically isolated, co-culture. The results show that upon indirect stimulation, using KCl (25 mM) and glutamate (100 µM), the $Ca^{2+}$ activity increases. This is a significant change in the number of $Ca^{2+}$ events, from that which occurs spontaneously during indirect vehicle application, to the increased number of events during indirect chemical stimulation. The only mechanism by which this change is possible is synaptic communication between the co-cultured networks.

High $K^+$ solution and glutamate both can directly stimulate cells but work using different mechanisms. High extracellular $K^+$ directly depolarises the cell by changing the concentration gradient of $K^+$ between the inside and the outside of the cell. Normally, during an action potential, once a neuron is depolarised (due to the influx of $Na^+$ ions) it is subsequently repolarised by the efflux of $K^+$ ions [2]. Under normal conditions $K^+$ leaves the cell due to the concentration gradient that is maintained by the sodium-potassium pumps. However, under high extracellular $K^+$ conditions the altered chemical concentration gradient prevents the net movement of $K^+$ ions from leaving the cell. Indeed, the higher extracellular concentration of $K^+$ will cause the concentration of $K^+$ inside the cell to increase and force the cell to remain depolarised. Alternatively, glutamate is a neurotransmitter and so will act on iGluRs and mGluRs present in the cell membrane. These receptors are naturally occurring mechanisms for initiating action potentials (see Section 1.1.1.4). While both methods of stimulating neurons were effective, glutamate provides a more pharmacologically relevant means of stimulating neurons.

It was not reasonable to directly compare the response of the cultures to the different treatments of glutamate and KCl. The control conditions for each treatment varied considerably between experiments, from an average of 0.21 events/min for V' in the KCl experiment to an average of 0.01 events/min for V' in the glutamate experiment. This difference between control conditions highlights the variability that can be experienced from culture to culture. It also demonstrates a limitation of the system where, without being able to wash drugs off of the system, it is not possible to test and compare multiple treatments in a single device. The variability between cultures

and experiments is also shown in the ratio of analysed astrocytes to neurons. This may be due to the variations in cultures observed in Figure 3.5, where groups of neurons appear to cluster making it more difficult to identify astrocytes, or it is possibly due to the fact that astrocytes are never directly stimulated for identification. This means that dormant astrocytes may be excluded from the results as all non-active signals are discarded. Both of these factors could contribute to the apparent lower number of astrocytes analysed in the glutamate experiment (Figure 3.18) compared to the KCl experiment (Figure 3.17). The apparent discrepancy between the experiments again highlights the variability between cultures as well as the inability to perform multiple control stages within the current system.

The displayed synaptic connectivity is in agreement with other literature which largely assumes that synapses between connected co-cultures are functional [74], [86], [89]. Other studies that have directly addressed the question of functional synaptic connectivity between co-cultures have been reliant on microelectrode arrays [95], [98]. One limitation of such studies is that they cannot detect any direct response of astrocytes present within the culture. While the primary focus of this study was to prove synaptic connectivity it was found that astrocytic signals were also affected during indirect stimulation. The mechanisms for the astrocytic response have not been investigated here however they are thought to be in response to the increase in neuronal activity as no astrocytes were observed extending across the entirety of the central microfluidic barrier. Astrocytes are able to uptake glutamate and have been shown to express glutamate receptors of their own [21]. Stimulation of the astrocytes may be caused by the local release of neurotransmitters from the indirectly stimulated neurons. With interest in the astrocyte's role of synaptic regulation increasing [30], [118], the ability to detect astrocytic activity is potentially advantageous for future studies using this platform.

## 3.6.3. Fluidic Isolation

A fundamental principle of the live cell experiment devised is that the chemically targeted culture is fluidically isolated from the monitored co-culture. It is essential to prove this within the system to show that cross-contamination of chemicals does not confound the results. Modelling was required to estimate how fluid flow varied over

short term and long term conditions. This was used to inform a computational model that was able to simulate the competing phenomenon of fluid flow against diffusion. The model was validated against an experimental condition using fluorescein and subsequently used to show that $K^+$ would not contaminate the opposing chamber under the same experimental conditions. These results are comparable with other models of similar structures [80], [84], [88] however, as each variation in structure used changes the fluid dynamics of the system, it is necessary to simulate each device individually to ensure its suitability.

## 3.6.4. Evaluation

A microfluidic system, similar to those previously described for neuroscience research, has been used here to validate a new methodology for the evaluation of functional synaptic communication between fluidically isolated hippocampal co-cultures. The device and assay developed show that co-cultures are indeed synaptically connected, and can be quantitatively evaluated. While the system is potentially useful for evaluating drugs or proteins that affect synaptic communication, there are a few drawbacks to the current system described in this chapter. The manual application of fluids during each experiment is difficult to perform and requires a very steady pipetting technique to avoid nudging the device during the recording. The single application of a stimulus is also a drawback as other standard *in vitro* techniques will wash on and off a chemical of interest to evaluate the recovery process of the cells being targeted. Both of these problems may be addressed with an integrated perfusion system which could provide the automated application and washing of cells within the microfluidic system. The development of such an integrated perfusion system will be described in the following chapter, *Chapter 4. Development of a Microfluidic Perfusion System for Compartmentalised Hippocampal Co-cultures.*

Other assays could also be devised to improve the supporting literature of the system described here. The use of tetrodotoxin (TTX) to prevent action potential propagation, by blocking voltage gated $Na^+$ channels, or glutamate blockers to inhibit glutamatergic synaptic transmission would be useful to evaluate situations where synaptic transmission should decrease. Unfortunately this is difficult to perform in

the system used here, where only single applications of compounds can be reliably applied.

Overall the device and methodology developed here achieved its initial purpose of proving that synaptic communication occurs between fluidically isolated co-cultures. In addition, it was found that the system has the ability to detect and monitor astrocyte activity which may be advantageous in future studies of astrocyte-neuron interactions.

# Chapter 4. Development of a Microfluidic Perfusion System for Compartmentalised Hippocampal Co-cultures

The system described in the previous chapter was able to demonstrate functional communication between two isolated neuronal cultures; however, its applications are limited due to the dependence on a single stimulus that has to be manually applied. The inability to wash solutions on and off the cell cultures restricts investigations to single applications of drugs which has limitations if the devices were to be used for drug discovery where ideally a novel compound should be compared to a known drug on the same preparation. To address these problems a perfusion system was developed to allow experiments involving multiple solution exchanges and is described in this chapter.

## 4.1. Introduction to Perfusion

In traditional *in vitro* neuronal culture experiments, a laminar flow perfusion system can be used to apply and subsequently remove a drug of interest from a culture [106], [107]. This allows both the immediate effect on cells to be evaluated as well as the recovery of cells following the removal of the drug. In addition, multiple compounds of interest can be sequentially applied to and removed from the cells in a continuous experiment [67]. In these systems, physiological pathways can be investigated as receptor antagonists may be applied to block specific mechanisms of action [67], [107].

In principle, an ideal perfusion system has to maintain a constant fluidic flow rate and be able to instantaneously switch between different perfusates. Changing perfusates is the primary method of applying drugs during an experiment *in vitro*. This allows different chemicals to be applied to the cells in a controlled manner with their effects observed. Instantaneous transitioning between solutions is desirable to know exactly when a drug is applied and the concentration that produces an effect. Slow transitions between perfusates will result in diffusion between solutions producing a gradual change in concentration. This makes it difficult to determine exactly when a compound reaches the target cells and what concentration produces

the initial effect on the cell. For long term studies, of several hours or days, precise control of changes in perfusate is not often required; however, for short applications of chemical stimulations, precise temporal control of perfusates is required. To reduce transition times between fluids, higher flow rates of perfusate must be used. It is desirable for the fluid flow to be kept constant to avoid changes in shear stress that may damage delicate cell structures. Additionally, to minimise the shear stress on the cells, the flow rate should be as low as possible. However, as this would hinder the production of a fast transition between perfusates, a compromise must be found.

Traditional perfusion setups used for $Ca^{2+}$ imaging and electrophysiological experiments require flow rates of 1–2 mL/min [67], [106], [107], [119] for *in vitro* primary neuronal cultures, or up to 6 mL/min for brain slices [120]. Typical perfusion baths volumes range from 0.5–1 mL and can be even larger for slice chambers [49]. Therefore a change in perfusate will take approximately 30 s to completely flood the bath. This does not take into account any lead time required due to the connected piping that supplies the solutions. The perfusate flow is typically gravity fed, from a series of connected inlets, to the perfusion chamber via a length of tubing [121]. This results in a time delay, of approximately 20–40 seconds, between the switching of perfusates at the inlets to the perfusate reaching the perfusion chamber. While these systems excel at providing laminar flow at a consistent flow rate to cell cultures being assessed, they can use a large volume of fluid during experiments and the perfusion of a drug cannot be located to a single sub-population of cells in the culture. Local perfusion can be implemented within the traditional perfusion setup with the use of a micro-pipette placed near the cell or sub-cellular structure of interest [68], [70]. However, this method can be difficult to implement, requiring significant time and skill to setup precisely, and is generally used to target single neurons or individual neurites, making it a low-throughput system.

In this chapter, the development of a microfluidic perfusion system for neuronal sub-network targeting, based on Chapter 3, will be described. The system has been optimised for $Ca^{2+}$ imaging studies of 1 hour duration, where fast transitions between

perfusates are required. Finally, the system has been evaluated with primary neuronal cultures to ensure that the cells remain functionally viable under perfusion.

## 4.2. Theory of Perfusion between Two Open Wells

For perfusion to be a viable and robust procedure in the current microfluidic system a model was developed and the system was experimentally characterised.

### 4.2.1. Flow Path

In the compartmentalised system described earlier (see Chapter 3), perfusion can either be applied directly to the cell culture chambers via a series of connected inlet and outlet ports, or via ports connected to the open wells. To connect ports directly to the chambers would result in the connected open well volume being stagnant and so might contaminate changes in perfusate by storing drugs and slowly diffusing them back into the solution. Blocking the open wells from the system would reduce the dead volume, however, this also removes the beneficial dampening effect they have on fluid flow within the culture chamber. Alternatively, perfusion via the open wells preserves the dampening effect which reduces the impact of changes in shear stress on the cells in culture. Adding the open wells to the perfusion flow path also prevents the fluid they contain becoming stagnant so that they cannot contaminate changes in perfusate.

Syringe pumps were chosen to drive the perfusion due to the precise control of flow rate that can be achieved, where pressure systems require additional calibration to compensate for the fluidic resistance of pipes and channels. The syringe pumps used also have the ability to both infuse and withdraw fluid as required which is necessary for maintaining perfusion over longer durations.

### 4.2.2. Steady State Flow

As an approximation, the fluidic system comprising the two open wells connected via a culture chamber can be assessed in isolation, without any influence from the microfluidic barrier and the opposing chamber and wells as described earlier (Figure 3.11). When there is an equal volume present in both wells, there is no flow in the microchannel. Since a volume difference between the wells induces a flow in the

chamber, sustaining a constant volume difference will maintain a constant fluid flow over the cell culture (Figure 4.1). This can be achieved by constant injection of fluid to one well and withdrawal from the other.
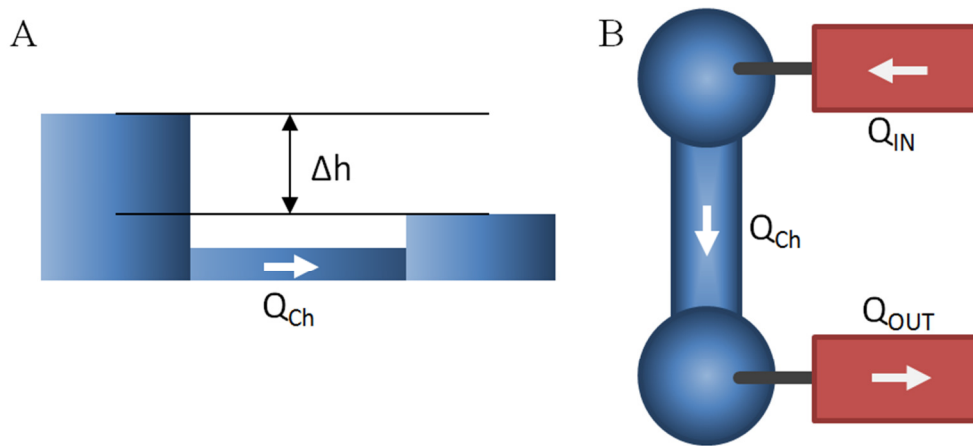


**Figure 4.1 Under steady state conditions perfusion remains constant. (A) A volume difference between open wells results in a potential energy difference that drives fluid flow in the culture chamber, $Q_{Ch}$. (B) By maintaining the volume difference, with syringe pumps, the system will reach a steady state where $Q_{Ch} = Q_{IN} = Q_{OUT}$.**

Initially, if the inlet and outlet well volumes are equal, then applying an equal and opposite flow rate to the inlet and outlet wells will result in a transition to a steady state condition. The expected steady state is achieved when the volume difference between the inlet and outlet well remains constant. This condition results in a constant flow rate induced in the cell culture chamber which is equal to the applied infusion and withdrawal rates to the inlet and outlet wells. This is assuming that the inlet well can hold a sufficient volume to maintain the flow rate to the outlet well.

The relationship between volume difference and induced flow rate depends on the hydraulic resistance of the channels and the hydraulic capacitance of the open wells, Equation 9.

$$Q = \frac{\Delta V}{R_h C_h}$$
**Equation 9**

Where $Q$ is the volumetric flow rate due to volume difference, $\Delta V$ is the volume of fluid maintained between the loading and the draining wells, $C_h$ is the hydraulic capacitance of the well and $R_h$ is the hydraulic resistance of the chamber connecting the wells. Assuming the hydraulic resistance of the channel is identical to the

previously described system ($7.36\times10^{10}$ Pa·s·m$^{-3}$, see Section 3.4.2), it is possible to calculate the volume differences required for open wells of different diameters (Figure 4.2).
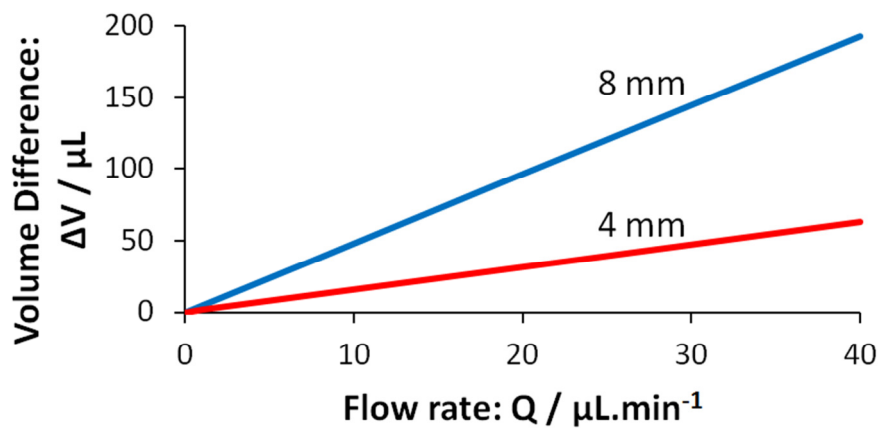


**Figure 4.2 The relationship between flow rate and induced volume difference between open wells in the perfusion system. The graph shows the volume difference between two open wells (of 4 mm or 8mm diameter) for any steady state flow rate, where the wells are connected by a channel with a hydraulic resistance $7.36\times10^{10}$ Pa·s·m$^{-3}$.**

The graph shows the linear relationship between $\Delta V$ and $Q$, from Equation 9, as both $R_h$ and $C_h$ remain constant. This graph is useful for determining the maximum flow rate possible in the device for different well diameters and volumes. The volume of a well, which for a given diameter will be determined by its height (see Section 3.4.2), limits the flow rates possible between the open wells. Since the flow rate was required to be less than 10 µL/min, to minimise the shear stress on cell cultures, only very small volume differences must be maintained to sustain constant perfusion.

## 4.2.3. Perfusate Transitions

Once perfusion is established within the system it is possible to estimate the time taken to change from one solution to another solution. This characterisation is required for exposing cell cultures to different drugs at predictable times. The overall time it takes for a solution transfer to reach the culture chamber depends on the combination of advective transport and diffusive transport.

A newly introduced substance will be transported by both the flow rate of the solution and the concentration gradient that exists between the previous solution and

the new solution containing the substance. It is possible to determine which of these is more significant given the parameters of the system by calculating the associate Péclet number.

## 4.2.4. Péclet Number

The Péclet number is a unitless measure of how diffusion and advection provide transport of substances in solution [122], [123]. It is a product of the Reynolds number and Schmidt number [124], which reduces to Equation 10. A Péclet number, *Pe*, greater than 1 implies that advection is the dominant source of mass transfer, while a value of less than 1 implies that diffusion is dominant.

$$Pe = \frac{LU}{D}$$ 
**Equation 10**

$$D_h = \frac{4A}{P}$$ 
**Equation 11**

Where *L* is the characteristic length of the system which, for fluid flow through a pipe, is given by $D_h$ (the hydraulic diameter of the system), *U* is the average velocity of the solution and *D* is the mass diffusion coefficient for the substance of interest in the fluid. The hydraulic diameter is a function of the cross sectional area of perpendicular to the fluid flow, *A*, and the wetted perimeter, *P*, as shown in Equation 11. In general, if *Pe* >> *1* diffusive transport can effectively be ignored, while at lower *Pe* numbers diffusion will play a more significant role in mass transfer and must be considered.

Using fluorescein as a relevant target molecule, with a diffusion coefficient of $6.4 \times 10^{-6}$ cm$^2$s$^{-1}$ in water [113], it is possible to calculate the Péclet number for a range of flow rates in different structures. The Péclet numbers calculated here are for simplified systems and can only give an indication of what transitions between solutions would be like in practise. The inconsistent dimensions of the system as well as the non-uniform flow profile through the open well cause detailed modelling of the system to be impractical.

For very large Péclet numbers then loading a well purely depends on the time taken to transport fluid across the entire well. This will result in a time delay, lag time, between the switching of solutions and a sharp transition between perfusates being

observed in the culture chamber. For lower Péclet numbers, diffusion will cause the transition between solutions to be gradual and may significantly increase the time taken to switch between 0% and 100% of a solution. Following the lag time, a time constant, $\tau$, can be used to measure the time taken for the perfusate to transition from 0% to 63.2% of the new solution. A period of $3\tau$ is therefore the time taken to reach 95% of the source perfusate's concentration.

## 4.3. Device 1 – A Basic Perfusion System

### 4.3.1. Design

The device implemented in Chapter 3 was initially altered to provide injection of the perfusate solution to one open well and withdrawal from the other (Figure 4.3). Both injection and withdrawal were driven by syringe pumps connected to the device via tubing. This allowed the flow rate to be controlled in one culture chamber (side B) while the other culture chamber was fluidically isolated using a larger volume to prevent diffusion and cross-contamination (see Section 3.4.3).
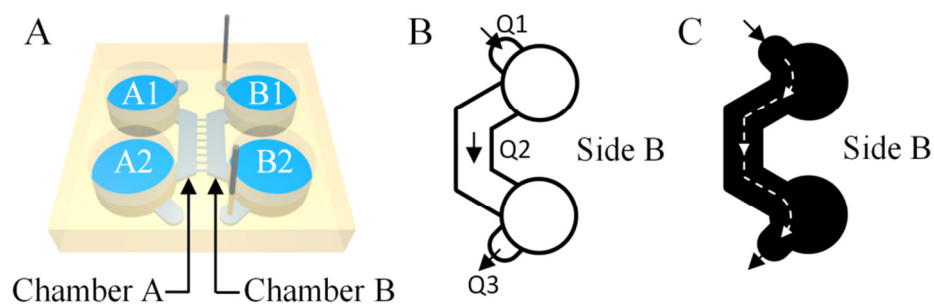


**Figure 4.3 The device was altered to provide perfusion to the culture chamber. (A) The configuration of the device is shown with additional features that allow each well to be connected to a syringe pump. (B) The schematic (not to scale) shows that the loading well *B1* is connected to an infusion source *Q1* and that the draining well *B2* is connected with a withdrawal source *Q3*. Under steady state conditions *Q1 = Q2 = Q3*. (C) An approximate representation of the fluid flow path through *Side B* of the device.**

### 4.3.2. Péclet Number

For the single flow path between the inlet and the outlet port (consisting of: inlet port → loading well → culture chamber → draining well → outlet port), the flow rate is the same for the loading well and the culture chamber. If this flow rate is set to

1 mL/hour (16.7 µL/min), then for the loading well $Pe = 66$, and for the culture chamber $Pe = 400$. The lower $Pe$ number for the loading well suggests that diffusion will have a noticeable effect on the transition between solutions.

## 4.3.3. Characterisation

To determine how the system performs with changes of solution, fluorescein was used to fluorescently monitor a change in solution. Under steady state conditions fluorescein (15 µM) was introduced to the loading well, with a flow rate of 16 µL/min. This was then washed off with water, while the fluorescence across the chamber was recorded (Figure 4.4). A 2.5× objective was used to record the entire width of the microchannel and the excitation intensity was reduced to 2% (FL attenuator, position 6) to minimise photobleaching of the fluorescein solution. The camera settings were adjusted to have an exposure of 0.4 s for a frame rate of 0.5 s, and pixel binning was set to 4×4, as detailed image resolution was not required. The image sequence acquired was analysed using a region of interest (encompassing 80% of the channel width) placed in the centre of the culture chamber directly between two supporting structures. The mean intensity of this region was taken over time and normalised to the maximum intensity observed during the recording.
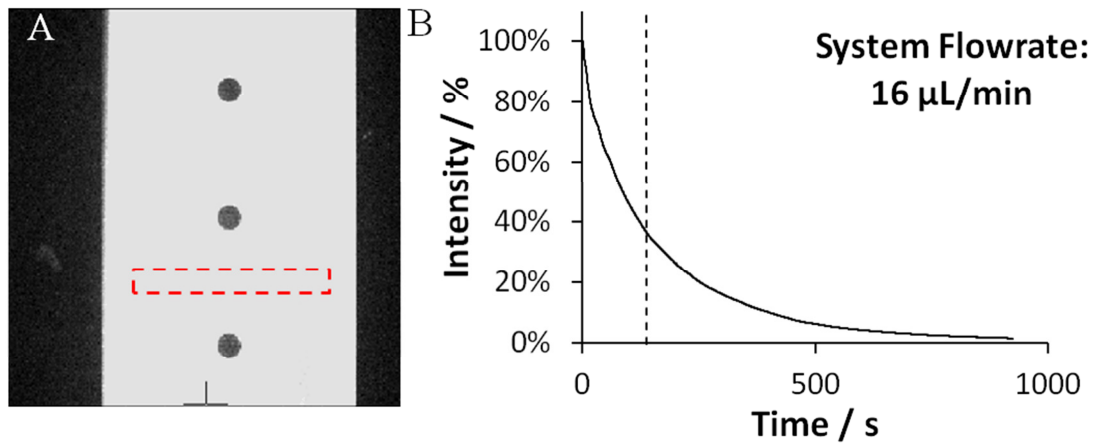
**Figure 4.4 Characterisation of Device 1 using fluorescein. (A) A video of the device undergoing a change in perfusate (from fluorescein to water) was used to measure the change in concentration of fluorescein by measuring its fluorescent intensity. (B) The normalised fluorescent intensity of the region marked in part A (red dotted line) was measured over time to show how the concentration of fluorescein changes. The dotted line (at 137 s) marks the time taken to make 63.2% reduction in the concentration of fluorescein.** *(A) The channel width is 2 mm*

This experiment shows that it is possible to change between solutions using a single flow path within the system and manual changing of perfusates. However, the transition between solutions is long, taking several minutes to change between solutions, which poses a problem given the short applications of drugs required during $Ca^{2+}$ imaging experiments. As a result, this device was not evaluated with cell culture and a new method of perfusion was devised to allow for fast transitions between perfusates in the device.

## 4.4. Device 2 – A Method for Fast Perfusate Exchange

### 4.4.1. Design

To overcome the limitations of having a low flow rate within the open well, a method of fast media exchange was developed to provide a fast flow rate isolated to the open well. An additional outlet and inlet were added to the loading well B1 to increase the flow rate in the loading well whilst maintaining a suitably slow flow rate within the culture chamber (Figure 4.5).
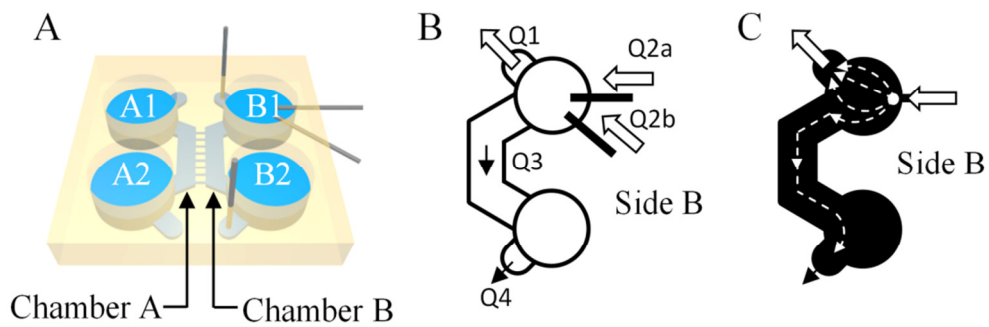
**Figure 4.5 Configuration of the device used to provide fast perfusate transfer. (A) The configuration of inlets and outlets connected to each well is shown, where each inlet/outlet is connected to an individual syringe pump. (B) A schematic (not to scale) of the device shows how multiple inlets feed into the open well, while the previous inlet is now used as an outlet to provide faster medium exchange. In this setup Q2a and Q2b are never active at the same time. (C) An approximate representation of the fluid flow path through *Side B* of the device when one of the inlets is active.**

Under steady state conditions, the sum of the flows into and out of the loading well, B1, must equal zero, Equation 12. This is important to calculate what flow rates were required to have a high flow rate in the well and a low flow rate in the channel.

$$Q1 + Q2 + Q3 = 0 \qquad \textbf{Equation 12}$$

Where $Q$ is the volumetric flow rate at each point labelled in Figure 4.5B. The flow rates for each infusion and withdrawal were determined using this relationship prior to each experiment.

## 4.4.2. Péclet Number

The system is now split into two flow paths (consisting of: inlet port → loading well → outlet port, as well as; inlet port → loading well → culture chamber → draining well → outlet port) so it is possible to produce a higher flow rate in the loading well than in the culture chamber. Setting the loading well flow rate to 200 µL/min gives the loading well a *Pe* number of 830. Reducing the culture chamber flow rate to 4 µL/min, which is more appropriate for cell culture, gives the chamber a *Pe* number of 99. These Péclet numbers are high enough to suggest that diffusion would have little effect on the transitions between solutions.

An additional benefit of the altered layout is that the inlets can pass fluid into the system at a different height than the outlet, allowing for the entire volume of fluid

within the open well to be exposed to the flow path (Figure 4.6). This reduces the volume of stagnant fluid in the system which can alter the time it takes to completely transition between perfusates.
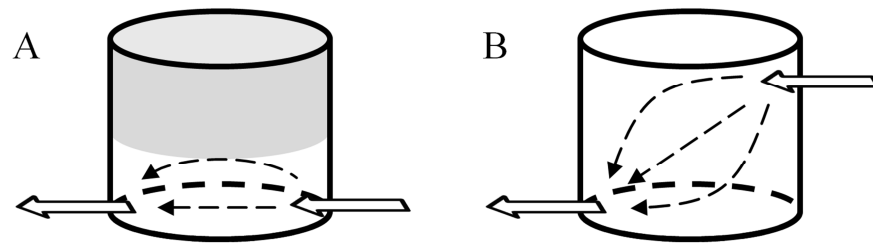


**Figure 4.6 Fluid flow within an open well. (A) Approximate fluid flow within an open well when the inlet and outlet to the well are located on the same plane. A significant volume of fluid (grey region) is not exposed to the flow path and so may adversely affect the transition between perfusates. (B) Approximate fluid flow path within an open well when the inlet and outlet to the well are located on different planes. Here the majority of fluid within the well forms part of the flow path, allowing changes in perfusate to be unaffected by stagnant volumes of fluid.**

## 4.4.3. Characterisation

To evaluate the performance of the altered configuration, fluorescein was used to fluorescently monitor perfusate exchange (Figure 4.7). During this characterisation; the loading well flow rate $Q1$ was set at 200 µL/min, the chamber flow rate $Q3$ & $Q4$ was set at 5 µL/min, and the infusion rate $Q2$ was set at 205 µL/min. Water was used as the initial perfusate to establish steady state conditions prior to fluorescein being washed on for 2 minutes and washed off again with water. The microscope and camera were setup as described earlier in section 4.3.2.
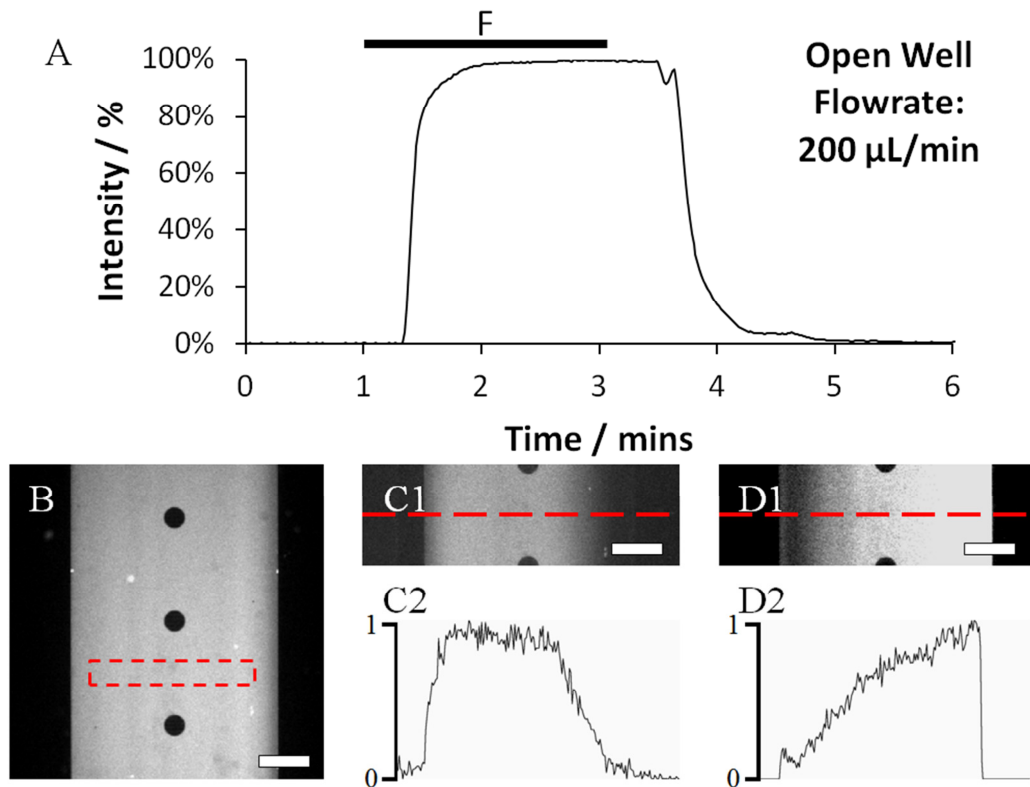
**Figure 4.7 Fluorescein was used to characterise the perfusate transfer times in Device 2. (A & B) A video of the system was taken, where the fluorescent intensity in a selected region (B) was measured to show the change in concentration of fluorescein within the chamber. (A) There is initially a time delay between changing the solutions (at 60 s) and a change in fluorescence (at 80 s). Following the delay there is a sharp change in fluorescence, 0–63.2% in 7 s. There is a similar delay and sharp change in concentration of fluorescein when the perfusate is switched back to water 2 minutes later. For some perfusate transitions, non-uniform loading of the chamber was observed (C1 & D1). The corresponding line plots (C2 & D2) show that in these cases the system was not loaded uniformly across the whole chamber. (B–D) Scale bars 500 μm.**

This alternative method of perfusion successfully demonstrated that fast transitions between perfusates were possible while maintaining a suitably low flow rate within the culture chamber itself. This is expected as the *Pe* numbers for the loading well and the culture chamber were high, 830 and 99 respectively, showing that diffusion does not play a significant role in perfusate transitions. However, the uniformity of the loading profile was inconsistent as the fluorescent perfusate occasionally was biased to loading one side of the chamber (Figure 4.7C & D). This effect is most likely caused by the asymmetrical flow path within the loading well combined with the presence of central supporting pillars that effectively divide the chamber into two

streams. To reduce this effect and improve the uniformity of loading perfusates a new fluidic design was required to alter the flow paths.

## 4.4.4. Experimental Evaluation on Cell Cultures

The main purpose of the perfusion system is to provide the ability to wash drugs on and off neuronal cell cultures in order that assays using multiple applications of the drugs could be carried out in the compartmentalised system. To investigate if the perfusion system affected the viability of neuronal cell cultures, $Ca^{2+}$ imaging was used to measure functional responses to glutamate stimulation. Two syringe pumps were prepared to provide infusion of either external solution or glutamate solution (glutamate 100 µM dissolved in external solution).

Primary neuronal cultures (10–14DIV) grown in appropriate devices were prepared for $Ca^{2+}$ imaging experiments as described earlier (see Section 2.5). During all experiments the culture chambers were kept under constant perfusion with external solution at 4 µL/min, while the loading well flow rate was set to 200 µL/min. After 20 minutes of perfusion, with external solution, cultures were repeatedly stimulated with bursts of glutamate solution lasting 60 seconds duration. Following 3 repeats of glutamate stimulation the neurons were finally depolarised with potassium solution (final concentration 25 mM KCl) to determine if $Ca^{2+}$ signal origins were neuronal. The potassium solution was applied manually via pipette as described earlier (see Section 2.5).

$Ca^{2+}$ imaging recordings, of 3 to 5 minutes duration, were taken featuring a short period immediately prior to each glutamate application. These recordings were processed as described previously (see Section 2.5.3). Between chemical stimulations of cells, no $Ca^{2+}$ imaging was performed to allow the stimulated cells to recover with no fluorescent excitation and to limit the size of the files obtained. During one experiment, the cell culture was perfused whilst sustaining the fluorescent excitation between glutamate stimulations. This was to determine if continuous fluorescent excitation affected cell viability and recovery. The two conditions tested used two devices with cells from the same culture.
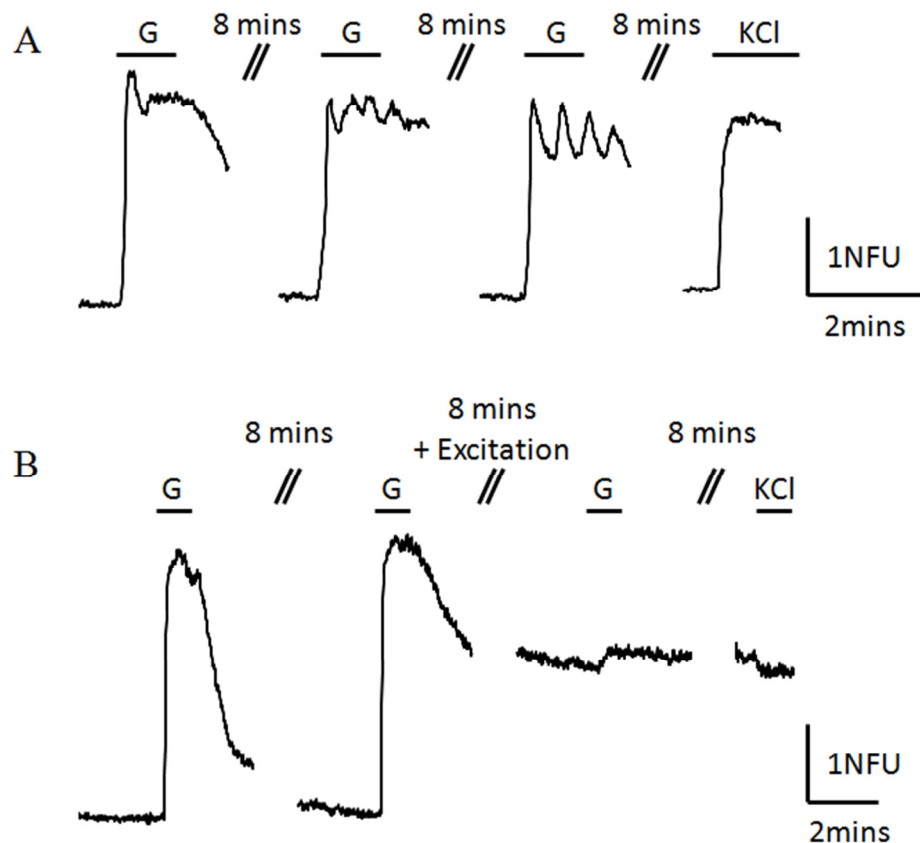
**Figure 4.8 Cultures under perfusion responded to repeated glutamate applications. Glutamate (100 μM) was applied for 1 minute durations while the culture was under constant perfusion. (A) A typical response from a neuron that was repeatedly exposed to glutamate showing an increase in intracellular $Ca^{2+}$ upon stimulation. Between stimulations and recordings the culture was allowed to recover with no fluorescent excitation. (B) A typical response from a neuron that was not allowed to recover between stimulations. The prolonged fluorescent excitation rendered the cell non-responsive to glutamate or KCl. In both cases the total time under perfusion was longer than 60 minutes.**

## 4.5. Device 3 – Optimisation of the Fast Perfusate Exchange System

### 4.5.1. Design

Further modifications to the system were made, based on Device 2, to improve the efficiency of solution use and the uniformity of chamber loading (Figure 4.9). The well diameter was reduced to 4 mm, lowering the volume of unused solution in the loading well required to achieve equivalent flow rates in the culture chamber. A lower volume of solution also reduces the flow rate required to quickly change solutions compared to the previous larger wells. A further alteration was made to include microfluidic channels to assist in the movement of fluid through the open

well. These microchannels allow fluid in the well to be withdrawn evenly from both sides of the inlet to the culture chamber, which assists in creating a uniform flow across the width of the chamber.
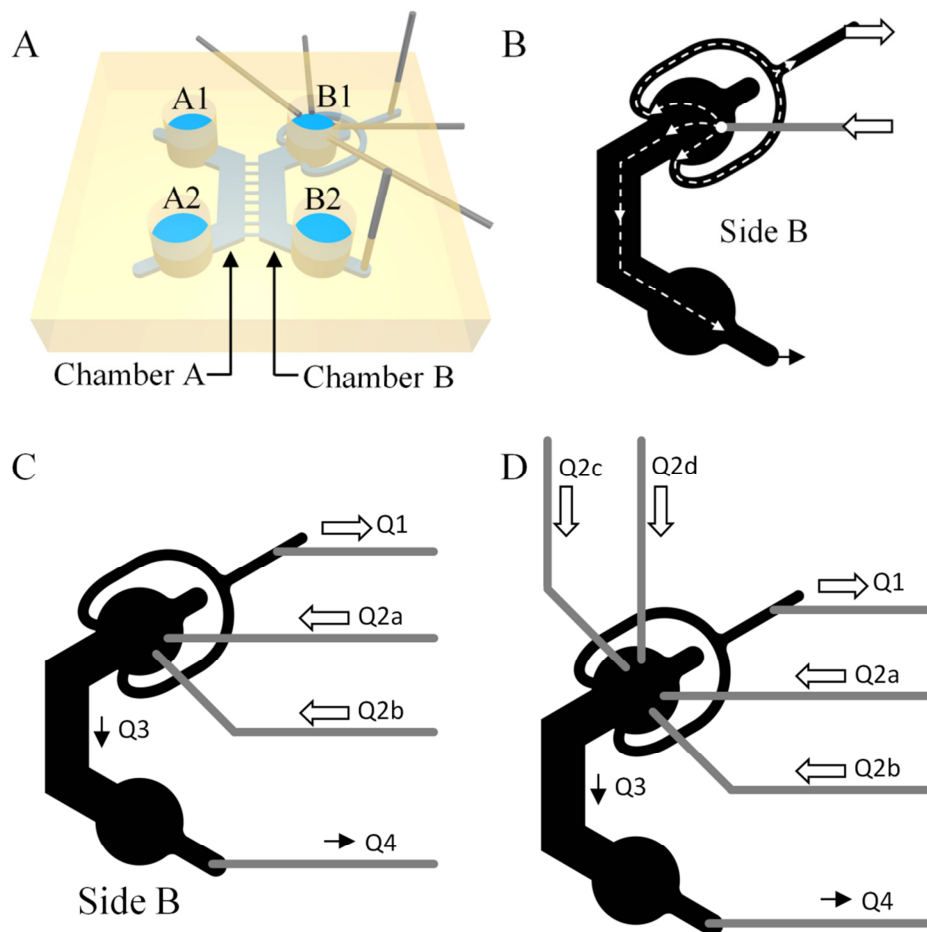


**Figure 4.9 Alterations made to the device design. (A) The diameter of the open wells was decreased to reduce the volume required to be replaced during perfusate transitions. The layout of the fluidic layer was altered to provide withdrawal from both sides of the culture chamber inlet at *B1*. (B) The approximate flow path for fluid injected into the well at a single inlet. (C) The diagram shows both the layout of the fluidic layer (black) and the location of connections to syringe pump drivers (grey). In this configuration two types of perfusate can be connected to the device. (D) Additional perfusates can be added to the loading well as required. In both configurations vertically punched inlets are used to connect to Q1 & Q4 while horizontally punched inlets are used to connect to Q2.**

## 4.5.2. Péclet Number

Reducing the diameter of the well is an additional method to achieve a high Péclet number whilst also reducing the flow rate in the loading well. If the well diameter is

halved to 4 mm, then reducing the loading well flow rate to 50 µL/min maintains a high Péclet number of 410. The culture chamber is unaltered and so the *Pe* number remains at 99, providing the flow rate through the chamber does not change. This suggests that perfusate transitions should not be significantly affected by diffusion.

## 4.5.3. Characterisation

Fluorescein (15 µM) was used to characterise how altering loading well flow rates affects the loading of solutions within the chamber. The chamber flow rate Q3 & Q4 was set at 4 µL/min, while the loading well flow rate Q1 was set between 10 µL/min and 80 µL/min (Figure 4.10). Once steady state conditions were established using water as the perfusate, the solution was switched to fluorescein for 1 minute, before being switched back to water.
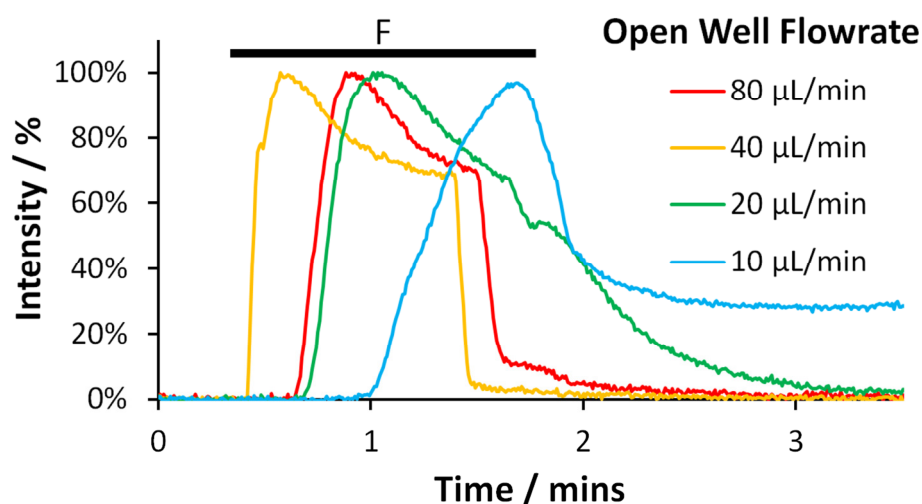


**Figure 4.10 The change of perfusate was characterised for the new device at various loading well flow rates. In each case perfusion of water was established at a specified flow rate (10, 20, 40, 80 µL/min) followed by perfusion of fluorescein solution into the loading well as indicated (black line, F). The chamber flow rate was kept constant at 4 µL/min. For each graph the lag time (the delay between introduction of fluorescein to the loading well and a measured increase in fluorescence in the channel) was measured as well as the time taken to increase to 63.2% fluorescein in the channel. (10 µL/min) Lag time = 40 s, time constant 18 s. (20 µL/min) Lag time = 21 s, time constant 7.8 s. (40 µL/min) Lag time = 9.6 s, time constant 3.9 s. (80 µL/min) Lag time = 19 s, time constant 6.5 s. At lower flow rates (10 & 20 µL/min) washing off the fluorescein took significantly longer than the loading times, while at the two highest flow rates used (40 & 80 µL/min) the washing off characteristics were similar to the loading times.**

During the fluorescent characterisation of Device 3, it was observed that the distribution of fluorescein throughout the chamber was consistently uniform across the width of the culture chamber (Figure 4.11). The uniform distribution of perfusates is desirable as it means that a drug can be reliably applied to the entire culture within the chamber and not inconsistently to a smaller proportion of the chamber.
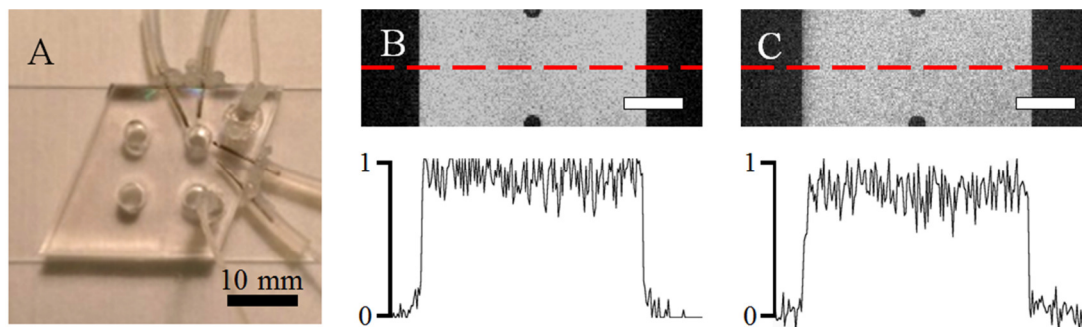


**Figure 4.11 The distribution of fluorescein in Device 3 during cycles of perfusion at different flow rates. (A) Device 3 is connected to multiple infusion ports horizontally, with the two withdrawal port connected vertically. During fluorescein perfusion only two infusion ports are required for water and fluorescein solution. (B & C) The loading of fluorescein had better uniformity than in Device 2, across the width of the culture chamber at both low loading well flow rates (B: 10 µL/min) and high loading well flow rates (C: 80 µL/min). (B, C) Scale bars: 500 µm.**

The uniform distribution of the fluorescent perfusate shows that the flow path in the loading well is more consistent here than in Device 2. The reduced flow rates required to change perfusates quickly is also an improvement meaning that less solution will be required during experiment involving cell cultures.

## 4.5.4. Experimental Evaluation

To determine that primary neuronal cell cultures could be successfully stimulated and remain viable under perfusion, functional testing was carried out as described in section 4.4.4, with appropriate alterations made for the reduced well diameter. The loading well flow rate was reduced to 50 µL/min. A culture grown with one device was repeatedly stimulated with glutamate solution (100 µM) for 1 minute durations, with time to recover without illumination between applications (Figure 4.12).
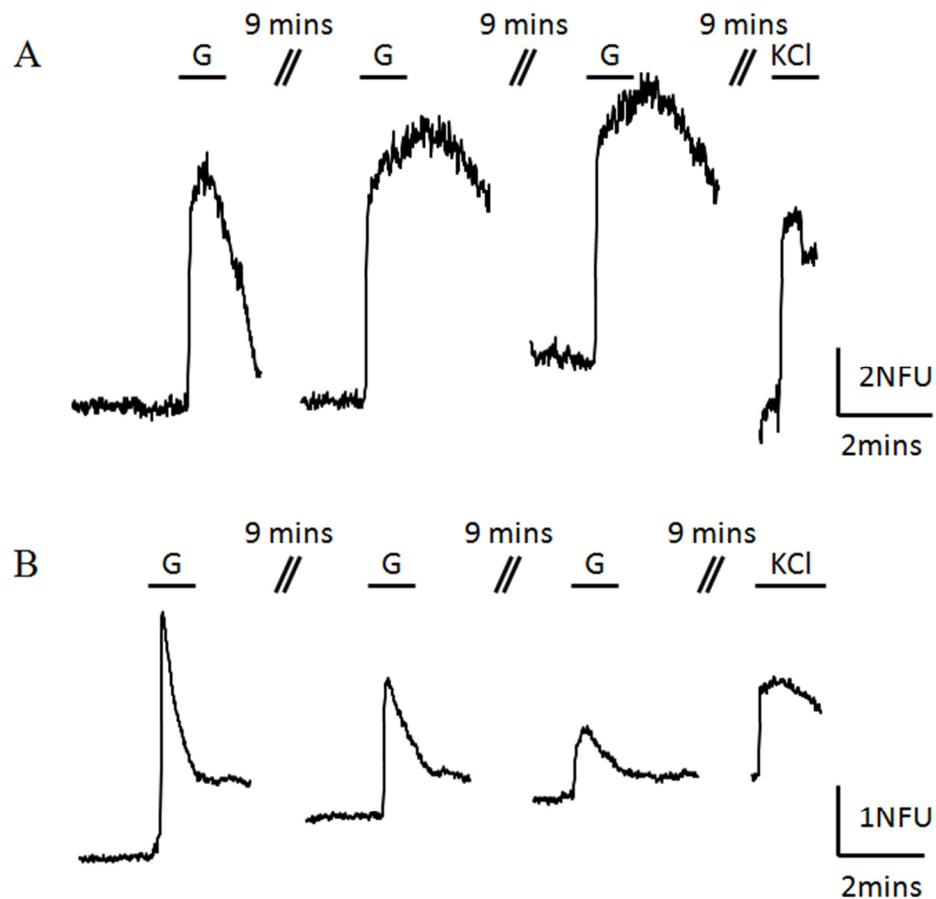
**Figure 4.12 Neuronal responses to repeated glutamate stimulation while under perfusion in the reduced volume device. Glutamate (100 µM) was applied for 1 minute durations while the culture was under constant perfusion. (A & B) Both signals show responses to each direct application of glutamate. (A) An example of a neuron showing consistent responses to glutamate even though there is an apparent shift in its baseline level of $Ca^{2+}$. (B) An example of a neuronal signal where the response to glutamate stimulation decreases with each application of glutamate.**

## 4.6. Demonstration of a Multiphase Experiment Using Glutamate Receptor Antagonists

To demonstrate the capability of experiments in a compartmentalised neuronal culture, involving multiple washing procedures, glutamate receptor activation was blocked using competitive antagonists (Figure 4.13). For the multistage functional test four infusion pumps were prepared containing: external solution; glutamate (100 µM dissolved in external solution); glutamate blocking solution (NBQX 20 µM, DL-AP5 100 µM, MCPG 500 µM, all dissolved in external solution); and a

combined glutamate and glutamate blocking solution (glutamate 100 µM dissolved in glutamate blocking solution).

A device containing primary hippocampal cultures, 13 DIV, was prepared for $Ca^{2+}$ imaging as described earlier. These were connected to the syringe pumps via the appropriate tubing to provide perfusion to chamber B. The syringe pumps were networked together to be controlled from a single user interface on a computer. The flow rate for the cell culture chamber was set to 4 µL/min while the flow rate in the loading well was set to 50 µL/min. The open wells connected to chamber A were topped up with 50 µL of external solution to prevent diffusion of the perfusate from chamber B.

Initially perfusion was established using external solution for over 10 minutes. Cells were stimulated with a single pulse of glutamate solution (30s duration), and allowed to recover for 10 minutes after which the perfusate was changed to glutamate blocking solution for 10 minutes. The perfusate was then changed to glutamate and glutamate blocking solution for 1 minute, before being changed back to glutamate blocking solution. The perfusate was then changed back to external solution for 7 minutes before another pulse of glutamate was applied. Following a period of recovery the cells were finally stimulated by manual injection of potassium solution (25 mM) to depolarise the neurons. This entire procedure was repeated on a fresh device, 14 DIV, with a lower concentration of glutamate (10 µM) used in all solutions.

In the first device tested (using 100 µM glutamate), it was possible to record $Ca^{2+}$ imaging from both sides of the fluidic barrier (Figure 4.13A & B). In the second device tested (using 10 µM glutamate) it was not possible to record from the indirect side due to poor uptake of the Fluo4 AM, and therefore only effects on the direct side were recorded (Figure 4.13C & D).
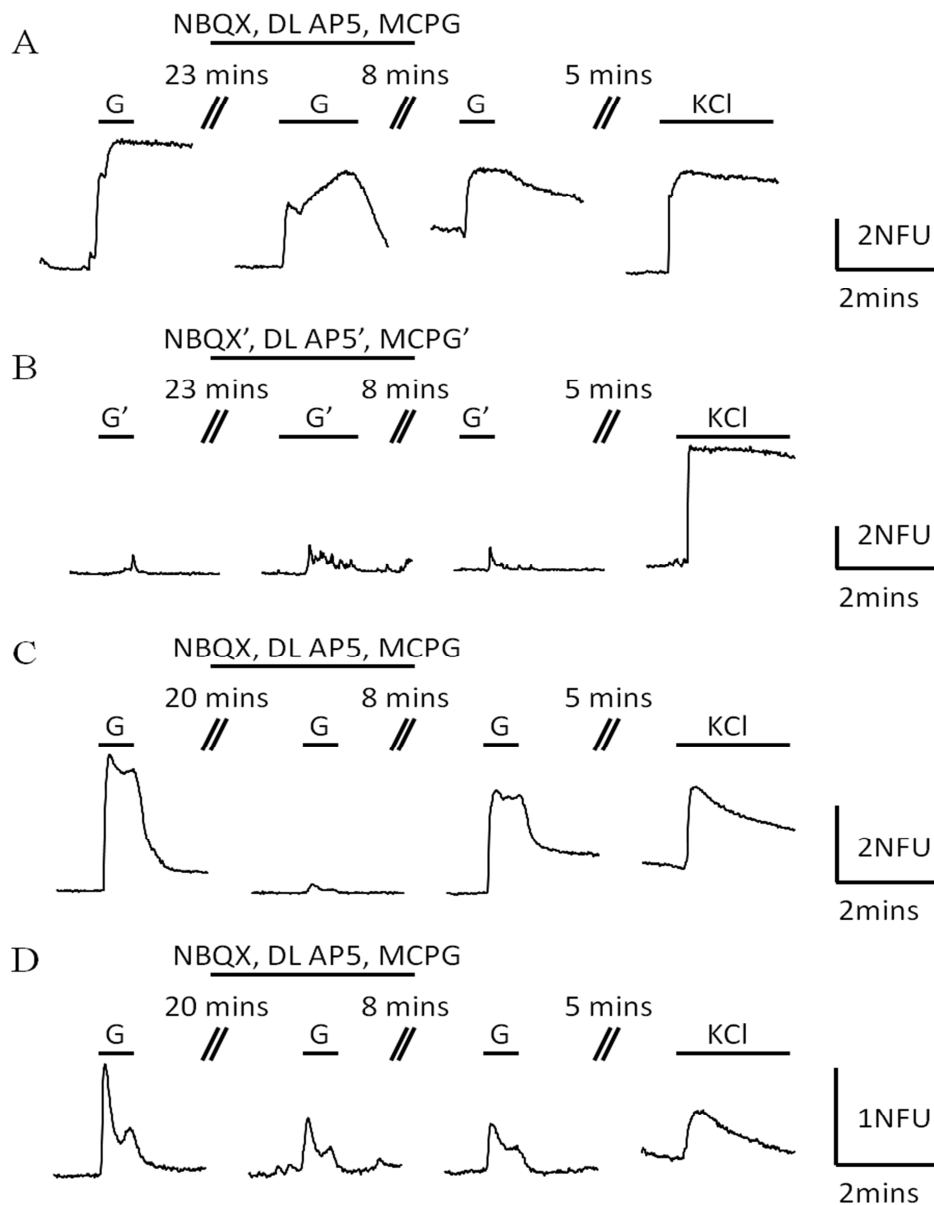
**Figure 4.13 Neuronal cell cultures showed mixed responses to glutamate inhibition. (A) A typical neuronal response to 100 μM glutamate stimulation showed no effect of the antagonists NBQX, DL AP5, and MCPG. The magnitude of the response to glutamate whilst being perfused with glutamate blocking solution is similar to that when there is no glutamate blocking solution. (B) A typical neuronal response (n = 75) from the indirectly stimulated culture chamber. Upon each indirect application of glutamate solution (with or without glutamate blocking solution) the neuron shows a burst of $Ca^{2+}$ activity that coincides with activity from the directly stimulated neurons. (C) A typical neuronal signal (55%, n = 59) that shows a suppressed response to glutamate solution (10 μM) while being perfused with glutamate blocking solution. The neuron responds to glutamate solution both before and after glutamate blocking solution is applied. (D) An example trace, taken from some neuronal signals (45%) of the neuronal signals, which shows a response to glutamate solution (10 μM) during the perfusion glutamate blocking solution.**

## 4.7. Discussion

In this chapter a new system for perfusion in compartmentalised cell culture chambers has been shown. Three different configurations of applying perfusion have been described, with each system characterised and evaluated using the fluorescent probe fluorescein. Two methods were also evaluated with live cell studies using $Ca^{2+}$ imaging to examine neuronal functional responses while under perfusion and the final evaluation involved a multiphase experiment including glutamate and glutamate antagonists.

## 4.7.1. Device Development and Characterisation

There were three methods of perfusion described in this chapter which succeeded at perfusion to varying degrees. The first device developed featured a single inlet to the loading well which limited the flow rate of perfusion that could be applied to the cell culture chamber. The low flow rate resulted in a minimum switching time of over 2 minutes to change between solutions of water and fluorescein. The concentration profile of switching between solutions is gradual which makes determining the concentration at a specific time difficult. Overall this makes the system unsuitable for fast transitions between solutions. However, for long term studies, this simple method of perfusion is potentially a viable option for sustaining a volume difference between the two sides of the fluidic barrier within the device, therefore maintaining fluidic isolation of one culture chamber from the other over several days. Such a system could be used for long term studies that require a single sub-culture to be treated for several hours, e.g. during viral transfection [83].

The second device developed included an additional withdrawal port connected to the loading well, allowing the solution within the well to be switched quickly whilst maintaining a lower flow rate within the cell culture chamber. From the fluorescent characterisation, using fluorescein solution and water as the perfusates, it was shown that while there was a noticeable lag of 20 seconds, between the switching of infusion syringe pumps and a change in fluorescence, the transition between solutions occurs in only 7 seconds. This transition time between solutions is suitable for short term experiments involving $Ca^{2+}$ imaging, where fast transitions

(<1 minute) between solutions is required. The lag is due to the time taken to replace the fluid within the loading well, where a higher flow rate could be used to reduce the time taken. There were inconsistent problems with Device 2 found during the characterisation of the device with fluorescein. Occasionally the system preferentially loaded or cleared one side of the culture chamber as seen in Figure 4.7. This is due to the asymmetrical flow present in the loading well where the outlet port is located to one side of the culture chamber inlet. In these instances perfusing fluorescein for a long duration resulted in uniform fluorescence. However, this is still undesirable as inconsistent and uneven changes in perfusate may influence cell cultures adversely in an uncontrolled manner which is not desirable in functional studies that require precise timing and drug application.

The third device described in this chapter included modifications to improve the efficiency of changing solutions in the loading well in addition to improving the concentration profile of perfused solutions. The addition of microchannels to connect the loading well withdrawal port to either side of the culture chamber was sufficient to provide consistent uniform loading of the culture chamber. Using 4 mm wells made it possible to reduce the loading well flow rate (compared to the 8 mm wells) which reduced the total volume of solutions required for experiments. The switching of solutions was measured using fluorescein solution and water over a range of loading well flow rates to determine what flow rate had the best transition time between solutions. A loading well flow rate of 40 µL/min was found to have the best loading profile. Using lower flow rates involved longer delays before switching between solutions, and the transition itself took a significant amount of time. In both cases (10 µL/min and 20 µL/min) the wash off period took significantly longer than the wash on time, potentially due to residual fluorescein within the loading well. The transition cannot be attributed to residual fluorescein within the chamber as the flow rate within the chamber remained constant for each loading well flow rate used. At the faster flow rate of 80 µL/min, it was found that the loading profile deteriorated. As all other conditions within the system are kept constant the less suitable loading profile is potentially due to the faster flow altering the laminar flow profile within the open well resulting in unstable well loading.

In practise it was found that the draining well required a priming volume to function properly, ensuring that there was a continuous stream of fluid, across the draining well, between the channel opening and inlet to the withdrawal port on the device. This resulted in a dead volume of approximately ¼ of the open well volume (50 µL for the 8 mm diameter wells, and 10 µL for the 4 mm diameter wells), however this did not significantly affect the switching of solutions due to the high loading well flow rate.

The device was optimised for low perfusion rates within the culture chamber and fast switching between solutions in the loading well. The flow rate of 4 µL/min used in the cell culture chamber here is similar to that found in other forms of perfusion microfluidic systems [86], [97], however lower flow rates are generally used for longer term perfusion lasting several hours [125], [126]. The flow rate in the loading well does not affect the cells in culture, however, it does influence the time taken to switch between solutions being perfused. In general, faster loading well flow rates reduce the time taken to exchange volumes within the loading well, although this benefit comes at a cost of inducing potentially unstable flow to the system.

The syringe pumps and rigid glass/plastic syringes were found to be reliable at the flow rates used. Using a pump based system of this nature will introduce a number of phenomena that can adversely affect performance. The syringe plunger, and tubing between the syringe and the device will experience elastic deformation as the pump applies pressure to meet the required flow rate of fluid. This produces a small capacitive effect which ultimately delays the onset of fluid flow which may affect the start/stop time of the solution being perfused. However, this time is insignificant compared to the time taken to replace the solution within the open well. Additionally, during the start/stop motion of the pump, the initial deformation can cause a slight overshoot in flow rate which is possibly the cause of the rise and fall in fluorescence observed during the steady state conditions seen in the characterisation of Device 3 (Figure 4.10). Syringe pumps in microfluidic system can also cause pulsatile flow within the fluidic chamber due to the motor action of the pumps used. The changes of flow rate are dampened in this system, by connecting all infusion and withdrawal ports to open wells prior to the confined microchannel which acts to reduce the

impact of sharp changes in flow rate. While this leads to smoother continuous flow over the cell culture, it cannot completely remove all the effects of flow rate changes caused by the syringe pumps. In the future, pressure systems may be used to drive the fluid flow as an alternative to syringe pumps since they do not exhibit any pulsatile flow (see Chapter 5).

## 4.7.2. Functional Viability of Cells During Microfluidic Perfusion

To evaluate the viability of primary neuronal cell cultures experiencing perfusion $Ca^{2+}$ imaging was performed while the cells were repeatedly stimulated with glutamate (100 μM). Glutamate is one of the most common neurotransmitters present in the brain and acts on glutamate receptors which include NMDA, AMPA, kainite and mGluRs. During an action potential the intracellular $Ca^{2+}$ inside the neuron increases (due to influx via voltage gated $Ca^{2+}$ channels), where bursts of action potentials produce a sufficient change in intracellular $Ca^{2+}$ to be detected via the $Ca^{2+}$ imaging setup used (as seen previously in Chapter 3). During functional testing, it was shown that the neuronal signals behave as expected upon glutamate application, and finally $K^+$ (25 mM) stimulation. This shows that the cells remain viable even after an hour of constant perfusion at a flow rate 4 μL/min. However, it was found that prolonged fluorescent excitation prevents the neurons recovering from glutamate stimulation and renders them unresponsive to both glutamate and $K^+$ stimulation, presumably due to phototoxicity known to be induced following prolonged light exposure [127], [128]. For subsequent experiments, a non-illuminated recovery period, following all stimulations, was included to maintain cell viability. Both the device structures tested with cells cultures showed that neurons do remain viable while under perfusion over at least 1 hour as this was the longest time demonstrated. While Device 2 required a loading well flow rate of 200 μL/min to make the transition between external and glutamate solutions, Device 3 required 50 μL/min to switch between solutions which resulted in the total use of a quarter of the solutions that were used for the same experiment in Device 2.

## 4.7.3. Blockade of Glutamate Receptors During Microfluidic Perfusion

To demonstrate the capability of Device 3 for multiphase experiments, glutamate blocking solution was used along with glutamate stimulations to show that the device could wash on and off multiple solutions on demand. The glutamate blocking solution consisted of NBQX and DL-AP5 (ionotropic glutamate receptor antagonists [67], [107]) as well as MCGP (a metabotropic glutamate receptor antagonist [106], [129]). The blockers used are all competitive antagonist for glutamate receptors and therefore had to be perfused both prior to glutamate application and during glutamate application to be effective receptor antagonists.

Both concentrations of glutamate used (10 µM and 100 µM) were found to produce reliable bursts of $Ca^{2+}$ activity during short applications of the compound in isolation. It was important to establish that the neurons were responsive to glutamate both before and after the perfusion of glutamate blocking solution which, as a competitive antagonist, should only be effective when it is present in sufficient quantities to suppress the normal action of glutamate binding to its receptors.

While it was shown that the glutamate blocking solution was not able to block 100 µM glutamate stimulation, it was sufficient to suppress the majority of induced neuronal activity when the applied glutamate concentration was reduced to 10 µM. The presence of competitive antagonists reduces the probability of glutamate binding but does not prevent them from doing so. Since not all glutamate receptors have to be bound to glutamate for excitation to occur, it follows that a reduced number may still induce synaptic activity. Therefore, it is reasonable for the glutamate blocking solution to be only partially effective at preventing glutamate activation especially when a high concentration of glutamate (100 µM) is applied. It also follows that the glutamate blocking solution will be more effective at suppressing glutamate activation when a lower concentration of glutamate (10 µM) is used.

During the glutamate blocking experiments it was also shown that synaptic activity occurs across the microfluidic barrier. The indirect side responded to glutamate stimulation of the direct side which was not prevented with the application of

glutamate blocking solution to the direct side. The indirect side's response is to be expected as the solution failed to reduce activity on the direct side. As fluidic isolation of the indirect side, side A (Figure 4.9), was maintained throughout the experiment it can be seen that synaptic activity was present between the cell culture chambers even in the presence of perfusion, demonstrating that the fluid flow does not prevent neuronal cells from signalling normally.

## 4.7.4. Evaluation

The development of a novel platform has been described for the perfusion of interconnected neuronal cultures in a compartmentalised microfluidic device. Successive iterations of the device used results from previous attempts in order to improve the characteristics of the device.

It has been shown that during perfusion neurons within the system remain functional and are capable of synaptic communication between compartments within the device. A multiphase experiment demonstrated the ability of the device to perform multiple solutions exchanges to wash on and off drugs of interest.

The system developed here is comparable to other microfluidic systems that are used to perfuse neuronal cultures in different configurations. Taylor *et al.*[86] developed a system, based on their previous work [80], [84], for the perfusion of synapses located within a microfluidic barrier between co-cultures. While they showed that they can selectively target the synaptic region, they did not show functional communication between the cultures involved, instead focusing on local activity within a single neuron. Their system was only capable of switching between two solutions without intervening at the device directly and the applications were controlled manually via pipette. Another microfluidic system that uses perfusion with neuronal sub-cultures [97] is not capable of functional communication between the sub-cultures, instead using one as a control while the other is chemically targeted. In contrast to these systems, the platform developed here has the ability to perfuse multiple solutions individually controlled via a graphical user interface on a computer. A further advantage of this system is also the ability to selectively target individual sub-networks of neurons within a larger interconnected network, making

this system suitable for studying how compounds of interest affect functional communication between neuronal cells.

In comparison to standard *in vitro* perfusion systems there are a number of advantages to using this microfluidic system. Due to the lower flow rates used (50 µL/min compared to 2–10 mL/min [106], [120]) there is a significant reduction in fluid required for experiments of equivalent duration. Further refinement could be made to the operation of the syringe pumps to dramatically reduce this. As the higher flow rate of 50 µL/min is only required to switch between solutions in the loading well, the loading well flow rate can be reduced during longer periods where only a single perfusate is required. This would limit the flow rate in the loading well to that of the culture chamber flow rate, saving much of the solution that is wasted by maintaining a higher flow rate with the loading well. The reduction in volume of solutions required is essential for testing of novel compounds where producing small quantities can be time consuming and expensive.

A potential drawback of this platform is the ability of PDMS to absorb small hydrophobic molecules [130]. This is a drawback of all PDMS devices where the polymer structure allows molecules to passively diffuse into the bulk structure. Absorption of hydrophobic substances could significantly alter drug discovery outcomes where nanomolar concentrations may be used [131]. This highlights an additional benefit of integrating perfusion, where the reduced time that drugs of interest are present in the system can minimize any diffusion that occurs from the solution to the PDMS. Additionally, as the perfusate is being continually refreshed the effects of partial absorption and emission of small molecules by the PDMS becomes insignificant.

Overall the system developed here is a reliable platform for perfusion targeted to a single chamber within a compartmentalised microfluidic device. Combined with previously described $Ca^{2+}$ imaging techniques (see Section 2.5) it is able to monitor the functional activity of neurons connected between compartments. This makes the platform suitable for advanced neuron-neuron interaction studies that involve multiple stages and where both the direct and indirect effects of novel compounds are of interest.

# Chapter 5. Discussion

## 5.1. Introduction

So far, this thesis has examined the capabilities of *in vitro* neuroscience research methods and the recent impact made by microfluidics techniques applied to the field. The combination of methods has created a new approach for the construction of neurological networks *in vitro* as well as the sub-network control of cellular environments. Potential limitations in the literature were identified, such as the lack of methods for assessing the synaptic communication between compartmentalised co-cultures and the absence of suitable perfusion systems for selected compartments within the systems. Initially it was required to devise a method for demonstrating that functional connectivity could be detected, using a $Ca^{2+}$ indicator, between co-cultures in a compartmentalised system and that this connectivity could be pharmacologically manipulated. Once this capability was established, a perfusion system was developed to allow multiple stage experiments to be conducted and even partially automated.

In the previous chapters (Chapter 3 & Chapter 4), the work carried out has been described and the results of these were presented and discussed with particular reference to their validity and suitability for purpose. The potential impact from these chapters shall now be discussed with reference to the wider fields of neuronal microfluidics and *in vitro* neuroscience research. Ongoing collaborative work relating to this project will also be described as well as possible areas of future work that have been identified.

## 5.2. Chapter 3 Outcomes

In Chapter 3, a method was developed for assessing the functional connectivity of neurons grown in a compartmentalised system. This method involved manual applications of drugs and was evaluated on primary rat hippocampal co-cultures. Using $Ca^{2+}$ imaging it was possible to detect both direct and indirect responses of neurons to KCl and glutamate stimulation. It was noted that using this method also allowed the simultaneous observation of changes in astrocyte activity. Additionally, modelling of the fluidic isolation of one compartment was carried out to show that there was no cross contamination of stimulating solution between the co-cultures.

The work in this chapter represents a fusion of existing technologies and techniques including; microfluidic compartmentalisation [84], $Ca^{2+}$ imaging [62], and neuropharmacology [17]. This combination has been used here to provide a new method of assessing both the direct and indirect effects of drugs on neuronal and astrocytic communication *in vitro*.

This work is similar to other neuronal microfluidic studies that have used compartmentalised networks in conjunction with either $Ca^{2+}$ imaging [89], [132], or MEAs [95]. However, $Ca^{2+}$ imaging so far has not been used to demonstrate the manipulation of activity between co-cultures. In that respect this work is more closely related to studies recently carried out with MEAs, where the connectivity between co-cultures was assessed under selective pharmacological stimulation [95]. While some principles are comparable between $Ca^{2+}$ imaging and MEAs, the method of assessing connectivity is very different and each has its own advantages and disadvantages. Using MEAs provides monitoring of electrical activity of large cell networks allowing multiple compartments to be monitored simultaneously, and with a high enough temporal resolution to form network connectivity maps [98]. However, as activity from a group of cells is generally recorded it is difficult to attribute activity to individual neurons. In addition, MEAs are restricted to monitoring neuronal polarisation activity only and cannot detect activity from astrocytes which are not excitable and are thought to play a role in synaptic regulation [30], [31]. On the other hand, $Ca^{2+}$ imaging is able to detect the $Ca^{2+}$ activity of non-neuronal cells such as astrocytes and can monitor large networked

regions as demonstrated here. However, while individual signals are automatically attributed to individual cells, the low temporal resolution used means that only large bursts of activity were measured and it would not be possible to form network connectivity maps.

The new method described in this chapter provides a useful means of assessing both direct and indirect consequences of drug application to connected neuronal networks. The ability to monitor induced astrocyte activity could also prove beneficial in furthering the understanding of neuron-astrocyte interactions. Additionally, the techniques shown are also relevant to other studies that currently do not assess the functional communication between networked sub-compartments. Overall, while only a simple network was demonstrated in this chapter, the method described was validated and is suitable for a wide range of neurological studies that use more complex models of the brain and neurodegenerative disorders.

## 5.3. Chapter 4 Outcomes

There is currently a gap in the literature regarding perfusion methods for compartmentalised neurological co-cultures. This has been a key motivation for the work carried out in Chapter 4, which has built on previously described techniques to develop an integrated perfusion system which may eventually lead to automated experiments.

The system developed here involves an array of syringe pumps and is capable of applying repeated stimulations to a single chamber in isolation as well as conducting multiphase pharmacological tests on the communication between the chambers. While a method for manually applied repeated stimulations of glutamate has been previously shown [86], it was not possible to control the flow rate experienced by the cell and there was no ability to quickly change between multiple solutions *in situ*. An alternative study, that involved multiple solutions in a staggered experiment, again applied each solution manually and was not able to continue recording during the experiment because of the multiple washes that were required between each step [95]. In general, the growing field of neuronal microfluidic devices has primarily focussed on the development of physiologically relevant brain structures

and been restricted to simple one or two stage experiments [89]. The addition of a perfusion system could simplify experimental routines and enable experiments of greater complexity that require multiple applications of various solutions *in situ*.

In Chapter 4, the method of perfusion demonstrated utilised a computer controlled interface to selected solutions to be perfused over the cells which enabled experiments to be automated. Automated perfusion of solutions is of particular interest in terms of drug discovery where thousands of novel compounds may be developed and must be tested in a robust manner. High throughput systems are required to perform these tests and computer controlled automated systems are well-suited to the repetitive nature of the tasks involved. However, the current setup still requires several inlets and outlets to be manually attached to the device so, while the control during experiments can be readily automated, it is not currently possible to automate the preparation of the devices.

## 5.4. Collaborative Work

In collaboration with Andrew Samson and Professor Chris Connolly (University of Dundee), a compartmentalised *in vitro* system for modelling stroke has been developed. Specifically the system is designed to examine the spread of excitotoxic insults using a series of five connected compartments to represent local regions of the brain. An excitotoxic insult in the brain is a condition where neurons are hyper-stimulated until a point that they are damaged and may experience cell death. In stroke there is a directly affected ischemic region that undergoes cell death, while secondary neural damage can spread to the surrounding penumbral regions via glutamate excitotoxicity. The compartmentalised structure is well suited to model this condition where each chamber can be kept in isolated environments while a selected chamber undergoes an excitotoxic insult. The model is used to study the spread of cell death to the surrounding chambers that did not experience the insult, mimicking what occurs in the brain.

Fluidically isolated chambers; *A, B, D, E*
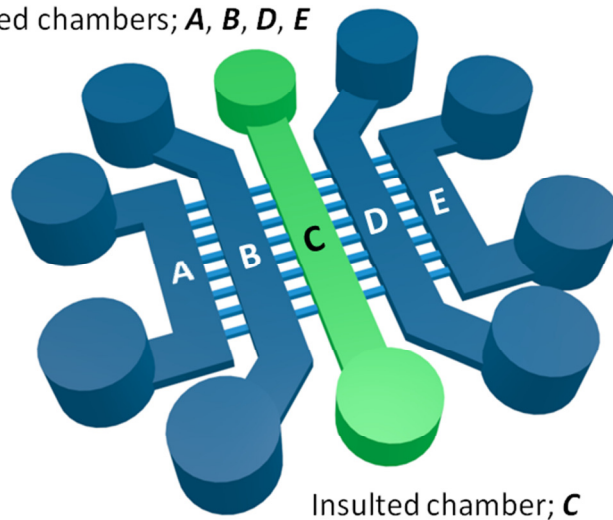
Insulted chamber; *C*

**Figure 5.1 An *in vitro* system to model the spread of excitotoxic insults. The image shows the 5 chambers of the device connected by arrays of microchannels. Neurons are cultured in all chambers (*A–E*) of the device, forming synaptic connections between each compartment. The target chamber (*C*) can be fluidically isolated and an excitotoxic insult is applied (typically glutamate [100 µM] for one hour). This allows secondary effects to be observed in *B & D*, and tertiary effects observed in *A & E*. Any chamber can be selectively preconditioned or postconditioned as required.**

The work presented here is useful in determining that synaptic communication occurs between compartments, and so the spread of cell death is thought be synaptically modulated. Using this device, it has been found that cell death in the surrounding regions may be prevented by preconditioning the surrounding chambers with a sub-toxic glutamate insult, as previously shown [133]. Interestingly, it has also been found that postconditioning can also increase cell viability (data not shown), and work is currently underway to determine the underlying mechanisms for this.

## 5.5. Future Work

There are many areas relating to this work that need to be investigated in the future including the development and evaluation of new *in vitro* models relevant to CNS disorder as well as continued refinement of the microfluidic devices used in their investigation.

While the perfusion system described in Chapter 4 was an improvement on the system described in Chapter 3, further optimisations still have to be carried out before it is a comprehensive tool for neuroscience research. In the current perfusion

system, optimisations of the device geometry and experimental procedures can be made.

With regards to the geometry of the device, the structure of the cell culture chambers could be altered. Currently, along the centre of each chamber, there are several pillars that are required to support the wide chamber structure. By reducing the width of the chamber, the central pillars can be removed which should improve the loading profile through the chamber. However, the new system would have to be evaluated to ensure that fluidic isolation and cell viability are maintained during an experiment. Additionally, altering the device setup to have a single/combined solution inlet would be beneficial as it should reduce the variability between each solution's lag time due to the manual positioning of each inlet.

Further optimisations should be carried out on the experimental procedure with regards to the perfusion of solutions, as previously described in Section 4.7. These include the reduction of flow rate within the culture chamber as this may improve cell viability, and the alternation of loading well flow rates to reduce the total volume of solutions required. It is important to ensure that altering flow rates during an experiment does not alter the flow rate in the culture chambers itself, as doing so may stimulate cells and confound the results.

It may also be preferred to change the driver of the system from syringe pumps to a pressure system. A current disadvantage of using syringe pumps as a driver is their intrinsic onset and offset delays, and the fact that they produce semi-pulsatile flow in the system. Pressure driven systems provide non-pulsatile flows and could be used as an alternative method of perfusion; however, measurement and feedback systems would have to be included to ensure that the desired flow rates were produced in the cell culture chamber.

Until now, this work has exclusively exploited $Ca^{2+}$ imaging to detect and quantify cell activity. However, as previously discussed in Section 3.6, $Ca^{2+}$ imaging is generally limited to detecting bulk activity of the neuron and is not easily adapted to detecting single action potentials or creating network maps. Alternatively, voltage sensitive dyes could be used to optically detect electrophysiological activity within

the networks [134]. By looking directly at the cell signalling activity, and not the indirect $Ca^{2+}$ activity, greater clarity could be found on the effects that compounds of interest have on connected co-cultures.

Aside from the improvements to the device that can be made, the models of CNS disorders require further development. Currently the system has only been tested on one of the simplest models of the brain, specifically featuring two compartments of connected hippocampal neurons. While some models of brain structures already exist [74], [75], [85], [89], new models can be developed that capitalise on the recent development of induced pluripotent stem cells (IPSCs). Human IPSCs can be differentiated into neurons and have the potential to provide further insight into neurodegenerative disorders. This is particularly relevant to forms of disease that are genetically linked where fibroblast cells can be harvested from patients with genetic mutations and be used to create IPSCs that can then be differentiated into neurons to be studied *in vitro* [135]. A significant advantage of studying these neurons is that they can be created from humans instead of animals, reducing the number of animals required to be sacrificed for research and increasing the human relevance of any results. However, at this early stage of development there are still concerns about how neuron-like these iPSC derived neurons actually are.

The microfluidic devices and techniques described here are well suited to studying these neurons and evaluating their physiological properties that affect synaptic communication. In addition, the compartmentalised structure can be used to characterise the progression of a disease between compartments, for example the tauopathies that occur during dementia, and to evaluate strategies that aim to limit the progression of neurological disorders. Such a project has recently been funded, and work will be carried out to characterise how specific genetic mutations affect synaptic communication and the spread of tauopathies between diseased and healthy neurons shall be investigated [136], [137].

Separately, the novel system for studying the spread of toxicity has several areas of future work that will be carried out in Dundee University. While so far both neurodegenerative and neuroprotective effects have been observed, the exact mechanisms are yet to be established. Once these underlying mechanisms are

understood it will then be possible to target these in search of therapeutic strategies that can help patients to prevent, or recover from, excitotoxic insults such as stroke. These therapies may be screened first in multicompartment devices such as this device to assess their viability prior to the more expensive assessments of animal testing and clinical trials.

## 5.6. Conclusions

This work has aimed to develop new tools for investigating neurological mechanisms using *in vitro* microfluidic devices. To do this a new method was developed for analysing the functional communication between co-cultures in a compartmentalised microfluidic device. Furthermore, a system for perfusing selected compartments was developed which could successfully switch between multiple solutions without the need for manual intervention between stages to perform washing steps. The approaches described here could greatly benefit both existing models of disorders and enable new models to be created as they allow functional communication between cultures to be assessed and multiple solutions to be applied sequentially to probe physiological mechanisms. Overall, progress has been made towards providing new techniques that can aid in the understanding of CNS disorders. The systems developed here may be used to model and evaluate neurological diseases *in vitro*, providing on chip screening platforms for new drugs and therapeutic strategies targeted at these disorders.

# References

[1]     Z. M. Weil, G. J. Norman, A. C. DeVries, and R. J. Nelson, "The injured nervous system: A Darwinian perspective," *Progress in Neurobiology*, vol. 86, no. 1. pp. 48–59, 2008.

[2]     J. Martini, F.H & Nath, *Fundamentals of Anatomy and Physiology*, vol. 7th. 2009, p. 1123.

[3]     M. F. Bear, B. W. Connors, and M. A. Paradiso, *Neuroscience: Exploring the brain (3rd ed.).* 2007, p. 898.

[4]     M. Carter and J. C. Shieh, *Guide to Research Techniques in Neuroscience.* 2010, pp. 91–118.

[5]     E. R. Kandel, J. H. Schwartz, and T. M. Jessell, *Principles of Neural Science*, vol. 3. 2000, p. 1414.

[6]     T. H. Bullock, "Neuron doctrine and electrophysiology.," *Science*, vol. 129, no. 3355, pp. 997–1002, 1959.

[7]     H. Fodstad, "The neuron saga," *International Congress Series*, vol. 1247. pp. 645–650, 2002.

[8]     S. R. Y. Cajal, "The structure and connexions of neurons," *Nobel Lect. Physiol. or Med. 1901-1921*, pp. 220–253, 1906.

[9]     P. C. Caldwell, A. L. Hodgkin, R. D. Keynes, and T. I. Shaw, "THE EFFECTS OF INJECTING 'ENERGY-RICH' PHOSPHATE COMPOUNDS ON THE ACTIVE TRANSPORT OF IONS IN THE GIANT AXONS OF LOLIGO," *J. Physiol.*, pp. 561–590, 1960.

[10]    P. Glees and K. Meller, "The Finer Structures of Synapses and Neurones. A Review of Recent Electronmicroscopical Studies.," *Paraplegia*, vol. 2, no. 1957, pp. 77–95, 1964.

[11]    B. D. Clark, E. M. Goldberg, and B. Rudy, "Electrogenic tuning of the axon initial segment.," *Neuroscientist*, vol. 15, pp. 651–668, 2009.

[12]    A. F. Huxley and R. Stampfli, "Evidence for saltatory conduction in peripheral myelinated nerve fibres.," *J. Physiol.*, vol. 108, no. 3, pp. 315–339, 1949.

[13]    B. Katz and R. Miledi, "A Study of Synaptic Transmission in the Absence of Nerve Impulses," *J. Physiol.*, pp. 407–436, 1967.

References

[14]    J. G. Nicholls, P. A. Fuchs, A. R. Martin, and B. G. Wallace, *From Neuron to Brain*, 4th ed. Sinauer Associates, 2001.

[15]    D. Purves, G. Augustine, D. Fitzpatrick, L. Katz, A.-S. LaMantia, J. McNamara, and M. Williams, "Neuroscience. 2nd edition," *Sunderland (MA): Sinauer Associates; 2001.*, 2001. .

[16]    M. G. Rae, D. J. Martin, G. L. Collingridge, and a J. Irving, "Role of Ca2+ stores in metabotropic L-glutamate receptor-mediated supralinear Ca2+ signaling in rat hippocampal neurons.," *J. Neurosci.*, vol. 20, no. 23, pp. 8628–8636, 2000.

[17]    S. R. Platt, "The role of glutamate in central nervous system health and disease--a review.," *Vet. J.*, vol. 173, no. 2, pp. 278–86, Mar. 2007.

[18]    D. M. Treiman, "GABAergic mechanisms in epilepsy," *Epilepsia*, vol. 42, no. 2, pp. 8–12, 2001.

[19]    M. J. Niciu, B. Kelmendi, and G. Sanacora, "Overview of glutamatergic neurotransmission in the nervous system.," *Pharmacol. Biochem. Behav.*, vol. 100, no. 4, pp. 656–64, Feb. 2012.

[20]    Q. Liu, Q. Xu, G. Arcuino, J. Kang, and M. Nedergaard, "Astrocyte-mediated activation of neuronal kainate receptors.," *Proc. Natl. Acad. Sci. U. S. A.*, vol. 101, no. 9, pp. 3172–3177, 2004.

[21]    C. J. Swanson, M. Bures, M. P. Johnson, A.-M. Linden, J. a Monn, and D. D. Schoepp, "Metabotropic glutamate receptors as novel targets for anxiety and stress disorders.," *Nat. Rev. Drug Discov.*, vol. 4, no. 2, pp. 131–44, Feb. 2005.

[22]    P. Clapp, S. V Bhave, and P. L. Hoffman, "How Adaptation of the Brain to Alcohol Leads to Dependence: A Pharmacological Perspective.," *Alcohol Res. Health*, vol. 31, pp. 310–339, 2008.

[23]    Y. Ben-ari, J. Gaiarsa, R. Tyzio, and R. Khazipov, "GABA : A Pioneer Transmitter That Excites Immature Neurons and Generates Primitive Oscillations," pp. 1215–1284, 2007.

[24]    B. Bettler, K. Kaupmann, J. Mosbacher, M. Gassmann, and M. Structure, "Molecular Structure and Physiological Functions of GABA B Receptors," *Fisiol Rev*, vol. 84, pp. 835–867, 2004.

[25]    R. K. Wong, R. D. Traub, and R. Miles, "Cellular basis of neuronal synchrony in epilepsy.," *Adv. Neurol.*, vol. 44, pp. 583–592, 1986.

References

[26] C. Rubio, M. Rubio-Osornio, S. Retana-Márquez, M. L. Verónica Custodio, and C. Paz, "In vivo experimental models of epilepsy.," *Cent. Nerv. Syst. Agents Med. Chem.*, vol. 10, pp. 298–309, 2010.

[27] V. Parpura, M. T. Heneka, V. Montana, S. H. R. Oliet, A. Schousboe, P. G. Haydon, R. F. Stout, D. C. Spray, A. Reichenbach, T. Pannicke, M. Pekny, M. Pekna, R. Zorec, and A. Verkhratsky, "Glial cells in (patho)physiology," *Journal of Neurochemistry*, vol. 121, no. 1. pp. 4–27, 2012.

[28] M. Tsacopoulos and P. J. Magistretti, "Metabolic coupling between glia and neurons.," *J. Neurosci.*, vol. 16, no. 3, pp. 877–885, 1996.

[29] D. A. Turner and D. C. Adamson, "Neuronal-astrocyte metabolic interactions: understanding the transition into abnormal astrocytoma metabolism.," *J. Neuropathol. Exp. Neurol.*, vol. 70, no. 3, pp. 167–176, 2011.

[30] M. Santello, C. Calì, and P. Bezzi, "Gliotransmission and the tripartite synapse.," *Adv. Exp. Med. Biol.*, vol. 970, pp. 307–31, 2012.

[31] G. Perea and A. Araque, "GLIA modulates synaptic transmission.," *Brain Res. Rev.*, vol. 63, no. 1–2, pp. 93–102, May 2010.

[32] D. J. Nutt, "The full cost and burden of disorders of the brain in Europe exposed for the first time.," *Eur. Neuropsychopharmacol.*, vol. 21, no. 10, pp. 715–7, Oct. 2011.

[33] D. J. Nutt and J. Attridge, "CNS drug development in Europe - Past progress and future challenges.," *Neurobiol. Dis.*, p. In Press, May 2013.

[34] N. A. Fineberg, P. M. Haddad, L. Carpenter, B. Gannon, R. Sharpe, A. H. Young, E. Joyce, J. Rowe, D. Wellsted, D. J. Nutt, and B. J. Sahakian, "The size, burden and cost of disorders of the brain in the UK.," *J. Psychopharmacol.*, vol. 27, no. 9, pp. 761–70, Sep. 2013.

[35] P. Y. Collins, V. Patel, S. S. Joestl, D. March, T. R. Insel, and A. S. Daar, "Grand challenges in global mental health © 2011," *Nature*, vol. 475, pp. 27–30, 2011.

[36] G. Miller, "Is pharma running out of brainy ideas?," *Science (New York, N.Y.)*, vol. 329, no. July 2010. pp. 502–504, 2010.

[37] A. Domínguez, A. Álvarez, E. Hilario, B. Suarez-Merino, and F. Goñi-de-Cerio, "Central nervous system diseases and the role of the blood-brain barrier in their treatment," *Neurosci. Discov.*, vol. 1, p. 11, 2013.

[38] A. Wimo and M. Prince, "World Alzheimer Report 2010," 2010.

References

[39] National Institute on Aging, "Alzheimer's Disease Fact Sheet," *NIH Publication*. NIH Public Access, 2011.

[40] National Institute on Aging, "Alzheimer's Disease Unraveling the mystery." NIH Public Access, pp. 1–84, 2008.

[41] J. Hardy and D. J. Selkoe, "The amyloid hypothesis of Alzheimer's disease: progress and problems on the road to therapeutics.," *Science*, vol. 297, pp. 353–356, 2002.

[42] R. B. Maccioni, G. Farías, I. Morales, and L. Navarrete, "The Revitalized Tau Hypothesis on Alzheimer's Disease," *Arch. Med. Res.*, vol. 41, pp. 226–231, 2010.

[43] T. Bartsch, "The Clinical Neurobiology of the Hippocampus: An Integrative View," 2012, pp. 1–16.

[44] P. Winn, T. J. Bushell, J. Pratt, and B. Picard, "The future of neuroscience," *Public Serv. Rev. UK Sci. Technol.*, no. 3, pp. 1–2, 2011.

[45] P. Anderson, R. Morris, D. Amaral, T. Bliss, and J. O'Keefe, *The Hippocampus Book*. 2007, p. 872.

[46] H. Keshishian, "Ross Harrison's 'The outgrowth of the nerve fiber as a mode of protoplasmic movement'.," *J. Exp. Zool. A. Comp. Exp. Biol.*, vol. 301, no. January, pp. 201–203, 2004.

[47] A. N. Van Den Pol, K. Obrietan, A. B. Belousov, Y. Yang, and H. C. Heller, "Early synaptogenesis in vitro: Role of axon target distance," *J. Comp. Neurol.*, vol. 399, no. May, pp. 541–560, 1998.

[48] A. M. Hopkins, E. DeSimone, K. Chwalek, and D. L. Kaplan, "3D in vitro modeling of the central nervous system," *Prog. Neurobiol.*, vol. 125, pp. 1–25, 2015.

[49] B. G. Kornreich, "The patch clamp technique: principles and technical considerations.," *J. Vet. Cardiol.*, vol. 9, no. 1, pp. 25–37, May 2007.

[50] J. Halliwell, M. Whitaker, and D. Ogden, "Using microelectrodes," *Microelectrode Tech. Plymouth Work. Handb.*, vol. 3, pp. 1–15, 1949.

[51] O. P. Hamill, a. Marty, E. Neher, B. Sakmann, and F. J. Sigworth, "Improved patch-clamp techniques for high-resolution current recording from cells and cell-free membrane patches," *Pflügers Arch. Eur. J. Physiol.*, vol. 391, pp. 85–100, 1981.

[52] Biolin Scientific, "QPatch," 2014. [Online]. Available: http://www.biolinscientific.com/sophion/products/?card=SP4. [Accessed: 01-Jan-2015].

[53] S. B. Kodandaramaiah, G. T. Franzesi, B. Y. Chow, E. S. Boyden, and C. R. Forest, "Automated whole-cell patch-clamp electrophysiology of neurons in vivo.," *Nat. Methods*, vol. 9, no. 6, pp. 585–7, Jun. 2012.

[54] F. Hofmann and H. Bading, "Long term recordings with microelectrode arrays: studies of transcription-dependent neuronal plasticity and axonal regeneration.," *J. Physiol. Paris*, vol. 99, no. 2–3, pp. 125–32, 2006.

[55] L. A. Geddes, *Electrodes and the Measurement of Bioelectric Events*. Wiley-Interscience, 1972.

[56] F. Scholz, *Electroanalytical methods: Guide to experiments and applications*. 2010, pp. 1–359.

[57] S. B. Jun, M. R. Hynd, N. Dowell-Mesfin, K. L. Smith, J. N. Turner, W. Shain, and S. J. Kim, "Low-density neuronal networks cultured using patterned poly-l-lysine on microelectrode arrays.," *J. Neurosci. Methods*, vol. 160, no. 2, pp. 317–26, Mar. 2007.

[58] R. Morales, M. Riss, L. Wang, R. Gavín, J. A. Del Río, R. Alcubilla, and E. Claverol-Tinturé, "Integrating multi-unit electrophysiology and plastic culture dishes for network neuroscience.," *Lab Chip*, vol. 8, no. 11, pp. 1896–905, Nov. 2008.

[59] W.-C. Li, S. R. Soffe, and A. Roberts, "A direct comparison of whole cell patch and sharp electrodes by simultaneous recording from single spinal neurons in frog tadpoles.," *J. Neurophysiol.*, vol. 92, pp. 380–386, 2004.

[60] M. E. Spira and A. Hai, "Multi-electrode array technologies for neuroscience and cardiology.," *Nat. Nanotechnol.*, vol. 8, no. 2, pp. 83–94, Feb. 2013.

[61] H. Hirase, L. Qian, P. Barthó, and G. Buzsáki, "Calcium dynamics of cortical astrocytic networks in vivo.," *PLoS Biol.*, vol. 2, no. 4, p. E96, Apr. 2004.

[62] C. Grienberger and A. Konnerth, "Imaging calcium in neurons.," *Neuron*, vol. 73, no. 5, pp. 862–85, Mar. 2012.

[63] H. Westerblad and D. G. Allen, "Methods for calibration of fluorescent calcium indicators in skeletal muscle fibers.," *Biophys. J.*, vol. 66, no. March, pp. 926–928, 1994.

[64] N. Takahashi, T. Sasaki, A. Usami, N. Matsuki, and Y. Ikegaya, "Watching neuronal circuit dynamics through functional multineuron calcium imaging (fMCI).," *Neurosci. Res.*, vol. 58, no. 3, pp. 219–25, Jul. 2007.

References

[65] J. G. G. Borst and B. Sakmann, "Calcium current during a single action potential in a large presynaptic terminal of the rat brainstem," *J. Physiol.*, vol. 506, pp. 143–157, 1998.

[66] N. Takahashi, Y. Takahara, D. Ishikawa, N. Matsuki, and Y. Ikegaya, "Functional multineuron calcium imaging for systems pharmacology.," *Anal. Bioanal. Chem.*, vol. 398, no. 1, pp. 211–8, Sep. 2010.

[67] T. J. Bushell, R. Plevin, S. Cobb, and A. J. Irving, "Characterization of proteinase-activated receptor 2 signalling and expression in rat hippocampal neurons and astrocytes.," *Neuropharmacology*, vol. 50, no. 6, pp. 714–25, May 2006.

[68] H. J. Song, G. L. Ming, and M. M. Poo, "cAMP-induced switching in turning direction of nerve growth cones.," *Nature*, vol. 388, pp. 275–279, 1997.

[69] C. D. Harvey and K. Svoboda, "Locally dynamic synaptic learning rules in pyramidal neuron dendrites.," *Nature*, vol. 450, no. 7173, pp. 1195–1200, 2007.

[70] M. A. Sutton, A. M. Taylor, H. T. Ito, A. Pham, and E. M. Schuman, "Postsynaptic Decoding of Neural Activity: eEF2 as a Biochemical Sensor Coupling Miniature Synaptic Transmission to Local Protein Synthesis," *Neuron*, vol. 55, pp. 648–661, 2007.

[71] J. H. Schwartz and E. R. Kandel, *Principles of neural science*, 2nd editio. New York: Elsevier, 1985, p. 979.

[72] L. J. Millet and M. U. Gillette, "Over a century of neuron culture: From the hanging drop to microfluidic devices," *Yale J. Biol. Med.*, vol. 85, pp. 501–521, 2012.

[73] J. Wang, L. Ren, L. Li, W. Liu, J. Zhou, W. Yu, D. Tong, and S. Chen, "Microfluidics: a new cosset for neurobiology.," *Lab Chip*, vol. 9, no. 5, pp. 644–52, Mar. 2009.

[74] A. Kunze, R. Meissner, S. Brando, and P. Renaud, "Co-pathological connected primary neurons in a microfluidic device for Alzheimer studies.," *Biotechnol. Bioeng.*, vol. 108, no. 9, pp. 2241–5, Sep. 2011.

[75] H.-L. Song, S. Shim, D.-H. Kim, S.-H. Won, S. Joo, S. Kim, N. L. Jeon, and S.-Y. Yoon, "β-Amyloid is transmitted via neuronal connections along axonal membranes.," *Ann. Neurol.*, vol. 75, no. 1, pp. 88–97, Jan. 2014.

[76] E. K. Sackmann, A. L. Fulton, and D. J. Beebe, "The present and future role of microfluidics in biomedical research.," *Nature*, vol. 507, no. 7491, pp. 181–9, 2014.

[77] L. Kang, B. G. Chung, R. Langer, and A. Khademhosseini, "Microfluidics for drug discovery and development: From target selection to product lifecycle management," *Drug Discovery Today*, vol. 13. pp. 1–13, 2008.

[78] S. Halldórsson, E. Lucumi, R. Gómez-Sjöberg, and R. M. T. Fleming, "Advantages and challenges of microfluidic cell culture in polydimethylsiloxane devices," *Biosens. Bioelectron.*, Jul. 2014.

[79] R. B. Campenot, "Local control of neurite development by nerve growth factor," *Proc. Natl. Acad. Sci. USA*, vol. 74, pp. 4516–4519, 1977.

[80] A. M. Taylor, S. W. Rhee, C. H. Tu, D. H. Cribbs, C. W. Cotman, and N. L. Jeon, "Microfluidic Multicompartment Device for Neuroscience Research.," *Langmuir*, vol. 19, no. 5, pp. 1551–1556, Mar. 2003.

[81] Y. Gao, D. Majumdar, B. Jovanovic, C. Shaifer, P. C. Lin, A. Zijlstra, D. J. Webb, and D. Li, "A versatile valve-enabled microfluidic cell co-culture platform and demonstration of its applications to neurobiology and cancer biology.," *Biomed. Microdevices*, vol. 13, no. 3, pp. 539–48, Jun. 2011.

[82] T. Honegger, M. a Scott, M. F. Yanik, and J. Voldman, "Electrokinetic confinement of axonal growth for dynamically configurable neural networks.," *Lab Chip*, vol. 13, no. 4, pp. 589–98, Jan. 2013.

[83] B. a Walker, U. Hengst, H. J. Kim, N. L. Jeon, E. F. Schmidt, N. Heintz, T. a Milner, and S. R. Jaffrey, "Reprogramming axonal behavior by axon-specific viral transduction.," *Gene Ther.*, vol. 19, no. 9, pp. 947–55, Sep. 2012.

[84] A. M. Taylor, M. Blurton-Jones, S. W. Rhee, D. H. Cribbs, C. W. Cotman, and N. L. Jeon, "A microfluidic culture platform for CNS axonal injury, regeneration and transport," *Nat. Methods*, vol. 2, no. 8, p. 599, 2005.

[85] B. Deleglise, B. Lassus, V. Soubeyre, A. Alleaume-Butaux, J. J. Hjorth, M. Vignes, B. Schneider, B. Brugg, J.-L. Viovy, and J.-M. Peyrin, "Synapto-protective drugs evaluation in reconstructed neuronal network.," *PLoS One*, vol. 8, no. 8, p. e71103, Jan. 2013.

[86] A. M. Taylor, D. C. Dieterich, H. T. Ito, S. a Kim, and E. M. Schuman, "Microfluidic local perfusion chambers for the visualization and manipulation of synapses.," *Neuron*, vol. 66, no. 1, pp. 57–68, Apr. 2010.

[87] J. Park, H. Koito, J. Li, and A. Han, "A multi-compartment CNS neuron-glia Co-culture microfluidic platform.," *J. Vis. Exp.*, no. 31, pp. 6–8, Jan. 2009.

[88] A. Kunze, S. Lengacher, E. Dirren, P. Aebischer, P. J. Magistretti, and P. Renaud, "Astrocyte-neuron co-culture on microchips based on the model of SOD mutation to mimic ALS.," *Integr. Biol. (Camb).*, vol. 5, no. 7, pp. 964–75, Jul. 2013.

References

[89] J.-M. Peyrin, B. Deleglise, L. Saias, M. Vignes, P. Gougis, S. Magnifico, S. Betuing, M. Pietri, J. Caboche, P. Vanhoutte, J.-L. Viovy, and B. Brugg, "Axon diodes for the reconstruction of oriented neuronal networks in microfluidic chambers.," *Lab Chip*, vol. 11, pp. 3663–3673, Sep. 2011.

[90] T. T. Kanagasabapathi, P. Massobrio, R. A. Barone, M. Tedesco, S. Martinoia, W. J. Wadman, and M. M. J. Decré, "Functional connectivity and dynamics of cortical-thalamic networks co-cultured in a dual compartment device.," *J. Neural Eng.*, vol. 9, no. 3, p. 036010, Jul. 2012.

[91] S. Hosmane, A. Fournier, R. Wright, L. Rajbhandari, R. Siddique, I. H. Yang, K. T. Ramesh, A. Venkatesan, and N. Thakor, "Valve-based microfluidic compression platform: single axon injury and regrowth.," *Lab Chip*, vol. 11, no. 22, pp. 3888–95, Nov. 2011.

[92] H. J. Kim, J. W. Park, J. W. Park, J. H. Byun, B. Vahidi, S. W. Rhee, and N. L. Jeon, "Integrated Microfluidics Platforms for Investigating Injury and Regeneration of CNS Axons.," *Ann. Biomed. Eng.*, vol. 40, no. 6, pp. 1268–1276, Feb. 2012.

[93] L. Li, L. Ren, W. Liu, J.-C. Wang, Y. Wang, Q. Tu, J. Xu, R. Liu, Y. Zhang, M.-S. Yuan, T. Li, and J. Wang, "Spatiotemporally controlled and multifactor involved assay of neuronal compartment regeneration after chemical injury in an integrated microfluidics.," *Anal. Chem.*, vol. 84, no. 15, pp. 6444–53, Aug. 2012.

[94] A. M. Kaufman, A. J. Milnerwood, M. D. Sepers, A. Coquinco, K. She, L. Wang, H. Lee, A. M. Craig, M. Cynader, and L. a Raymond, "Opposing roles of synaptic and extrasynaptic NMDA receptor signaling in cocultured striatal and cortical neurons.," *J. Neurosci.*, vol. 32, no. 12, pp. 3992–4003, Mar. 2012.

[95] T. T. Kanagasabapathi, M. Franco, R. A. Barone, S. Martinoia, W. J. Wadman, and M. M. J. Decré, "Selective pharmacological manipulation of cortical-thalamic co-cultures in a dual-compartment device.," *J. Neurosci. Methods*, vol. 214, no. 1, pp. 1–8, Mar. 2013.

[96] D. A. Links, "Lab on a Chip Valve-based microfluidic compression platform : single axon injury and," pp. 3888–3895, 2011.

[97] E. Biffi, F. Piraino, A. Pedrocchi, G. B. Fiore, G. Ferrigno, A. Redaelli, A. Menegon, and M. Rasponi, "A microfluidic platform for controlled biochemical stimulation of twin neuronal networks.," *Biomicrofluidics*, vol. 6, no. 2, pp. 24106–2410610, Jun. 2012.

[98] T. T. Kanagasabapathi, D. Ciliberti, S. Martinoia, W. J. Wadman, and M. M. J. Decré, "Dual-compartment neurofluidic system for electrophysiological

measurements in physically segregated and functionally connected neuronal cell culture.," *Front. Neuroeng.*, vol. 4, no. Article 13, pp. 1–11, Jan. 2011.

[99]   V. Jokinen, P. Sakha, P. Suvanto, C. Rivera, S. Franssila, S. E. Lauri, and H. J. Huttunen, "A microfluidic chip for axonal isolation and electrophysiological measurements.," *J. Neurosci. Methods*, vol. 212, no. 2, pp. 276–82, Jan. 2013.

[100]  L. Vitzthum, X. Chen, D. B. Kintner, Y. Huang, S.-Y. Chiu, J. Williams, and D. Sun, "Study of Na+/H+ exchange-mediated pHi regulations in neuronal soma and neurites in compartmentalized microfluidic devices.," *Integr. Biol. (Camb).*, vol. 2, no. 1, pp. 58–64, Jan. 2010.

[101]  A. Taylor and N. Berchtold, "Axonal mRNA in uninjured and regenerating cortical mammalian axons," *J. ...*, vol. 29, no. 15, pp. 4697–4707, 2009.

[102]  J. Harris, H. Lee, B. Vahidi, C. Tu, D. Cribbs, C. Cotman, and N. L. Jeon, "Non-plasma bonding of PDMS for inexpensive fabrication of microfluidic devices.," *J. Vis. Exp.*, no. 9, p. 410, Jan. 2007.

[103]  J. W. Park, B. Vahidi, A. M. Taylor, S. W. Rhee, and N. L. Jeon, "Microfluidic culture platform for neuroscience research.," *Nat. Protoc.*, vol. 1, no. 4, pp. 2128–36, Jan. 2006.

[104]  J. C. McDonald, D. C. Duffy, J. R. Anderson, D. T. Chiu, H. Wu, O. J. Schueller, and G. M. Whitesides, "Fabrication of microfluidic systems in poly(dimethylsiloxane).," *Electrophoresis*, 2000.

[105]  F. Katzenberg and F. B.- Chemieingenieurwesen, "Plasma-bonding of poly ( dimethylsiloxane ) to glass," no. 060, pp. 1–5, 2005.

[106]  J. Gan, S. M. Greenwood, S. R. Cobb, and T. J. Bushell, "Indirect modulation of neuronal excitability and synaptic transmission in the hippocampus by activation of proteinase-activated receptor-2.," *Br. J. Pharmacol.*, vol. 163, no. 5, pp. 984–94, Jul. 2011.

[107]  C. J. Ledgerwood, S. M. Greenwood, R. R. Brett, J. a Pratt, and T. J. Bushell, "Cannabidiol inhibits synaptic transmission in rat hippocampal cultures and slices via multiple receptor pathways.," *Br. J. Pharmacol.*, vol. 162, no. 1, pp. 286–94, Jan. 2011.

[108]  T. J. Bushell, C. C. Lee, R. Shigemoto, and R. J. Miller, "Modulation of synaptic transmission and differential localisation of mGlus in cultured hippocampal autapses.," *Neuropharmacology*, vol. 38, no. 10, pp. 1553–67, Oct. 1999.

[109]  T. Fellin and G. Carmignoto, "Neurone-to-astrocyte signalling in the brain represents a distinct multifunctional unit.," *J. Physiol.*, vol. 559, no. Pt 1, pp. 3–15, Aug. 2004.

References

[110] K. W. Oh, K. Lee, B. Ahn, and E. P. Furlani, "Design of pressure-driven microfluidic networks using electric circuit analogy.," *Lab Chip*, vol. 12, no. 3, pp. 515–45, Feb. 2012.

[111] H. Bruus, *Theoretical Microfluidics*. New York: Oxford University Press Inc, 2008.

[112] S. A. Rani, B. Pitts, and P. S. Stewart, "Rapid diffusion of fluorescent tracers into Staphylococcus epidermidis biofilms visualized by time lapse microscopy," *Antimicrob. Agents Chemother.*, vol. 49, pp. 728–732, 2005.

[113] P. Galambos and F. K. Forster, "Micro-Fluidic Diffusion Coefficient Measurement," in *Micro Total Analysis Systems '98*, 1998, pp. 189–192.

[114] W. R. Holmes, "Modeling the effect of glutamate diffusion and uptake on NMDA and non-NMDA receptor saturation.," *Biophys. J.*, vol. 69, no. 5, pp. 1734–47, Nov. 1995.

[115] V. M. M. Lobo, A. C. F. Ribeiro, and L. M. P. Verissimo, "Diffusion coefficients in aqueous solutions of potassium chloride at high and low concentrations," *J. Mol. Liq.*, vol. 78, pp. 139–149, 1998.

[116] F. Bianco, N. Tonna, R. D. Lovchik, R. Mastrangelo, R. Morini, A. Ruiz, E. Delamarche, and M. Matteoli, "Overflow microfluidic networks: application to the biochemical analysis of brain cell interactions in complex neuroinflammatory scenarios.," *Anal. Chem.*, vol. 84, no. 22, pp. 9833–40, Nov. 2012.

[117] M. Shi, D. Majumdar, Y. Gao, B. M. Brewer, C. R. Goodwin, J. a McLean, D. Li, and D. J. Webb, "Glia co-culture with neurons in microfluidic platforms promotes the formation and stabilization of synaptic contacts.," *Lab Chip*, vol. 13, no. 15, pp. 3008–21, Jul. 2013.

[118] D. Rossi and A. Volterra, "Astrocytic dysfunction: insights on the role in neurodegeneration.," *Brain Res. Bull.*, vol. 80, no. 4–5, pp. 224–32, Oct. 2009.

[119] M. a Sutton, H. T. Ito, P. Cressy, C. Kempf, J. C. Woo, and E. M. Schuman, "Miniature neurotransmission stabilizes synaptic function via tonic suppression of local dendritic protein synthesis.," *Cell*, vol. 125, no. 4, pp. 785–99, May 2006.

[120] C. Schauer and T. Leinders-Zufall, "Imaging calcium responses in GFP-tagged neurons of hypothalamic mouse brain slices.," *J. Vis. Exp.*, no. 66, p. e4213, Jan. 2012.

[121] T. Leinders-zufall, "Technique for setting up the perfusion of a recording chamber for physiological studies with cultured and acutely dissociated cells," 1998.

References

[122] Y.-H. Hsu, M. L. Moya, P. Abiri, C. C. W. Hughes, S. C. George, and A. P. Lee, "Full range physiological mass transport control in 3D tissue cultures.," *Lab Chip*, vol. 13, no. 1, pp. 81–9, Jan. 2013.

[123] H. D. Baehr and K. Stephan, *Heat and Mass Transfer*, 3rd ed. Berlin, Heidelberg: Springer Berlin Heidelberg, 2011.

[124] S. Patankar, "Numerical heat transfer and fluid flow," in *Series in coputational methods in mechanics and thermal sciences*, 1980, pp. 1–197.

[125] L. Xiao, S. K. Mahto, and S. W. Rhee, "Axon orientation by gradient of cytochalasin D inside microfluidic device," vol. 6, pp. 335–341, 2012.

[126] S. Giulitti, E. Magrofuoco, L. Prevedello, and N. Elvassore, "Optimal periodic perfusion strategy for robust long-term microfluidic cell culture.," *Lab Chip*, vol. 13, no. 22, pp. 4430–41, Nov. 2013.

[127] B. F. Godley, F. A. Shamsi, F. Liang, S. G. Jarrett, S. Davies, and M. Boulton, "Blue Light Induces Mitochondrial DNA Damage and Free Radical Production in Epithelial Cells *," vol. 280, no. 22, pp. 21061–21066, 2005.

[128] T. Nishigaki, C. D. Wood, K. Shiba, S. A. Baba, and A. Darszon, "Stroboscopic illumination using light-emitting diodes reduces phototoxicity in fluorescence cell imaging," vol. 41, no. 2, pp. 191–197, 2006.

[129] M. Cedex, "Molecular , Functional , and Pharmacological Characterization Metabotropic Glutamate Receptor Type 5 Splice Variants : Comparison with mGluR1," vol. 75, no. May, pp. 3970–3981, 1995.

[130] J. D. Wang, N. J. Douville, S. Takayama, and M. Elsayed, "Quantitative analysis of molecular absorption into PDMS microfluidic channels," *Ann. Biomed. Eng.*, vol. 40, pp. 1862–1873, 2012.

[131] M. W. Toepke and D. J. Beebe, "PDMS absorption of small molecules and consequences in microfluidic applications.," *Lab Chip*, vol. 6, no. c, pp. 1484–1486, 2006.

[132] A. M. Taylor and N. L. Jeon, "Micro-scale and microfluidic devices for neurobiology.," *Curr. Opin. Neurobiol.*, vol. 20, no. 5, pp. 640–7, Oct. 2010.

[133] R. A. Stetler, R. K. Leak, Y. Gan, P. Li, F. Zhang, X. Hu, Z. Jing, J. Chen, M. J. Zigmond, and Y. Gao, "Preconditioning provides neuroprotection in models of CNS disease: Paradigms and clinical significance," *Prog. Neurobiol.*, vol. 114, pp. 58–83, 2014.

[134] Y. Wang, G. Jing, S. Perry, F. Bartoli, and S. Tatic-Lucic, "Spectral characterization of the voltage-sensitive dye di-4-ANEPPDHQ applied to

probing live primary and immortalized neurons.," *Opt. Express*, vol. 17, no. 2, pp. 984–990, 2009.

[135] S. Wray, M. Self, P. a. Lewis, J. W. Taanman, N. S. Ryan, C. J. Mahoney, Y. Liang, M. J. Devine, U. M. Sheerin, H. Houlden, H. R. Morris, D. Healy, J. F. Marti-Masso, E. Preza, S. Barker, M. Sutherland, R. a. Corriveau, M. D'Andrea, A. H. V Schapira, R. J. Uitti, M. Guttman, G. Opala, B. Jasinska-Myga, A. Puschmann, C. Nilsson, A. J. Espay, J. Slawek, L. Gutmann, B. F. Boeve, K. Boylan, a. Jon Stoessl, O. a. Ross, N. J. Maragakis, J. Van Gerpen, M. Gerstenhaber, K. Gwinn, T. M. Dawson, O. Isacson, K. S. Marder, L. N. Clark, S. E. Przedborski, S. Finkbeiner, J. D. Rothstein, Z. K. Wszolek, M. N. Rossor, J. Hardy, J. F. Gusella, M. E. MacDonald, V. C. Wheeler, C. a. Ross, S. Akimov, J. Arjomand, L. M. Thompson, A. King, N. Hermanowicz, S. Winokur, C. N. Svendsen, V. Mattis, M. Onorati, E. Cattaneo, N. D. Allen, P. J. Kemp, K. S. Kim, S. Przedborski, J. Feng, V. M. Y. Lee, J. Q. Trojanowski, D. James Surmeier, C. E. Henderson, T. Maniatis, K. Eggan, and M. E. Cudowicz, "Creation of an open-access, mutation-defined fibroblast resource for neurological disease research," *PLoS One*, vol. 7, no. 8, pp. 1–8, 2012.

[136] NC3Rs, "Challenge 12: UnTangle," *CRACK IT*, 2014. [Online]. Available: https://www.crackit.org.uk/challenge-12-untangle. [Accessed: 01-Feb-2015].

[137] NC3Rs, "CRACK IT Challenge winners awarded £4.9 million to further their research," *CRACK IT*, 2014. [Online]. Available: https://www.nc3rs.org.uk/crackit-news/crack-it-challenge-winners-awarded-£49-million-further-their-research. [Accessed: 01-Feb-2015].

# Appendix

## Publications

**1.**     G. Robertson, T. Bushell, M. Zagnoni "Chemically induced synaptic activity between mixed primary hippocampal co-cultures in a microfluidic system"

Integr. Biol., 2014,6, 636-644 DOI: 10.1039/C3IB40221E

Received 25 Oct 2013, Accepted 27 Apr 2014

First published online 28 Apr 2014


**(2.)**     A. Sampson, G. Robertson, C. Moffat, M. Zagnoni, C. Connolly "Recruiting rapidly spreading neuroprotective signalling to combat neurotoxicity"

*(Pre-submission)*


**(3.)**     Cover Image of *Nature Reviews Neurology 2015* (12 issues)

## Conference Presentations

29/10/2014    MicroTAS 2014 (San Antonio, Texas, USA) : "A Microfluidic Platform for Human Tau Mutation Neurons"(Poster presentation)

24/08/2014    Scottish Neuroscience Group 2014 (Glasgow University, UK): "A Microfluidic Perfusion System for Neuronal Network Communication Study" (Poster presentation)

17/03/2014    SET for Britain 2014 (Houses of Parliament, London, UK) "Healthy Communication: Brain Disorders on a Chip"
(Poster Presentation) *Biological and Biomedical Sciences Gold Award and winner of the GW Mendel Medal*

17/01/2014    Glasgow Neuroscience Day 2014 (Glasgow, UK): "Developing novel microfluidic platforms for neuroscience research" (Oral presentation)

30/08/2013    Scottish Neuroscience Group 2013 (Glasgow, UK): "A Microfluidic Tool for Neuroscience Research" (Poster presentation)

11/07/2013    PGBiomed 2013 (Surrey, UK): "A Microfluidic Tool for Neuronal Network Signalling Studies" (Oral presentation)

08/04/2013    BNA Festival of Neuroscience 2013 (London, UK): "A Microfluidic Tool for Neuroscience Research" (Poster presentation)

23/01/2013    Glasgow Neuroscience Day 2013 (Glasgow, UK): "A Microfluidic Tool for Neuroscience Research" (Poster presentation)

31/08/2012    Scottish Neuroscience Group 2012 (Dundee, UK): "A Microfluidic Tool for Neuroscience Research" (Poster presentation)

# MATLAB Files – Processing Ca$^{2+}$ Imaging

## FormatData.m

```
%%  PART1: Run this as soon as the data is loaded.

%   Manually load the dataset from the excel spreadsheet
%        Select the raw intensity values of all signals
%        Copy them into a new matrix called "data"

%   Inputs:     data
%
%   Defined:    BKGROWS
%               NRNG
%               TRUNC_START
%               TRUNC_END
%
%   Locals:     rawIntT
%               Bkgdata
%               filterINT
%               rmbINT
%               shiftINT
%               i, k, j
%
%   Outputs:    tInt
%               noRegions
%               noFrames

%% Initial Check
if ~exist('data','var'); error('Error: Variable ''data'' does not
         exist. Please load the data and call it ''data''.'); end;

%% Settings and defaults
    % The first rows are assumed to be the background.
    % This is the number of rows that are the background.
    % The default is assumed to be 1 background row.
if ~exist('BKGROWS','var'); BKGROWS = 1; end;

    % Moving average over nRng values, Must be ODD!
    % The default is assumed to be a window of 11.
if ~exist('NRNG','var'); NRNG = 3; end;

    % Number of samples at the start and end to remove.
    % Default for both is set to be 10.
if ~exist('TRUNC_START','var'); TRUNC_START = 1; end;
if ~exist('TRUNC_END','var'); TRUNC_END = 0; end;

% Trigger Information. While not used here, it is required for later
         use.

    % Number of Triggers
if ~exist('NTRIG','var'); NTRIG = 4; end; % Default 3
    % Location of Triggers, what frames they occur.
if ~exist('TRIGS','var'); TRIGS = [85 825 1445 1805]; end;
    % Names of Triggers
if ~exist('NAMET','var')
```

# Appendix

```matlab
        NAMET = {...
                'Indirect Vehicle',...
                'Indirect Glutamate',... %'Indirect Potassium',...
                'Direct KCL1',...
                'Direct KCL2'};
end;

%%  Truncate the dataset

% Remove any zero filled rows or columns
rawIntT = data;

rawIntT( ~any(rawIntT,2), : ) = []; % Clear empty rows
rawIntT( :, ~any(rawIntT,1) ) = []; % Clear empty columns

% Get the number of frames (noFrames)
% Get the number of traces (noTraces)
[noRegions, noFrames] = size(rawIntT);

Bkgdata = rawIntT(1:BKGROWS,:);      % Grab the background values
          from the truncated raw data. The background is assumed to
          be the first row.
BkgAr = mean(Bkgdata,1);             % Find background average if
          necessary.

%% Filter and format the dataset

rmbINT = rawIntT;
filterINT = rawIntT;
shiftINT = filterINT;
fInt = filterINT;

% Stores the filtered data in filterInt
for i = BKGROWS+1:noRegions
    rmbINT(i,:)      = rawIntT(i,:)-BkgAr;
         % Remove background
    filterINT(i,:)  = filter(ones(1,NRNG)/NRNG,1,rmbINT(i,:));
         % filters filterInt
    shiftINT(i,1:noFrames-(NRNG-1)/2)   =
         filterINT(i,(NRNG+1)/2:noFrames);     % Shift the filtered
         data to correct for filter induced offset
    shiftINT(i,1:(NRNG-1)/2)               = shiftINT(i,(NRNG+1)/2);
         % Change start
    shiftINT(i,noFrames-(NRNG-1)/2:noFrames) = shiftINT(i,noFrames-
         (NRNG-1)/2); % Change end
end

shiftINT(1,:) = BkgAr;                               % Make the
         first row of fInt the averaged background
for i = 1:noRegions-BKGROWS+1
    for k = 1:noFrames
        j = i+BKGROWS-1;                            % Provides
         the shift upwards if there are empty rows of background.
        fInt(i,k) = shiftINT(j,k)/shiftINT(j,TRUNC_START);     %
         Normalise to first displayed value.
    end
end
```

```
k = BKGROWS;
while(k>1)                              % Remove the excess rows.
        Deletes the bottom row until all empty rows are removed.
    fInt(noRegions-BKGROWS+k,:) = [];
    k = k-1;
end
noRegions = noRegions-BKGROWS+1;    % redefine the number of regions
        to have only one background trace.

%% Truncate start and end

tInt = fInt(1:noRegions,TRUNC_START:(noFrames-TRUNC_END));
noFrames = noFrames - TRUNC_START+1 - TRUNC_END;

TRIGS = TRIGS - TRUNC_START;

clearvars i k j shiftINT filterINT rmbINT rawIntT Bkgdata BkgAr fInt
clearvars NRNG BKGROWS TRUNC_END TRUNC_START

disp('Datasets formatted!')

%% Save Progress
disp('Saving Progress...')
save('TEMP_PROGRESS1')
disp('Progress Saved!')
```

## ChooseCategories.m

```
%%  PART2: Run this to put the traces into categories.

%   Must run FormatData before this routine.
%   Manually select which trace goes where.

%   Inputs:     tInt
%               noRegions
%               noFrames
%
%   Defined:    MCS
%               NTRIG
%               TRIGS
%               NAMET
%               TOL
%
%   Outputs:    cTrace      % Stores the selected category of each
        trace.
%               nuTrace     % Stores the number of each traces in
        each category.
%               bkgTime     % Stores potentially misleading frame
        numbers.


%% Initial Check
if ~exist('tInt','var'); error('Error: Variable ''tInt'' does not
        exist. Please load the data and run ''FormatData''.'); end;

% For debugging just doing 10 regions
% noRegions = 10;
```

Appendix

```matlab
%% Definitions

% Menu Content
MCS = { 'Neuron : ~ / ',...
        'Astroc : ~ \ ',...
        'Errors / Unsure'};

TOL = 0.05;       % Used to define the tolerance that triggers a grey
          area.
SIG = 1.5;        % Used to determine what is a significant increase.


%% Find and Display Background Grey Areas

% Background grey areas are regions where the background
          significantly deviates from the standard which suggests
          that an external influence may affect a recording
% Work out the linear best fit line for the background trace
p = polyfit(1:1:noFrames,tInt(1,:),1);  % Bestfit coefficients
bkgfit = (1:1:(noFrames))*p(1)+p(2);      % Line of bestfit
          coordinates

tempJK = 0;       % Used to define if in or out of a grey area.
bkgTime = [];     % Used to store the frame stamps of the grey areas.
k = 0;            % Floating index for iTime.
for i = 1:1:noFrames
    if bkgfit(i) > (tInt(1,i)+TOL) || bkgfit(i) < (tInt(1,i)-TOL) %
          Conditions of grey area.
        if tempJK == 0       % Start a grey area.
            tempJK = 1;
            k = k+1;
            bkgTime(k)=i;
        end
    else
        if tempJK == 1       % End a grey area.
            tempJK = 0;
            k = k+1;
            bkgTime(k)=i;
        end
    end
end

if mod(k,2) == 1             % Check and ensure that iTime is even.
    k = k+1;
    bkgTime(k) = i;
end

% Plot Background Data.
figH1 = figure;
set(figure(figH1),'Color',[0.95 0.95 1]);
hold on;

n = size(bkgTime,2)/2;
for i=1:n                                    % Plot the grey
          areas.
    area([round(bkgTime(2*i-1)) round(bkgTime(2*i))], [2 2],
          0,'FaceColor',[0.8 0.8 0.9],'LineStyle','none');
end
```

```
plot(1:1:noFrames,tInt(1,:),'Color',[0 0 0])     % Plot the
         background trace.
plot(1:1:noFrames,bkgfit(:),'Color',[0 0 1])     % Plot the bestfit
         background trace.
axis([1, noFrames, 0, 2]);                        % Scale the axis
         accordingly.
clear title xlabel;
title('Background reading that is subtracted from all other
         traces.');


clearvars tempJK n k i p bkgfit     % Clear non-essential variables


%% Draw the traces and categorise them

figH2 = figure;  % Create a new figure
set(gca,'Color',[1 1 1]);
set(figure(figH2),'Color',[0.9 0.95 1]);

if ~exist('cTrace','var')

    cTrace = zeros(noRegions,1);     % Define cTrace for the first
         time.
    hold on
    if exist('iTime','var')                          % Check
         if background grey areas have been stored
        n = size(bkgTime,2)/2;
        for j = 1:n                                  % Draw
          the Background grey areas
            area([round(bkgTime(2*j-1)) round(bkgTime(2*j))], [10
        10], 0,'FaceColor',[0.8 0.8 0.9],'LineStyle','none');
        end
    end

    plot(1:1:noFrames,tInt(1,:),'Color',[0,0,0.5])        % Draw
         the background trace
    for j = 1:NTRIG                                       %
         Display all of the defined trigger lines.
        line([TRIGS(j);TRIGS(j)],[0;10],'Color',[0.5 0 0]);
    end

    for i = 2:1:noRegions;        % Display each trace and ask user to
         select it's category
        mymax = max(tInt(i,:)); % Find the maximum (min 2)
        if mymax < 2
            mymax = 2;
        end

        hLine = plot(1:1:noFrames,tInt(i,:),'Color',[0.2 0.2 0.5]');
         % Plot the Graph
        axis([1, noFrames, 0, mymax]);
         % Scale the axis correctly
        str = sprintf([ 'Trace ID#: %d\n'...
                        'Select the category of this trace.'], i);
        title(str);

        while(cTrace(i) == 0)   % Let the user select a category.
            cTrace(i) = menu(  'Choose a category',MCS);
        end
```

```
        delete(hLine);              % Clear the line before the next
            trace.
    end
else
    disp('Not Run: cTrace already exists!')
end


%% Count the types of traces

nuTrace = zeros(1,3);
for i=2:noRegions;       % Work out how many of each type of trace
        there are.
    switch cTrace(i)
        case 1
            nuTrace(1) = nuTrace(1) + 1;
        case 2
            nuTrace(2) = nuTrace(2) + 1;
        case 3
            nuTrace(3) = nuTrace(3) + 1;
    end
end
disp('nuTrace updated!')

clearvars i j n mymax hLine str cookie

%% Close

close all
clearvars figH1 figH2

%% Save Progress
disp('Saving Progress...')
save('TEMP_PROGRESS2')
disp('Progress Saved!')
```

## ChooseEvents.m

```
%%  PART3: Run this to select the event locations and peaks

%   Must run FormatData and ChooseCategories before this routine.
%   Manually select which trace goes where.
%
%   Inputs:      tInt
%
%   Defined:     HBUF
%
%   Outputs:     caTime  % Store the time of each event
%                caRise  % Store the magnitude of each event
%

%% Initial Check
if ~exist('cTrace','var'); error('Error: Variable ''cTrace'' does
        not exist.'); end;

% For debugging just doing 10 regions
%noRegions = 10;
```

```matlab
%% Definitions

% Horizontal buffer of selection
HBUF = 20;

%% Script

figH1 = figure;  % Creat a figure and make it pretty
set(gca,'Color',[1 1 1]);
set(figure(figH1),'Color',[0.9 0.95 1]);

hold on
if exist('bkgTime','var')    % Check if background grey areas have
        been selected
    n = size(bkgTime,1)/2;

    for j = 1:n              % Draw the Background grey areas
        area([round(bkgTime(2*j-1)) round(bkgTime(2*j))], [mymax
        mymax], 0,'FaceColor',[1 0.95 0.95],'LineStyle','none');
    end
end
                               % Plot the Background
plot(1:1:noFrames,tInt(1,:),'Color',[0,0,0])
for k = 1:NTRIG             % Display all of the defined trigger
        lines.
    line([TRIGS(k);TRIGS(k)],[0;10],'Color',[0.5 0 0]);
end


if ~exist('caTime','var') % Check that this has not been run already
    caTime = zeros(noRegions,2);    % Create an array to store the
        times of each event
    caRise = zeros(noRegions,2);    % Create an array to store the
        magnitude of the event

    for i=2:1:noRegions; % 2:1:noRegions; Display each trace and ask
        user to select the peaks
        if cTrace(i)<3
            mymax=max(tInt(i,:));    % Find the maximum (min = 2)
            if mymax < 2; mymax = 2; end

            hLine = [0 0];
            hLine(1) = plot(HBUF:1:noFrames-
        HBUF,tInt(i,HBUF:noFrames-HBUF),'Color',[0.2 0.2 0.5]');%
        Plot the Graph

            axis([HBUF, noFrames-HBUF, 0, mymax]);    % Scale the
        axis correctly
            str = sprintf([ 'Trace ID#: %d'...
                            '\n%s'...
                            '\nSelect the Start, and Peak of each
        event.'...
                            '\nMust be a multiple of 2!!!'], i,
        MCS{cTrace(i)});
            title(str);

            cookie = 0;
            n = 0;
```

```
        while(cookie == 0 || mod(n,2) ~=0)   % User selects
    individual event starts and peaks.
            temp1 = ginput(1);                % Get the user's
    selected frame number.
            if isempty(temp1)
                if n ~= 0
                    cookie = 1;
                end
            else
                n = n+1;
                temp1 = round(temp1(1));     % Round selection to
    the nearest whole number.
                if mod(n,2) == 0              % Determine if this
    is the first or second line of an event.
                    mycol = [1 0 0];         % Red for Max of
    event.
                    [~, temp2] = max(tInt(i,temp1-
    HBUF:temp1+HBUF));    % Sweeps right and left to find local
    max.
                else
                    mycol = [0 1 0];         % Green for Start of
    event.
                    [~, temp2] = min(tInt(i,temp1-
    HBUF:temp1+HBUF));    % Sweeps right and left to find local
    min.
                end
                temp1 = temp1 + temp2 - HBUF -1; % need to
    include a -1 here to account for an array that does not
    start at element 0.
                                              % Draw the line to
    show what is selected.
                hLine(n+1) =
    line([temp1;temp1],[0;mymax],'Color',mycol);
                caTime(i,n) = temp1;          % Store the location
    of the line.
                caRise(i,n) = tInt(i,caTime(i,n));
            end
        end
        if n ~=0
            delete(hLine);
        else
            i = i-1;
        end
    end
    end
else
    disp('Not Run: caTime already exists!')
end

close(figH1)
clearvars mycol hLine n i k j figH1 tempvar mymax cookie str temp1
         temp2
clearvars HBUF


%% Save Progress
disp('Saving Progress...')
save('TEMP_PROGRESS3')
disp('Progress Saved!')
```

# EditEvents.m

```
%%  PART4: Run this to Edit the event locations and peaks

%   Must run FormatData, ChooseCategories and ChoosePeaks before
          this routine.
%   Manually reselect where each maximum and minimum is.
%

%% Initial Check
if ~exist('caTime','var'); error('Error: Variable ''caTime'' does
          not exist.'); end;

% For debugging just doing 10 regions
%noRegions = 10;


%% Definitions

% Horizontal buffer of selection
HBUF = 10;


%% Script

figH1 = figure;  % Creat a figure and make it pretty
set(gca,'Color',[1 1 1]);
set(figure(figH1),'Color',[0.9 0.95 1]);

hold on
if exist('bkgTime','var')    % Check if background grey areas have
          been selected
    n = size(bkgTime,1)/2;

    for j = 1:n              % Draw the Background grey areas
        area([round(bkgTime(2*j-1)) round(bkgTime(2*j))], [mymax
          mymax], 0,'FaceColor',[1 0.95 0.95],'LineStyle','none');
    end
end
plot(1:1:noFrames,tInt(1,:),'Color',[0,0,0])% Plot the Background
for k = 1:NTRIG              % Display all of the defined trigger
          lines.
    line([TRIGS(k);TRIGS(k)],[0;10],'Color',[0.5 0 0]);
end

for i=2:1:noRegions; % Display each trace and ask user to select the
          peaks
    if cTrace(i)<3
        mymax=max(tInt(i,:));   % Find the maximum
        if mymax < 2
            mymax = 2;
        end

        hLine = [0 0];          % Plot the Graph
        hTLine = plot(HBUF:1:noFrames-HBUF,tInt(i,HBUF:noFrames-
          HBUF),'Color',[0.2 0.2 0.5]');
```

```
axis([HBUF, noFrames-HBUF, 0, mymax]);    % Scale the axis
 correctly
str = sprintf([ 'Trace ID#: %d\n'...
               'Select the Start, and Peak of each
 event.'...
               '\nMust be a multiple of 2!!!'], i);
title(str);
choice = 1;     % Lets the user edit the graph until
 satisfied.
while (choice ~= 2)

    sample = caTime(i,:);   % Load all the events for the
 current trace.
    sample = sample(1:find(sample,1,'last'));   % Remove all
 non-events.
    if ~isempty(sample)     % If there are events to plot,
 then plot all event lines.
        for m = 2:2:size(sample,2)
            hLine(m-1)=line([sample(m-1);sample(m-
1)],[0;mymax],'Color',[0 1 0]);    % Start of event

hLine(m)=line([sample(m);sample(m)],[0;mymax],'Color',[1 0
0]);          % End of event
        end
    end

    choice = menu('Edit?', 'Edit', 'Keep'); % Lets the user
 edit the graph until satisfied.
    delete(hLine)       % Clears all of the event lines
 currently projected.
    hLine = [0 0];      % Defines array for handles of the
 new event lines.
    if choice == 1
        caTime(i,:) = zeros(1,size(caTime(i,:),2)); % Clear
 the previously stored event locations.
        %caRise(i,:) = zeros(1,size(caRise(i,:),2)); % Clear
 the previously stored event magnitudes.
        cookie = 0;     % Watch the cookie crumble.
        n = 0;          % What's your n-number...?
        while(cookie == 0 || mod(n,2) ~=0)  % User selects
 individual event starts and peaks.
            temp1 = ginput(1);              % Get the user's
 selected frame number.
            if isempty(temp1)
                if n ~= 0
                    cookie = 1;
                end
            else
                n = n+1;
                temp1 = round(temp1(1));    % Round
 selection to the nearest whole number.
                if mod(n,2) == 0            % Determine if
 this is the first or second line of an event.
                    mycol = [1 0 0];        % Red for Max of
 event.
                    [~, temp2] =
 max(tInt(i,temp1:(temp1+HBUF)));
```

**170**

```
                                        temp1 = temp1 + temp2 -1;              %
            Sweeps right from selection, -1 here as array does not
            start at element 0.
                                else
                                    mycol = [0 1 0];         % Green for
            Start of event.
                                    [~, temp2] = min(tInt(i,(temp1-
            HBUF):temp1));
                                    temp1 = temp1 + temp2 - HBUF -1;      %
            Sweeps right from selection - HBUF (i.e. left), -1 here as
            array does not start at element 0.
                                end
                                                            % Draw the line
            to show what is selected.
                                hLine(n) =
            line([temp1;temp1],[0;mymax],'Color',mycol);
                                caTime(i,n) = temp1;           % Store the
            location of the line.
                                %caRise(i,n) = tInt(i,caTime(i,n));
                             end
                        end
                        if n ~=0
                            delete(hLine);
                        else
                            i = i-1;
                        end
                    end
                end
            end
            delete(hTLine)  % Clear the Trace.
        end
end


close(figH1)
clearvars mycol hLine hTLine n m i k j figH1 tempvar mymax cookie
        str temp1 temp2 choice sample HBUF


%% Save Progress
disp('Saving Progress...')
save('TEMP_PROGRESS4')
disp('Progress Saved!')
```

## EventEvaluation.m

```
%% PART5: Look at all of the chosen peaks and determine which are
        significant events.


%% Initial Check
if ~exist('caTime','var');     error('Error: Variable ''caTime'' does
        not exist.'); end;


%% Definitions

if ~exist('SIG','var')
    SIG = 1.5;
    disp('Significance set to 0.5 Normalised Fluorescence Units.');
```

```matlab
end

MYZONES = [1 TRIGS noFrames];


%% Script
% Finds significant events

events = zeros(noRegions,2,1);
keptEvents = 0;
removedEvents = 0;
NuConflicts = 0;
conflicts = [0];
for i = 2:1:noRegions
    if cTrace(i) < 3
        sample = caTime(i,:);
        sample(sample == 0) = [];
        sizesample = size(sample, 2);
        if sizesample > 0 % Checks that there are samples available
            k = 0;
            for j = 1:1:(sizesample/2)
                tTime  = (caTime(i,j*2-1)+caTime(i,j*2))/2;
                tRise  = tInt(i,caTime(i,j*2))-tInt(i,caTime(i,j*2-
        1));
                %tpRise =
        tInt(i,(caTime(i,j*2)))/tInt(i,(caTime(i,j*2-1)));

                if tRise >= (SIG-1) %|| tpRise >= SIG   % Determines
        if event is significant.
                    k = k+1;
                    events(i,1,k) = tTime;               % Store the
        event location.
                    events(i,2,k) = tRise;               % Store the
        event magnitude.
                    keptEvents = keptEvents+1;          % Count the
        number of events.
                else
                    removedEvents = removedEvents+1;     % Count the
        number of dropped events.
                end
            end
            if k == 0
                NuConflicts = NuConflicts+1;             % Count the
        number of signals with no events.
                conflicts(NuConflicts) = i;              % Store the
        location of signals with no events.
            end
        end
    end
end

str = sprintf(  ['Events Evaluated;\n%d events kept.\n%d events
        removed.'...
                '\n%d conflicts.\nConflict Traces;'],...
                keptEvents,removedEvents,NuConflicts);
disp(str)
disp(conflicts)
clearvars i j k tTime tRise tpRise sample sizesample keptEvents
        removedEvents str NuConflicts conflicts
```

## **EventAnalysis.m**

```
%% PART6: Analyse the events, convert them to frequencies.


%% Initial Check
if ~exist('events','var');     error('Error: Variable ''events'' does
        not exist.'); end;


%% Definitions
MYZONES = [TRIGS noFrames];%[1 TRIGS noFrames];
NTRIG = 3; %temp for debugging


%% Find the number of events in each region

eventreg = zeros(noRegions,NTRIG+1);
eventM = zeros(noRegions,NTRIG+1);

NuConflicts = 0;
Conflicts = 0;
for i = 2:1:noRegions
    sample = events(i,1,:);        % Get all of the event times for
        the trace
    sample(sample == 0) = [];      % Change all of the zero values
        to null []
    sample = squeeze(sample);      % Remove all of the empty
        dimensions
    sizesample = size(sample, 1);  % Get the number of events
        present

    sampleM = events(i,2,:);       % Get all of the event
        Magnitudes for the trace
    sampleM(sampleM == 0) = [];     % Change all of the zero values
        to null []
    sampleM = squeeze(sampleM);     % Remove all of the empty
        dimensions

    if ~isempty(sample)             % Checks that there are events
        to categorise
      nuEvent = zeros(1,NTRIG+1);     % Create a temporary event
       catalogue. Number of events in each region.
      tempMag = zeros(1,NTRIG+1);
      for j = 1:1:NTRIG+1             % Loop through all of the
       Areas
         for k = 1:1:(sizesample)        % Loop through all of
        the events in the sample
             if sample(k) >= MYZONES(j) && sample(k) <=
        MYZONES(j+1)
                 nuEvent(j) = nuEvent(j)+1;  % Add 1 to the total
        number of events in the Trace area
                 tempMag(j) = tempMag(j) + sampleM(k);
             end
         end
      end
      eventreg(i,:) = nuEvent;    % Store the temporary event
       catalogue in the overall array
```

```
        eventM(i,:) = tempMag./nuEvent;
        eventM(i,isnan(eventM(i,:))) = 0;
    else
        if cTrace(i) < 3
            NuConflicts = NuConflicts+1;
            Conflicts(NuConflicts) = i;
        end
    end
end

clearvars i j k sample sampleM sizesample nuEvent tempMag


%% Convertion from instances to frequencies require duration of
        zones: myTimes

myTimes = zeros(1,NTRIG+1);

for i = 1:1:NTRIG+1
    myTimes(i) = MYZONES(i+1) - MYZONES(i);
end
% Modifier to remove grey areas...
% myTimes(2)= myTimes(2)- 110;
clearvars i


%% Get the positions that need to be stored

positions = zeros(noRegions, 2);

if exist('ROIxywh','var')
    for i = 1:1:noRegions
        positions(i,1) = ROIxywh(i,1) + (ROIxywh(i,3)/2);
        positions(i,2) = ROIxywh(i,2) + (ROIxywh(i,4)/2);
    end
end


%%  Gather frequencies of events for Neurons: eNeuro
%   Gather frequency of events for active Neurons: reNeuro
%   Gather Frequency of events for active Astrocytes: reAstro
if exist('eventreg','var')
    eNeuro = zeros(1,NTRIG+1);  % Number of events Neuron
    reNeuro = zeros(1,NTRIG+1); % Number of responsive events Neuron
        - Removes inactive neurons
    reAstro = zeros(1,NTRIG+1); % Number of responsive events
        Astrocyte

    FeNeuro = zeros(1,NTRIG+1); % Frequency of events Neuron
    FreNeuro = zeros(1,NTRIG+1);% Frequency of responsive events
        Neuron
    FreAstro = zeros(1,NTRIG+1);% Frequency of responsive events
        Astrocyte

    eNeuroP = zeros(1,2);       % Store reletive position of the
        Neuron
    reNeuroP = zeros(1,2);      % Store reletive position of the
        responsive Neurons
```

```
reAstroP = zeros(1,2);      % Store reletive position of the
     responsive Astrocyte

eNeuroM = zeros(1,NTRIG+1); % Number of events Neuron
reNeuroM = zeros(1,NTRIG+1);% Number of responsive events Neuron
     - Removes inactive neurons
reAstroM = zeros(1,NTRIG+1);% Number of responsive events
     Astrocyte

index_eNeuro = 0;
index_reNeuro = 0;
index_reAstro = 0;
for i = 2:1:noRegions
    if sum(eventreg(i,:)) > 0   % Final check for significant
    events
       switch cTrace(i)
           case 1          % It's a neuron
               index_eNeuro = index_eNeuro+1;
               eNeuro(index_eNeuro,:) = eventreg(i,:);
    % Store the number of events per region
               FeNeuro(index_eNeuro,:) =
    eventreg(i,:)./myTimes;    % Store the frequecy of events
    per region
               eNeuroM(index_eNeuro,:) = eventM(i,:);
    % Store the average magnitude of events per region
               if exist('positions','var');
    eNeuroP(index_eNeuro,:) = positions(i,:); end;

               k = 0;
               for j = 1:1:NTRIG
                   if eventreg(i,j) > 0
                       k = 1;
                   end
               end
               if k == 1   % It's a responsive neuron
                   index_reNeuro = index_reNeuro+1;
                   reNeuro(index_reNeuro,:) = eventreg(i,:);
                   FreNeuro(index_reNeuro,:) =
    eventreg(i,:)./myTimes;
                   reNeuroM(index_reNeuro,:) = eventM(i,:);
                   if exist('positions','var');
    reNeuroP(index_reNeuro,:) = positions(i,:); end;
               end

               if eventreg(i,(NTRIG+1)) == 0
                   NuConflicts = NuConflicts+1;
                   Conflicts(NuConflicts) = i;
               end

           case 2          % It's an astrocyte
               index_reAstro = index_reAstro+1;
               reAstro(index_reAstro,:) = eventreg(i,:);
               FreAstro(index_reAstro,:) =
    eventreg(i,:)./myTimes;
               reAstroM(index_reAstro,:) = eventM(i,:);
               if exist('positions','var');
    reAstroP(index_reAstro,:) = positions(i,:); end;
       end
    end
```

```
    end
end


str = sprintf(  ['Events Evaluated;\n%d Neurons, (%d)
        responsive.\n%d Astrocytes.'...
            '\n%d conflicts.\nConflict IDs;'],...

        length(FeNeuro),length(FreNeuro),length(FreAstro),NuConflic
        ts);
disp(str)
disp(Conflicts)

clearvars i j k index_eNeuro index_reNeuro index_reAstro myTimes
        MYZONES str


%% Save Progress
disp('Saving Progress...')
save('TEMP_PROGRESS6')
disp('Progress Saved!')
```

## ProduceStatistics.m

```
function
        ProduceStatistics(MyArr,MyTitle,MyVar,MyUnits,MyModifier,Pa
        ired)
%Displays a few sets of data. For both Frequency and magnitude.
%   The bargraphs of region Mean and Standards Error, quoting the
        standard
%   deviation too.
%   The p values associated with paired t-tests between regions.


%% Definitions

%MyArr = NeuroAF;

%MyTitle = 'Neuron';
MyRegions = {'Background','Indirect Vehicle','Indirect
        Glutamate','Direct Glutamate'};
MyLineWid = 2;
MyBkgCol  = [1 1 1];
MyAxWid   = MyLineWid;
MyFonSiz  = 12;
MyBarCol  = [1 1 1];
MyEdgeCol = [0 0 0];
MyEdgeWid = MyLineWid;
MyErrCol  = [0 0 0];
MyErrWid  = MyLineWid;

if ~exist('NZONE','var'); NZONE = size(MyArr,2); end;
if ~exist('DZONE','var'); DZONE = NZONE; end;
if ~exist('START','var'); START = 1; end;
if ~exist('END','var'); END = size(MyArr,1); end;

tmean = zeros(NZONE,1);
tstd  = zeros(NZONE,1);
tste  = zeros(NZONE,1);
```

**176**

```
tmax  = zeros(NZONE,1);
tH    = zeros(NZONE);
tP    = zeros(NZONE);


%% Modifier
% Scales the value to something more managable, such as *1000 to
         make mHz
MyArr = MyArr.*MyModifier;


%% Stats - Mean, STD, STE

if Paired == 1
    for i = 1:1:NZONE
        tmean(i) = mean(MyArr(START:END,i));
        tstd(i)  = std(MyArr(START:END,i));
        tste(i)  = tstd(i)/sqrt(END-START+1);
        tmax(i)  = tmean(i) + tste(i)*2;
    end
end


%% Stats - ignoring 0s... Mean, STD, STE

if Paired ~= 1
    for i = 1:1:NZONE
        tmean(i) = mean(MyArr(MyArr(START:END,i)~=0,i));
        tstd(i)  = std(MyArr(MyArr(START:END,i)~=0,i));
        tste(i)  = tstd(i)/sqrt(END-START+1);
        tmax(i)  = tmean(i) + tste(i)*2;
    end
end


%% Stats - Paired T-Test H & P MATRIX

if Paired == 1
    for i = 1:1:NZONE
        for j = 1:1:NZONE
            [tH(i,j) tP(i,j)] =
          ttest(MyArr(START:END,i),MyArr(START:END,j));
        end
    end
end


%% Stats - unPaired T-Test H & P MATRIX

if Paired ~= 1
    for i = 1:1:NZONE
        for j = 1:1:NZONE
            [tH(i,j) tP(i,j)] =
          ttest2(MyArr(MyArr(START:END,i)~=0,i),MyArr(MyArr(START:END
          ,j)~=0,j));
        end
    end
end
```

Appendix

```matlab
%% Display stats, 2 samples

% Create the figure and make it pretty
figBar1 = figure('Color', MyBkgCol, 'NumberTitle', 'off', 'Name', ...
        MyTitle);

% Create axes
axes1 = axes(  'Parent',        figBar1,...
               'XTickLabel',    MyRegions(1:DZONE),...
               'XTick',         1:1:DZONE,...
               'LineWidth',     MyAxWid,...
               'FontSize',      MyFonSiz);
xlim(axes1,[0 (DZONE+1)]);
ylim(axes1,[0 round(max(tmax(1:DZONE))+0.5)]);
hold(axes1,'all');

% Plot the Barchart
bar(tmean(1:DZONE), 'FaceColor',    MyBarCol,...
                    'EdgeColor',    MyEdgeCol,...
                    'LineWidth',    MyEdgeWid,...
                    'BarWidth',     0.4);

% Add the error bars
errorbar(tmean(1:DZONE),tste(1:DZONE), 'LineStyle',    'none',...
                                       'LineWidth',    MyErrWid,...
                                       'Color',        MyErrCol);

% Titles and labels etc.
title(MyTitle,  'FontWeight',   'bold',...
                'FontSize',     MyFonSiz);
str = sprintf(  'n: %d Traces\n', (END - START + 1));
xlabel(str,     'FontSize', MyFonSiz);
ylabel([MyVar ' / ' MyUnits], 'FontSize', MyFonSiz);


%% Display for each region the MEAN STD and STE

TabWid = 600;
TabHei = DZONE*25+1;
MySpac = 25;
ColWid = {(TabWid/4)};
NAMESCOL = {'Region', ['Mean / ' MyUnits], ['STD / ' MyUnits], ...
        ['STError / ' MyUnits]};

figTab1 = figure('Color', MyBkgCol, 'Position', [200 200 ...
        (TabWid+(2*MySpac)) ((TabHei*2) + (MySpac*3))], ...
        'NumberTitle','off', 'Name', MyTitle);

tableM = uitable('Parent', figTab1, 'Position', [MySpac ((MySpac*2) ...
        + TabHei) TabWid+2 TabHei+1]);

mydata = {};
mydata(:,1) = MyRegions;
mydata(:,2:4) = num2cell([tmean tstd tste]);
set(tableM, 'Data', mydata(1:DZONE,:), 'ColumnWidth', ColWid, ...
        'ColumnName', NAMESCOL, 'RowName', []);
```

```
%% Display the H and P values in a table

ColWid = {(TabWid/(2*DZONE+1))};
NAMESCOL = {'Comparison'};

for i = 1:1:DZONE
    NAMESCOL(i+1) = {sprintf('H(#,%d)', i)};
    NAMESCOL(i+DZONE+1) = {sprintf('P(#,%d)', i)};
end

tableHP = uitable('Parent', figTab1, 'Position', [MySpac MySpac
        TabWid+1 TabHei+1]);

mydata = [[1:1:DZONE]' tH(1:DZONE,1:DZONE) tP(1:DZONE,1:DZONE)];
set(tableHP, 'Data', mydata, 'ColumnWidth', ColWid, 'ColumnName',
        NAMESCOL, 'RowName', []);
```

## DisplayTraces.m

```
%% Display the traces once they have been categorised. Can be used
        after PART2.


%% Initial Check
if ~exist('tInt','var');    error('Error: Variable ''tInt'' does not
        exist.'); end;

if ~exist('MCS','var');     error('Error: Variable ''MCS'' does not
        exist.'); end;

if ~exist('cTrace','var');  error('Error: Variable ''cTrace'' does
        not exist.'); end;
% For debugging just doing 10 regions
%noRegions = 10;


%% Display The Traces in their groups

figH3 = figure;  % Creat a figure and make it pretty
set(gca,'Color',[1 1 1]);
set(figure(figH3),'Color',[1 1 1]);%[0.9 0.95 1]);

selection = 1;      % Default selection
displaytype = 1;
while 1;            % Loop so that current selection can be changed
        on the fly

    if displaytype > 0 && displaytype < 4
        mymax = 2;  % Default maximum
        c = jet(nuTrace(selection));

        figure(figH3);
        cla
        hold all
        k=0;
        for j=2:noRegions;  % Draw the current selection
            if cTrace(j)==selection;
                k=k+1;
```

```matlab
            plot(1:1:noFrames,tInt(j,:),'Color',c(k,:)');

            if max(tInt(j,:))>mymax       % Find the max value
      displayed
                mymax = max(tInt(j,:));
            end
        end
    end

    axis([1, noFrames, 0, mymax]);  % Redo the axis scales

    str = sprintf(' : %d Traces',nuTrace(selection));
    title([MCS{selection} str],'interpreter','none');
    xlabel('Time (0.5s)');
    ylabel('Intensity f()/f(0)');

    hold off
end

    % Choose what Category to highlight
displaytype = 0;
while (displaytype == 0)
    displaytype = menu( 'Choose a category',...
                        MCS{1},MCS{2},MCS{3},...
                        'Expand',...
                        'Individual',...
                        'Exit');
end

if displaytype == 6;    % Exit the process and close the figures
    break;
end

if displaytype == 4     % Expand the current selection
    cla
    hold all
    k=0;
    for j=2:noRegions;  % Draw the expanded current selection
        if cTrace(j)==selection;
            temptrace = tInt(j,:)+2*k;
            k=k+1;
            plot(1:1:noFrames,temptrace(:),'Color',c(k,:)');
        end
    end

    for i=1:NTRIG       % Display all of the defined trigger
      lines.
        line([TRIGS(i);TRIGS(i)],[0;mymax+(2*k)],'Color',[0.5 0
      0]);
    end
    axis([1, noFrames, 0, mymax+(2*k)]);
    hold off
end

if displaytype == 5     % Show individual selection
    cla
    hold all

    sel=1;
```

**180**

```
        myRange = num2cell(1:1:nuTrace(selection)+1);
        myRange(nuTrace(selection)+1) = {'Exit'};
        while(sel ~= nuTrace(selection)+1)
            j=0;
            k=0;
            while (k ~= sel)     % Find the selected trace reference
          number
                j=j+1;
                if cTrace(j) == selection
                    k=k+1;
                end
            end
            temptrace = tInt(j,:);
            mymaxt = 2;
            plot(1:1:noFrames,temptrace(:),'Color',c(k,:)');

            if max(temptrace(:))>mymaxt      % Find the max value
          displayed
                mymaxt = max(temptrace(:));
            end

            for i=1:NTRIG       % Display all of the defined trigger
          lines.
                line([TRIGS(i);TRIGS(i)],[0;mymaxt],'Color',[0.5 0
          0]);
            end

            axis([1, noFrames, 0, mymaxt]);

            str = sprintf('Selection: %d\nTrace ID: %d',sel,j);
            title(str,'interpreter','none');
            xlabel(MCS{selection},'interpreter','none');

            hold off

            sel = menu('Choose a Trace',myRange);
        end
    end

    if displaytype < 4; selection = displaytype; end
end


%% Close

if exist('figH3','var'); close(figH3); end
clearvars k j i c displaytype selection mymax mymaxt temptrace str
        hLine figH3 sel myRange
```

## MATLAB Files – Syringe Pump Control

### MultiPumpInterface.m

```matlab
function MultiPumpInterface

% Various parameters that need to be defined
DIR             = {'INF','WDR'};
RUNITS          = {'UM','MM','UH','MH'};
STATES          = {'STP','RUN'};
default_values  =
          {'00','Vehicle','10.3','10',[RUNITS{1}],[DIR{1}],[STATES{1}
          ],[STATES{1}]};
%CODEWORDS      = {'Hardward Name', 'Software Name', 'DIA', 'RAT',
          'RAT', 'DIR'};
nopumps         = 6;     % Number of pumps to generate an interface
          for

% Open a channel...
serialcom1 = open_comms('COM1',9600);

% Variables used to store a log of what is going on
captainslog     = '';
filling         = 0;
timelog         = 0;
statelog        = 0;
LogDateTime     = 'HH-MM-SS-FFF : ';

% On Screen!
hFig = figure('position',[100 100  820 500],'name','Multi Pump
          Control','Numbertitle','off','menubar','none','resize','off
          ',...
    'DeleteFcn',@exit_routine);

pumps = cell(nopumps,2,8);       % Register to store all of the
          pumps, their variabls and the handles to each of the on
          screen inputs.
for i=1:1:nopumps                % Create the pumps and display them
    pumps(i,:,:) = generate_pump(hFig,i);
    refresh_pump(i);
end

generate_interface(hFig,nopumps);

set_states();

%% Functions
    function set_states()
        setmypumps(char(pumps{:,1,1}),char(pumps{:,1,8}));
    end

    function mypump = generate_pump(hFig, PumpNo)
        % Pump variables: Hardware Name, Software Name, Diameter,
         Rate,
        % Units, Direction, Next state, Current State
        % Handles for each variable
```

Appendix

```
    mypump = default_values; %default settings for a pump
    mypump(2,:) = generate_pump_interface(hFig, PumpNo);
end

function pumphandles = generate_pump_interface(hFig, PumpNo)
    % Pump handles: Hardware Name, Software Name, Diameter,
      Rate, Units, Direction
    hHName     = uicontrol(hFig, 'Style','text');%,
      'Callback', {@set_param,PumpNo,1});
    hSName     = uicontrol(hFig, 'Style','edit',   'Callback',
      {@set_param,PumpNo,2});
    hDia       = uicontrol(hFig, 'Style','edit',   'Callback',
      {@set_param,PumpNo,3});
    hRateVal   = uicontrol(hFig, 'Style','edit',   'Callback',
      {@set_param,PumpNo,4});
    hRateUni   = uicontrol(hFig, 'Style','popup',  'Callback',
      {@set_list_param_1,PumpNo});
    hDir       = uicontrol(hFig, 'Style','popup',  'Callback',
      {@set_list_param_2,PumpNo});
    hTogOnOff  = uicontrol(hFig, 'Style','togglebutton',...
                                              'Callback',
      {@set_next_state,PumpNo});
    hLblOnOff  = uicontrol(hFig, 'Style','text');

    set(hHName,'String', sprintf('%02d',PumpNo),  'Position',
      [020 20*PumpNo 80 20]);
    set(hSName,     'String', default_values{2},  'Position',
      [120 20*PumpNo 80 20]);
    set(hDia,       'String', default_values{3},  'Position',
      [220 20*PumpNo 80 20]);
    set(hRateVal,   'String', default_values{4},  'Position',
      [320 20*PumpNo 80 20]);
    set(hRateUni,   'String', RUNITS,             'Position',
      [420 20*PumpNo 80 20]);
    set(hDir,       'String', DIR,                'Position',
      [520 20*PumpNo 80 20]);
    set(hTogOnOff,  'String', STATES(1),
        'Position', [620 20*PumpNo 80 20]);
    set(hLblOnOff,  'String', STATES(1),
        'Position', [720 20*PumpNo 80 18]);

    pumphandles =
      {hHName,hSName,hDia,hRateVal,hRateUni,hDir,hTogOnOff,hLblOn
      Off};
end

function generate_interface(hFig,noPumps)   % Creates labels for
    all of the inputs and a big command button to update the
    pumps.
    uicontrol(hFig, 'Style','text', 'String','PumpID#',
      'Position',[020 20*(noPumps+1) 80 20]);
    uicontrol(hFig, 'Style','text', 'String','Fluid',
      'Position',[120 20*(noPumps+1) 80 20]);
    uicontrol(hFig, 'Style','text', 'String','Diameter',
      'Position',[220 20*(noPumps+1) 80 20]);
    uicontrol(hFig, 'Style','text', 'String','Flow Rate',
      'Position',[320 20*(noPumps+1) 80 20]);
    uicontrol(hFig, 'Style','text', 'String','Units',
      'Position',[420 20*(noPumps+1) 80 20]);
```

```matlab
    uicontrol(hFig, 'Style','text', 'String','Direction',...
      'Position',[520 20*(noPumps+1) 80 20]);
    uicontrol(hFig, 'Style','text', 'String','Next State',...
      'Position',[620 20*(noPumps+1) 80 20]);
    uicontrol(hFig, 'Style','text', 'String','Current State',...
      'Position',[720 20*(noPumps+1) 80 20]);

    uicontrol(hFig, 'Style','pushbutton', 'String','Update',...
      'Position',[820 20 60 20*(noPumps)],...
        'Callback',@set_current_states);    % The pushbutton
      called Update calls the function "set_current_states"
    set(hFig, 'Position', [200 200 900 20*(noPumps+3)]);
end

function set_param(~,~,pumpID,param)    % Used to set all of the
    basic string components
    pumps{pumpID,1,param} = get(pumps{pumpID,2,param},'String');
    disp_param(pumpID);
end

function set_list_param_1(~,~,pumpID)    % Used to set the rate
    units
    pumps{pumpID,1,5} = RUNITS{get(pumps{pumpID,2,5},'Value')};
    disp_param(pumpID);
end

function set_list_param_2(~,~,pumpID)    % Used to set the pump
    direction
    pumps{pumpID,1,6} = DIR{get(pumps{pumpID,2,6},'Value')};
    disp_param(pumpID);
end

function set_next_state(~,~,pumpID)    % Used to load the next
    state for the pump
    pumps{pumpID,1,7} =
      char(STATES(get(pumps{pumpID,2,7},'Value') + 1));
    set(pumps{pumpID,2,7},'String',[pumps{pumpID,1,7}]);
    disp_param(pumpID);
end

function set_current_states(~,~)    % Used to switch onto
    the next state for all of the pumps
    noPumps = size(pumps,1);
    for scsi = 1:1:noPumps;
        pumps{scsi,1,8} = pumps{scsi,1,7};
        set(pumps{scsi,2,8},'String',[pumps{scsi,1,8}]);
        update_pump_details(scsi);
    end;
    set_states();
    simplelog;
end

function update_pump_details(pumpID)

    setmypumps(char(pumps{pumpID,1,1}),'DIA',char(pumps{pumpID,
    1,3}));

    setmypumps(char(pumps{pumpID,1,1}),'RAT',[char(pumps{pumpID
    ,1,4}) char(pumps{pumpID,1,5})]);
```

**184**

```matlab
        setmypumps(char(pumps{pumpID,1,1}),'DIR',char(pumps{pumpID,
        1,6}));
        % Pump variables: Hardware Name, Software Name, Diameter,
         Rate,
        % Units, Direction, Next state, Current State
    end

    function refresh_pump(pumpID)
        for rpj = 1:1:4;  set_param('','',pumpID,rpj);  end;
        set_list_param_1('','',pumpID);
        set_list_param_2('','',pumpID);
    end

%% Miscellaneous functions
    function disp_param(pumpID) % Display a specific pumps current
         parameters.
        message = char([pumps{pumpID,1,:}]);
        disp(message);
    end

%% Communication functions
    function close_comms(myserial)
        fclose(myserial);
    end
    function myserial = open_comms(commport,baudrate)
        myserial = serial(commport,'BaudRate',baudrate);
        fopen(myserial);
    end
    function setmypumps(name,property,value)

        if ~exist('value', 'var') || isempty(value)
            value = '';
        end

        NoInst = size(name,1);

        if size(property,1) < NoInst;
            property = repmat(property,[NoInst 1]);
        end
        if size(value,1) < NoInst
            value = repmat(value,[NoInst 1]);
        end

        for spi=1:1:NoInst
            command=[name(spi,:) property(spi,:)];
            if ~isempty(value); command = [name(spi,:)
     property(spi,:) value(spi, :)]; end;
            message = sprintf([command '\r']);
            disp(message);
            fwrite(serialcom1, message)
            mylog(message);
        end
    end

%% Logging and save functions
    function mylogintro() % Adds the preamble to the captain's log
        mydate = datestr(now,'yy-mm-dd');
        noPumps = size(pumps,1);
```

```matlab
        captainslog = sprintf(['New Log: ' mydate '\r']);
        temp = '';
        for mli = 1:1:noPumps % Get all of the Hardware and software
         pump names used
            temp = strcat(temp, [sprintf('\r') [pumps{mli,1,1}]
         [pumps{mli,1,2}]]);
        end
        captainslog = [captainslog temp sprintf('\r\rInstructions
         Sent...\r')];
    end

    function mylog(event)
        if isempty(captainslog); mylogintro(); end;
        stardate = datestr(now,LogDateTime);
        captainslog = [captainslog stardate event];
    end

    function simplelog()
        if filling == 0; tic; end;
        filling = filling + 1;
        timelog(filling) = toc;

        noPumps = size(pumps,1);

        for sli = 1:1:noPumps
            if      pumps{sli,1,8} == STATES{1}
                statelog(sli,filling) = 0;
            elseif  pumps{sli,1,8} == STATES{2}
                statelog(sli,filling) = 1;
            else
                statelog(sli,filling) = 2;
            end
        end
    end

    function quicksave(qsName, qsVal)
        assignin('base', qsName, qsVal);
    end

%% Closing functions
    function exit_routine(~,~)
        quicksave('tlog', timelog);
        quicksave('slog', statelog);
        quicksave('vlog', captainslog);

        close_comms(serialcom1);

        delete(serialcom1);
        clearvars filling timelog statelog captainslog
    end
end
```

## MPRoutine.m

```matlab
function MPRoutine

% Various parameters that need to be defined
DIR             = {'INF','WDR'};
```

```
RUNITS          = {'UM','MM','UH','MH'};
STATES          = {'STP','RUN'};
default_values  =
        {'00','Vehicle','10.6','10',[RUNITS{1}],[DIR{1}],[STATES{1}
        ],[STATES{1}]};
%CODEWORDS       = {'Hardward Name', 'Software Name', 'DIA', 'RAT',
        'RAT', 'DIR'};


% Variables used to store a log of what is going on
captainslog     = '';
filling         = 0;
timelog         = 0;
statelog        = 0;
LogDateTime     = 'HH-MM-SS-FFF : ';


%% Rough design
% Create an basic interface that states all of the pumps parameters.
% loading the defaults of the pump parameters, assuming identical
        pumps.
% Include a button to start the routine.
% Procedure to carry out the routine, maintaining a software log.
% Once completed, inform user of time taken, save the log to the
        workspace.


%% Operational parameters - Timings for the program to follow
last_cycle = 4;
P1t = [80 660 660 600];
P2t = [60 60 60 0];


pump_diameter   = '10.3';    % mm
channel_rate    = '4.5UM';     % ul/min
well_rate       = '50UM';  % ul/min
inf_rate        = '54UM';  % ul/min


time_estimate = sum( [P1t P2t] );


mydetails = sprintf (  ['DETAILS\n---------------------------\n'
        ...
                        'Pump Diameter : %s\n'...
                        'Channel Rate : %s\n'...
                        'Well Rate : %s\n'...
                        'Infusion Rate : %s\n---------------------
        -----\n'...
                        'Estimated Time : %ds\n'...
                        'Estimated Frames : %d'],...
                        pump_diameter,...
                        channel_rate,...
                        well_rate,...
                        inf_rate,...
                        time_estimate,...
                        (time_estimate*2));

%% Create displayed interface

% Open a channel...
serialcom1 = open_comms('COM1',9600);

% On Screen!
hFig = figure(  'position',[100 100 270 160],...
```

```
                    'name','Routine3 Pulsed Glutamate',...
                    'Numbertitle','off',...
                    'menubar','none',...
                    'resize','off',...
                    'DeleteFcn',@exit_routine);
% Send a hail
        uicontrol(  hFig,...
                    'Style','text',...
                    'Position', [10 10 140 140],...
                    'String',mydetails);


hbtn =  uicontrol(  hFig,...
                    'Style','pushbutton',...
                    'String','Start',...
                    'Position',[160 90 100 60],...
                    'Callback',@liftoff);


hclk =  uicontrol(  hFig,...
                    'Style','text',...
                    'Position', [160 10 100 30]);


hcd  =  uicontrol(  hFig,...
                    'Style','text',...
                    'Position', [160 40 100 30]);


%% Setup the pumps
%   Pump     Note
%   00       Secondary well withdrawl pump / Channel withdrawal pump
%   01       Primary well withdrawal pump
%   02       Primary well infusion - default liquid
%   03       Primary well infusion - target liquid

setup_pump('00',pump_diameter,'WDR',channel_rate);
setup_pump('01',pump_diameter,'WDR',well_rate);
setup_pump('02',pump_diameter,'INF',inf_rate);
setup_pump('03',pump_diameter,'INF',inf_rate);


%% Create a time machine
% setup the time machine
tardis = timer( 'TimerFcn',@mytimer,...
                'Period', 0.1,...
                'StopFcn','disp(''Timer has stopped.'')',...
                'StartFcn','disp(''Timer has started.'')',...
                'ExecutionMode','fixedrate',...
                'StartDelay',0.5);
% make sure that the timer isn't running
stop(tardis);


%% Settings required for functions
clock_val = 0;
countto = 0;

button_state = 0;

counting_phase = 0;
current_cycle = 0;
completed_cycles = 0;
```

```matlab
%% Functions for operation
    function liftoff(~,~)
        if button_state == 0
            set(hbtn,'String','Stop')
            button_state = 1;

            counting_phase = '0';
            current_cycle = 0;
            completed_cycles = 0;

            start(tardis);
        else
            set(hbtn,'String','Start')
            button_state = 0;
            stop(tardis);
        end
    end


    function mytimer(~,~)
        switch counting_phase
            case '0'
                counting_phase = 'A';
                current_cycle = 0;
                countto = clock_val + P1t(current_cycle+1);
                    start_pumps();
            case 'A'  % Pump A is running with vehicle
                if  clock_val >= countto
                    completed_cycles = completed_cycles + 1;
                    current_cycle = current_cycle + 1;
                    if (completed_cycles >= last_cycle);
                        liftoff();
                        set(hbtn,'enable','off');
                        stop_pumps();
                    else
                        counting_phase = 'B';
                        toggle_pumps(counting_phase);
                        countto = clock_val + P2t(current_cycle);
                    end
                end
            case 'B'  % Pump B is running with fluo
                if  clock_val >= countto
                    counting_phase = 'A';
                    toggle_pumps(counting_phase);
                    countto = clock_val + P1t(current_cycle+1);
                end
        end

        clock_val = clock_val + 1;

        set(hclk, 'String', [num2str(clock_val) 's Pump '
          counting_phase])
        set(hcd, 'String', [num2str(countto) 's Phase:'
          num2str(current_cycle)])
    end

    function start_pumps()
        quick_set_state('RUN','RUN','RUN','STP')
    end
```

```matlab
    function stop_pumps()
        quick_set_state('STP','STP','STP','STP')
    end

    function toggle_pumps(token)
        switch token
            case 'A'
                setmypumps('03','STP');
                setmypumps('02','RUN');
            case 'B'
                setmypumps('02','STP');
                setmypumps('03','RUN');
        end
    end

    function quick_set_state(ps0,ps1,ps2,ps3)
        setmypumps('00',ps0);
        setmypumps('01',ps1);
        setmypumps('02',ps2);
        setmypumps('03',ps3);
    end

    function setup_pump(name, diameter, direction, rate)
        setmypumps(name,'DIA',diameter);
        pause(0.01);
        setmypumps(name,'DIR',direction);
        pause(0.01);
        setmypumps(name,'RAT',rate);
        pause(0.01);
    end

%% Communication functions
    function close_comms(myserial)
        fclose(myserial);
    end
    function myserial = open_comms(commport,baudrate)
        myserial = serial(commport,'BaudRate',baudrate);
        fopen(myserial);
    end
    function setmypumps(name,property,value)

        if ~exist('value', 'var') || isempty(value)
            value = '';
        end

        NoInst = size(name,1);

        if size(property,1) < NoInst;
            property = repmat(property,[NoInst 1]);
        end
        if size(value,1) < NoInst
            value = repmat(value,[NoInst 1]);
        end

        for spi=1:1:NoInst
            command=[name(spi,:) property(spi,:)];
            if ~isempty(value); command = [name(spi,:)
        property(spi,:) value(spi, :)]; end;
```

```matlab
            message = sprintf([command '\r']);
            disp(message);
            fwrite(serialcom1, message)
            mylog(message);
        end
    end

%% Logging and save functions
    function mylogintro() % Adds the preamble to the captain's log
        mydate = datestr(now,'yy-mm-dd');
        captainslog = sprintf(['New Log: ' mydate '\r']);
        captainslog = [captainslog mydetails
          sprintf('\r\rInstructions Sent...\r')];
    end

    function mylog(event)
        if isempty(captainslog); mylogintro(); end;
        stardate = datestr(now,LogDateTime);
        captainslog = [captainslog stardate event];
    end

    function simplelog()
        if filling == 0; tic; end;
        filling = filling + 1;
        timelog(filling) = toc;

        noPumps = size(pumps,1);

        for sli = 1:1:noPumps
            if      pumps{sli,1,8} == STATES{1}
                statelog(sli,filling) = 0;
            elseif  pumps{sli,1,8} == STATES{2}
                statelog(sli,filling) = 1;
            else
                statelog(sli,filling) = 2;
            end
        end
    end

    function quicksave(qsName, qsVal)
        assignin('base', qsName, qsVal);
    end


%% Closing functions
    function exit_routine(~,~)
        quicksave('tlog', timelog);
        quicksave('slog', statelog);
        quicksave('vlog', captainslog);

        close_comms(serialcom1);

        delete(serialcom1);
        stop(tardis);
        delete(tardis);
        clearvars filling timelog statelog captainslog
    end

end
```

# Paper

*Robertson et al., Integrative Biology, 2014*

## Integrative Biology

**PAPER**

# Chemically induced synaptic activity between mixed primary hippocampal co-cultures in a microfluidic system†

Graham Robertson,[a] Trevor J. Bushell*[b] and Michele Zagnoni*[c]

Primary neuronal cultures are an invaluable *in vitro* tool for examining the fundamental physiological changes that occur in diseases of the central nervous system. In this work, we have used a microfluidic device to grow twin cultures of primary hippocampal neuronal/glia cells which are synaptically connected but environmentally isolated. Immunocytochemical staining, for β-III-Tubulin and synaptophysin, indicated that the two neuronal populations were physically connected and that synapses were present. By dispensing predefined volumes of fluids into the device inlets, one culture was chemically stimulated and the consequent increase in neuronal activity in the opposing culture was monitored using calcium imaging. To optimise the experimental procedures, we validated a numerical model that estimates the concentration distribution of substances under dynamic fluidic conditions, proposing that no cross contamination of chemical stimuli occurred during the experiments. Calcium imaging and local chemical stimulation were used to confirm synaptic connectivity between the cultures. Chemical stimulation of one population, using KCl or glutamate, resulted in a significant increase of calcium events in both neurons and astrocytes of the connected population. The integration of the system and techniques described here presents a novel methodology for probing the functional synaptic connectivity between mixed primary hippocampal co-cultures, creating an *in vitro* testing platform for the high-throughput investigation of synaptic activity modulation either by novel compounds or in *in vitro* disease models.

### Insight, innovation, integration

We have developed an *in vitro* system for monitoring the functional connectivity of primary hippocampal co-culture networks by integrating microfluidics with calcium imaging techniques. The microfluidic structure is essential for patterning the cell growth and regulating the local application of chemical stimuli, while calcium imaging allows the simultaneous recording of cellular activity from both networks in a high-throughput format. This novel approach enables the consequence of manipulating neuronal activity to be monitored in environmentally isolated, but synaptically connected, neuronal networks. This system has the potential to provide insights for modelling and understanding altered synaptic communication and astrocytic behaviour that are associated with central nervous system disorders.

## Introduction

Brain disorders are top of the World Health Organisation's agenda because of their impact and prevalence; many will occur more frequently as life expectancy continues to grow. Indeed, recent reports have highlighted the economic burden of mental and neurological disorders in Europe with an estimated annual cost of €798 billion.[1,2] Within the UK alone, approximately 45 million cases of brain disorders were highlighted in a 2010 survey as a cost of €134 billion.[3] Strikingly, this cost is likely to increase due to long term impact of these disorders especially with the ageing population.[2,3] Understanding the central nervous system (CNS) is one of the 'grand challenges' of our age[4] and there is a growing need to develop and adopt innovative technologies to increase our understanding of CNS disorders.[5] A significant contribution to this has been provided by advances in high-throughput genomics which has identified a number of pathways that may be linked to CNS disorders.[5] However, how many of these genes affect neuronal activity and synaptic communication

[a] Department of Biomedical Engineering, University of Strathclyde, Glasgow, G4 0NW, UK
[b] Strathclyde Institute of Pharmacy and Biomedical Sciences, University of Strathclyde, Glasgow, G4 0RE, UK. E-mail: trevor.bushell@strath.ac.uk
[c] Centre for Microsystems and Photonics, Electronic and Electrical Engineering, University of Strathclyde, Glasgow, G1 1XW, UK.
E-mail: michele.zagnoni@strath.ac.uk
† Electronic supplementary information (ESI) available. See DOI: 10.1039/c3ib40221e

# Appendix

is still largely unknown. To this end, *in vitro* techniques are an invaluable tool for investigating cellular changes and dysfunctions associated with CNS disorders.

Mixed primary cultures, including both neurons and astrocytes, have proven to be a useful method associated with neurobiological research.[6,7] However, it is difficult to gain control over the parameters that influence the cellular microenvironment and neuronal connectivity. Indeed, creation of patterned neuronal networks that are environmentally isolated or the localised transfection of cell populations is difficult to achieve using conventional cell culture techniques. As a consequence, it is often impossible to separate and simplify the mechanisms underlying cellular activity, obtaining only average responses observed on global cell populations. A viable solution to these problems lies in the use of microfluidic procedures which enable greater control of cell patterning, manipulation and regulation of extracellular environments whilst retaining the ability to interface the system with conventional microscopy.

Excellent examples of how neuronal cell cultures can be grown, manipulated and studied in microfluidic devices has been provided in the last 10 years.[8–13] Microfluidic systems and procedures, that were originally developed to compartmentalise neurons to study their axons in isolation and their response to injury,[9] have led to a range of analytical applications addressing neuron/glia co-cultures, cortical/thalamic neuronal co-cultures and neuron–neuron cultures, as well as studying synapse formation.[10,13,14] These systems allow for increasingly complex but "ordered" models of the CNS to be created *in vitro*, facilitating the application of localised chemical stimuli, increasing the throughput of monitored responses and reducing the amount of drugs required per experiment, a factor particularly important for screening novel or expensive compounds. This makes microfluidic systems a versatile, low-cost and useful tool to screen new drugs and/or examine the genetic changes associated with CNS conditions.

Typically, methods of analysing neuronal activity in primary cultures include the use of microelectrode arrays (MEAs) and patch clamping. On one side, MEAs provide extracellular recordings that do not interfere with the growth of cells and can cover a large area of patterned neurons within a microfluidic environment.[15] However, each electrode in the array (due to its size and position) is not guaranteed to always interface with a cell. This often results in poor signal quality, with a proportion of the array providing no useful information. On the other side, patch clamping is the gold standard in electrophysiology, enabling the acquisition of high quality signals and the ability to record individual action potentials from single cells, including those cultured in microfluidic devices.[16] However, the process of patching a cell and obtaining high quality recordings is often slow and impractical for high-throughput assays. Therefore, several advantages, such as parallel throughput and ease of use, can be obtained from using optical techniques to analyse functional responses of neuronal networks.

In this work, we present a method of integrating multi-neuron calcium imaging with an *in vitro* microfluidic system for the analysis of synaptic communication between two interconnected populations of mixed primary hippocampal co-cultures. Each culture containing both neurons and astrocytes can be

monitored simultaneously *via* calcium imaging. A computational model was validated to characterise the system's fluidic properties and to optimise experimental procedures, ensuring that no cross-contamination of substances occurred between co-cultures. Sub-networks of synaptically connected neurons were formed *via* microchannels, as demonstrated using immuno-cytochemistry to visualise neurite growth and synapse formation with co-culture communication measured using calcium imaging.

Overall, we have demonstrated that our system is capable of monitoring the connectivity of neuronal cell populations and causality between mixed primary hippocampal co-cultures due to chemical stimulation. This work shows the potential of combining calcium imaging with microfluidic technologies to provide low-cost solutions for screening processes related to identifying the functional role of novel genes associated with CNS disorders in addition to screening programmes for novel compounds.

## Materials and methods

### Device preparation

Microfluidic devices were fabricated in polydimethylsiloxane (PDMS) using standard soft lithography techniques. Silicon masters were produced using two layers of SU8 photoresist (3000 series, MicroChem, US) onto a silicon wafer following the manufacturer's protocol. The first layer (SU8 3010) formed the microchannels connecting the two chambers (Fig. 1), achieving a final resist thickness of 7 μm. The second layer (SU8 3035) formed the side chambers achieving a final resist thickness of 90 μm. The resist was exposed through a photomask (JD Photo-Tools, UK) to UV light and was developed in MicroPosit EC solvent (Rohm and Haas, US). To prevent PDMS adhesion to the resulting silicon master, the silicon surface was silanised by vapour deposition of $1H,1H,2H,2H$-perfluorooctyl-trichlorosilane (Sigma Aldrich, UK) for 1 hour. PDMS was then poured onto the silicon master at a 10:1 ratio of base to curing agent, degassed in a vacuum desiccator chamber and cured at 80 °C for 3 hours. The PDMS devices were then peeled from the mould, cut to the desired size, and holes were punched (8 mm diameter) to obtain the inlet and outlet wells for each chamber. PDMS devices were then cleaned and irreversibly bonded to glass microscope slides or coverslips using oxygen plasma. Bonded devices were then flooded with a solution of poly-L-lysine (PLL, 10 μg ml$^{-1}$) for 1 hour to coat the chambers and microchannels. Finally, devices were washed with DI water, UV sterilised and washed with Neurobasal-A medium prior to cell injection.

### Primary hippocampal culture

Primary hippocampal cells were prepared as described previously.[6,7] Briefly, Sprague Dawley rat pups (1–2 days old) were killed *via* cervical dislocation in accordance to UK Home Office guidelines and the hippocampus dissected out. This was chopped and incubated in papain solution (1.5 mg ml$^{-1}$) before trituration in a solution containing bovine serum albumin (BSA, 10 mg ml$^{-1}$). The solution was spun down and resuspended
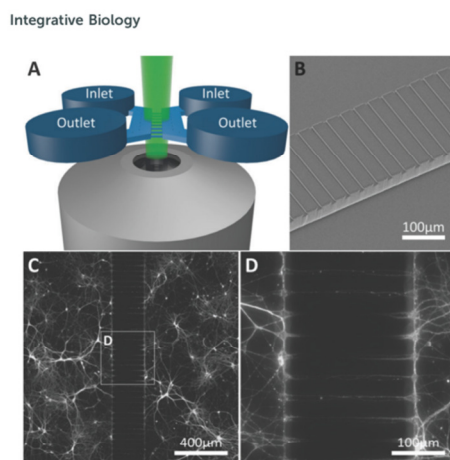
**Fig. 1** Device structure and fluorescent microscopy setup. (A) The device consists of two parallel chambers (8 mm long, 2 mm wide and 90 μm deep) which are fed by open inlet and outlet wells at each end of the chamber. The area between the two parallel chambers is bridged by an array of 200 microchannels (250 μm long, 10 μm wide and 7 μm deep) allowing both axons and dendrites to enter and form synapses with the opposing culture. (B) Scanning electron microscope image of the barrier of microchannels between the two chambers. (C, D) Two neuronal networks on either side of the barrier become connected *via* the microchannels (neurites stained with β-III-Tubulin).

in culture medium containing Neurobasal-A supplemented with ʟ-glutamine (2 mM) and B27 (2% v/v), at a density of $3.5 \times 10^6$ cells per ml. Cells were loaded into the inlet well of each chamber and incubated for 1 hour before each well was filled with 200 μl of culture medium. Devices were kept in a humidified incubator at 37 °C/5% $CO_2$ for up to 17 days prior to functional studies, with 100 μl of medium replaced from each well every 2–3 days.

**Immunocytochemistry**

Immunocytochemical staining was carried out on cultures 3–17 days *in vitro* (DIV). Cultures within the devices were washed with phosphate buffered saline (PBS) and fixed in paraformaldehyde (4% w/v, 10 min) followed by ice cold 100% methanol (10 min). The cells were then washed in PBS and permeabilised with 0.01% Triton-X100 (10 min). Non-specific binding was prevented by incubation in a blocking solution containing foetal bovine serum (5% v/v) and BSA (1% w/v) for 1 hour.

Primary antibodies for β-III-Tubulin (neuron specific cytoskeleton marker, 1 : 500 dilution), GFAP (astrocytic marker, 1 : 500 dilution), and synaptophysin (synaptic vesicle marker, 1 : 500 dilution) diluted in blocking solution were incubated with the cultures at 4 °C overnight. The cultures were then washed with PBS and incubated with fluorescently labelled secondary antibodies (Alexa 555 conjugated donkey anti-rabbit, Alexa 488 conjugated donkey anti-mouse, Alexa 488 conjugated goat anti-chicken) diluted in blocking solution (1 : 200) for 1 hour at room temperature. Epifluorescent images were taken on an

inverted microscope (Axio Observer A1, Zeiss) with 5×, 10×, 20× and 50× objectives using a cooled EM-CCD camera (LucaR, Andor Technologies) and processed using Andor SOLIS for Imaging (version 4.19.30001.0) and GIMP (version 2.8). Synaptophysin images were taken with the device inverted on an upright microscope (BX51WI, Olympus) with 40× and 60× water immersion objectives, using a cooled CCD camera (QImaging) and processed using WinFluor imaging software (J. Dempster, University of Strathclyde) and ImageJ (version 1.47). These images were used to examine cell growth (β-III-Tubulin and MAP2 3-17 DIV) and subsequently to confirm synapse formation (synaptophysin, 12 DIV).

**Modelling active and passive fluid transport**

To reliably analyse cause-effect events between co-cultures within the device, the delivery of substances to cells must occur under precise spatial and temporal conditions, avoiding undesired cross-contamination effects between the co-cultures. Therefore, it is important that the active and passive transport of substances dissolved within fluids is predicted within a certain degree of accuracy. This will depend on the overall duration of the assay, the rate of change of fluid volume within the wells, the type of molecules suspended in solution and on the microchannel network geometry. Under static conditions (equal volumes in each well) only diffusion is responsible for chemical transport. When, instead, a hydrostatic pressure gradient is formed either between the chamber inlets/outlets or across the microchannels, a laminar flow will also be present. This will either facilitate or oppose the diffusive transport of substances depending on the gradient direction.

In our experiments, the aim was to avoid cross-contamination of substances between the chambers to ensure that co-culture response was solely induced *via* synaptic communication across the microchannels. To model this process and ensure that chemical isolation of one chamber was maintained for the duration of the experiment, a dual approach was carried out. Firstly, a simplified analytical model describing the volumetric fluid transport across the four wells was developed based on the geometrical features of the microchannels and wells. As described elsewhere,[17] this is analogous to an electrical circuit featuring the culture chambers and microchannels as a resistive network, $R_B$ and $R_C$ respectively, and each open well as a capacitor, $C_{1-4}$ (Fig. 2). By setting the initial volumes in each well and therefore the hydrostatic pressures (electrical potentials) for a given channel network geometry, the volumetric flow rates (electrical currents) could be estimated in simplified conditions.

$$V(t) = \frac{\Delta V}{2}\left(1 - e^{-\frac{2t}{RC}}\right) \qquad (1)$$

$$P(t) = R\frac{dV}{dt} \qquad (2)$$

where the flow rate $V(t)$ is the differential volume between wells over time and $P(t)$ is the differential hydrostatic pressure between the wells over time. Depending on the values of $C$ and $R$ and the initial conditions, the time constant $\tau = RC/2$ provides an estimate of the rate of change of the pressure and, consequently, allows to estimate how long it takes for the system to reach
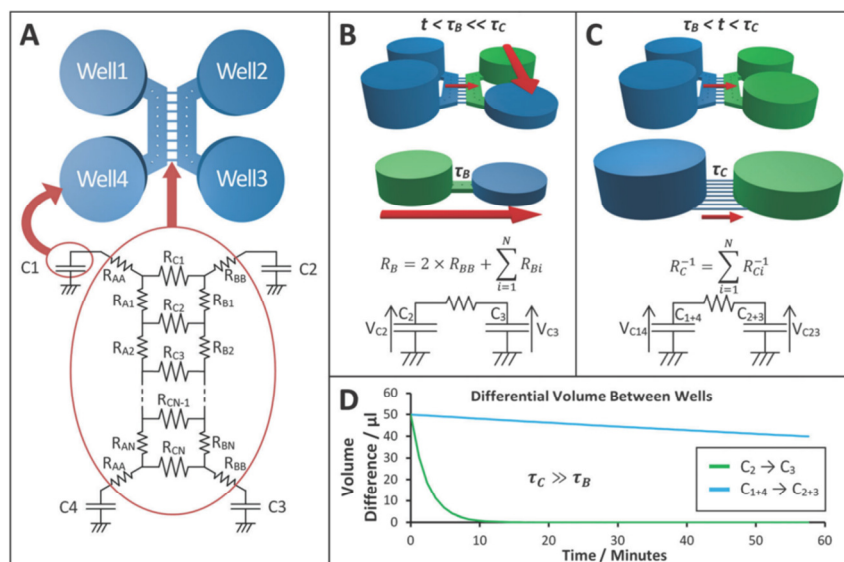
**Fig. 2** Electrical circuit analogue of the device microfluidic network. (A) The fluidic system between the 4 open wells of the device was modelled as an electrical circuit comprising a resistive network connected to 4 capacitors.[17] The height of the fluid in an open well determines the value of hydrostatic pressure (equivalent to an electrical potential). All open wells share the same geometry, therefore C1≡C2≡C3≡C4. Depending on the direction of the pressure gradient, the system can be simplified and modelled as a basic RC circuit, allowing the dynamic effects of volume changes between wells to be evaluated in a simplified manner. (B) When a volume difference is created between Well 2 and Well 3, the discharge effects due to the central microchannels can be ignored, as $\tau_C \gg \tau_B$. (C) For the procedure adopted, once the liquid volume in Well 2 and Well 3 has been equilibrated, a flow between the two culture chambers is the only one present. (D) Plot of the temporal variation of differential volume between wells for the two configurations described in B and C, showing a few orders of magnitude difference in equilibration rates.

equilibrium. In addition, this analytical procedure is useful during the device design, enabling optimisation of the relationship between the assay to be performed and the microchannel geometry. Secondly, to estimate the substance concentration within the chambers and its temporal dependency within the device, a 3 dimensional (3D) model replica of the channel network was built using COMSOL 3.5 (Fig. 4A). This numerical model was used to simulate the experimental conditions of Fig. 2B and C. This was achieved by solving the Navier–Stokes equations to model pressure driven fluid transport together with Fick's law to model the diffusive transport in 3D.

To validate the models described with respect to the microfluidic procedures, experiments using fluorescein as a target molecule were performed by fluorescence microscopy and the results were compared to the simulations (Fig. 4B–D). Further simulations were also performed to estimate the concentration distribution of K+ ions and glutamate for the calcium imaging experiments.

### Calcium imaging

Calcium ($Ca^{2+}$) imaging was performed based on techniques described previously.[6,18] After 10–14 DIV two hippocampal cultures within the system were loaded with the $Ca^{2+}$-sensitive dye, Fluo-4 AM (5 μM, 60 min, room temperature) prior to imaging. $Ca^{2+}$ transients on both sides were recorded using an inverted microscope (Axio Observer A1, Zeiss) with a cooled EM-CCD camera (LucaR, Andor Technologies) at a frame rate of 2.0 Hz and exposure time of 0.4 s using a 5× objective that gave a field of view of 2.68 $mm^2$. Images were analysed and data processed using Andor SOLIS and Matlab R2011b.

The external solution used in all $Ca^{2+}$ imaging consisted of (in mM): NaCl 140, KCl 5, $MgCl_2$ 2, HEPES 10, D-glucose 10, $CaCl_2$ 2. A procedure was developed to test the functional communication between co-cultures in the left and right chambers (Fig. 3) by which a hydrostatic pressure gradient was created by filling the wells of the left culture with 150 μl of external solution and the wells of the right culture with 50 μl of external solution. Vehicle (external solution) and KCl (45 or 85 mM) or glutamate (200 μM) solutions were applied to the right culture by injecting 50 μl into the inlet of the right chamber, creating a flow over the culture until equilibrated by adding a further 50 μl of the same solution to the outlet. Injection of solutions was performed *in situ*, allowing a non-interrupted recording of the cellular $Ca^{2+}$ responses to be taken.
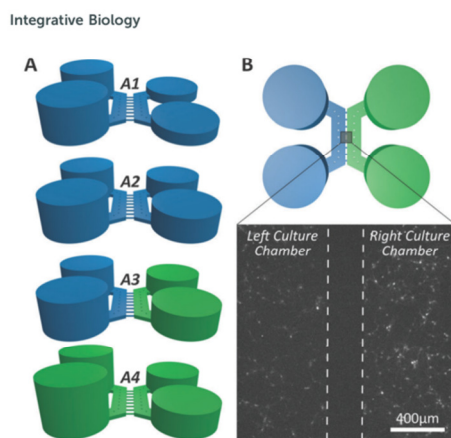
Integrative Biology

**Fig. 3** Experimental procedure for calcium imaging. (A) The wells and culture chambers were initially filled with 50 μl of external solution (blue) and subsequently selectively stimulated with KCl solution (green). (A1) A pressure difference across the microchannels was established between the two culture chambers by adding 100 μl of external solution to the wells that supply the left culture. (A2) After background recording, the right culture is stimulated by adding 50 μl vehicle to both wells for 300 s. (A3) 50 μl of external solution was removed from both wells of the right culture and 50 μl of KCl solution (final concentration 25 mM) was injected in both wells. (A4) Following indirect stimulation, the left culture is depolarised by adding 50 μl KCl solution to both wells (final concentration 25 mM) to identify neurons. (B) Example of the field of view image used to assess the activity of both cultures centred across the microchannel barrier monitoring direct and indirect effects of chemical stimulation (see Video S1 in ESI†).

In all of the experiments, cells in the right culture were depolarised by adding 50 μl of KCl (45 mM) *via* the wells, which given the initial 5 mM KCl present in the external solution, results in a final concentration of 25 mM KCl, this is the indirect stimulation. Following a period of at least 4 minutes the cells of the left culture were depolarised by injecting 50 μl KCl (85 mM) to the open wells resulting in a final concentration of 25 mM KCl, this is the direct stimulation. In another set of experiments, 50 μl of L-glutamate (200 μM) was used instead of the first indirect KCl treatment, resulting in a final concentration of 100 μM glutamate.

From each recording, approximately 100 regions of interest (ROIs) (minimum area size of 50 pixels) were selected per chamber, where each ROI contained the soma of one cell. The average pixel intensity in each region was converted to time variant intensity signals representative of the $Ca^{2+}$ activity. Signals were filtered (moving average filter, window size 11) and normalised (by dividing each data set by the first value: frame(n)/frame(0)) with responses and characterisation performed manually. A 'significant response' was defined as an increase in fluorescence greater than 0.5 normalised fluorescence units (NFU) of the preceding background intensity. Signals that did not exceed the background by 10% were discarded, as were signals that displayed either no significant response during the recordings

(background, vehicle, indirect and direct stimulus) or experienced significant drift that could not be reliably attributed to an event. Multiple responses from the same ROI were included in the analysis providing that the previous response had sufficiently recovered or a significant secondary increase above the peak of the primary response occurred. Comparisons between frequencies of events were performed with a paired student's *T*-test to determine significance.

### Materials

Cell culture medium, supplements, β-III-Tubulin, all secondary antibodies and Fluo4 AM were supplied by Life Technologies (UK). Other compounds (PLL, BSA, papain, FBS, MAP2, GFAP) were obtained from Sigma Aldrich (UK) and L-glutamic acid was obtained from Tocris Bioscience (UK). Synaptophysin antibodies were obtained from Millipore UK.

## Results

### Numerical model validation

The fluid flow in the device was first estimated using a simplified analytical model (Fig. 2). Two configurations (flow paths) were considered: a pressure gradient between wells connecting a culture chamber (Fig. 2B) and a pressure gradient across the microchannels (Fig. 2C). The estimated time constants for the pressure to equilibrate were 189 s across each chamber ($\tau_B$) and 39 956 s across the microchannels ($\tau_C$) respectively (Fig. 2D), implying that the same differential pressure along the chambers will discharge faster than when across the smaller microchannels. Given that $\tau_C$ is two orders of magnitude greater than $\tau_B$, as a first order approximation, the two chambers can be considered fluidically isolated over short periods of time (from seconds to few minutes). However, to obtain a more accurate prediction of the fluid transport within the device, 3D numerical simulations were required to estimate how substance concentrations within the microchannels changed over time depending on the experimental conditions during application of chemical stimuli.

Simulations were performed mimicking the experimental conditions used for calcium imaging (Fig. 3), as detailed in the Material and methods section. Simulation results closely matched the outcomes from the control experiment (Fig. 4). The model was then used to simulate the experimental procedure when KCl and glutamate solutions were used, confirming that no chemical stimulus directly affected the opposite culture in the time frame of the assay (Fig. 4E and F).

### Neurite growth and synapse formation within the device

Primary hippocampal cultures (3–17 DIV) were stained to visualise neurite growth through the microchannels towards the opposing culture. Neurite growth was observed within a few days (3 DIV, Fig. 5A–C) using β-III-Tubulin and MAP2 staining, continuing until 17 DIV. Our staining indicates neurite growth throughout the microchannels but whether individual processes fully traverse the microchannel barrier cannot be elucidated
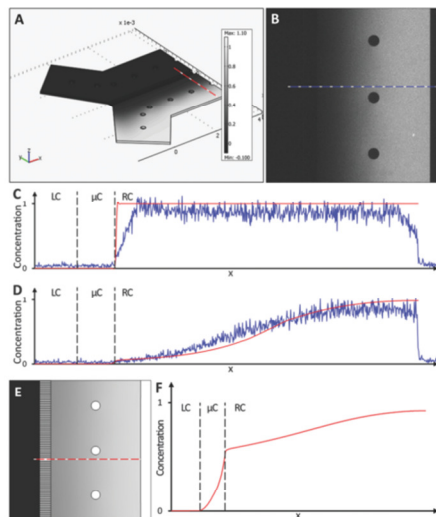
Paper

**Fig. 4** A numerical model was used to simulate the diffusion of fluorescein molecules and K+ ions across the central microchannel barrier. (A) 3D view of the finite element model of the microfluidic system simulating the experimental procedure described in Fig. 3. (B) Microscope image showing fluorescein (30 μM) concentration within a chamber after 300 s, following the procedure described in Fig. 3. Neutral density filters were used to minimise bleaching of fluorescein. (C and D) Comparison between fluorescent intensity profiles from the simulation (━━) and the experiment (━━) at 0 s and 300 s, respectively. Dashed lines indicate the boundaries between left chamber (LC), microchannels (μC) and right chamber (RC). (E and F) 2D view of simulation result and profile of K+ ion distribution within a chamber after 300 s, showing that no cross contamination should take place for the time frame of the assay.
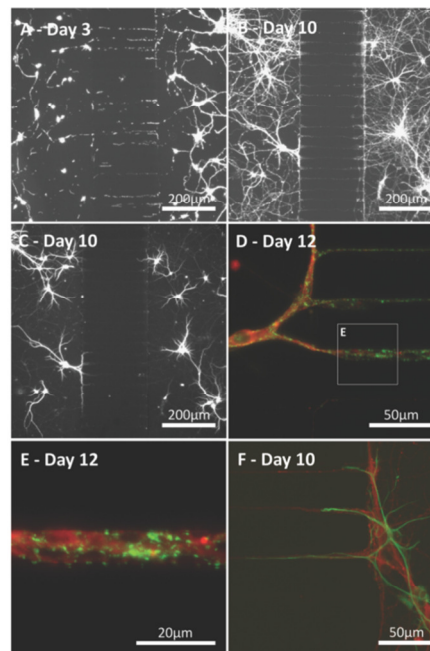


**Fig. 5** Neuronal and astrocytic processes project within the microchannels. (A, B) Representative images of cultures (3 and 10 DIV) revealing neurite growth across the microchannel barrier (β-III-Tubulin: neuron specific cytoskeleton marker). (C) As β-III-Tubulin staining extends across the microchannels, staining with the somatodendritic marker MAP2, confirms neurons extend both axonal and dendritic projections into the microchannels. (D, E) Representative images of a culture (12 DIV) showing punctate synaptophysin staining, indicating synapse formation outside and inside the microchannels (green: β-III-Tubulin, red: synaptophysin, a synaptic vesicle marker). (F) Astrocytes are identified (green: GFAP) projecting into the microchannels along with neurites (red: β-III-Tubulin).

from the current study. Interestingly, astrocytes, identified with GFAP (Fig. 5D), could be seen projecting into the microchannels along with the neurites. However, no astrocytic projections completely traversed the microfluidic barrier and the furthest projection observed extended up to 118 μm into the channel. In order to identify whether the neurites growing within the microchannels were forming synaptic connections, cultures were stained with the synaptic vesicle marker synaptophysin at 12 DIV,[19] an age at which synaptic activity is present when investigated using standard patch clamp techniques.[6,7] Punctate synaptophysin staining was clearly evident, indicating that synapse formation occurred both inside and outside the microchannels in these cultures (Fig. 5D and E).

### Functional synaptic communication between neuronal networks

Having established that synapse formation occurred, we then used $Ca^{2+}$ imaging to confirm that the synapses were functional and that synaptic communication occurred between the two co-cultures.

An area comprising both chambers and the central microchannels was monitored over 5–10 minutes using 7 different devices (4 for KCl experiments and 3 for glutamate experiments). Signals were classed as neuronal or astrocytic, using established protocols used previously in our laboratory,[6,18] depending on their response to direct KCl solution injection, with neurons showing a significant increase in fluorescence directly after KCl application (Fig. 6 and Fig. S1 in ESI†).

To determine whether synaptic communication occurred between the two fluidically isolated networks, $Ca^{2+}$ events in the non-stimulated chamber were examined to assess the induced activity of these cells. Stimulation of neurons in the right culture significantly increased the number of neuronal calcium events in the left culture by 41% ($n = 235$, $p < 0.001$) from $3.54 \times 10^{-3} \pm 0.33 \times 10^{-3}$ events per second to
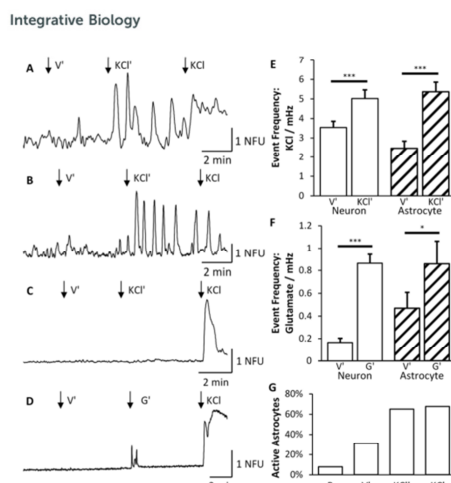
**Fig. 6** KCl stimulation of the right culture (KCl') elicits Ca²⁺ events in both neurons and astrocytes of the left culture. Arrows (↓) indicate time points for injection of vehicle (V'), indirect (KCl') and direct (KCL) solutions. (A) Example trace from a single neuron, identified by its response to direct KCl stimulation, showing an increase in the number of calcium events following indirect stimulation. (B) Example trace from a single astrocyte, identified by no response to direct KCl stimulation, showing an increase in calcium events following indirect stimulation. (C) Trace revealing that not all neurons respond to indirect KCl stimulation. (D) Typical trace from a single neuron demonstrating that activity can be induced *via* indirect stimulation from glutamate (G'). (E) Calcium imaging analysis revealed that the event frequency of neurons (□) and astrocytes (▨) under indirect vehicle and indirect stimulation increased significantly. (F) Glutamate application also increased astrocytic and neuronal activity. (G) The total number of astrocytes that are active approximately doubles during indirect and direct applications of KCl.

$5.01 \times 10^{-3} \pm 0.45 \times 10^{-3}$ events per second (Fig. 6). These results further confirmed that the two chambers were fluidically isolated as a number of neurons remained silent during indirect KCl application but responded to the subsequent direct KCl application (Fig. 6C). Whilst an increase in the frequency of Ca²⁺ events was observed, there was no change in the average magnitude of the events observed in the absence or presence of indirect KCl stimulation ($0.64 \pm 0.068$ NFU compared to $0.60 \pm 0.059$ NFU). Therefore, with no direct stimulus being applied to the cells, this increase in Ca²⁺ events must be driven by an increase in synaptic activity from the other cell population (see Video S1 in ESI†).

Interestingly, Ca²⁺ events were also evident in a number of cells that did not respond to direct KCl stimulation suggesting that these are glial cells, presumably astrocytes.[6,18] These events significantly increased by 117%, from $2.47 \times 10^{-3} \pm 0.37 \times 10^{-3}$ events per second to $5.36 \times 10^{-3} \pm 0.51 \times 10^{-3}$ events per second ($n = 152$, $p < 0.001$, Fig. 6E). Only astrocytes that were significantly active were included in this analysis as all non-active ROIs were discarded. As the traces

recorded for astrocytes varied substantially during each stage of the experiment, the number of astrocytes that were active during each stage was counted (Fig. 6G). 31% of the total astrocyte population were active during the indirect application of vehicle which doubled to 65% being active during indirect application of KCl and 68% during direct stimulation of KCl.

In order to provide a more physiologically relevant stimuli in the right culture, we used the major excitatory neurotransmitter within the CNS, namely glutamate. Application of glutamate (100 μM) on the right culture similarly produced an increased response in neuronal activity of the left culture (Fig. 6F). The indirect culture's response to vehicle was $1.68 \times 10^{-4} \pm 0.38 \times 10^{-4}$ events per second which rose to $8.64 \times 10^{-4} \pm 0.8 \times 10^{-4}$ events per second upon glutamate being applied to the right side. This is a significant increase of 415% ($n = 286$, $p < 0.001$) which is much greater than the KCl system due to the reduced activity prior to glutamate application. Astrocytes were again deduced from their lack of response to direct KCl stimulation and were found to increase in activity by 83%, from $4.70 \times 10^{-4} \pm 1.4 \times 10^{-4}$ events per second to $8.6 \times 10^{-4} \pm 2.1 \times 10^{-4}$ events per second ($n = 57$, $p < 0.05$).

## Discussion

In this study, we have successfully demonstrated the use of a microfluidic system combined with calcium imaging for investigating how the activity of one primary hippocampal cultured network is modulated by the changes in activity in a second, environmentally isolated, network *via* functional synaptic connections.

### Modelling fluidic isolation

The validated numerical model shows that cross-contamination of substances across chambers does not occur in the timescales under which the experiments were carried out. The simulation results are also in agreement with previously described models.[9,12,20] From our models, it is possible to predict the duration for which fluidic isolation is maintained and, furthermore, to estimate the optimum time for withdrawal and injection of solutions that is required to sustain a desired substance concentration condition within the device chambers. This information is particularly important for the future optimisation of co-culture transfection within the device, leading to localised genetic manipulation of a cell population, thus opening the way to studying proteins of interest and their effects on synaptic communication.

However, one phenomenon that has not been taken into account in our model is the evaporation of aqueous solutions. Contrary to what happens in bulk systems used for conventional calcium imaging experiments, fluid evaporation due to the reduced volumes in microchannels and the water permeability through PDMS can potentially have significant effects in fluid volumes over long-term experiments. Nonetheless, since the on-chip experiments were limited to 20 minutes and carried out at room temperature, the effect of evaporation was not significant in this work.

### Imaging neurite growth and synapse formation

To demonstrate synaptic communication between the chambers, it was first essential to confirm that both neurite growth and synapse formation were indeed present within the microchannels. Our data clearly indicates that neuronal processes were present and synapse formation occurred within the microchannels. Neurons grew processes which at an early stage, within 3 DIV, were already within the microchannels, as seen previously.[8] The synaptic vesicle marker, synaptophysin, is commonly used to identify synapse formation[11,19] which was clearly identified here to have occurred at 12 DIV (as expected from other studies of synaptic activity using standard electrophysiological techniques[6,7]). Punctate synaptophysin staining was present around the entrances/exits of the microchannels as well as within the microchannels themselves. This is a clear indication that the cultures form synapses. However, their functionality can only be confirmed by monitoring cellular activity using calcium imaging or electrophysiology.

### Calcium imaging and synaptic communication

Neuronal depolarisation is known to cause an increase in neuronal activity and this was evident in the present study by the increase in frequency of observed $Ca^{2+}$ events monitored in the left chamber, following KCl application in the opposing right chamber. It was also shown that the excitatory neurotransmitter, glutamate, induced an increase in the frequency of $Ca^{2+}$ events observed in the left chamber when applied to the right chamber.

Calcium imaging is an established technique for monitoring neuronal activity[6,18,21] and can be effectively used to increase the throughput of simultaneously acquired signals.[22,23] Some studies have even shown that it is possible to detect single action potentials from captured $Ca^{2+}$ signals.[23] Similar calcium imaging techniques have previously been used within microfluidic devices to examine how a cell responds to locally applied chemical insults,[14] as well as in cortico-striatal co-cultures to construct orientated synaptic networks.[21] However, while these studies demonstrate the use of calcium imaging as a method for monitoring cell activity within microfluidic devices, the technique was not used in a dynamic assay to show how one stimulated culture can synaptically influence the activity of the connected culture.

Here, we have demonstrated that a chemically induced effect on neuronal activity, *via* the application of KCl or glutamate, can dynamically influence the neuronal activity in a fluidically isolated co-culture. Since the chemical stimulus was contained within one chamber, as proposed by our modelling, these data indicate that the increase in activity in both neurons and astrocytes resulted from functional synaptic communication between the two networks. To the best of our knowledge this is the first time, using solely calcium imaging and chemical stimuli, that the formation of functional synapses between two fluidically isolated cultures has been confirmed. Furthermore, an increase in $Ca^{2+}$ events was also observed in the astrocyte population indicating that changes in neuronal activity can alter the activity of neurons

and astrocytes alike. Other studies demonstrating live signalling between neuronal co-cultures have been reliant on microelectrode arrays[10,15] that cannot detect this activity from astrocytes. However, underlying mechanisms for the astrocytic response are beyond the scope of this study. Nevertheless, with the understanding of astrocytic function under both physiological[24,25] and pathophysiological conditions[26,27] increasing dramatically, one could speculate that the proposed methodology could be useful in further increasing our understanding of the role that neuron–astrocyte interactions play under these conditions. This approach opens numerous possibilities for the use of these systems in drug discovery programmes or to further increase our understanding of the synaptic mechanisms that underlie certain CNS disorders. However, we cannot confirm that this synaptic communication occurs solely within the microchannels as we cannot rule out an effect from neurites from the opposing culture that have crossed the central barrier. Further development of the device by utilising different chamber configurations and microchannels of different geometries[14,28] will allow this to be examined.

## Conclusion

We have shown a novel approach integrating microfluidic systems with calcium imaging for the purpose of monitoring neuronal and astrocytic activity in functionally connected, but fluidically isolated primary hippocampal cultures. This method has high-throughput capability to monitor effects on neuronal synaptic communication in response to controlled local stimuli that could be useful for drug screening. In addition, there is the potential to extend this approach for investigating the consequence on synaptic function of genetic alterations observed in certain CNS disorders and thus highlight novel therapeutic targets.

## Acknowledgements

## Notes and references

1  D. J. Nutt, The full cost and burden of disorders of the brain in Europe exposed for the first time, *Eur. Neuropsychopharmacol.*, 2011, **21**, 715–717.

2  D. J. Nutt and J. Attridge, CNS drug development in Europe - Past progress and future challenges, *Neurobiol. Dis.*, 2013, **61**, 6–20.

3  N. A. Fineberg, *et al.*, The size, burden and cost of disorders of the brain in the UK, *J. Psychopharmacol.*, 2013, **27**, 761–770.

4  P. Y. Collins, *et al.*, Grand challenges in global mental health © 2011, *Nature*, 2011, **475**, 27–30.

5  P. Winn, T. J. Bushell, J. Pratt and B. Picard, The future of neuroscience, *Public Serv. Rev. UK Sci. Technol.*, 2011, 1–2.

6  J. Gan, S. M. Greenwood, S. R. Cobb and T. J. Bushell, Indirect modulation of neuronal excitability and synaptic

# Appendix

Integrative Biology

transmission in the hippocampus by activation of proteinase-activated receptor-2, *Br. J. Pharmacol.*, 2011, **163**, 984–994.

7 C. J. Ledgerwood, S. M. Greenwood, R. R. Brett, J. a. Pratt and T. J. Bushell, Cannabidiol inhibits synaptic transmission in rat hippocampal cultures and slices *via* multiple receptor pathways, *Br. J. Pharmacol.*, 2011, **162**, 286–294.

8 A. M. Taylor, Microfluidic multicompartment device for neuroscience research, *Langmuir*, 2003, **19**, 1551–1556.

9 A. M. Taylor, A microfluidic culture platform for CNS axonal injury, regeneration and transport, *Nat. Methods*, 2005, **2**, 599–605.

10 T. T. Kanagasabapathi, *et al.*, Selective pharmacological manipulation of cortical-thalamic co-cultures in a dual-compartment device, *J. Neurosci. Methods*, 2013, **214**, 1–8.

11 M. Shi, *et al.*, Glia co-culture with neurons in microfluidic platforms promotes the formation and stabilization of synaptic contacts, *Lab Chip*, 2013, **13**, 3008–3021.

12 A. Kunze, *et al.*, Astrocyte-neuron co-culture on microchips based on the model of SOD mutation to mimic ALS, *Integr. Biol.*, 2013, **5**, 964–975.

13 J. Park, H. Koito, J. Li and A. Han, A multi-compartment CNS neuron-glia Co-culture microfluidic platform, *J. Visualized Exp.*, 2009, 6–8, DOI: 10.3791/1399.

14 A. M. Taylor, D. C. Dieterich, H. T. Ito, S. A. Kim and E. M. Schuman, Microfluidic local perfusion chambers for the visualization and manipulation of synapses, *Neuron*, 2010, **66**, 57–68.

15 T. T. Kanagasabapathi, D. Ciliberti, S. Martinoia, W. J. Wadman and M. M. J. Decré, Dual-compartment neurofluidic system for electrophysiological measurements in physically segregated and functionally connected neuronal cell culture, *Front. Neuroeng.*, 2011, **4**, 1–11.

16 V. Jokinen, *et al.*, A microfluidic chip for axonal isolation and electrophysiological measurements, *J. Neurosci. Methods*, 2013, **212**, 276–282.

17 K. W. Oh, K. Lee, B. Ahn and E. P. Furlani, Design of pressure-driven microfluidic networks using electric circuit analogy, *Lab Chip*, 2012, **12**, 515–545.

18 T. J. Bushell, R. Plevin, S. Cobb and A. J. Irving, Characterization of proteinase-activated receptor 2 signalling and expression in rat hippocampal neurons and astrocytes, *Neuropharmacology*, 2006, **50**, 714–725.

19 T. J. Bushell, C. C. Lee, R. Shigemoto and R. J. Miller, Modulation of synaptic transmission and differential localisation of mGlus in cultured hippocampal autapses, *Neuropharmacology*, 1999, **38**, 1553–1567.

20 A. M. Taylor, *et al.*, Microfluidic multicompartment device for neuroscience research, *Langmuir*, 2003, **19**, 1551–1556.

21 J.-M. Peyrin, *et al.*, Axon diodes for the reconstruction of oriented neuronal networks in microfluidic chambers, *Lab Chip*, 2011, **11**, 3663–3673.

22 N. Takahashi, T. Sasaki, A. Usami, N. Matsuki and Y. Ikegaya, Watching neuronal circuit dynamics through functional multineuron calcium imaging (fMCI), *Neurosci. Res.*, 2007, **58**, 219–225.

23 N. Takahashi, Y. Takahara, D. Ishikawa, N. Matsuki and Y. Ikegaya, Functional multineuron calcium imaging for systems pharmacology, *Anal. Bioanal. Chem.*, 2010, **398**, 211–218.

24 G. Perea and A. Araque, GLIA modulates synaptic transmission, *Brain Res. Rev.*, 2010, **63**, 93–102.

25 M. Santello, C. Calì and P. Bezzi, Gliotransmission and the tripartite synapse, *Adv. Exp. Med. Biol.*, 2012, **970**, 307–331.

26 D. Rossi and A. Volterra, Astrocytic dysfunction: insights on the role in neurodegeneration, *Brain Res. Bull.*, 2009, **80**, 224–232.

27 V. Parpura, *et al.*, Glial cells in (patho)physiology, *J. Neurochem.*, 2013, **121**, 4–27.

28 A. Kunze, R. Meissner, S. Brando and P. Renaud, Co-pathological connected primary neurons in a microfluidic device for Alzheimer studies, *Biotechnol. Bioeng.*, 2011, **108**, 2241–2245.

**200**